INFORMATION TO USERS

This manuscript has been reproduced from the microfilm master. UMI films the text directly from the original or copy submitted. Thus, some thesis and dissertation copies are in typewriter face, while others may be from any type of computer printer.

The quality of this reproduction is dependent upon the quality of the copy submitted. Broken or indistinct print, colored or poor quality illustrations and photographs, print bleedthrough, substandard margins, and improper alignment can adversely affect reproduction.

In the unlikely event that the author did not send UMI a complete manuscript and there are missing pages, these will be noted. Also, if unauthorized copyright material had to be removed, a note will indicate the deletion.

Oversize materials (e.g., maps, drawings, charts) are reproduced by sectioning the original, beginning at the upper left-hand corner and continuing from left to right in equal sections with small overlaps.

UMI®

Before earth and sea and heaven were created, all things wore one aspect, to which we give the name of Χάος – a confused and shapeless mass, nothing but dead weight, in which, however, slumbered the seeds of things. Earth, sea and air were all mixed up together; so the earth was not solid, the sea was not fluid, and the air was not transparent.

Thomas Bulfinch, *Mythology*

Chaos umpire sits,
And by decision more embroils the fray
By which he reigns: next him high
Chance governs all.

John Milton, *Paradise Lost*

University of Alberta

On the drag experienced by particles in fluid

by

Paweł Buczek ©

A thesis submitted to the Faculty of Graduate Studies and Research in partial
fulfillment of the requirements for the degree of Master of Science

Department of Department of Physics

Edmonton, Alberta
Fall 2005

Canada

University of Alberta

Library Release Form

NAME OF AUTHOR: Paweł Buczek

TITLE OF THESIS: On the drag experienced by particles in fluid

DEGREE: Master of Science

YEAR THIS DEGREE GRANTED: 2005

Permission is hereby granted to the University of Alberta Library to reproduce single copies of this thesis and to lend or sell such copies for private, scholarly or scientific research purposes only.

The author reserves all other publication and other rights in association with the copyright in the thesis, and except as herein before provided neither the thesis nor any substantial portion thereof may be printed or otherwise reproduced in any material form whatever without the author's prior written permission.

June 22, 2005

University of Alberta

Faculty of Graduate Studies and Research

The undersigned certify that they have read, and recommend to the Faculty of Graduate Studies and Research for acceptance, a thesis entitled **On the drag experienced by particles in fluid** submitted by **Paweł Buczek** in partial fulfillment of the requirements for the degree of Master of Science.

_____
Dr. Andrzej Czarnecki (Supervisor)

_____
Dr. Krishnaswamy Nandakumar (External)

_____
Dr. Richard Sydora

_____
Dr. Zbigniew Gortel

DATE: _____

Abstract

Description of multiphase flows, such as mixtures of gas and solid particles, requires knowledge of the coupling between the momenta of the granular and fluid phases - the interphase drag. The determination of this quantity is the main topic of this thesis. After an extensive review of previous approaches, the Navier-Stokes equation for the flow between particles is solved by means of an "electric network analogy". Since the calculations are easy in the case of a flow of irregular assemblages of particles, the main part of the analysis is devoted to the investigation of the impact of disorder. It is found that irregular weighted hydraulic networks feature significant correlations, in contrast to regular networks. Additionally, the disorder causes local flows to develop large spatial fluctuations.

To

my Parents

Preface

If you live in Edmonton you can easily get to the real origins of this work. Pack your car on early Saturday morning and drive it north sticking to Highway 63; after couple of hours you will reach Athabasca Oil Sands Deposit. Athabasca Fields contain more oil than all known reserves in the Middle East, trapped in greasy soils just beneath Alberta's plains, but as distinguished from light green-gold stocks of Southern Arabia, that you could almost directly feed your motor with, oil extracted in Fort McMurray resembles more black tar. This unpleasant substance is called bitumen or "energetic future of Canada".

The long hydrocarbons it contains are useless, unless in the process of thermocracking they are cut into smaller chains. The catalytic reaction is performed on the surface of fine coke particles suspended in the stream of pressurized steam in huge chemical reactors. Mixture of bitumen and steam is injected into the reactor using sonic nozzles and in the perfect picture every fine droplet of oil meets coke particle, which it covers. Coke particles decrepitated in external burner serves as a source of energy for the cracking to occur and the light fractions of oil produced in this process are collected at the top of the reactor. Unfortunately the reality does not match this idealized description: oil and coke form large conglomerates, which are to heavy to be suspended by steam. They fall down, slowly blocking the reactor; at some point the process need to be stopped and the chamber cleared. The right design of the reactors is the key to achieve high productivity and small losses. Efficient reactors mean minimization of the costs of energy and what follows maximization of profit, but also the protection of natural environment. Unfortunately it is almost impossible to experiment with the real reactors, so instead models need to be created. They may be laboratory miniatures of real chemical plants, but also numerical simulations of such systems. My group concentrates on the second task.

Computer studies of multiphase flows, which essentially occur in our reactors, are still in the phase of development. One of the most important phenomenon they must grasp is that the discrete solids phase (coke particles) can exchange momentum with the conveying fluid. Understanding of this process became the major goal of this thesis.

Part I of the work opens with the exposition of hydrodynamical formalism and its generalizations leading to the description of multiphase flows (Chapter 1). In this chapter the quantity of main interest, i.e. the momentum exchange or interphase drag, is formally defined. Next, in Chapter 2, I review the existing experimental and theoretical work devoted to this quantity and introduce several important concepts, especially the notion of momentum transfer coefficient, β, which is central in the subsequent considerations. Chapter 3 deals with the especially promising hydraulic network method for describing flows in complicated geometries. From now on, in Part II, the thesis concentrates solely on this approach. Chapters 4 and 5 contain analytical studies. The first one deals with flow in periodic media, which are the starting point for modeling realistic, i.e. disordered, systems. In the latter several concepts developed for regular arrays of particles are translated into language of irregular sets of points, especially the "uniform gradient

hypothesis". To verify it a series of direct numerical simulations of hydraulic networks is undertaken; the simulations are presented in Chapter 6 with the attention focused on the impact of disorder. Chapter 7, summarizing the work, points also the directions of further research.

Acknowledgements

This document would never have come to life in any form without the legendary supervision of Dr. Andrzej Czarnecki. His contagious enthusiasm and unceasing support – stretching far beyond the standard duties of academic supervisor – have earned my deepest gratitude and respect. Andrzej Czarnecki showed me that students could gain much more from their masters than mere knowledge.

I am also grateful to Dr. Alexander Yelkhovsky, who guided me throughout my research at the University of Alberta. He protected me against numerous traps and the influence of his scientific expertise permeates this thesis.

Special thanks go to my friends in Canada and Poland. In Edmonton, I am greatly indebted to Eun Ah Lee and Alexey Pak, who helped me survive my first – and therefore coldest – winter in Alberta. In Kraków and Halle, to Krzysztof Fitta and Martyna Polok, partly for taking care of my eccentric educational business in Europe, but mainly for not forgetting about their fellow-countryman on the other side of the globe. I would also like to take this opportunity to express my appreciation to Dr. Andrzej Lenda and my supervisor in Poland Dr. Janusz Wolny for their support and patience.

I am also indebted to professors Kokichi Sugihara and Masao Iri, the creators of the VORONOI2 library, who granted me permission to use their software.

This work was generously supported by the Alberta Energy Research Institute and Syncrude Canada Ltd. under the COURSE grant program.

Contents

CONTENTS

CONTENTS

List of Tables

List of Figures

LIST OF FIGURES

Part I

Preliminaries

Chapter 1

Formulation of the problem

The importance of fluid mechanics need not to be emphasized. The spectrum of application ranging from the construction of airplanes to the design of chemical reactors clearly reveals the great practical importance of our work. Fluid mechanics has deeply rooted in the landscape of human scientific and technical activity. Flows intrigue us nowadays in the same way as rain and wind used to absorb our wood-dwelling forefathers, forcing them to become cave-dwellers, and like for Archimedes fluids are still a source of revelations, making excited εὕρηκα's sound in numerous graduate offices around the world. Furthermore hydrodynamics repeatedly does not fail to be an inspiration and source of decent living. Exactly like in the times of Vikings, who built their ships to travel to distant and prosperous lands to share their cultural experience and European sense of humor, it allows us to travel and earn money, however a bit faster. But apart from this earthen mission hydrodynamics appears as one of the greatest scientific achievements of physics though, like any decent scientific quest, it still avoids our full understanding.

The first formulation of the modern hydrodynamics is associated with the turn of eighteen and nineteen century and the remarkable names like Claude Louis Navier, Siméon Poisson, George Stokes, Leonhard Euler or Joseph Louis Lagrange, to mention just the few. Their understanding of fluid mechanics did not differ from the modern one, at least as far as laminar flows are concerned, nevertheless the mankind had to wait another half of the century for the explanation of the flow phenomena, especially viscosity, in terms of the first principles. It was statistical mechanics, which facilitated that. Forming the cornerstone of the heat theory, works of Ludwig Boltzmann and especially his H theorem initiate the kinetic theory of gases and hence modern hydrodynamics, where viscosity appears as a calculable parameter of the system and does not need to be taken solely from the experiment. The twentieth century fluid mechanics went beyond laminar approximation and brought up its own heroes, whose names again sound familiar to almost everybody: Ernst Mach, Theodore von Kármán and Ludwig Prandtl (the fathers of modern aeronautics) and of course Osborne Reynolds, again to perform unjust selection.

In this chapter I present theoretical foundations of the hydrodynamics to celebrate the joy once more. First a brief introduction to kinetic theory is given, which is then followed by the sketch of a derivation of Navier-Stokes equation from the Boltzmann transport

equation. Subsequently I investigate the possibilities of solution of the Navier-Stokes equation and some of its general properties, discussing several important examples. Next a theory of two phase flow is exposed for the limited case of dilute suspension of spheres and supplemented with a heuristic generalization. In this point I am able to formulate the main goal of the thesis which is a calculation of the interphase drag **F**. The chapter ends with a few comments on the granular gases, which used to be (and still are) of our great interest.

1.1   Hydrodynamics as the problem of kinetic theory

The contents of this section is based primarily on the classic textbook *Statistical mechanics* by Kerson Huang ([47]).

We are interested in a collection of N molecules in a container of volume V. Let's set the right length scales first. We assume that the temperature T is high enough and the density is sufficiently low so that the each molecule may be considered as a classical particle with well defined position and momentum; particles are in general distinguishable. This requires the average de Broglie wavelength to be smaller then average interparticle separation

$$\frac{\hbar}{\sqrt{2mk_{\mathrm{B}}T}}\left(\frac{N}{V}\right)^{1/2} \ll 1,$$

where $k_{\mathrm{B}} \approx 1.38 \times 10^{-8}\,\mathrm{JK}^{-1}$ is a Boltzmann constant and $\hbar \approx 1.055 \times 10^{-34}\,\mathrm{Js}$ is a Planck's constant. This means that we do not need to worry about quantum effect such as superfluidity and we will work with Boltzmann energy distribution, not differentiating between fermions and bosons. Furthermore we will assume that masses of the fluids under consideration are small enough so the "self-gravitation" effects do not matter and we will not end up in a black hole (however we do not discard the effects of gravitational interactions of the fluid with other bodies). Clearly Newtonian mechanics applies. This statement of the ontological status still leaves us a lot of space.

The molecules are further assumed to be of the single kind, having equal masses m and interacting via collisions with scattering cross section $\sigma(\Omega)$, where Ω stands for the scattering angle.

1.1.1   Boltzmann transport equation

We are not interested in the history of the particular molecules, but rather in their distribution function $f(\mathbf{r}, \mathbf{v}, t)$, which is so defined that

$$f(\mathbf{r}, \mathbf{v}, t)d^3r d^3v$$

denotes the number of molecules in the element $d^3r d^3v$ of position-velocity phase space around $(\mathbf{r}, \mathbf{v})$ at time t. $\mathbf{r}$ is a position of the particle and $\mathbf{v}$ its velocity. The function is

normalized as follows

$$\int f(\mathbf{r}, \mathbf{v}, t) d^3r \, d^3v = N.$$

The equation for the evolution of $f(\mathbf{r}, \mathbf{v}, t)$ can be obtained from the particle number conservation law and second Newton law

$$\left(\frac{\partial}{\partial t} + \mathbf{v} \cdot \nabla_{\mathbf{r}} + \frac{\mathbf{F}}{m} \cdot \nabla_{\mathbf{v}}\right) f(\mathbf{r}, \mathbf{v}, t) = \left(\frac{\partial f}{\partial t}\right)_{\text{coll}}. \tag{1.1.1}$$

$\mathbf{F}$ is an external force acting on a particle. If the particles did not interact they would move in the phase space on the trajectories characterized by 0 on the RHS of the equation (1.1.1). The term $(\partial_t f)_{\text{coll}}$ describes therefore the rate of change of these trajectories due to collisions and it can be calculated from the analysis of particles' interaction. The equation is useless without explicit determination of this term; the method to deal with it is due to Boltzmann.

The following simplification are necessary

i. only the collisions between two particles (binary collisions) are important, since the fluid is not too dense. Particles 1 and 2 with velocities $\{\mathbf{v}_1, \mathbf{v}_2\}$ collide conserving momentum and energy and enter the state $\{\mathbf{v}_1', \mathbf{v}_2'\}$.

ii. the velocity of the molecule in uncorrelated with its position. This is the famous Boltzmann's *assumption of molecular chaos*. This is exactly the moment where the *irreversibility* enters our formalism.

Few more technical assumption have to made; they are listed in [47].

Under these assumptions we are able to calculate RHS in terms of f and parameters of binary collision and write *Boltzmann transport equation*

$$\left(\frac{\partial}{\partial t} + \mathbf{v}_1 \cdot \nabla_{\mathbf{r}} + \frac{\mathbf{F}}{m} \cdot \nabla_{\mathbf{v}_1}\right) f_1 = \int d\Omega \int d^3v_2 \sigma(\Omega) |\mathbf{v}_1 - \mathbf{v}_2| (f_2' f_1' - f_2 f_1), \tag{1.1.2}$$

where $\sigma(\Omega)$ is differential cross-section for the collision

$$\{\mathbf{v}_1, \mathbf{v}_2\} \rightarrow \{\mathbf{v}_1', \mathbf{v}_2'\}$$

and the following notation was used

$$f_1 \equiv f(\mathbf{r}, \mathbf{v}_1, t)$$
$$f_2 \equiv f(\mathbf{r}, \mathbf{v}_2, t)$$
$$f_1' \equiv f(\mathbf{r}, \mathbf{v}_1', t)$$
$$f_2' \equiv f(\mathbf{r}, \mathbf{v}_2', t).$$

Note that only $\mathbf{v}_1$ is an independent variable in this equation since an integration is performed over $\mathbf{v}_2$ and pair $\{\mathbf{v}_1', \mathbf{v}_2'\}$ is single valued function of the velocities before collision.

This integro-differential equation was published together with the famous H-theorem by Boltzmann in 1872. Function $f(\mathbf{r}, \mathbf{v}, t)$ used as a weight enables us to calculate macroscopic properties of our system.

Let us note, following Huang, that (1.1.2) is only an approximation based on the validity of the assumption of molecular chaos; it cannot predict for example the emergence of Brownian motion.

It is relatively easy to construct the solution of (1.1.2) for isotropic system in equilibrium (when $f(\mathbf{r}, \mathbf{v}, t)$ depends explicitly neither on time nor on $\mathbf{r}$) and when the external forces may be neglected. This solution is called *Maxwell-Boltzmann distribution* and has the following form

$$f_0(\mathbf{v}) = C \exp\left[-A(\mathbf{v} - \mathbf{v}_0)^2\right], \tag{1.1.3}$$

where $\mathbf{v}_0$ denotes average velocity of molecules. C and A are constants and we will come back to them later.

There are two interesting facts about (1.1.3). It is independent of the details of molecular interactions. As long as the latter exist the gas in equilibrium will be described by (1.1.3). Second, it may be proved that this is the *most probable* distribution, i.e. (overwhelming) majority of the systems composing an ensemble is characterized by f_0.

1.1.2   Conservation theorem

Let us assume that we obtained a solution to Boltzmann transport equation. Now we are able to build macroscopic quantities (averages) by using f as a weight

$$\langle A \rangle (\mathbf{r}, t) \equiv \frac{1}{n} \int A f d^3 v,$$

where

$$n(\mathbf{r}, t) \equiv \int f d^3 v.$$

For the quantities χ, which are conserved in the binary collision, we can derive from Boltzmann transport equation the following *conservation theorem*

$$\frac{\partial}{\partial t} \langle n\chi \rangle + \frac{\partial}{\partial x_i} \langle n v_i \chi \rangle - n \left\langle v_i \frac{\partial \chi}{\partial x_i} \right\rangle - \frac{n}{m} \left\langle F_i \frac{\partial \chi}{\partial v_i} \right\rangle - \frac{n}{m} \left\langle \frac{\partial F_i}{\partial v_i} \chi \right\rangle = 0. \tag{1.1.4}$$

We are particularly interested in the following invariants

$$\chi = m \qquad\qquad \text{(mass)}, \tag{1.1.5a}$$

$$\chi = m v_i, \quad (i = 1, 2, 3) \qquad\qquad \text{(momentum)}, \tag{1.1.5b}$$

$$\chi = \frac{1}{2} m (\mathbf{v} - \langle \mathbf{v} \rangle)^2 \qquad\qquad \text{(thermal energy)}, \tag{1.1.5c}$$

for which the following three conservation laws can be derived

$$\frac{\partial \rho}{\partial t} + \nabla \cdot (\rho \mathbf{u}) = 0 \qquad \text{(conservation of mass)}, \qquad (1.1.6a)$$

$$\rho \left(\frac{\partial}{\partial t} + \mathbf{u} \cdot \nabla \right) \mathbf{u} = \frac{\rho}{m} \mathbf{F} - \nabla \cdot \overleftrightarrow{P} \qquad \text{(conservation of momentum)}, \qquad (1.1.6b)$$

$$\rho \left(\frac{\partial}{\partial t} + \mathbf{u} \cdot \nabla \right) \theta = -\frac{2}{3} \nabla \cdot \mathbf{q} - \frac{2}{3} \overleftrightarrow{P} : \overleftrightarrow{\Lambda} \qquad \text{(conservation of energy)}, \qquad (1.1.6c)$$

using the following definitions

$$\rho(\mathbf{r}, t) \equiv m n(\mathbf{r}, t) \qquad \text{(mass density)}, \qquad (1.1.7a)$$

$$\mathbf{u}(\mathbf{r}, t) \equiv \langle \mathbf{v} \rangle \qquad \text{(average local velocity)}, \qquad (1.1.7b)$$

$$\theta(\mathbf{r}, t) \equiv \frac{1}{3} m \langle (\mathbf{v} - \mathbf{u})^2 \rangle \equiv k_\mathrm{B} T \qquad \text{(average particle energy – temperature)}, \quad (1.1.7c)$$

$$\mathbf{q}(\mathbf{r}, t) \equiv \frac{1}{2} m \rho \langle (\mathbf{v} - \mathbf{u})(\mathbf{v} - \mathbf{u})^2 \rangle \qquad \text{(heat flux vector)}, \qquad (1.1.7d)$$

$$P_{ij}(\mathbf{r}, t) \equiv \rho \langle (v_i - u_i)(v_j - u_j) \rangle \qquad \text{(pressure tensor)}, \qquad (1.1.7e)$$

$$\Lambda_{ij}(\mathbf{r}, t) \equiv \frac{1}{2} m \left(\frac{\partial u_i}{\partial x_j} + \frac{\partial u_j}{\partial x_i} \right). \qquad (1.1.7f)$$

Word about notation. $\overleftrightarrow{T}$ denotes tensor quantity and the operation $\overleftrightarrow{T}^1 : \overleftrightarrow{T}^2$ stands for the product that saturates both pairs of indexes, $\sum_{i,j} T_{ij}^1 T_{ij}^2$.

These relations are exact, but do not bring anything interesting unless we are able to calculate the above averages. It turns out however that they are sufficient to give meaning to constants A and C in (1.1.3)

$$f_0(\mathbf{v}) = n \left(\frac{m}{2\pi\theta} \right)^{3/2} \exp \left[-\frac{m}{2\theta} (\mathbf{v} - \mathbf{v}_0)^2 \right]. \qquad (1.1.8)$$

1.1.3 Approximate solutions

Let us take a look on function f_0 given by (1.1.8). It describes spatially homogeneous system in its steady state and therefore does not really interests us, because in such system neither flow (different from trivial case $\mathbf{v} = \mathbf{v}_0 \neq \mathbf{0}$) nor even variations of the temperature are possible – we want to go beyond equilibrium states. Nevertheless as a first approach the following picture may be taken. Let us assume that the system is in equilibrium everywhere and all the time, but only *locally*, i.e. that time and spatial variations exist, but are small. More precisely n, θ and $\mathbf{u}$ in (1.1.8) are slowly varying functions of t and $\mathbf{r}$.

This approximation can be put on more quantitative footing. If we have initially system out of equilibrium (say because different spatial parts of the system have different temperatures) we expect that after some time it will reach the steady, homogeneous state. The mechanism responsible for the energy transport are clearly molecular collisions. We can estimate so called *mean free path* λ, i.e. average distance traveled by a molecule

between the collisions

$$\lambda \sim \frac{1}{n\sigma_{\text{tot}}}, \tag{1.1.9}$$

σ_{tot} is the collision cross-section integrated over angles. We may now say that if the spatial variations are on the scales much large than λ our approximation should work quite well. In the same manner we can treat time variations by an introduction of *collision time* (average time between collisions)

$$\tau \sim \frac{\lambda}{\bar{v}}, \tag{1.1.10}$$

where $\bar{v} = \sqrt{2k_{B}T/m}$. Exemplary values (nitrogen in normal conditions) are

$$\lambda \sim 10^{-7}\,\text{m}$$
$$\tau \sim 10^{-9}\,\text{s}$$

and clearly indicate that in the most cases our zeroth-order approximation should be at least reasonable. Of course we can treat in the same manner quantities other than temperature.

If we take $f = f_0$ to calculate averages our mass conservation law (1.1.6a) will not change and the latter two ((1.1.6b) & (1.1.6c)) will take the following form

$$\rho\Big(\frac{\partial}{\partial t} + \mathbf{u}\cdot\nabla\Big)\mathbf{u} = \frac{\rho}{m}\mathbf{F} - \nabla p \qquad \text{(Euler's equation)}, \tag{1.1.11a}$$

$$\Big(\frac{\partial}{\partial t} + \mathbf{u}\cdot\nabla\Big)\theta = -\frac{1}{c_V}(\nabla\cdot\mathbf{u})\theta, \tag{1.1.11b}$$

where $c_V = \frac{3}{2}$ and p denotes local hydrostatic pressure. The first of the above equations was given by Euler in 1755 and describes the flow of nonviscous fluid. The slow flow patterns run forever and there is no energy dissipation; it is apparently in the contradiction with experiment (if we pass over superfluidity). Thermal energy flow is solely due to mass flow (*convection*); such medium does not conduct heat. The model can be nevertheless useful, since it reflects properly the propagation of adiabatic elastic sound waves. Their velocity is:

$$c = \sqrt{\frac{5}{6}}\bar{v}. \tag{1.1.12}$$

It appears that equation of state for such a fluid are simply given by:

$$p = \frac{\rho\theta}{m}, \tag{1.1.13}$$

what is nothing else than the equation of an *ideal gas*. This system never converges spontaneously to a *global* equilibrium state starting from the transient states.

Clearly to make any progress we must include non-equilibrium effects. It has been shown that a stunning progress can be made under assumption that the real function f differs from f_0 only slightly and hence the following approximation can be put forward:

$$\left(\frac{\partial f}{\partial t}\right)_{\text{coll}} \approx -\frac{f - f_0}{\tau}. \tag{1.1.14}$$

This facilitates the solution of equation (1.1.2), calculation of the averages and rewriting of the conservation laws (continuity equation remains the same)

$$\rho\left(\frac{\partial}{\partial t} + \mathbf{u} \cdot \nabla\right)\mathbf{u} = \mathbf{b} - \nabla\left(p - \left(\mu_b + \frac{1}{3}\mu\right)\nabla \cdot \mathbf{u}\right) + \mu\nabla^2\mathbf{u} \quad \text{(Navier-Stokes equation)} \tag{1.1.15a}$$

$$\left(\frac{\partial}{\partial t} + \mathbf{u} \cdot \nabla\right)\theta = -\frac{1}{c_V}(\nabla \cdot \mathbf{u})\theta + \frac{K}{\rho c_V}\nabla^2\theta \qquad \text{(heat conduction equation)}. \tag{1.1.15b}$$

Here I denoted $\mathbf{b} \equiv \rho\mathbf{F}/m$; this is a *body force*, i.e. external force acting on the fluid per unit volume.

Navier-Stokes equation (NS equation) is the foundation of hydrodynamics. It was first written down by Navier in 1821 and rediscovered by Stokes in 1842. The parameters μ, μ_b and K are respectively the *viscosity* (responsible for energy loss due to internal shear), *bulk viscosity* and *thermal conductivity* coefficients. The first and the last are equal in our approximation

$$\mu \approx K \approx \frac{\sqrt{mk_{\mathrm{B}}T}}{a^2}, \tag{1.1.16}$$

where a is an effective molecule diameter.

The SI unit of viscosity is Pa·s = kg/(ms). The latter unit is sometimes called poiseuille, Pl.

The pressure (stress) tensor $\overleftrightarrow{P}$ in Navier-Stokes equation written explicitly in Cartesian coordinates reads

$$P'_{ij} = P_{ij} - \left(\mu' + \frac{2}{3}\mu\right)\delta_{ij}\nabla \cdot \mathbf{u},, \tag{1.1.17a}$$

$$P_{ij} = \delta_{ij}p - \mu\left(\left(\frac{\partial u_i}{\partial x_j} + \frac{\partial u_j}{\partial x_i}\right) - \frac{2}{3}\delta_{ij}\nabla \cdot \mathbf{u}\right), \tag{1.1.17b}$$

where μ' is so called *second viscosity coefficient* and $\mu_b = \mu' + \frac{2}{3}\mu$. The force exerted by the fluid along direction $\hat{\xi}$ equals $-\hat{\xi} \cdot \overleftrightarrow{P}$. For incompressible fluid μ_b drops out from our equation.

We can now discuss briefly, what it means that something can flow. The difference between solids and fluids lies in the response to applied stress: solids can sustain stress without yielding, while fluids are materials that flows when the stress is applied.
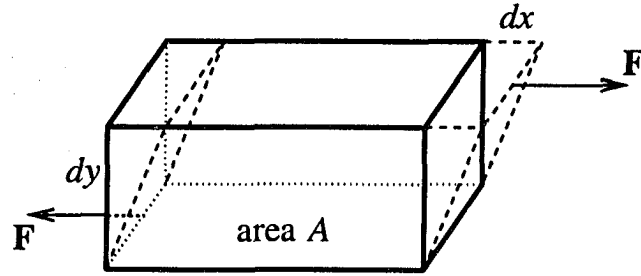
Figure 1.1: A body under shear deformation. The Figure comes from [54].

To make the statement a bit more mathematical let us refer to Figure 1.1. The discussion comes from [54]. We are observing the body under shear stress σ

$$\sigma = \frac{F}{A},\tag{1.1.18}$$

where A is the area on which the force F acts. In the case of *Hookean solids* the applied stress results in static deformation, so called shear strain

$$e = \frac{dx}{dy}\tag{1.1.19}$$

and these two quantities are connected by Hook law

$$\sigma = Ge,\tag{1.1.20}$$

where proportionality constant G is called shear modulus. The picture is completely different for *Newtonian fluids*. The shear stress applied to them causes flow with some velocity gradient

$$\sigma = \mu\frac{dv}{dy} = \mu\dot{e}.\tag{1.1.21}$$

$\dot{e}$ is called strain rate and the proportionality constant in the above law is exactly viscosity. Generalization of above equation leads exactly to the stress tensor given by equation (1.1.17b).

There exists however a whole family of materials that are neither simple liquids or crystalline solids. They are classified as *soft condensed matter* and include material as glues, paints, soaps, polymers, colloids, liquid crystals and almost all material of biological provenience. If they can flow, they are sometimes referred to as *non-Newtonian* liquids. For an introduction to the field please refer to [54].

When velocity u vanishes everywhere in the fluid equation (1.1.15b) takes a form of

well known *Fourier thermal diffusion equation*

$$\rho c_V \frac{\partial \theta}{\partial t} - K \nabla^2 \theta = 0. \tag{1.1.22}$$

Navier-Stokes equation can be derived starting from experimental definition of the viscosity. This derivation works fine for a rarefied gases and for dense liquids, what means that the Navier-Stokes equation validity may be extended beyond low density regime under usual conditions.

There exists general method allowing expansion of f in powers $\frac{\lambda}{L}$, where L is the characteristic length of the spatial variations (e.g. a sound wavelength). This quantity is called *Knudsen number*

$$\mathfrak{Kn} = \frac{\lambda}{L}. \tag{1.1.23}$$

The expansion is called *Chapman-Enskog scheme*. Euler's equation can be regarded as zeroth-order approximation, while Navier-Stokes equation is $\mathcal{O}(\mathfrak{Kn})$.

It appears that Navier-Stokes equation works perfectly well for $\mathfrak{Kn} < 0.01$. In this regime flow vanishes on external surfaces, this is so called *no-slip condition*. For $0.01 < \mathfrak{Kn} < 0.1$ NS equation is still valid, however we must account for slip velocity on the walls. For larger Knudsen numbers molecular effects become important and continuum approximation breaks down. Please refer to [44].

1.2 Some properties of Navier-Stokes equation

This section deals with some basics concepts of single phase hydrodynamics. I start with three simple but profound examples of usage of Navier-Stokes equation. Next a more general approach is presented. The section ends with the discussion of possible simplifications of NS equation.

1.2.1 Important examples

Effective mass of a sphere

Let us start with the simplest possible situation and consider movement of a sphere of radius a in infinite, nonviscous, incompressible liquid of constant velocity. I follow [47]. There are no external forces. The sphere moves with velocity $\mathbf{u_0}$, the velocity field of the fluid is $\mathbf{u}$. (1.1.15a) reduces to Euler's equation

$$\rho \left(\frac{\partial}{\partial t} + \mathbf{u} \cdot \nabla \right) \mathbf{u} = -\nabla p. \tag{1.2.1}$$

Since there is no viscosity in the problem boundary condition on the surface of the sphere requires only the normal component of the velocity to vanish. The fluid must be also

motionless in the infinity

$$\mathbf{r} \cdot \big(\mathbf{u}(\mathbf{r}) - \mathbf{u}_0\big)\Big|_{r=a} = 0, \qquad (1.2.2\text{a})$$

$$\mathbf{u} \xrightarrow[r\to\infty]{} \mathbf{0}. \qquad (1.2.2\text{b})$$

In addition the solution must obey continuity equation

$$\nabla \cdot \mathbf{u} = 0. \qquad (1.2.3)$$

The basic approach for $\mu = 0$ case is to prove *circulation conservation law*. Let us take curl of the both sides of (1.2.1)

$$\frac{\partial}{\partial t}(\nabla \times \mathbf{u}) + \nabla \times (\mathbf{u} \cdot \nabla)\mathbf{u} = 0 \qquad (1.2.4)$$

and recall the well known formula (e.g. [30])

$$\nabla \times (\mathbf{u} \cdot \nabla)\mathbf{u} = (\mathbf{u} \cdot \nabla)(\nabla \times \mathbf{u}) - ((\nabla \times \mathbf{u}) \cdot \nabla)\mathbf{u} + (\nabla \cdot \mathbf{u})(\nabla \times \mathbf{u}). \qquad (1.2.5)$$

If we recall property (1.2.3) we can rewrite (1.2.4) as

$$\Big(\frac{\partial}{\partial t} + \mathbf{u} \cdot \nabla\Big)\mathbf{c} = (\mathbf{c} \cdot \nabla)\mathbf{u}, \qquad (1.2.6)$$

where $\mathbf{c} = \nabla \times \mathbf{u}$ is called *vorticity*. If at some moment the fluid has no vorticity the RHS of (1.2.6) becomes zero and $\mathbf{c}$ is conserved along streamline. Therefore fluid with zero vorticity will never acquire it and thus

$$\nabla \times \mathbf{u} = \mathbf{0} \qquad (1.2.7)$$

therefore $\mathbf{u}$ can be rewritten as a gradient of a certain function (called *velocity potential*)

$$\mathbf{u} = \nabla \Phi. \qquad (1.2.8)$$

Let us rewrite the problem in terms of Φ

$$\nabla^2 \Phi = 0, \qquad (1.2.9\text{a})$$

$$\frac{\partial \Phi}{\partial r}\bigg|_{r=a} = u_0 \cos \vartheta, \qquad (1.2.9\text{b})$$

$$\Phi(\mathbf{r}) \xrightarrow[r\to\infty]{} 0, \qquad (1.2.9\text{c})$$

where ϑ is an angle between $\mathbf{u}_0$ and $\mathbf{r}$. Problem is reduced to solving Laplace equation (1.2.9a). The general solution is a combination of spherical harmonics, but it is an established experimental fact, that flow around a sphere (both in viscous and nonviscous regime) has characteristic dipole-like shape. Let us therefore take only the first term

(obviously we do not have ϕ dependence)

$$\Phi(\mathbf{r}) = C\frac{\cos\vartheta}{r^2}. \tag{1.2.10}$$

C is obtained immediately from boundary conditions and thus

$$\Phi(\mathbf{r}) = -\frac{1}{2}u_0 a^3 \frac{\cos\vartheta}{r^2} \quad (r \geq a). \tag{1.2.11}$$

Let us contemplate the physical situation for a while. The motion of the sphere requires that the fluid also moves and thus possesses some kinetic energy. Therefore, while accelerating the sphere, we must supply some energy both to the sphere and the surrounding fluid. The sphere appears therefore to be heavier than in the empty space, it acquires some *effective mass*. The latter can be obtained by calculating the kinetic energy of the fluid

$$\frac{\rho}{2}\int_\Omega d^3r\, \mathbf{u}\cdot\mathbf{u} = \frac{\rho}{2}\left(\frac{u_0 a^3}{2}\right)^2 \int_{r\geq a} d^3r\, \nabla\frac{\cos\vartheta}{r^2}\cdot\nabla\frac{\cos\vartheta}{r^2}.$$

The last integrand may be written in the following form

$$\nabla\cdot\left(\frac{\cos\vartheta}{r^2}\nabla\frac{\cos\vartheta}{r^2}\right),$$

once we note that $\nabla^2(\cos\vartheta/r^2) = 0$, because the function is harmonic. We apply now Gauss theorem (minus sign comes from the fact we integrate over an exterior of the sphere)

$$\begin{aligned}
&\frac{\rho}{2}\left(\frac{u_0 a^3}{2}\right)^2 \int_{r\geq a} d^3r\, \nabla\cdot\left(\frac{\cos\vartheta}{r^2}\nabla\frac{\cos\vartheta}{r^2}\right)\\
&= -\frac{\rho}{2}\left(\frac{u_0 a^3}{2}\right)^2 \int_{r=a} d\mathbf{S}\cdot\left(\frac{\cos\vartheta}{r^2}\nabla\frac{\cos\vartheta}{r^2}\right) =\\
&= -\frac{\rho}{2}\left(\frac{u_0 a^3}{2}\right)^2 2\pi a^2 \int_{-1}^{1} d(\cos\vartheta)\left(\frac{\cos\vartheta}{r^2}\frac{\partial}{\partial r}\frac{\cos\vartheta}{r^2}\right)\Big|_{r=a},
\end{aligned} \tag{1.2.12}$$

where the form of the last integral comes from the fact that $d\mathbf{S}$ has only radial component. Let us integrate to the end and obtain that kinetic energy of the fluid is

$$\frac{1}{2}m_{\text{eff}}u_0^2, \tag{1.2.13}$$

where $m_{\text{eff}} = \frac{1}{2}\left(\frac{4}{3}\pi a^3\rho\right)$ is the effective mass of the surrounding fluid and equals exactly half of the of the mass displaced. The quantity $m + m_{\text{eff}}$ may be regarded as effective mass of the sphere.

Stokes formula

Now I will turn on the viscosity and we will try to calculate the drag exerted on the sphere moving slowly in the unbound, viscous and incompressible fluid. The problem is very well known; the treatment presented comes from [47]; another approach can be found in famous Landau's textbook [61].

The only case, when the NS equation can be solved analytically and exactly, is *creeping flow (Stokes)* regime for which the nonlinear term $\mathbf{u} \cdot \nabla \mathbf{u}$ can be neglected. (1.1.15a) takes then the following form

$$\nabla\left(p - \frac{\mu}{3}\nabla \cdot \mathbf{u}\right) = \mu\nabla^2\mathbf{u}. \tag{1.2.14}$$

When supplemented by mass conservation equation, the problem can be rewritten as

$$\nabla^2\mathbf{u} = \frac{1}{\mu}\nabla p, \tag{1.2.15a}$$

$$\nabla \cdot \mathbf{u} = 0, \tag{1.2.15b}$$

with the non-slip conditions on the surface of the sphere; in infinity fluid should have constant velocity $\mathbf{u}_0$, therefore

$$\mathbf{u(r)}\big|_{r=a} = \mathbf{0}, \tag{1.2.16a}$$

$$\mathbf{u(r)} \xrightarrow[r\to\infty]{} \mathbf{u}_0. \tag{1.2.16b}$$

Divergence applied to both sides of (1.2.15a) gives

$$\nabla^2 p = 0. \tag{1.2.17}$$

Our coordination system has $\hat{\mathbf{z}}$ axis along $\mathbf{u}_0$; the sphere rests in the origin.

To solve (1.2.17) we should write p as general combination of spherical harmonics, but once again experimental evidence suggests that the following should be a good guess

$$p = P_0 + \mu P_1 \frac{\cos\vartheta}{r^2}, \tag{1.2.18}$$

leading us to inhomogeneous Laplace equation

$$\nabla^2\mathbf{u} = P_1\nabla\frac{\cos\vartheta}{r^2}. \tag{1.2.19}$$

Let us show that one of the particular solutions to (1.2.19) is

$$\mathbf{u}_1 = -\frac{P_1}{6}r^2\nabla\frac{\cos\vartheta}{r^2}. \tag{1.2.20}$$

By writing this expression explicitly in Cartesian coordinates ($r \equiv \sqrt{x^2 + y^2 + z^2}$)

$$(\mathbf{u}_1)_x = -\frac{P_1}{6}\frac{3xz}{r^3}, \tag{1.2.21a}$$

$$(\mathbf{u}_1)_y = -\frac{P_1}{6}\frac{3yz}{r^3}, \tag{1.2.21b}$$

$$(\mathbf{u}_1)_z = -\frac{P_1}{6}\frac{3z^2}{r^3} + \frac{P_1}{6}\frac{1}{r} \tag{1.2.21c}$$

we obtain

$$\mathbf{u}_1 = -\frac{P_1}{6}\left(\frac{\hat{\mathbf{z}}}{r} - 3\mathbf{r}\frac{z}{r^3}\right). \tag{1.2.22}$$

Laplacian $\nabla^2 \mathbf{u}_1$ turns to be

$$\frac{P_1}{r^5}\left(-3xy, -3yz, r^2 - 3z^2\right) = -\frac{6}{r^2}\mathbf{u}_1 = P_1\nabla\frac{\cos\vartheta}{r^2}. \tag{1.2.23}$$

To obtain full solution a proper homogeneous solution $\mathbf{u}_h$ must be added to fulfill our boundary conditions (1.2.16). Again, in principle, the solution should be a general combination of "vector" spherical harmonics, but clearly we need to incorporate only terms similar to those found in $\mathbf{u}_1$. We are lucky, because it appears that RHS of equation (1.2.23) is a solution of homogeneous Laplace equation

$$\nabla^2 \nabla\frac{\cos\vartheta}{r^2} = 0, \tag{1.2.24}$$

which can be verified by performing explicit calculations. We make therefore an educated guess, by adding to this function a constant and Coulomb-like term, and obtain homogeneous solution, which turns out to be sufficiently rich to assure non-slip conditions on the surface of the sphere

$$\mathbf{u}_h = \mathbf{A} + B\frac{\hat{\mathbf{z}}}{r} + C\nabla\frac{\cos\vartheta}{r^2}. \tag{1.2.25}$$

The full solution

$$\mathbf{u} = \mathbf{u}_1 + \mathbf{u}_h$$

$$= \mathbf{A} + B\frac{\hat{\mathbf{z}}}{r} + \left(C - \frac{P_1}{6}r^2\right)\nabla\frac{\cos\vartheta}{r^2}, \tag{1.2.26}$$

where (1.2.22) was used to express $\mathbf{u}_1$. The unknown constants can be found from the boundary conditions.

Let us start with the requirements given by (1.2.16a)

$$\mathbf{u}(\mathbf{r})\big|_{r=a} = \mathbf{A} + B\frac{\hat{\mathbf{z}}}{a} + \frac{1}{a^2}\left(C - \frac{P_1}{6}a^2\right)\left(\frac{\hat{\mathbf{z}}}{a} - 3\hat{\mathbf{r}}\frac{\cos\vartheta}{a^3}\right), \tag{1.2.27}$$

where once again (1.2.22) and (1.2.23) were used. The latter results immediately gives

$$C = \frac{P_1 a^2}{6} \tag{1.2.28a}$$

$$B\hat{z} = -\mathbf{A}a. \tag{1.2.28b}$$

(1.2.16b) allows to find $\mathbf{A} = \mathbf{u}_0$. Armed with this knowledge, we can calculate the divergence of $\mathbf{u}$

$$\nabla \cdot \mathbf{u} = (2P_1 + 3au_0)\frac{z}{3r^3}, \tag{1.2.29}$$

which according to (1.2.15b) must be zero, yielding

$$P_1 = -\frac{3}{2}au_0. \tag{1.2.30}$$

The full solution has therefore the following form

$$\mathbf{u} = \mathbf{u}_0\left(1 - \frac{a}{r}\right) + \frac{1}{4}u_0 a\left(1 - \frac{a^2}{r^2}\right)\frac{1}{r}\left(\hat{z} - 3\frac{z}{r}\hat{r}\right). \tag{1.2.31}$$
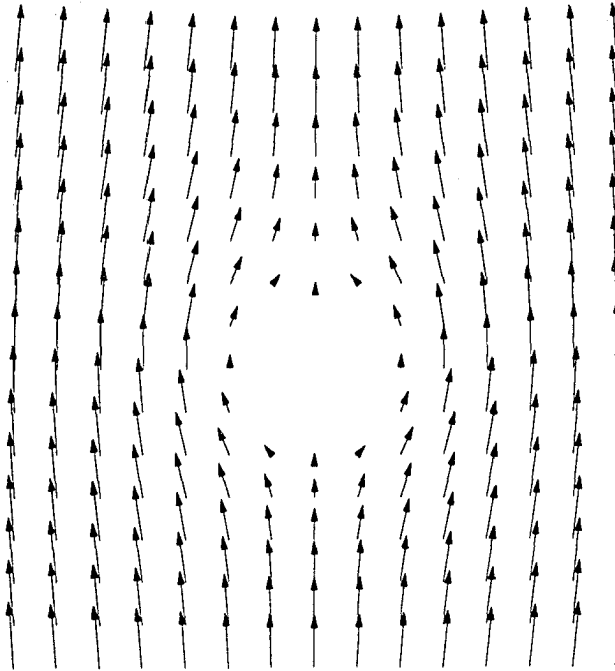
Figure 1.2: The Stokes flow field $\mathbf{u}$ given by (1.2.31). Unperturbed flow $\mathbf{u}_0$ points upward.

The force acting on the sphere is

$$\mathbf{F} = \int_{r=a} dS(-\hat{\mathbf{r}} \cdot \overleftrightarrow{P}), \tag{1.2.32}$$

with $\overleftrightarrow{P}$ given by (1.1.17a), with pressure term given by (1.2.18). The explicit calculation of $\mathbf{F}$ were one of my first exercises with *Mathematica*. It appears that after switching to spherical parametrization Cartesian components of $-\hat{\mathbf{r}} \cdot \overleftrightarrow{P}$ are

$$-\hat{\mathbf{r}} \cdot \overleftrightarrow{P} = \left(-P_0 \cos\phi \sin\vartheta, -P_0 \sin\phi \sin\vartheta, -P_0 \cos\vartheta + \frac{3}{2}\frac{\mu}{a}u_0\right). \tag{1.2.33}$$

Integration yields

$$\mathbf{F} = 6\pi\mu a \mathbf{u}_0. \tag{1.2.34}$$

This is the Stokes law [82]; drag force is proportional to relative velocity of the bodies, fluid viscosity and linear size of the sphere.

It is important to examine the approximation made in the beginning and compare quantities $\|\mu\nabla^2\mathbf{u}\|$ and $\|\mathbf{u}\cdot\nabla\mathbf{u}\|$. It appears that approximation works well if the *Reynolds number* is a small quantity

$$\mathfrak{Re} = \frac{\rho u_0 D}{\mu} \ll 1. \tag{1.2.35}$$

$D = 2a$ is the sphere diameter. When $\mathfrak{Re}$ becomes large (order of 1 for a moving sphere) the description breaks (eddies appear).

2D flow past a cylinder

It is well established fact (see for example [44]), that in 2D Stokes approximation may not exist, like for the case of the flow past a circular cylinder with main axis perpendicular to the flow direction. Let us quote a simple dimensional argument from the same source. In the creeping flow ρ is not a parameter and F, force per unit length of, say, a cylinder should depend only on μ, U (fluid velocity) and a (cylinder radius). The only dimensional group, which can be formed out of these quantities is $F/\mu U$, and we must have $F \sim U$, hence $F/\mu U = const$, what indicates, that force does not depend on the size of the body. Furthermore for $a \to 0$, the drag does not vanish. This is so called *Stokes paradox*. It corresponds to the fact that in two dimensional systems perturbation theory with Reynolds number as a small parameter becomes singular.

Lamb [60] obtained a first approximation for the drag per unit length of the cylinder of radius a

$$F = \frac{4\pi\mu U}{1/2 - \gamma - \log(Ua\rho/4\mu)}, \tag{1.2.36}$$

where $\gamma \approx 0.677$ is the Euler's constant. Rigorous justification using techniques of singu-

lar perturbation theory can be found in [73]. I show in the one of the subsequent chapters how to obtain, utilizing Fourier series techniques, similar result for flow past arrays of cylinders.

1.2.2 Green's function for NS equation

There exists the following theorem for the solutions of time independent, linearized NS equation. A point like force $\mathbf{F}$ applied to fluid in the point $\mathbf{x}'$ in the absence of any boundaries, will induce additional flow

$$\mathbf{v}(\mathbf{x}) = \frac{1}{8\pi\mu} I(\mathbf{x} - \mathbf{x}') \cdot \mathbf{F}(\mathbf{x}'), \qquad (1.2.37)$$

where the Green's function is

$$I_{ij}(\mathbf{x}) = \frac{\delta_{ij}}{\|\mathbf{x}\|} + \frac{x_i x_j}{\|\mathbf{x}\|^3}. \qquad (1.2.38)$$

The theorem is proved in [44]; the presented formulation comes from [6].

The usual application concerns with the perturbation of the flow due to introduction of a rigid body, in the simplest case a sphere. Let us suppose that before sphere was put into the flow a distribution $\mathbf{u}(\mathbf{x})$ of velocity existed. Center of the sphere is $\mathbf{x}_0$ and the radius is a. The flow velocity in the fluid is

$$\mathbf{u}(\mathbf{x}) + \frac{1}{8\pi\mu} \int_{A_0} (I(\mathbf{x} - \mathbf{x}') \cdot \mathbf{f}(\mathbf{x}')) \cdot d\mathbf{A}(\mathbf{x}'), \qquad (1.2.39)$$

where $\mathbf{f}(\mathbf{x})$ denotes a projection of a pressure-stress tensor, and integration is performed over surface A_0 of the sphere. If sphere moves with a velocity $\mathbf{U}$ it can be proved ([6]), that

$$\mathbf{U} = \frac{1}{4\pi a^2} \int_{A_0} \mathbf{u}(\mathbf{x}) dA(\mathbf{x}) + \frac{1}{6\pi a\mu} \int_{A_0} \mathbf{f}(\mathbf{x}) dA(\mathbf{x}), \qquad (1.2.40)$$

which is sometimes referred to as the *first Faxen law*. For $\mathbf{u} = 0$ we immediately get Stokes law (1.2.34). Let us note that in the case, when the particle is settling (or fluidized), i.e. has no acceleration, the last integral is simply equal to excess weight of the sphere and last term represent according to (1.2.34) the terminal velocity of the sphere in the unbound fluid.

In the subsequent chapters I will show how to construct similar Green's function for certain 2D problems.

1.2.3 NS equation in various limiting cases

One of the possible simplification, creeping flow corresponding to small $\Re\mathfrak{e}$ regime, has been already discussed. As I mentioned there exists perturbation solution to movement of the sphere in powers of $\Re\mathfrak{e}$; it can be found in [73] and correction to the force exerted

on a moving sphere are

$$\mathbf{F} = 6\pi\mu a \mathbf{u}_0 \left(1 + \frac{3}{16}\mathfrak{Re} + \frac{9}{160}\mathfrak{Re}^2 \log \mathfrak{Re} + \mathcal{O}(\mathfrak{Re}^2) \right). \qquad (1.2.41)$$

Please compare this expression to (1.2.34) and note presence of logarithmic terms.

In the limit of large $\mathfrak{Re}$ numbers we can neglect the viscosity term $\mu\nabla^2\mathbf{u}$ in comparison to $\mathbf{u}\cdot\nabla\mathbf{u}$. This is a useful method, but unfortunately cannot give any estimates of the drag exerted on the bodies. It is often possible, however, to overcome this difficulty by subdividing the field of flow around a body into an external region, where the flow is usually irrotational and a thin layer near the body together with a wake behind it, where viscous effects are not negligible. This is the so called *boundary layer method*. The technique was introduced by Prandtl and is extremely powerful for the description of flows with well developed turbulence.

In the case of air compressibility may be neglected for Mach numbers smaller than 0.3.

"Limiting case" usually means that the problem can be approximately solved by some kind of perturbation scheme. Exhaustive review of such methods is presented in reference [90].

1.3   Two-phase flows

In this section I outline briefly a way of formal introduction of simultaneous flow of two phases mixture of Newtonian incompressible fluid and a collection of identical spherical particles of radius a. The procedure is due to Jackson and comes from [51] (with errata in [52]) and [4]. The treatment is valid only for small concentrations of particles, but the concepts may be easily extended to more concentrated systems. Other methods must be utilized when flow of particulate phase consisting of fluid droplets is considered (rain), see e.g. [49].

1.3.1   Spatial averages

Any treatment of the system under consideration which attempts to describe motion of the spheres separately is analytically intractable and as far as I know it is still a challenge for computational fluid dynamics (CFD). The only possibility is to assume that spheres constitute a continuum phase, granular gas, which under some conditions behaves like Newtonian fluid. I leave the discussion of this approximation to Section 1.4.

Transition granular-continuous requires a method of spatial averaging, which washes out the details of the dynamics of single spheres. Obviously we will not loose any important information in averaging procedure, if our system exhibits proper scale separation, i.e. characteristic dimension of the flow patterns L is much larger than particle radius a.

There exist many possibilities of building averages: over time, over an ensemble or local space averages. Jackson uses the latter one defined with a help of weighting function $g(r)$, which is a monotoneously decreasing function of the separation r between a pair of

points of space. It is normalized to unity

$$4\pi \int_0^\infty g(r)r^2 dr = 1. \tag{1.3.1}$$

The function has a characteristic radius l, which is defined as follows

$$4\pi \int_0^l g(r)r^2 dr = 4\pi \int_l^\infty g(r)r^2 dr = \frac{1}{2}. \tag{1.3.2}$$

We require $a \ll l \ll L$.

Let us start from the definition of the *local void volume fraction*

$$\epsilon(\mathbf{x}) = \int_{V_f} g(\|\mathbf{x} - \mathbf{y}\|)d^3y, \tag{1.3.3}$$

where V_f denotes integration over the region taken by fluid. $\epsilon(\mathbf{x})$ states what is the ratio of the volume taken by a gas to the total volume of the system "around" point $\mathbf{x}$.

Using $g(r)$ several possible types of averages can be constructed. *Fluid phase average* of point property (pressure, velocity, etc.) f is

$$\langle f \rangle^f (\mathbf{x}) = \frac{1}{\epsilon(\mathbf{x})} \int_{V_f} f(\mathbf{y})g(\|\mathbf{x} - \mathbf{y}\|)d^3y. \tag{1.3.4}$$

Solid phase average is defined in the equivalent way

$$\langle f \rangle^s (\mathbf{x}) = \frac{1}{\phi(\mathbf{x})} \sum_p \int_{V_p} f(\mathbf{y})g(\|\mathbf{x} - \mathbf{y}\|)d^3y, \tag{1.3.5}$$

where summation is over all particles, and V_p denotes volume of the particle p and *solids volume fraction* $\phi(\mathbf{x})$ is defined as

$$\phi(\mathbf{x}) = \sum_p \int_{V_p} g(\|\mathbf{x} - \mathbf{y}\|)d^3y. \tag{1.3.6}$$

Finally it is useful to build *particle-phase average*. *Number density of particles* is

$$n(\mathbf{x}) = \sum_p g(\|\mathbf{x} - \mathbf{x}^p\|); \tag{1.3.7}$$

here $\mathbf{x}^p$ denotes position of the center of particle p. The following relations hold (ν – particles' volume)

$$\phi = \nu n = 1 - \epsilon. \tag{1.3.8}$$

If we consider some property f^p of the particle as a whole, say velocity, mass, etc.,

then the particle-phase average may be expressed as follow

$$\langle f\rangle^p(\mathbf{x}) = \frac{1}{n(\mathbf{x})}\sum_p f^p g(\|\mathbf{x}-\mathbf{x}^p\|). \tag{1.3.9}$$

Since particles are rigid bodies and "global" quantities for them are well defined, usage of particle-phase averages becomes more convenient for us than solid phase averages.

[4] presents a way to calculate the averages of derivatives. We will make use of the following ones

$$\epsilon(\mathbf{x})\Big\langle\frac{\partial f}{\partial x_k}\Big\rangle^f = \frac{\partial}{\partial x_k}\big(\epsilon(\mathbf{x})\,\langle f\rangle^f(\mathbf{x})\big) - \sum_p\int_{S_p} f(\mathbf{y})n_k(\mathbf{y})g(\|\mathbf{x}-\mathbf{y}\|)dS_y, \tag{1.3.10a}$$

$$\epsilon(\mathbf{x})\Big\langle\frac{\partial f}{\partial t}\Big\rangle^f = \frac{\partial}{\partial t}\big(\epsilon(\mathbf{x})\,\langle f\rangle^f(\mathbf{x})\big) + \sum_p\int_{S_p} f(\mathbf{y})n_k(\mathbf{y})u_k(\mathbf{y})g(\|\mathbf{x}-\mathbf{y}\|)dS_y \tag{1.3.10b}$$

and

$$n(\mathbf{x})\Big\langle\frac{\partial f}{\partial t}\Big\rangle^p = \frac{\partial}{\partial t}\big(n(\mathbf{x})\,\langle f\rangle^p(\mathbf{x})\big) + \frac{\partial}{\partial x_k}\sum_p f^p u_k^p g(\|\mathbf{x}-\mathbf{x}^p\|). \tag{1.3.11}$$

Few words about the notation. $\mathbf{n}$ denotes vector normal to the surface, while $\mathbf{u}(\mathbf{x})$ is a point velocity in the fluid and solid phases. S_p is the surface of particle p. The Einstein summation convention is used throughout the study.

1.3.2 Averaged equations of motion

Continuity equation reads $\partial u_k/\partial x_k = 0$. Let us take $f = u_k$ in (1.3.10a) and $f = 1$ in (1.3.10b) and sum up the results

$$\frac{\partial\epsilon}{\partial t} + \frac{\partial}{\partial x_k}\big(\epsilon\,\langle u_k\rangle^f\big) = 0. \tag{1.3.12}$$

Similarly having set $f = 1$ in (1.3.11) we get

$$\frac{\partial n}{\partial t} + \frac{\partial}{\partial x_k}\big(n\,\langle u_k\rangle^p\big) = 0. \tag{1.3.13}$$

Let us try something more complicated. (1.1.15a) written in Cartesian coordinates becomes

$$\rho_f\Big(\frac{\partial u_i}{\partial t} + \frac{\partial}{\partial y_k}\big(u_i u_k\big)\Big) = -\frac{\partial P_{ik}}{\partial y_k} + \rho_f g_i, \tag{1.3.14}$$

where ρ_f represents density of the fluid, g_i body forces (gravity) and P_{ij} is given by (1.1.17a). First we average both sides using $\langle\cdot\rangle^f$. With help of (1.3.10a) with $f = u_i u_k$ and (1.3.10b) with $f = u_i$ on the LHS and (1.3.10a) with $f = -P_{ik}$ on the RHS we get

the averaged momentum equation for fluid phase

$$\rho_f\left(\frac{\partial}{\partial t}(\epsilon\langle u_i\rangle^f) + \frac{\partial}{\partial x_k}(\epsilon\langle u_i u_k\rangle^f)\right) = -\frac{\partial}{\partial x_k}(\epsilon\langle P_{ik}\rangle^f) + \rho_f\epsilon g_i$$
$$+ \sum_p \int_{S_p} P_{ik}(\mathbf{y})n_k(\mathbf{y})g(\|\mathbf{x}-\mathbf{y}\|)dS_y. \qquad (1.3.15)$$

Momentum balance equation for particle p states

$$\rho_s\nu\frac{\partial u_i^p}{\partial t} = -\int_{S_p} P_{ik}(\mathbf{y})n_k(\mathbf{y})dS_y + \sum_{q\neq p} f_i^{pq} + \rho_s\nu g_i, \qquad (1.3.16)$$

where u_i^p is velocity of particle p. The first term on the RHS is the force exerted on the particle p by the fluid, f_i^{pq} is the force of interactions with other particles. ρ_s is a density of the material the particles are made of. The following averaged form may be obtained

$$\rho_s\nu\left(\frac{\partial}{\partial t}(n\langle u_i\rangle^p) + \frac{\partial}{\partial x_k}(n\langle u_i u_k\rangle^p)\right) = n\left\langle f_i^f\right\rangle^p + n\langle f_i^s\rangle^p + \rho_s\nu n g_i. \qquad (1.3.17)$$

The first term on the RHS represents interactions of particle phase with fluid, the next two are internal stress in the solids phase and the influence of body forces. Please note, what is the right meaning of this quantities: they are forces acting locally on the solids phase per total volume of the system.

The term

$$-n\left\langle f_i^f\right\rangle^p = \sum_p g(\|\mathbf{x}-\mathbf{x}^p\|)\int_{S_p}(P_{ik})(\mathbf{y})n_k(\mathbf{y})dS_y \qquad (1.3.18)$$

in not equal to the third term, denote it $\Im$, on the RHS of (1.3.15), but the following expansion with a/L as a small parameter is possible

$$\Im = n\left\langle f_i^f\right\rangle^p - \frac{\partial}{\partial x_j}\left(n\left\langle s_{ij}^f\right\rangle^p\right) + \frac{1}{2}\frac{\partial^2}{\partial x_j\partial x_m}\left(n\left\langle s_{ijm}^f\right\rangle^p\right) + \ldots, \qquad (1.3.19)$$

where

$$n\left\langle s_{ij}^f\right\rangle^p(\mathbf{x}) = a\sum_p g(\|\mathbf{x}-\mathbf{x}^p\|)\int_{S_p} t_i n_j dS, \qquad (1.3.20\text{a})$$

$$n\left\langle s_{ijm}^f\right\rangle^p(\mathbf{x}) = a^2\sum_p g(\|\mathbf{x}-\mathbf{x}^p\|)\int_{S_p} t_i n_j n_m dS, \text{ etc.,} \qquad (1.3.20\text{b})$$

and we put $\mathbf{t} = -\mathbf{n}\cdot\overleftrightarrow{P}$.

Using above expressions we arrive with averaged fluid-phase momentum balance

$$\rho_f \left(\frac{\partial}{\partial t} (\epsilon \langle u_i \rangle^f) + \frac{\partial}{\partial x_k} (\epsilon \langle u_i u_k \rangle^f) \right) = -\frac{\partial}{\partial x_k} (\epsilon \langle P_{ik} \rangle^f) + \rho_f \epsilon g_i$$
$$- n \left\langle f_i^f \right\rangle^p + \frac{\partial}{\partial x_j} \left(n \left\langle s_{ij}^f \right\rangle^p \right) - \frac{1}{2} \frac{\partial^2}{\partial x_j \partial x_m} \left(n \left\langle s_{ijm}^f \right\rangle^p \right). \qquad (1.3.21)$$

Let me stop here for a while. We are trying to build a macroscopic formulation of multiphase flow, resembling, as much as possible, single phase hydrodynamics. The quantities like n, ϵ, $\langle \mathbf{u} \rangle^f$ or $\langle \mathbf{u} \rangle^p$ may be easily identified as observables; the latter two are for example macroscopic velocities of fluid and solids phase respectively. Unfortunately we are not done yet, since not all quantities appearing in (1.3.17) and (1.3.21) have no straightforward macroscopic interpretation (e.g. $\langle u_i u_k \rangle^f$) and our equations must be supplemented with suitable *closure relations*.

1.3.3 Closure problem

First we need to know how to deal with terms like $\langle u_i u_k \rangle^f$. Jackson in [51] argues that they factorize, i.e.

$$\langle u_i u_k \rangle^f = \langle u_i \rangle^f \langle u_k \rangle^f \qquad (1.3.22a)$$
$$\langle u_i u_k \rangle^p = \langle u_i \rangle^p \langle u_k \rangle^p, \qquad (1.3.22b)$$

providing the motion of particles is *locally* Stokesian, i.e. particles move not too fast with respect to surrounding fluid. This assumption is probably very reasonable and as a matter of fact I utilize it throughout the whole work. Please note that it does not mean that the movement of the mixture with respect to the walls of the container must be laminar phases may move in rapid and turbulent manner, but their *relative* motion is usually slow.

There are other quantities we must be able to express

- $\langle P_{ij} \rangle^f$ – the average fluid stress tensor.

- $n \langle f_i^s \rangle^p$ – internal stress in the solids phase. Many researchers postulate it to have just simple Newtonian form. We will discuss this approximation briefly in the end of this chapter.

- $n \left\langle f_i^f \right\rangle^p$, defined by (1.3.18) – the momentum transfer between solids and fluid phase per unit time, per unit volume of the system.

- terms (1.3.20a) and (1.3.20b) may be adopted for example from [67].

1.3.4 Governing equations

I am able now to give the governing equations (1.3.17) & (1.3.21) in the form that is used in the modern theory of chemical reactors (for example [91] or [50])

$$\frac{\partial \epsilon}{\partial t} + \nabla \cdot (\epsilon \mathbf{u}) = 0 \qquad \text{(continuity eq. for fluid)} \qquad (1.3.23a)$$

$$\frac{\partial}{\partial t}(1 - \epsilon) + \nabla \cdot ((1 - \epsilon)\mathbf{v}) = 0 \qquad \text{(continuity eq. for solids)} \qquad (1.3.23b)$$

$$\rho_f \epsilon \left(\frac{\partial}{\partial t} + \mathbf{u} \cdot \nabla \right) \mathbf{u} = \epsilon \nabla \cdot \mathcal{F} - \mathbf{F} + \epsilon \rho_f \mathbf{g} \quad \text{(momentum balance eq. for fluid)}$$

$$(1.3.23c)$$

$$\rho_s(1 - \epsilon) \left(\frac{\partial}{\partial t} + \mathbf{v} \cdot \nabla \right) \mathbf{v} = \qquad \text{(momentum balance eq. for solids)}$$

$$= \nabla \cdot \mathcal{S} + (1 - \epsilon)\nabla \cdot \mathcal{F} + \mathbf{F} + (1 - \epsilon)\rho_s \mathbf{g}. \qquad (1.3.23d)$$

$\mathbf{u}$ and $\mathbf{v}$ are the average velocities of fluid and solids respectively, $\mathbf{F}$ denotes the force of interaction between fluid and solids phase per unit volume of the system with excluded buoyancy of the particles, $(1 - \epsilon)\nabla \cdot \mathcal{F}$. $\mathcal{F}$ and $\mathcal{S}$ are effective internal stress tensors for fluid and solids phases. They read

$$\mathcal{F}_{ij} = -p_{ij}^f + \mu_b^f(\epsilon)\delta_{ij}\nabla \cdot \mathbf{u} + \mu^f(\epsilon) \left(\frac{\partial u_i}{\partial x_j} + \frac{\partial u_j}{\partial x_i} - \frac{2}{3}\delta_{ij}\nabla \cdot \mathbf{u} \right), \qquad (1.3.24a)$$

$$\mathcal{S}_{ij} = -p_{ij}^s + \mu_b^s(\epsilon)\delta_{ij}\nabla \cdot \mathbf{v} + \mu^s(\epsilon) \left(\frac{\partial v_i}{\partial x_j} + \frac{\partial v_j}{\partial x_i} - \frac{2}{3}\delta_{ij}\nabla \cdot \mathbf{v} \right). \qquad (1.3.24b)$$

Effective viscosities may be obtained from kinetic theory and/or from experiment. The first analytical prediction of this quantity is due to Albert Einstein, [26]

$$\mu^f(\epsilon) = \mu \left(1 + \frac{5}{2}(1 - \epsilon) \right). \qquad (1.3.25)$$

The equations must be supplemented with energy balance equation if heat transport or dissipation is involved in the problem. Energy transport phenomena do not affect my future work.

I can formulate now the major goal of this thesis. I would like to concentrate on the calculations of the value of force $\mathbf{F}$. In the next chapter I will present experimental investigations of $\mathbf{F}$, which will give me a chance to discuss some of its basic properties. This quantity is crucial for the simulations of any multiphase system and the particular choice of its form affects the results much stronger than for example expressions for effective viscosities ([91]).

1.4 Some remarks upon granular gases

Although it is assumed that internal stress tensor for solids phase may have Newtonian form (1.3.24b) with effective parameters, we must keep in mind that the dynamics of such systems is generally much richer (see for example [71]). The typical example of granular material is sand: it can be regarded as a approximately Newtonian fluid only under special circumstances, for example when it is carried by water or air (as in the case of sand storm); this state is called *fluidized state*. The sand lying on the beach is *defluidized* and we know that it expresses completely different behavior: it can resist applied stress and form solid-like structures (cones, prisms, dunes, etc.), even when it is not glued by water.

Many of these properties can be understood on the molecular level in the contrast with the assumptions made upon derivation of Navier-Stokes equation in Section 1.1:

- Knudsen number $\mathfrak{Kn}$ is not small for usual granular gases: the "molecules" are much larger (typically we work with grain sizes of order hundreds of microns) than atoms and they move much slower. Chapman-Enskog method cannot be used.

- For the majority of the granular gases binary collision model is not valid – many body corrections become important especially for large ρ. Moreover due to irregular shapes of the grains collision cannot be usually described by a single collision parameter.

- Granular materials posses *memory* ([55]); especially the transitions packed-fluidized-defluidized.

- Collisions between particles are usually connected with the *dissipation* of energy. This is one the most important features: fluidization requires constant supply of kinetic energy. If we stop it, granular gas will cool and reach defluidized state after a time required for a few collisions per particle.

Chapter 2

The drag – the state of art

In the previous chapter I defined the quantity of my main interest, namely the momentum transfer between solids and fluid phase per unit time, per unit volume of the system, (1.3.18). In this chapter I describe, what has been already found about this quantity and as such the the goal of the chapter is two-fold. On one hand extensive literature is presented, and on the other I build a framework in which the future work will be rooted. Especially I introduce the notion of interphase drag coefficient, β, and list its major properties.

The real structure of drag is immensely complicated, even for a single particle in the unbound fluid, which may be considered as a limiting case $\epsilon = 1$; the force can be decomposed into several parts, which have been discovered independently. Fortunately the major contributions can be pointed out, even when their actual calculations are (almost) impossible. The discussion of forces acting on a single sphere (Section 2.1) is followed by the description of changes we observe when the concentration of bodies becomes significant (Section 2.2). Most of our knowledge comes from some kind of experiments and serious part of this chapter pertains to them; they help us to gain some qualitative insight into drag force but also provide us with numbers. Since β is never measured directly I describe in details, how to obtain it from data available. At the present moment we do not have any other reliable closure relations except the empirical laws mentioned. Their applicability is discussed. This is done in Section 2.3. Section 2.4 presents Batchelor treatment of the problem – the only existing analytic calculations based on direct attack on Navier-Stokes equation for the problem.

It should be noted that the phases may be coupled not only via momentum exchange, but also due to mass and energy transfer. These two latter mechanisms stay close to the heart of every chemical engineer, since they encompass such phenomena as evaporation, condensation and chemical reactions (examples of mass coupling) and radiation, convection and internal heating (energy coupling), but I do not deal with them in my thesis, concentrating on the drag.

Multiphase hydrodynamics is nowadays the separate branch of science with its own journals and textbooks devoted exclusively to it: [38] concentrates on applications in chemical engineering, [19] presents wider and a bit more formal view. Comprehensive

review of theoretical foundations of computational fluid dynamics for multiphase flows is given in [91], which was partially an inspiration for this chapter.

2.1 A body in the unbound fluid

A standard taxonomy of forces (as given for example in [19]) marks out the following families: *buoyancy*, *steady* and *unsteady motion forces* and different kinds of *lifts*. Buoyancy for a single body reduces usually to well known *Archimedes law*. Steady state forces act on a body when there are neither variations in static pressure field nor relative acceleration between the particle and the conveying fluid: they are *drag* or *Stokes force* and *Faxen force*. The following forces are counted into unsteady state interactions: *virtual mass effect* (discussed in Section 1.2.1) and *Basset force*. Finally lift occurs due to rotation of the particles. In the end of the section I briefly discuss other effects.

2.1.1 Steady state forces

Drag force for the general flow

Drag occurs due to viscosity and is usually given in the following form

$$\mathbf{F}_D = C_D \frac{\rho u^2}{2} A \hat{\mathbf{u}}, \tag{2.1.1}$$

where C_D is a dimensionless *drag coefficient*, A denotes an area of the cross section perpendicular to the flow, ρ is the density of the fluid, and $\hat{\mathbf{u}}$ is a velocity of the fluid in infinity in the rest frame of the body. For spheres $A = \pi D^2/4$, where D is the diameter.

We have already examined the low Reynolds number regime for this problem in Section 1.2.1. For this case the drag coefficient is given by

$$C_D \left(\mathfrak{Re} \right) = \frac{24}{\mathfrak{Re}}, \quad \mathfrak{Re} \ll 1. \tag{2.1.2}$$

The things start to complicate when $\mathfrak{Re}$ cannot be considered as a small quantity. The first corrections to C_D can be calculated exactly and are given by (1.2.41), but the approximation breaks down for $\mathfrak{Re} \approx 1.0$ and therefore researchers have to use expressions extracted from experimental data. A stunning review of available expressions can be found in [57]; the following taken from [20] seems to combine accuracy and simplicity and it is called Dalla Valle formula

$$C_D \left(\mathfrak{Re} \right) = \left(0.63 + \frac{4.8}{\mathfrak{Re}} \right)^2, \quad \mathfrak{Re} \le \mathfrak{Re}_c, \tag{2.1.3}$$

where $\mathfrak{Re}_c$ is the *critical Reynolds number*. In the so called *inertial range* $750 \le \mathfrak{Re} \le 3.5 \times 10^5 = \mathfrak{Re}_c$

$$D_D \approx 0.44; \tag{2.1.4}$$

it is also known as *Newton's law*. Beyond $\mathfrak{Re}_c$, C_D drops abruptly below 0.1. (2.1.2), (1.2.41) and (2.1.3) were compared for small $\mathfrak{Re}$ in the Figure 2.1a. 2.1b covers broader $\mathfrak{Re}$ regime.

Faxen force

Faxen force arises when the unperturbed flow (the flow existing before the body had been introduced) posses inhomogeneities and for a sphere with a small diameter D reads ([44])

$$\mathbf{F}_F = \mu\pi\frac{D^2}{2}\nabla^2\mathbf{u}.\qquad(2.1.5)$$

The Laplacian is evaluated at the center of the sphere.

2.1.2   Memory effects

Unsteady state forces may be regarded as memory effects, since they depend on the history of the flow. In a local system moving with the fluid all small perturbations are just sound waves, which we know to propagate with the finite velocity c given by (1.1.12). I have already presented the virtual mass effect, which accounts for the relative acceleration.

Basset force

Basset force is connected with the viscous effects and addresses the temporal delay in the boundary layer development as the relative velocity changes in time ([19])

$$\mathbf{F}_B = \frac{3}{2}D^2\sqrt{\pi\rho_f\mu}\int_0^t\frac{\dot{\mathbf{u}} - \dot{\mathbf{v}}}{t - \tau}d\tau.\qquad(2.1.6)$$

$\mathbf{u}$ is the fluid velocity, $\mathbf{v}$ is the particle velocity and $\dot{\mathbf{u}}$ should be understood as material derivative, $(\partial_t + \mathbf{u}\cdot\nabla)\mathbf{u}$.

[46] gives the conditions for which the memory effects may be discarded. They are

$$\rho_f/\rho_s \sim 10^{-3}\qquad(2.1.7a)$$

$$D\sqrt{\mu/\rho_f\omega} > 6,\qquad(2.1.7b)$$

where ω is the characteristic frequency of the stream oscillations.

2.1.3   Lift

The most important lift force is Magnus force, which appears when the particle (sphere) with linear velocity $\mathbf{v}$ and angular velocity ω is immersed in the fluid with the velocity
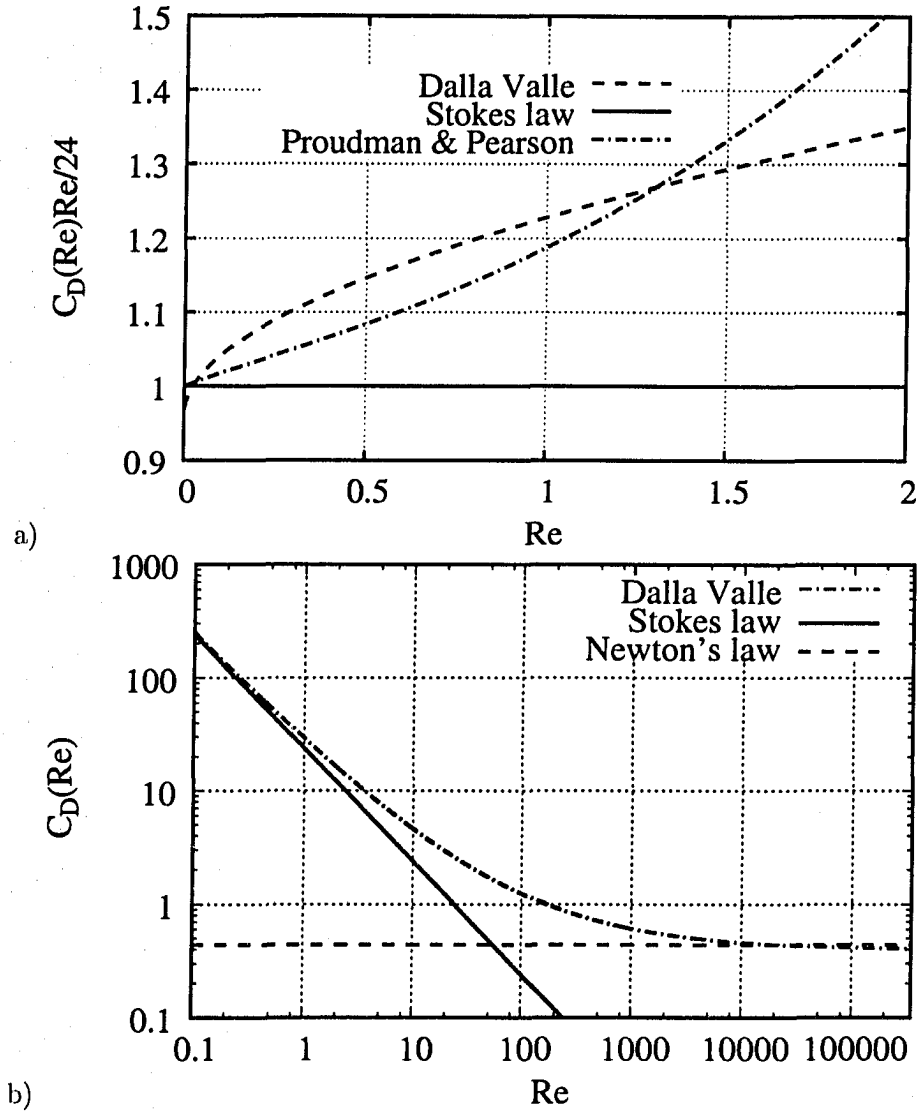
Figure 2.1: Drag coefficients as a function of Reynolds number $\Re e$. Panel a) presents respectively (2.1.3), (2.1.2) and (1.2.41) (rescaled). Panel b): (2.1.3), (2.1.2) and Newton's law (see page 26).

u ($\Re\mathfrak{e} \lesssim 1$):

$$\mathbf{F}_{\mathrm{M}} = \frac{\pi}{8} D^3 \rho \left(\left(\frac{1}{2} \nabla \times \mathbf{u} - \omega \right) \times (\mathbf{u} - \mathbf{v}) \right). \tag{2.1.8}$$

This force is present even in the nonviscous flows and can be understood as a simple consequence if of *Bernoulli law*. Due to rotation different sides of the sphere have different relative velocities with respect to the fluid and hence feel different dynamic pressures. Exactly the same mechanism is responsible for the lift force holding airplanes: their characteristic profile makes the air flow faster above the wing.

2.1.4 Other effects

First of all we have to have a method for dealing with nonsphericity of our bodies. We introduce the *shape factor* ([19])

$$\Psi = \frac{A_s}{A}, \tag{2.1.9}$$

where A is the surface area of the body and

$$A_s = \pi^{1/3} (6V)^{2/3} \tag{2.1.10}$$

is the surface area of the sphere having the same volume V as the investigated body. Since ancient Greek times we know that $\Psi \leq 1$.

It is believed that we can use (2.1.1) to calculate the force acting on the non-spherical body with C_D substituted by *effective drag coefficient* C_{Deff} and with the use of *effective diameter* D_{eff}, defined as

$$D_{\mathrm{eff}} = \left(\frac{6V}{\pi} \right)^{1/3}. \tag{2.1.11}$$

This is a diameter of a sphere with the same volume V as the body. C_{Deff} is a function of $\Re\mathfrak{e}$ and Ψ only. This approximation is widely accepted although it does not work well for oblate spheroids and cylinders.

Throughout the work it is assumed that bodies interact with the fluid by purely hydrodynamical means. We discard therefore the effects like *Brownian motion*, polarization of the fluid (which may lead to change in its viscosity) due to charges on the particles surface, etc.

2.2 Collection of particles

We could be tempted to think that the total force acting on the particle phase might be calculated as follows: each particle produces a flow disturbance (under special circumstances described given for example by (1.2.39)), which then are simply added; based on this velocity field we calculate the forces acting and sum them up. This approach

cannot give the right answer, moreover it leads to severe divergence. The first fact can be understood if we realize that the additional flow field introduced by the body must fulfill the non-slip boundary conditions on the surface of each other sphere: the bodies therefore "know" about themselves – they interact via the surrounding fluid. The divergence may be understood if we recall that Stokes velocity field, given by (1.2.31), vanishes like r^{-1}; any direct summation method bears the same pathologies as Coulomb field: to some extent the bodies in the real flow screen each other. I will be able to put this observations on a bit more quantitative footing at the end of this chapter; the next two sections deal with the experimental picture.

Let it be noted that the we have already excluded the buoyancy $(1 - \epsilon)\nabla \cdot \mathcal{F}$ from the general interaction in (1.3.23c) & (1.3.23d).

2.2.1   Interphase momentum transfer coefficient β

The experimental evidence makes chemical engineers believe that the force $\mathbf{F}$ appearing in the equations (1.3.23c) & (1.3.23d) can be written, following (2.1.1) as

$$\mathbf{F} = -\beta \mathbf{u}_r, \qquad\qquad (2.2.1)$$

where $\mathbf{u}_r = \mathbf{v} - \mathbf{u}$ is the velocity of solids phase in the (local) rest frame of fluid (we are using notation of the Section 1.3.4). β is so called *interphase momentum transfer coefficient*. This clearly indicates that the viscous forces (generalization of Stokes law) are the most important contribution to the interactions between phases. In general β could be a tensor, i.e. the drag not need to be a parallel to the relative velocity and we might ask why should not we include the generalizations of the other interactions described in the previous section (like [50], which adds virtual mass effect). The answer to this objections is two-fold. First, these phenomena are not observed experimentally (however it must be kept in mind that the experiments do not measure β directly and the effects mentioned would appear only as some kind of corrections). Second, it seems that the model (2.2.1) works in most applications, therefore capturing the essence of the underlying physics.

The average value of force acting on the particle in the cloud may be written as

$$F_1 = C_{D\text{eff}} \frac{\rho u_r^2}{2} \frac{\pi D^2}{4}, \qquad\qquad (2.2.2)$$

where D is a effective average diameter, as defined by (2.1.11) and $C_{D\text{eff}}$ is the effective drag coefficient – effective due to the shape, the presence of other bodies and the averaging procedure.

The interaction force $\mathbf{F}$ has according to this definition a value

$$F = nF_1, \qquad\qquad (2.2.3)$$

where n is defined by (1.3.7) and can be calculated from (1.3.8) as

$$n = \frac{1 - \epsilon}{\pi D^2/6},$$

(2.2.4)

yielding (we used (2.2.1))

$$\beta = \frac{3}{4} C_{D\text{eff}} \frac{(1 - \epsilon)\, \rho u_r}{D}.$$

(2.2.5)

We may reduce formally our problem to finding $C_{D\text{eff}}$. Let us list the factors that influence it

- Reynolds number $\mathfrak{Re}_r$ based on velocity u_r

- geometry of the system, which determines ϵ

- particles' shape and orientation, which to some extent may be described by the parameter Ψ

- roughness of the particles' surfaces

- distribution of the above parameters (the bodies not necessarily need to be identical)

- presence of walls and macroscopic geometry of the flow.

Let me discuss some of them. In the experimental work that I am going to present, the researchers were able to correlate data obtained, assuming some simplifications. It appears that for disordered systems the impact of detailed geometry, particle shapes and orientations may be included by simple dependence on ϵ. This is clearly a crude approximation, but seems to work. In general geometry is of a great importance and I will show it. I have not given any discussion of roughness factor, but there are empirical methods to include it in $C_{D\text{eff}}$. The presence of walls is usually neglected, which is justified for large containers.

Wide distribution of particles parameters (especially sizes) present however an important issue, since it leads to the several phenomena observed experimentally, especially *segregation* particles with different parameters tend to gather together, forming layers. It has extremely important industrial applications. The only successful approach to model this behavior was an introduction of more than one solids phase, each characterized by different set of effective parameters, and treating them independently (please refer to [86]).

2.3   Experimental methods for the estimation of β

The basic geometry for any experimental setup is quasi 1D *column*, as presented in the Figure 2.2, and there are in general three possible types of experiments that may be performed
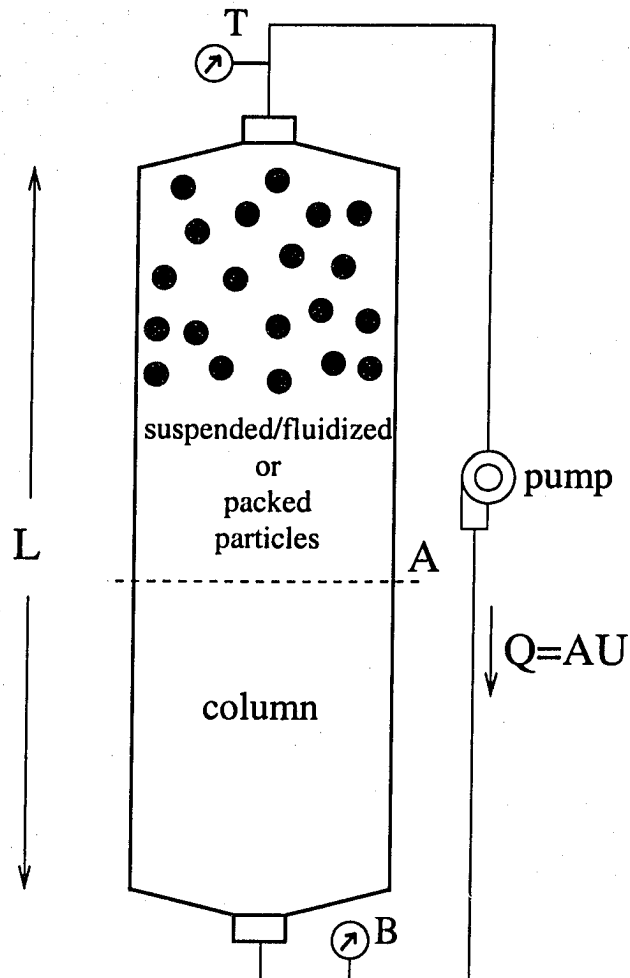
Figure 2.2: Basic geometry for a typical experiment involving interphase friction. The column is filled with a fluid, which may be forced by the pump to flow with the rate Q. The pressure drop is measured using a pair of manometers B and T, placed at the inlet and outlet of the column. When the orientation of the column is vertical it is possible to either observe fluidization $(Q \neq 0)$ or settling of the particles $(Q = 0)$. Duct may have horizontal direction, then the gravity is unimportant, and we may perform pressure drop measurements for packed column. The area of an empty cross section of the column is A and the superficial velocity is U.

1. **fluidization**: a cloud of particles is placed in the stream of fluid which suspends it. Depending on the velocity of fluidization gas u_r, the steady state in the column is reached for different value of ϵ. The process is in general very complicated and I will have a chance to return to it. Such a system is sometimes called *fluidized bed*.

2. **settling**: a cloud of particles with the specified ϵ is settling under the gravity force with some average velocity.

3. **pressure drop measurement**: the column may be *packed* with the material (i.e. the particles are immobilized by some means). We force the fluid to flow through such porous medium and the pressure drop is measured. To eliminate the influence of gravity usually the column has horizontal direction (and we would rather call it simply a pipe).

Please note first, that in all these cases the system is assumed to be macroscopically uniform. Second, the fluidization and settling are exactly the same phenomena, but observed from the different inertial reference frames. The distinction was made because of the way how the experiment is actually performed: for the case of fluidization we set the velocity and observe ϵ, but for settling the cloud of particles with the given ϵ is prepared and its velocity is measured.

The area of an empty cross-section of the column is denoted by A (and we assume it is constant). The volume of the fluid flowing through the column per unit time (*volumetric flow rate*) is denoted by Q and

$$Q = AU, \tag{2.3.1}$$

where U is so called *superficial velocity*, i.e. velocity of the fluid measured in the empty part of the column. If the solids are motionless with respect to the column, the relative velocity u_r between phases reads approximately

$$u_r = \frac{U}{\epsilon}. \tag{2.3.2}$$

If during the sedimentation the phases reach the equilibrium state (given by ϵ) with the relative velocity u_r, U is the velocity of sedimenting particles with respect to the column walls; the downward flow of the particles must be accompanied by the upward flux of fluid. It can be understood if we perform the following thought experiment. Fluidization and settling are exactly the same phenomena, if they occur for the same void volume ϵ, but simply seen from the two different reference frames; the relative velocity u_r between the phases is the same in both cases. Let us imagine that we observe settling particles standing on the floor of our laboratory, this is the column's wall coordinate system. The velocity of the fluid in the empty part of the column is obviously 0. Now let us move to the reference frame, where solids are motionless (we are observing fluidization). The gas in the region taken partially by solids has velocity u_r, therefore the velocity of the gas in the empty column region is U with respect to the particles. But by performing

simple Galilean velocity transformation we see that this velocity must be equal to the velocity of particles in the column stationary frame.

2.3.1   Fluidization and settling

Now, I will investigate the problem more quantitatively. Let us rewrite (1.3.23d) for the 1D case of flow along z axis, which points opposite to the gravity acceleration $\mathbf{g}$

$$\rho_s (1 - \epsilon) \left(\frac{\partial v}{\partial t} + v \frac{\partial v}{\partial z} \right) = - (1 - \epsilon) \rho_s g + f - (1 - \epsilon) \frac{\partial p}{\partial z}, \qquad (2.3.3)$$

where v denotes velocity of solids, p is the hydrostatic pressure in the fluid phase and f is the force acting on solids (due to internal stress in the solids phase and interactions both with the fluid and external objects) per unit volume of the whole system, excluding fluid hydrostatic pressure gradient influence. Exactly the same equation is derived in [93] from the first principles.

For steady and spatially uniform flow of solids the RHS of equation (2.3.3) is zero and therefore

$$f = (1 - \epsilon) \left(\rho_s g + \frac{\partial p}{\partial z} \right). \qquad (2.3.4)$$

When the particles are fluidized or they are settling, dynamic parts of the stress tensors (1.3.24a) & (1.3.24b) vanish, moreover, since the particles are fully supported by the fluid, their internal hydrostatic pressure may be neglected and the force f reads just

$$f = F = -\beta u_r, \qquad (2.3.5)$$

according to (2.2.1).

Usually the experimental data is presented as a dependence of *terminal velocity correlation* V_t on the set of dimensionless parameters characterizing the system. V_t is itself dimensionless and defined by

$$V_t = \frac{v_t}{v_{t0}}, \qquad (2.3.6)$$

where v_t is the terminal velocity of the group of particles and v_{t0} is the terminal velocity of a single sphere in the unbound fluid. Both of these quantities are measured in the fluid stationary frame.

For a single body, falling in the unbound fluid under terminal conditions, the drag force F_{Dt0} equals

$$F_{Dt0} = C_D(\Re_{t0}) \frac{\rho v_{t0}^2}{2} \frac{\pi D^2}{4} = \nu(\rho_s - \rho)g, \qquad (2.3.7)$$

where ν denotes particle volume and $\Re_{t0}$ is the Reynolds number based on v_{t0}. For the

particle in the cloud the terminal drag force F_{Dt} can be written according to (2.3.4) as

$$F_{Dt} = \nu \left(\rho_s g + \frac{\partial p}{\partial z} \right). \tag{2.3.8}$$

We require the mixture to be in the equilibrium, which yields the following expression for the pressure gradient

$$\frac{\partial p}{\partial z} = -g \left((1 - \epsilon) \rho_s + \epsilon \rho \right). \tag{2.3.9}$$

Combining the three previous equations we obtain

$$F_{Dt} = \nu(\rho_s - \rho) g \epsilon = F_{Dt0} \epsilon. \tag{2.3.10}$$

We can use this knowledge to compute C_{Deff} and subsequently β using (2.2.5), but first we must have closed expression for V_t.

2.3.2 Terminal velocity correlations

The classical reference is [74], where Richardson and Zaki, having performed set of original measurements and using available data, found that V_t may be expressed as follows

$$V_t = \epsilon^n, \tag{2.3.11}$$

where n, called *Richardson-Zaki* exponent, is a function of $\Re$ and ϵ. Unfortunately from their work n may be found only numerically and therefore a convenient correlation of n cried out to be created; the quest was fulfilled by Rowe in [76]

$$\frac{4.7 - n}{n - 2.35} = 0.175 \Re_t^{0.75}, \tag{2.3.12}$$

and $\Re_t$ pertains to the sphere moving with velocity v_t.

Another empirical correlation was found by Garside and Al-Dibouni and given in [35]

$$\frac{V_t - A}{B - V_t} = C \Re_{t0}, \tag{2.3.13}$$

with

$$A = \epsilon^{4.14}$$
$$B = \begin{cases} 0.8 \epsilon^{1.28} & (\epsilon \leq 0.85) \\ \epsilon^{2.65} & (\epsilon > 0.85) \end{cases}$$
$$C = 0.06. \tag{2.3.14}$$

2.3.3   Di Felice approach

Di Felice [22] found that satisfactory agreement with the experiment can be achieved by assuming that the drag force F_D acting on the particle in suspension is equal to the force acting on the sphere in the unbound fluid F_{D0} *multiplied* by a function $g(\epsilon, \mathfrak{Re})$

$$F_D = F_{D0} g(\epsilon, \mathfrak{Re}), \qquad (2.3.15)$$

providing that both of the forces in the above equation are evaluated at the same value of Reynolds number.

We can now write F_{Dt} twice, once using (2.3.10) and (2.1.1) and the second time using (2.3.15)

$$F_{Dt} = C_D(\mathfrak{Re}_{t0}) \frac{\rho v_{t0}^2}{2} \frac{\pi D^2}{4} \epsilon,$$

$$F_{Dt} = C_D(\mathfrak{Re}_t) \frac{\rho v_t^2}{2} \frac{\pi D^2}{4} g(\epsilon, \mathfrak{Re}),$$

which yields (using definition (2.3.6))

$$g(\epsilon, \mathfrak{Re}) = \frac{C_D(\mathfrak{Re}_t)}{C_D(\mathfrak{Re}_{t0})} \frac{1}{V_t^2} \epsilon.   \qquad (2.3.16)$$

De Felice used Dalla Valle formula for C_D (2.1.3) and Richardson and Zaki V_r correlations aided by Rowe formula (refer to (2.3.11) and (2.3.12)) and was able to successfully correlate available experimental data, giving the following formula

$$g(\epsilon, \mathfrak{Re}) = \epsilon^{-\alpha(\mathfrak{Re})},   \qquad (2.3.17)$$

where

$$\alpha(\mathfrak{Re}) = 3.7 - 0.65 \exp\left(-\frac{(1.5 - \log_{10}(\mathfrak{Re}))^2}{2}\right).   \qquad (2.3.18)$$

Note that limiting cases of large and small Reynolds numbers are characterized by almost the same value of $\alpha \approx -3.7$. Some authors take therefore α to be independent of $\mathfrak{Re}$.

Now we can compute $C_{D\text{eff}}$

$$C_{D\text{eff}}(\mathfrak{Re}) = C_D(\mathfrak{Re}) g(\epsilon, \mathfrak{Re})   \qquad (2.3.19)$$

and therefore β using (2.2.5).

2.3.4   Syamlal formula

Group of Madhava Syamlal created software package MFIX, open source code based on FORTRAN for hydrodynamical simulations of multiphase flows. In the documentation of this project [87] a different expression for β is given, although similarly based on terminal

velocity correlations. I could not find any published derivation of this formula, but I am able to give a plausible justification to it.

Average force acting on the particle in the suspension is given by

$$F_D = C_{D\text{eff}}(\mathfrak{Re}) \frac{\rho v^2}{2} \frac{\pi D^2}{4}. \tag{2.3.20}$$

Again we can express drag force under fluidization (terminal) condition twice using (2.3.20) and (2.1.1) & (2.3.10) to get

$$C_{D\text{eff}}(\mathfrak{Re}_t) = \frac{C_D(\mathfrak{Re}_{t0})\epsilon}{V_t^2}. \tag{2.3.21}$$

$\mathfrak{Re}_{t0} = \mathfrak{Re}_t/V_t$. Using Garside-Dibouni correlations (2.3.13) with (2.3.14) we can express V_t in terms of $\mathfrak{Re}_t$ and ϵ

$$\frac{V_t - A}{B - V_t} = 0.06 \mathfrak{Re}_t/V_t, \tag{2.3.22a}$$

$$V_t = \left(A - 0.06\mathfrak{Re}_t + \sqrt{(0.06\mathfrak{Re}_t)^2 + 0.12\mathfrak{Re}_t(2B - A) + A^2}\right)/2. \tag{2.3.22b}$$

Effective drag coefficient

$$C_{D\text{eff}}(\mathfrak{Re}_t) = \frac{C_D(\mathfrak{Re}_t/V_t)\epsilon}{V_t^2}, \tag{2.3.23}$$

where C_D may be calculated using (2.1.3). Now we can say that our sphere always moves with the terminal velocity, but for example in the fluid with different viscosity, since all the quantities in the above equation are dimensionless, and drop subscript t in $\mathfrak{Re}$. Once we know $C_{D\text{eff}}$ we can calculate β by means of (2.2.5).

2.3.5   Other experiments and models

Schiller-Naumann drag

When we are only interested in qualitative results (especially for small concentrations) the interactions between bodies may be neglected and we can assume that the effective drag coefficient equals just free sphere coefficient, with empirical $\mathfrak{Re}$ correction. I have already listed one of the numerous possibilities (2.1.3). Here is another one, *Schiller-Naumann coefficient* ([79])

$$\frac{24}{\mathfrak{Re}} \left(1 + 0.15\mathfrak{Re}^{0.687}\right). \tag{2.3.24}$$

Above $\mathfrak{Re} \approx 10^3$ Newton's 0.44 law, (2.1.4), is used. This is one of the models available in FLUENT package.

Ergun equation

In 1952 Sabri Ergun [27] found an empirical correlation allowing calculation of pressure drop in the packed column, i.e. for small void volumes

$$\frac{\Delta p}{L} = 150\frac{(1-\epsilon)^2}{\epsilon^3}\frac{\mu U}{D^2} + 1.75\frac{1-\epsilon}{\epsilon^3}\frac{\rho U^2}{D}, \qquad (2.3.25)$$

where L denotes length of the column (duct), ϵ is void volume in the system, U the superficial velocity and D is the effective diameter of the particle in the column, defined as

$$\frac{\pi}{6}D^3 = \frac{(1-\epsilon)V}{N}, \qquad (2.3.26)$$

where V is the total volume of the column, AL, and N is an estimation of the number of particles in the column. Let us note that that D is just a logic construction, since the bed may be packed for example with a crushed glass and therefore has void volume lower than $\epsilon_{cp}^{3D} \approx 0.36$, associated with closed packing of spheres.

The expression has two terms: the first one pertains to viscous energy loss and is important for small values of material flow; the second quadratic term represents the dissipation due to kinetic effects.

In such a system particles are maintained in fixed position and therefore we have to be rather concerned with the force that is exerted on the fluid, which is obviously ΔpA and may be written as

$$\Delta pA = N(\nu\Delta p/L + F_D), \qquad (2.3.27)$$

where $\nu\Delta p/L$ represents the average buoyancy force acting on the particle (ν being average particle volume $\pi D^6/6$) and F_D is an average force due to hydrodynamic interactions.

Total drag force reads

$$NF_D = A\Delta p - \frac{\Delta p}{L}(1-\epsilon)V = A\epsilon\Delta p. \qquad (2.3.28)$$

The force per total volume V, divided by the magnitude of relative velocity, gives β (using (2.3.2) and (2.3.25))

$$\beta = 150\frac{(1-\epsilon)^2}{\epsilon}\frac{\mu}{D^2} + \frac{7}{4}\frac{(1-\epsilon)}{D}\rho u_r. \qquad (2.3.29)$$

For the sake of future comparison, we might compute fictitious effective drag coefficient from (2.2.5)

$$C_{Deff} = 200\frac{1-\epsilon}{\epsilon}\frac{1}{\Re e} + \frac{7}{3}. \qquad (2.3.30)$$

Wen & Yu scheme

Wen and Yu in [95] were able to correlate data obtained and found that (this expression is explicitly written in their paper, eg. (47))

$$C_{D\text{eff}}(\mathfrak{Re}, \epsilon) = \epsilon^{-4.7} D_D(\mathfrak{Re}),\tag{2.3.31}$$

but they clearly neglected the influence of pressure gradient, which would results in additional factor ϵ on the RHS of the above equation (please refere to (2.3.10)). This is in obvious agreement with (2.3.17) & (2.3.18) and it should lead to results identical up to (small) $\mathfrak{Re}$ dependence in (2.3.18).

Nevertheless for the reasons completely unclear to me hydrodynamical packages (FLUENT) use the following formula, crediting it to the article mentioned

$$\beta = \frac{3}{4} C_D \frac{(1 - \epsilon)\epsilon\rho u}{D} \epsilon^{-2.65},\tag{2.3.32}$$

where

$$C_D(\mathfrak{Re}) = \begin{cases} 24\big(1 + 0.15(\epsilon\mathfrak{Re})^{0.687}\big)/(\mathfrak{Re}\epsilon) & \epsilon\mathfrak{Re} < 1000 \\ 0.44 & \epsilon\mathfrak{Re} \geq 1000 \end{cases}\tag{2.3.33}$$

The expression for the drag coefficient resembles Schiller-Naumann drag, but with the Reynolds number based on superficial velocity. The idea comes from [75] and seems to have no justification (I believe it is simply an error or misprint).

Gidaspow approach

Gidaspow wrote an acclaimed textbook on multiphase flow and fluidization, [38], where he presents a drag model based on combination of Ergun equation (2.3.29) and (2.3.32). There is a discontinuity in his expression in the matching point, which in general may lead to numerical instabilities, as suggested in [91].

2.3.6 Comparison of the available models

According to [91] the right choice of β model is crucial in all numerical experiments, strongly affecting the results. A comparison between described expression was presented in the Figure 2.3. The plots present Di Felice modifiers defined as $C_{D\text{eff}}(\epsilon, \mathfrak{Re})/C_D(\mathfrak{Re})$, where C_D is given by (2.1.3).

The immediate conclusion is such that the models do not agree with each other too well, which indicates that a theory better than just simple data matching must be developed. Di Felice work predicts much higher value of the drag than other models and, as was mentioned earlier, is insensitive to particle Reynolds number $\mathfrak{Re}$. An agreement with other models exists only for large void volumes. Other correlations express clearer dependence on $\mathfrak{Re}$. In the intermediate regime expression (2.3.32) and that of Syamlal agree, but they differ seriously for large relative flow velocities. It may be noted that matching of expressions of Wen & Yu and Ergun always leads to mentioned earlier discontinuity and
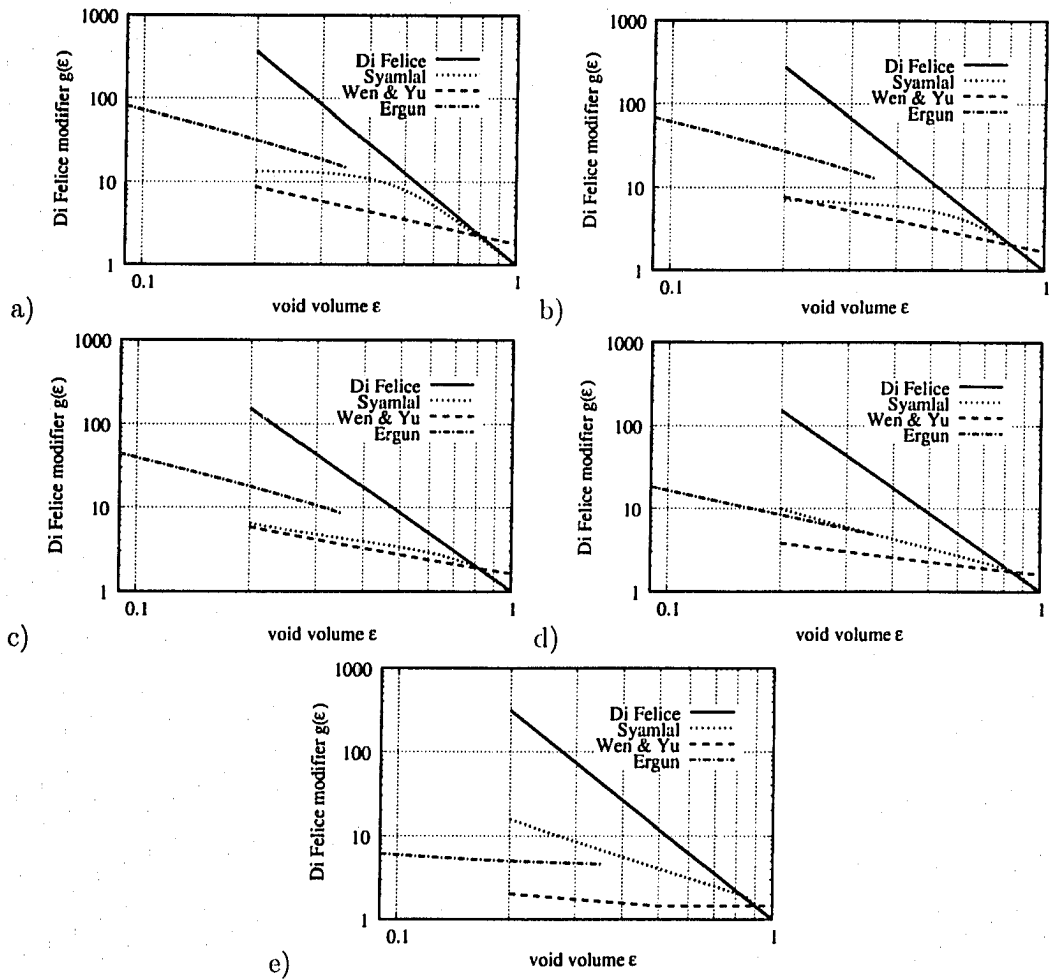
Figure 2.3: Comparison of different drag models as a function of ϵ for different $\mathfrak{Re}$. Panels a), b), c), d) and e) correspond to $\mathfrak{Re}$ = 0.1, 1, 10, 100 and 2000 respectively. Please refer to the discussion in text.

that the Syamlal model, developed for large ϵ, matches Ergun law (suitable for packed columns) much better. Finally the Wen & Yu prediction for C_{Deff} (based on (2.3.32) and (2.2.5)) does not converge to 1 while the suspension becomes infinitely dilute. This is an artifact of our comparison scheme – Schiller-Naumann coefficient (2.3.24) differs from the one due to Dalla Valle (2.1.3).

The assessment of validity of presented model is a delicate question, since we can apply different criteria to this problem. Should we choose the models that correlate the experimental data in the best way or that one, which yield the results of numerical simulations being closer to reality? It may sound paradoxical, but these two criteria do not need to be equivalent. The primary reason for that is of course the already mentioned fact that we never measure β directly in any experiment. Furthermore, often the results of the experiments must be extrapolated. For example, the procedure of extracting the value of drag from terminal velocities implies that properties of the suspensions under terminal conditions can be used also when the cloud moves with non-terminal velocity. The argument, based on dimensional analysis, sounds plausible, but we cannot assess how general it is. It is not too difficult to imagine that sand peacefully falling in the water has different properties than a cloud of dust suddenly dragged by a blast of wind.

We use the following rule of thumb in our group. Since all the reported correlations (except maybe for (2.3.32)) have at least decent justification in experimental data, the one is chosen, which yields the best agreement of numerical simulations with reality. It follows from our experience that the form of drag affects the whole picture of fluidized bed, beginning with the level of its free surface, through dynamics of eddies and ending with shape, volume, number and internal density of bubbles. It seems that the Syamlal model, (2.3.23), although still not completely free from discrepancies with experimental picture of the reactor, gives the best results. This opinion was strengthened by the interactions I had with the circle of chemical engineers working in Syncrude.

2.4 Analytical solution for small concentrations

Theoretical works devoted to flow of particulate systems concentrate around two major topic calculations of terminal velocities and effective viscosities of fluid-solids systems; the results originating from the first category, as it has already been noted, may be directly utilized to compute drag, therefore I will present shortly the literature devoted to it. These works are important from the theoretical point of view, but they cannot give the drag in the most interesting regime of high concentrations.

There were several attempts to obtain a analytic solution to a problem of the cloud of settling spheres, [81, 15, 33], none of them however was able to construct quantities that would be certain to converge. The first successful treatment is due to Batchelor, [6] and will be reported shortly.

There are also several heuristic theoretical attacks on the problem. For example [43] considers the following simplification of flow in the bed of spherical particles. Every sphere moves separately surrounded by a "fluid sphere" with a special radius. On the interface of the internal (solid) sphere no-slip boundaries conditions are imposed, on the

external surface the gradient of radial component of fluid velocity is zero. In this model the drop in the settling velocity is proportional to $\sqrt[3]{1-\epsilon}$.

2.4.1 Batchelor's treatment

A renormalization procedure introduced by Batchelor is now briefly summarized. Once again we are observing sedimentation in the container's walls reference frame. The total velocity of the arbitrarily chosen particle is written in the form

$$\mathbf{U} = \mathbf{U}_0 + \mathbf{V} + \mathbf{W}, \tag{2.4.1}$$

where the terms have the following interpretation. $\mathbf{U}_0$ is a velocity of the particle in the unbound fluid (no other particles present). $\mathbf{V}$ is the additional velocity that the particle acquires due to distortion of the velocity field caused by the other particles, but as if the non-slip conditions on the surfaces of other particles were released,

$$\mathbf{V} = \frac{1}{\pi D^2} \int_{A_0} \mathbf{u}\, dA, \tag{2.4.2}$$

with the integration performed over the surface of the particle, A_0. $\mathbf{u}$ is the local velocity in the fluid, that would exist in the absence of the chosen particle, coming from the summation of the influences of other particles; please confront the above expression with equation (1.2.40). The quantities are averages over particles' configurations' space. The configuration space should be understood here as $3N$-dimensional space (N stands for the number of particles); the points of this represent given configurations of particles. Not all points in this space might be available, since there are forbidden configurations (for example the configurations that violate hard-core distance). $\mathbf{W}$ is the already mentioned change in the velocity required to fulfill the no-slip conditions on the surfaces of the remaining solids. The danger of divergence comes in the contribution $\mathbf{V}$, since it is a sum over an infinite collection of Coulomb force centers; Batchelor avoids this catastrophe by expressing $\mathbf{V}$ in terms of converging quantities and the average velocity both in solids and fluid phase, which is known exactly to be zero. This is the renormalization procedure. Later, upon small concentration assumption, the velocity $\mathbf{W}$ is found, assuming that only *pair* interactions are important. Finally the result reads

$$\mathbf{U} = \mathbf{U}_0(1 - 6.55(1 - \epsilon)). \tag{2.4.3}$$

The profound assumption made in the cited work is that the suspension is statistically homogeneous; the averages calculated are taken over all spheres' configurations that obey the minimal interparticle distance D. First of all it means that the flow field does not influence the particles' configuration space. Second, the variation of particles' concentration takes place on the scale much larger than interparticle distance. Batchelor suggested the following shape of the pair correlation function for his collection of particles

$$g(r) = \mathbb{H}(r - D) + (1 - \epsilon)c\delta(r - D), \tag{2.4.4}$$

where $\mathbb{H}(x)$ stands for Heaviside (unit) function. The delta at the edge of excluded region represent the characteristic excess of nearly touching spheres. The matter will be discussed more fully in the Section 5.2.2. The actual calculations are performed for the constant c equal to zero.

The solution presented does not avoid the divergences completely. It appears that the variation of spheres' velocities is growing without limit for the large collection of spheres, [16]. Unfortunately this quantity is an observable, since it enters the expression for the granular temperature of solids phase. It should probably be understood as a sign, that renormalization procedure applied here is not complete.

The Batchelor solution, even though it is based on serious assumptions and still leads to unphysical results, is an important step. Partially, since it is the only analytic solution we have, but primarily, because it introduces some concepts (simplifications), that appear to be surprisingly good. I mean here the statistical homogeneity assumption (discussed above and in the introduction to Chapter 5) and the suggested shape of pair correlation function, (2.4.4). They both will be reused in future.

Chapter 3

The electric theory of friction

As I demonstrated in Chapter 2, the interphase drag force becomes significant for relatively small values of void volume ϵ (values close to the packing limit), exactly where the direct attempts to solve Navier-Stokes equation become helpless. The interaction between spheres become important and we can hardly describe the velocity field as a sum of "corrected" contributions due to particular spheres. Rather, the flow takes place in the random constrained geometry, (dynamical) porous medium. It is impossible, at the present time, to construct any exact analytic solution of Navier-Stokes equation with such boundary conditions. Traditional CFD simulations (taking advantage for example of finite volume method) appeared to be extremely expensive both by means of time required for the computations and money spent for the massive (usually parallel) supercomputers.

The first serious numerical models of flow in porous media became feasible only after Frisch and coworkers translated Navier-Stokes equation into the language of cellular automata (CA), creating famous LGA (Lattice Gas Automaton), [34]. Their main idea was to create a (seriously) simplified microdynamics, which would be easy to simulate and which in the macroscopic limit would reproduce equations describing motion of fluid, exactly in the same manner in which NS equations emerges from microscopic description given by Boltzmann transport equation. CA are fascinating for their own sake; they were invented by Stanisław Ulam and John von Neumann at Los Alamos Laboratory in the 1940's and later popularized by Stephen Wolfram in 1980's (see e.g. [96]). But even with the use of these methods the task of simulating the motion of the set of bodies in the fluid is non trivial.

Fortunately the problem of flow in the constrained geometries has already been deeply studied in the theory of soils, see e.g. [78]), and it appears that the results obtained (permeability of the materials) may be used for calculations of the friction. I became especially interested in the theory of hydraulic networks utilized by Steven Bryant, Peter King and David Mellor, [13], since their theoretical prediction for permeability as a function of void volume agreed well with the experimental data, spanning seven orders of magnitude. I decided to extended their theory and calculate the permeability (and subsequently β), for larger void volume fractions (or porosities, to use their terminology), observed in the chemical reactors.

The primary purpose of this chapter is to expose the hydraulic network method and show its connection to our problem of finding β. Since the work of Bryant and coworkers originates from the theory of porous media I start with the description of its fundamental equation, Darcy's law (Section 3.1). Additionally in that section the notions of hydraulic conductance and the permeability of porous medium are presented. I show how to use them to calculate interphase drag. Section 3.2 shows the attempts to model porous medium by means of spheres. After these introductory sections I am able to present the original works on the network model (Section 3.3). The latter section contains also the comparison of the network model and experimental data correlated by Ergun (equation (2.3.25)) and shows the excellent agreement mentioned. In Section 3.4 I present the mathematical theory of linear resistor networks. The networks have several important features that will be utilized in their analysis. The key points of the chapter are recapitulated in Section 3.5.

3.1 Darcy's law

3.1.1 Flow in the duct

From the theoretical point of view, an important geometry of flow is a duct. i.e. situation when the flow occurs in straight parallel lines, Figure 3.1. Velocity u depends on x and y and has only $\hat{z}$ component, u. In the laminar regime NS equation takes the form

$$\nabla^2 u = \frac{1}{\mu}G, \tag{3.1.1}$$

where $G = \partial_z p$ is the pressure gradient, a constant quantity.

The general solution to (3.1.1) reads

$$u = \psi + \frac{G}{4\mu}(x^2 + y^2), \tag{3.1.2}$$

where ψ is an harmonic function in 2D,

$$\nabla^2 \psi = 0, \tag{3.1.3}$$

satisfying the following boundary conditions on stationary surfaces

$$\psi = -\frac{G}{4\mu}(x^2 + y^2). \tag{3.1.4}$$

If the duct has length l and the pressure drop along it is Δp, then

$$G = -\frac{\Delta p}{l}. \tag{3.1.5}$$

The volumetric flow rate Q in a system is a measure of the volume of fluid passing a
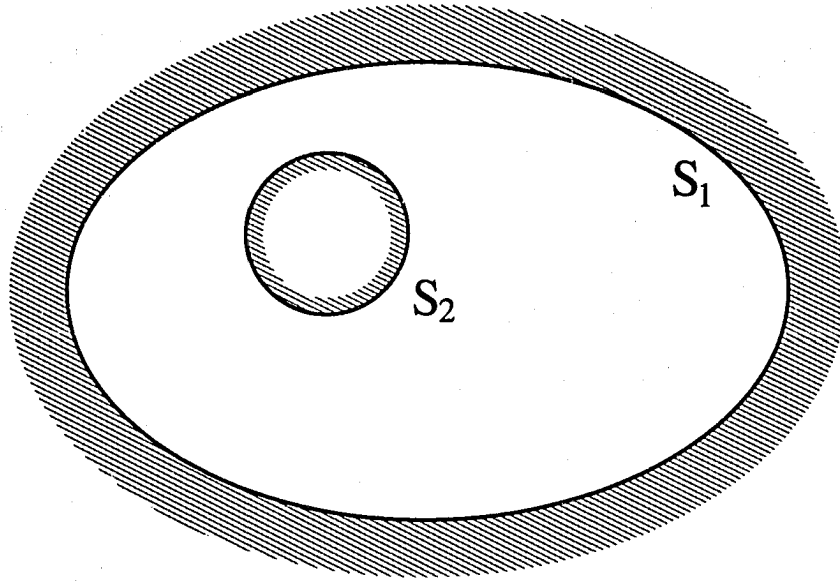
Figure 3.1: Laminar parallel flow in a duct; we are looking down the pipe, parallel to the flow. We must solve Poisson equation (3.1.1) with Dirichlet non-slip boundary conditions on external (S_1) and internal (S_2) surfaces. The picture was taken from [44].

stationary cross-section of the duct per unit time

$$Q = \int_A u(x, y) dA, \tag{3.1.6}$$

where A in an area of the cross section of the duct. In general we have

$$Q = g\Delta p, \tag{3.1.7}$$

for fixed l. This is sometimes referred to as Poiseuille law. The proportionality constant g is called *hydraulic conductance* and will be of our main interest. We can also define superficial velocity as

$$U = \frac{Q}{A}. \tag{3.1.8}$$

I will now analyze two important examples.

Hagen-Poiseuille flow

Hagen-Poiseuille flow pertains to motion of the fluid in the circular pipe of length l and radius R. If we write Laplacian in the cylindrical coordinates and discard the dependence

on φ we obtain

$$\frac{1}{r}\frac{d}{dr}\left(r\frac{du}{dr}\right) = -\frac{\Delta p}{\mu l},$$ (3.1.9)

which after straightforward integration yields

$$u = -\frac{\Delta p}{4\mu l}r^2 + a\log(r) + b.$$ (3.1.10)

Constant a must be taken to be zero to avoid singularity in the center of the tube and b can be obtained from boundary condition on the surface $r = R$, corresponding to the radius of the pipe.

The volumetric flow (cf. (3.1.6)) reads

$$Q = \frac{\pi R^4}{8\mu l}\Delta p.$$ (3.1.11)

and hence conductance for such a system can be written as

$$g = \frac{\pi R^4}{8l}\frac{1}{\mu}.$$ (3.1.12)

Let us note the strong dependence on R. Exactly this is the reason for which coronary artery disease is so dangerous: small blood vessels that supply blood (and oxygen) to the heart increase their resistance significantly when their walls become covered with a layer of fatty material and plaque.

Flow between two parallel walls

The geometry of the system was sketched in the Figure 3.2. Velocity u depends only on x.

We immediately get from (3.1.1) that

$$\frac{\partial^2 u}{\partial x^2} = \frac{G}{\mu},$$ (3.1.13)

what gives

$$u(x) = \frac{1}{2}\frac{G}{\mu}x\left(x - M\right),$$ (3.1.14)

after the boundary conditions are included. Volumetric flow is obtained by integration

$$Q = H\int u(x)dx = -\frac{1}{12}\frac{GH}{\mu}M^3,$$ (3.1.15)
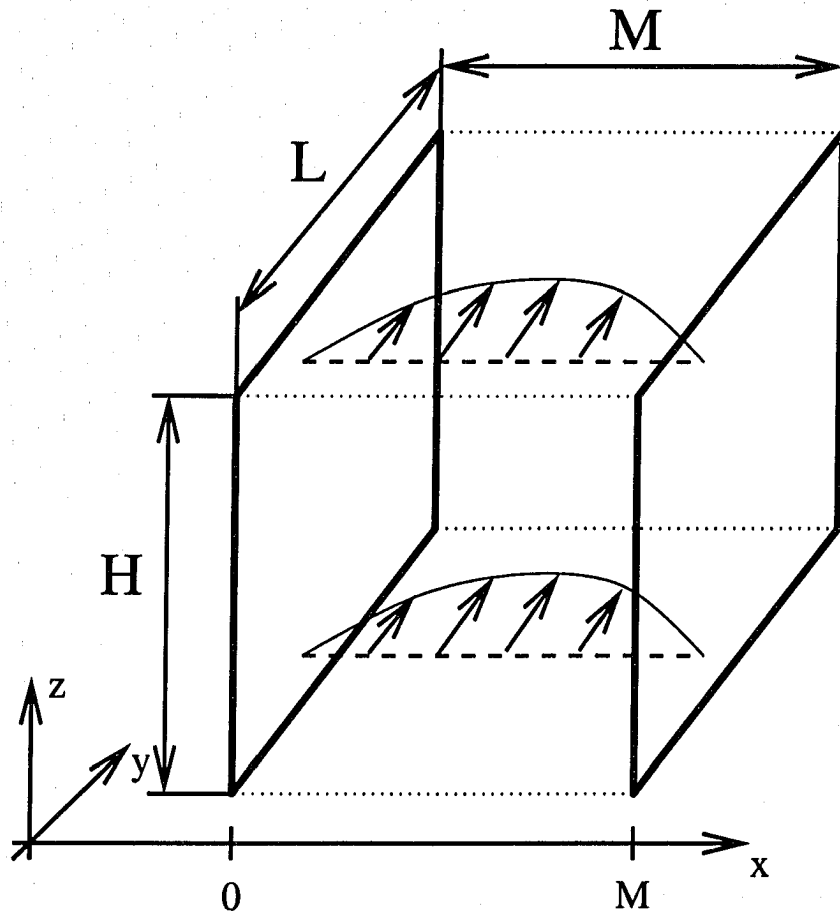
Figure 3.2: Flow between parallel walls. Discussion in the text.

yielding the following expression for the conductance of a section of height H

$$g = \frac{1}{12} \frac{HM^3}{L} \frac{1}{\mu}.$$ (3.1.16)

3.1.2 Permeability

Laminar flow in constrained geometries can be always proved to have linear flow pressure dependence. This law was first discovered by Henry Darcy in 1856 [21] and it is usually written in the following differential form for flow through fine materials (like sand)

$$\mathbf{U} = -\frac{k}{\mu} \nabla p,$$ (3.1.17)

where $\mathbf{U}$ denotes local superficial velocity, cf. equation (2.3.2). The quantity k is an intensive property of the medium called *permeability*. Such formulation again requires separation of scales, which is however natural for the case of soils. In general k may be a tensor.

Permeability describes the ability of the medium to transport fluids. In the SI system its unit is defined as:

> amount of permeability that permits $1\,m^3$ of fluid of viscosity $1\,Pa \cdot s$ to flow through a section of material $1\,m$ thick with a cross-section of $1\,m^2$ in $1\,s$ at a pressure difference of $1\,Pa$.

In fact this unit appears to be equal to m^2. SI unit it not quite handy, and in practice a unit called darcy (D) is used. Material has permeability $1D$ if

> in $1\,s$ $1\,cm^3$ of liquid with viscosity $1\,cP$ (centipoise) will flow through a section $1\,cm$ thick with cross-section $1\,cm^2$ when the pressure difference is 1 physical atmosphere.

Let us remind that $1\,cP = 1$ milipascal·second and the physical atmosphere is $101325\,Pa$.

$$1\,D = 9.869233 \cdot 10^{-13}\,m^2.$$

I will save the reader the questionable pleasure of defining units of permeability based on pound per square inch as the pressure unit.

The quantity of our interest, β, can be constructed from permeability k as follows. The pressure gradient in the material due to friction is $\epsilon \nabla p$ (please confront the presence of ϵ with (2.3.28) for example) and from the definition of β we get

$$\epsilon \nabla p = -\beta \frac{\mathbf{U}}{\epsilon},$$ (3.1.18)

hence

$$\beta = \epsilon^2 \frac{\mu}{k}.$$ (3.1.19)

Permeability may be formally computed from the knowledge of $C_{D\text{eff}}$ as follows

$$k = \frac{24}{\mathfrak{Re}} \frac{D^2}{18} \frac{\epsilon^2}{1-\epsilon} \frac{1}{C_{D\text{eff}}}.$$

(3.1.20)
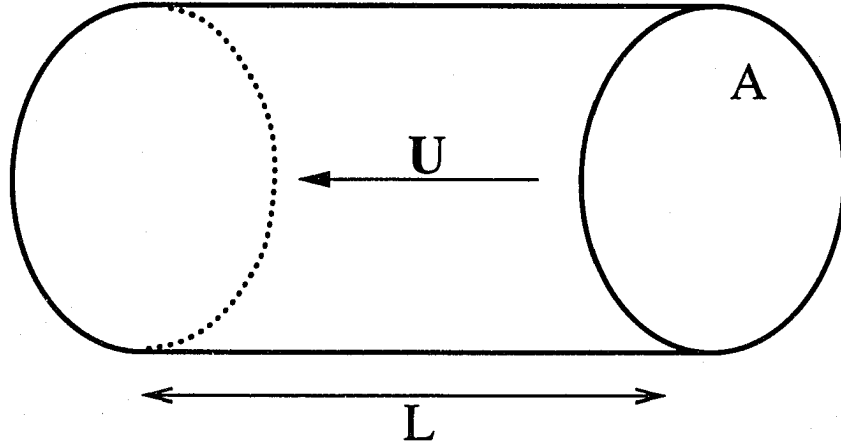
Figure 3.3: Porous medium sample.

Let us now imagine that a material of the permeability k was used to produce a cylindroidal sample, like on Figure 3.3, of the cross-section area A and length L. Such a sample has conductance

$$g = \frac{k}{\mu} \frac{A}{L}.$$

(3.1.21)

Combining (3.1.19) and (3.1.21) we get

$$\beta = \epsilon^2 \frac{A}{L} \frac{1}{g}.$$

(3.1.22)

3.2 Packing of spheres

The real soils are usually collection of irregular grains packed randomly and as such they proved to be extremely complicated to model. There are however materials (for example consolidated sandstone), which may be described roughly as a collection of (tiny) spheres. This kind of approximation was introduced in [80] and has been successfully developed up to these days. It may be therefore instructive to have a look at some work devoted to packing of spheres. The review comes partially from [94].

In 1611 Johannes Kepler hypothesized that in 3D the densest possible packing of spheres was *periodic close packing* (cp), yielding void volume $\epsilon_{cp}^{3D} = 1 - \pi/(3\sqrt{2}) \approx$ 0.25952. There are two regular Bravais lattices which form cp: face centered cubic (fcc) and hexagonal close packed (hcp). It took almost 400 years to prove this hypothesis.

Johann Carl Friedrich Gauss showed that cp is indeed the densest *periodic packing*, but the question whether there are no non-periodic packings of greater density remained open. The final proof was presented in 1998 by Hales, after a series of papers initiated by [41] – periodic cp of hard spheres is indeed the densest possible packing.

In any realistic model we must incorporate disorder and fortunately much of attention was paid to *random packings* of spheres. This term is not precisely defined ([88]), but there exist an experimental definition, namely collection of spheres vibrated upon action of gravity in the container and left in the rest. The first investigation of such a system was undertaken by Finney, who actually measured positions of 8000 spheres in random close pack ([31, 32]). His research showed serious short range correlations in the positions of spheres. The value of void volume obtained by him was $\epsilon_{rp}^{3D} \approx 0.362$, what agrees with contemporary results, [53].

It is worth noticing that the random packing of ellipsoids is denser than spheres, what was proved by direct experiment with packing 125 pounds of almond M&M's candies, [23]. The reported void volume was about 0.32, beating by 4% the spheres. After the experiment the sweets were eaten by undernourished graduate students.

3.3 Network model of permeability

The idea, that the flow in porous medium can be described as a flow in the duct (or system of ducts) is not new and has been utilized e.g. by Fatt in 1956, [29], but I am going to present here another work, [13, 10, 11]. As it was mentioned earlier, the researchers were able to predict correctly the permeability, having started from almost first principle model of porous medium.

To be more specific, they assumed that the soil may be described by a set of identical spherical particles of diameter D, placed in the positions taken from already mentioned Finney random packing. Further, they observed that the flow occurs along the well defined ducts (or throats) defined by the triads if neighboring spheres; the throats connect the tetrahedral cavities (nodes). The schematic picture of a node is presented in Figure 3.4.

If we recall now that the ducts have linear (Ohmic) flow-pressure dependence the resultant system is an analogue of a network of resistors (volumetric flow corresponds to the current and pressure is an analogue of potential). If we assign conductance g_k to each node and calculate the total network conductance g_{tot}, we will be able to obtain (providing we know the macroscopic dimensions of the sample) permeability of such a medium using (3.1.21).

There are several important issues now. First, we must reasonably identify the neighbors. Second, a suitable model of the throat must be used. Finally we have to calculate the net conductance; the latter task may be non-obvious once we deal with thousands of resistors connected in random.

The natural method of finding nearest neighbors is construction of *Voronoi diagram*. I will focus on this issue more precisely in the subsequent chapters, here I present only a brief discussion. Consider discrete set of points, so called generators, scattered in arbi-
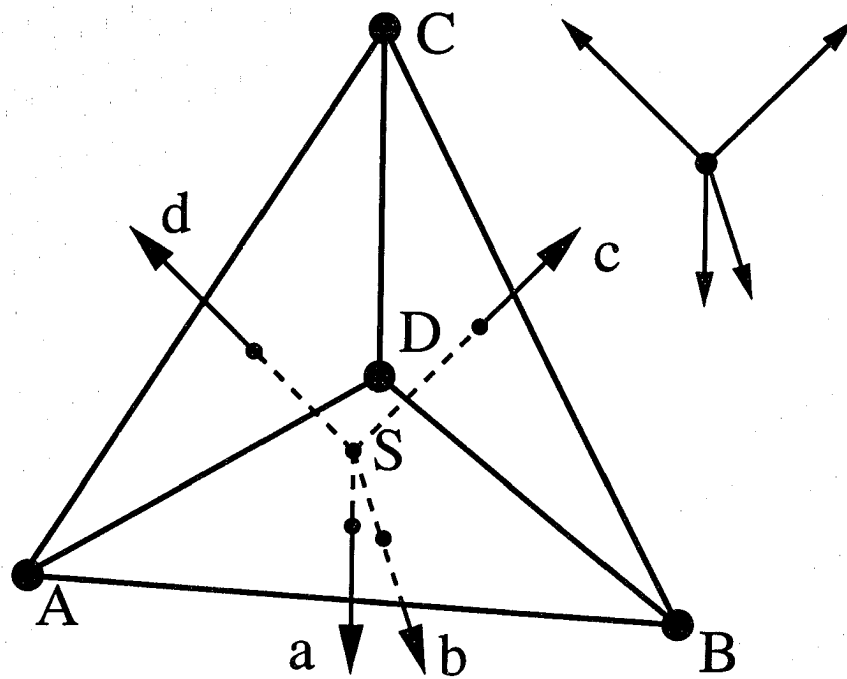
Figure 3.4: The schematic presentation of the node in the network model. A, B, C & D denote positions of the spheres. a, b, c & d represent throats' axii. All the nodes have four nearest neighbours. The center of the (irregular) tetrahedron ABCD is marked with S; S is understood as the center of the sphere circumscribed about the tetrahedron. The schema comes from [11].

trary manner in the Euclidean space Ω (of arbitrary dimensionality). For each generator G we define now *Voronoi region* as a subset of Ω, containing points which which are closer to G than to any other generator. It can be proved (see e.g. [69]) that Voronoi regions are always convex. In 3D two generators sharing the face of Voronoi region are naturally identified as nearest neighbors. In our problem the spheres' centers form the mentioned set of generators. If we connect each pair of nearest neighbors with a line we obtain so called Delaunay diagram, a set of simplexes (tetrahedra); their walls form the narrownesses of the throats, according to authors of the work mentioned. Centers of Delaunay cells are nodes of our resistor network. Each node has degree (i.e. the number of attached throats) exactly four. Schematic presentation of the node and four throats are presented in Figure 3.4.
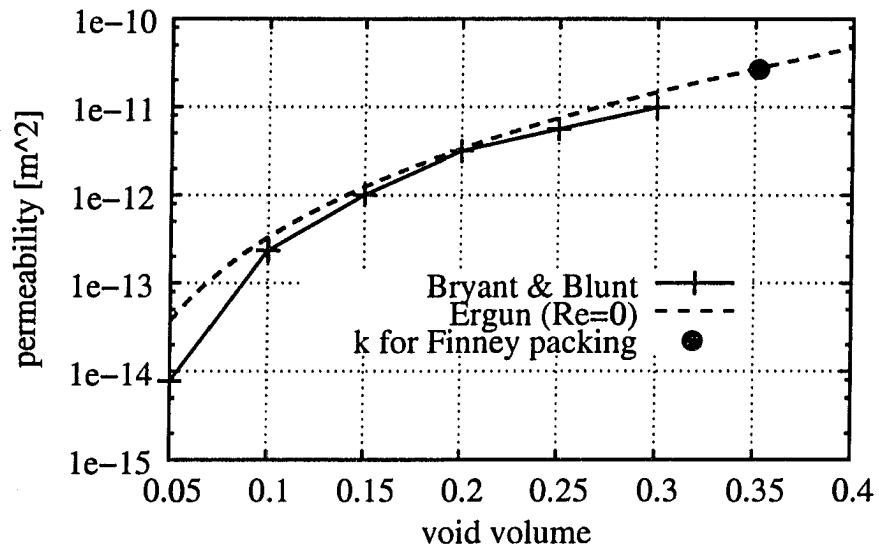
Figure 3.5: The results of Bryant and coworkers. The length scale for Finney packing was set with sphere diameter $D_0 = 0.2\,\text{mm}$, being the only experimental input. It can be seen that the theoretical prediction matches Ergun empirical formula very closely.

The following model of throat was adopted in the investigation. The duct formed by the three spheres was cut into "slices" perpendicular to the direction of the flow and each slice was regarded as conical frustum: a pipe with a radius changing linearly with distance. The resultant resistors were later connected in series. The inlet and outlet radii were calculated using carefully chosen linear dimensions of throat's slice; in general the procedure is involved and suitable only for numerical study; it was described in Appendix of [13]. The geometry of macroscopic flow was spherical: the inlet and outlet pressure was applied to two concentric spheres.

Ref. [13] reports two kinds of numerical experiments performed. First, the original topology of Finney packing was left unchanged and the whole structure was scaled: both positions of the grains and (proportionally) diameters D. This do not change the void

volume, $\epsilon \approx 0.362$. The permeability of the medium was found to be

$$k = \Gamma D^2,\tag{3.3.1}$$

where

$$\Gamma = 6.8 \cdot 10^{-4}\,\mathrm{m}^2.\tag{3.3.2}$$

The second type of experiment performed relied on the "squeezing" of the packing along one direction. The spheres started to overlap and it was assumed that the material corresponding to intersecting grains was removed from the system (in reality e.g. washed out by water). This changes the void volume and, in general, is supposed to mimic actual geological processes like cementation or grain overgrowth (in both additional material is deposited in the system by some means). It was found that some throats became completely blocked at $\epsilon = 0.1$. The percolation threshold was reached for $\epsilon = 0.03$, where 50% of the connections were closed and the permeability fell to zero.

The result of the calculations of permeability as the function of ϵ is presented in Figure 3.5. The only experimental input was an original grain diameter $D_0 = 0.2\,\mathrm{mm}$, understood as the grain size before deformation occurred (and as the original spheres' diameter used in simulation). There is an error in [10], fortunately resolved [12]: the diameter was falsely reported to be 0.4mm. Bryant compared their results to experimental data for Fontainebleau sandstone and noted perfect agreement; their model perfectly matched the effect of decreasing ϵ. For comparison a permeability obtained from Ergun formula was plotted

$$k_{\mathrm{E}} = \frac{1}{150}\frac{\epsilon^3}{(1-\epsilon)^2}D^2.\tag{3.3.3}$$

The expression was obtained from (3.1.20) and (2.3.30), in the limit $\mathfrak{Re} \to 0$. Both results are very close. Let it be noted that Ergun formula reaches permeability ΓD_0^2 exactly for the void volume found for Finney packing. Moreover we can see that the predictions easily span several orders of magnitude.

3.4 Networks of resistors

In this section I present the matrix formalism for dealing with the networks of conductances. As we have already noted, there is full analogy between electrical and hydraulic circuits in the limit of low Reynolds numbers. In this section I use electric terminology. It is assumed that all the elements express the linear (Ohmic) pressure-flow characteristic and that all the elements are passive (real), i.e. that they not not introduce current-voltage lags, or that we deal only with stationary flows. It would be straightforward to include the nonstationary effects into the formalism; non-linearity on the other hand poses a certain challenge.

There is a close connection between resistor's networks and random walks (especially

Markov chains), as suggested in Doyle and Snell monograph, [25], which contains all the result from this paragraph (and many more), although usually without proof. Abundant mathematical literature devoted to electrical networks exists, since they can be easily studied, as we shall soon see, using techniques of matrix theory (see e.g. [17] and references therein), but the formulation from this section is mine. Markov chains (and in general randoms walks) are deeply studied (for example [48, 56]). I believed that the theory of random graphs might be of some help for the investigation undertaken (see [3, 24] for a review), but I was not able to build any useful connection to the problem at hand, partially because the structures being studied are mainly trees (since they resemble "real world" networks like Internet), while our networks have systematic loops. Regular (square) network of random uncorrelated resistors was studied in [7, 39]; our nets are irregular and the values of resistors are correlated. Apart from that, we must be able not only investigate topological, but also spatial properties of arrangements of spheres (discs). At present, this requires numerical simulations.

The formalism presented is so called nodal-voltage approach. In electronics sometimes dual description, based on the loops of the circuit, is used (loop-current method). We do not use it since it is more difficult to implement.

3.4.1 Basic notions

Figure 3.6 presents the basic building block, conductance g. If there are voltages u_s and u_e applied to endings s and e respectively, then there will be current I flowing from s to e given by

$$I = g\left(u_s - u_e\right). \tag{3.4.1}$$

This is Ohm law. The power P dissipated at this element is

$$P = I\left(u_s - u_e\right) = g\left(u_s - u_e\right)^2. \tag{3.4.2}$$

We assume that g's are non-negative, therefore the power dissipated is also always non-negative.
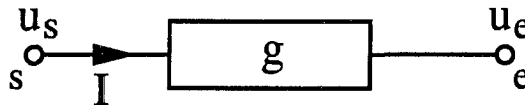
Figure 3.6: Single conductance.

By *electric network* we understand a set of nodes $\mathcal{N}$ connected with conductances. The set of conductances will be denoted by $\mathcal{G}$. Conductance connecting nodes $k, l \in \mathcal{N}$ will be denoted by $g_{kl} \in \mathcal{G}$. Schematic diagram of the network is presented in Figure 3.7.

We divide the nodes into two categories: *border nodes*, in which the voltage (by means of generator or battery) is maintained constant all the time and *core nodes*, for which we require a conservation of current. The set of border nodes is denoted by $\mathcal{B}$ and the set
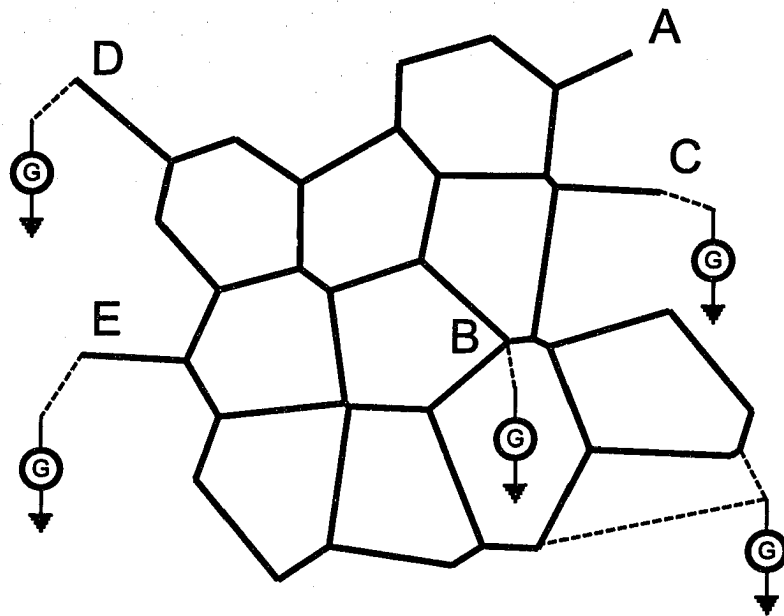
Figure 3.7: Circuit. G denotes generators. Border nodes do not need to lie necessarily on the edge of the circuit (like B). All nodes are connected to at least one other node, but the degree of the core node may be 1 (A). Node cannot be connected to itself. Border nodes are denoted with letters, the rest of the nodes are core nodes. Thick lines denotes conductances, thin and dashed lines are just wires with vanishing resistivity.

of core nodes by $\mathcal{C}$; clearly $\mathcal{N} = \mathcal{B} \cup \mathcal{C}$. The number of core nodes is denoted by κ and number of border nodes by β. We assume that there are at least one border and one core node. The total number of nodes is N and

$$\kappa + \beta = N. \tag{3.4.3}$$

Our term "network" is usually reserved for the type *directed graphs*, but we do not use it in this context. The graphs underlying our networks are assumed to be simple, weighted graphs and therefore posses the following properties ($k, l \in \mathcal{N}$, $k \neq l$)

- the underlying graph is *connected*, i.e. all nodes are connected to at least one other node. Further we require network of core nodes to be connected, without any loss of generality.

- the underlying graph is *non-degenerate*, what means that two nodes may be connected by only one conductance (or none, which corresponds to conductance 0).

- the graph has no "self-loops"; nodes are not connected to themselves

$$g_{kk} = 0. \tag{3.4.4}$$

- the graph is non-directed

$$g_{kl} = g_{lk}. \tag{3.4.5}$$

3.4.2 Matrix formulation

Let us denote by v_l, $l \in \mathcal{N}$, the potential in the node l and by the I_l current leaving (through a generator) this node. The law of current conservation reads

$$I_l = \sum_{k \in \mathcal{N}} g_{kl}(v_l - v_k) = \gamma_l v_l - \sum_{k \in \mathcal{N}} g_{kl} v_k, \tag{3.4.6}$$

where we denoted by γ_l the sum of conductances attached to node l

$$\gamma_l = \sum_{k \in \mathcal{N}} g_{kl}. \tag{3.4.7}$$

From (3.4.6) we immediately get the global current conservation law

$$\sum_{l \in \mathcal{N}} I_l = 0. \tag{3.4.8}$$

We will now order potentials and currents in the nodes into vectors $\mathbf{v}$ and $\mathbf{I}$ respectively. This requires the introduction of numeration of the nodes: from now on k, say, will denote both the node (element of $\mathcal{N}$) and the number of the node. We will understand that $(\mathbf{v})_k = v_k$ (in all expressions of this kind).

We introduce now matrix notation. According to (3.4.6) we may write

$$\mathbf{I} = \mathsf{K}\mathbf{v},\tag{3.4.9}$$

where K is a *Laplacian* of the network

$$\mathsf{K} = \mathsf{D} - \mathsf{A}.\tag{3.4.10}$$

D is diagonal matrix, which entries are γ_l

$$\mathsf{D}_{kl} = \delta_{kl}\gamma_l,\tag{3.4.11}$$

δ_{kl} being Kronecker symbol. A is called *adjacency matrix*

$$\mathsf{A}_{kl} = g_{kl}.\tag{3.4.12}$$

All entries of A are positive and the matrix has zeros on the diagonal.

It is now desirable to reorder indexing of nodes such that $\mathbf{v}$ and $\mathbf{I}$ could be written in the form

$$\mathbf{v} = (\mathbf{v}_b, \mathbf{v}_c)\tag{3.4.13a}$$
$$\mathbf{I} = (\mathbf{I}_b, \mathbf{I}_c),\tag{3.4.13b}$$

where subscripts b and c pertain to border and core nodes respectively. $\mathbf{v}_b, \mathbf{I}_b \in \mathbb{R}^\beta$ and $\mathbf{v}_c, \mathbf{I}_c \in \mathbb{R}^\kappa$. Notation $(\mathbf{v}_b, \mathbf{v}_c) \in \mathbb{R}^N$, should be understood as a vector, which first β components comes from $\mathbf{v}_b$ and the latter κ from $\mathbf{v}_c$.

The problem of *solution* of the electric network may be now stated as follows. There are given network defined by $\mathcal{N}$, $\mathcal{B}$ and $\mathcal{C}$ and fixed potentials in the border nodes $\mathbf{v}_b$. Additionally we require

$$\mathbf{I}_c = \mathbf{0}.\tag{3.4.14}$$

What are the potentials $\mathbf{v}_c$ at the core nodes?

This problem resembles strongly problem of finding electrostatic potential with Dirichlet boundary conditions

$$\nabla^2 \phi = 0.\tag{3.4.15}$$

Matrix K is nothing more than discretized Laplacian, up to the fact that neighbors are taken with weights given by g_{kl} and our network occupies rather some kind of topological than physical space. Let us note that the solution $\mathbf{v}_c$ is a *harmonic function*, i.e. that its value in the node k is given by the weighted average of values in the neighboring nodes ($k \in \mathcal{C}$)

$$v_k = \frac{1}{\gamma_k} \sum_{l \in \mathcal{N}} g_{kl} v_l,\tag{3.4.16}$$

according to (3.4.6) and (3.4.14). This is an echo of the well known fact that the average of continuous harmonic function (i.e. the function obeying Laplace equation (3.4.15)) over the surface of the sphere is equal to the value of the function in the center of the sphere.

We could write the Laplacian K in the following form, simply imposing on it its natural block structure

$$\begin{pmatrix} B & R \\ R^T & \widetilde{K}_c \end{pmatrix} \tag{3.4.17}$$

where all the internal matrices are parts of K: B denotes connections between border nodes, R is a scheme of connections between border and core nodes (^{T} stands for transposition) and $\widetilde{K}_c$ are connections within the set of core nodes. Let us note that $\widetilde{K}_c$ is not a proper Laplacian for core network (network of core nodes and core-core links), since its diagonal elements were built using conductances of core-border type together with core-core connections. This kind of pathology will be consequently denoted with a tilde.

3.4.3 Existence and the uniqueness of solution

Sticking to our block-like form we can write (3.4.9) as

$$\begin{pmatrix} B & R \\ R^T & \widetilde{K}_c \end{pmatrix} \begin{pmatrix} v_b \\ v_c \end{pmatrix} = \begin{pmatrix} I_b \\ 0 \end{pmatrix}. \tag{3.4.18}$$

We look for v_c such that

$$\widetilde{K}_c v_c = -R^T v_b. \tag{3.4.19}$$

This is simply a set of linear equations. We will investigate now the existence and the uniqueness of solution v_c.

Theorem 3.4.1 (Network fundamental theorem). *All eigenvalues α_i of the network Laplacian K are real, non-negative and its set of eigenvectors $\mathcal{K} = \{a_i\}$ forms orthogonal basis. Zero is an eigenvalue, its multiplicity is exactly one and corresponds to a eigenvector $\Theta/\sqrt{N}$, where Θ is a vector consisting of all 1's.*

Proof. The fact that all the eigenvalues are real and the eigenvectors form orthogonal basis follow immediately from the fact that the matrix K is real and symmetric (the proof can be found in any quantum mechanic textbook since K is exactly hermitian operator). The rest of the theorem may be proved as follows.

The power P dissipated in the system, when potentials and leaving currents in the

nodes are $\mathbf{u}$ and $\mathbf{I}$, is

$$
\begin{aligned}
P &= \frac{1}{2} \sum_{l \in \mathcal{N}} \sum_{k \in \mathcal{N}} g_{lk} \left(u_l - u_k \right)^2 \\
&= \frac{1}{2} \sum_{l \in \mathcal{N}} \sum_{k \in \mathcal{N}} g_{lk} u_l^2 - \sum_{l \in \mathcal{N}} \sum_{k \in \mathcal{N}} g_{lk} u_l u_k + \frac{1}{2} \sum_{l \in \mathcal{N}} \sum_{k \in \mathcal{N}} g_{lk} u_k^2 \\
&= \sum_{l \in \mathcal{N}} \gamma_l u_l^2 - \sum_{l \in \mathcal{N}} \sum_{k \in \mathcal{N}} g_{lk} u_l u_k = \mathbf{u} \mathsf{K} \mathbf{u} = \mathbf{u} \cdot \mathbf{I},
\end{aligned}
\tag{3.4.20}
$$

where in the last step (3.4.9) was used.

We may expand arbitrary potential distribution $\mathbf{u}$ in the basis $\mathcal{K}$

$$
\mathbf{u} = \sum_{i=1}^{N} a_i \mathbf{a}_i.
\tag{3.4.21}
$$

We assume that $\mathbf{a}_i$ are normalized hence

$$
a_i = \mathbf{u} \cdot \mathbf{a}_i.
\tag{3.4.22}
$$

It is easy to check that the power

$$
P = \sum_{i=1}^{N} \alpha_i a_i^2.
\tag{3.4.23}
$$

Since for arbitrary distribution of potentials (and thus arbitrary numbers a_i) power dissipated is non-negative, it follows that all the eigenvalues are non-negative. The zero eigenvalue is associated with constant vector $c\Theta$, where $c \in \mathbb{R}$. It is easy to check, that once we realize that $u_l = \mathrm{const}$ is the only vector which does not case any current flow in the system and hence power dissipation. Multiplicity of this eigenvalue is exactly one following the same argumentation – any other distribution causes heating. $\qquad \square$

Lemma 3.4.2. *If potentials $\mathbf{v}_b$ are set in the border nodes all the time, $\mathbf{v}_c$ obeys (3.4.19), $\delta \mathbf{v}_c \in \mathbb{R}^\kappa$ is an arbitrary vector and*

$$
\mathbb{R}^\kappa \ni \mathbf{v}_c' = \mathbf{v}_c + \delta \mathbf{v}_c,
\tag{3.4.24}
$$

then if we apply $\mathbf{v}_c'$ to core nodes, the power dissipated in the systems is

$$
P_0 + \delta \mathbf{v}_c \widetilde{\mathsf{K}}_c \delta \mathbf{v}_c,
\tag{3.4.25}
$$

where P_0 denotes the power dissipated when $\mathbf{v}_c$ is applied to core nodes.

Proof. The power dissipated in the system is according to (3.4.20)

$$(\mathbf{v}_b, \mathbf{v}_c + \delta\mathbf{v}_c) \begin{pmatrix} \mathsf{B} & \mathsf{R} \\ \mathsf{R}^\mathsf{T} & \widetilde{\mathsf{K}}_c \end{pmatrix} \begin{pmatrix} \mathbf{v}_b \\ \mathbf{v}_c + \delta\mathbf{v}_c \end{pmatrix}$$
$$= P_0 + \delta\mathbf{v}_c\widetilde{\mathsf{K}}_c\delta\mathbf{v}_c, \qquad (3.4.26)$$

where (3.4.19) was used to cancel cross-terms. □

The following min-max principle exists. Let us recall that power is always bounded from below by 0.

Theorem 3.4.3 (Thomson principle). *Among all distributions of core potentials $\mathbf{v}_c$ those obeying equation (3.4.19) minimize the power dissipated in the system, providing we keep $\mathbf{v}_b$ fixed.*

Proof. Let us apply the voltage $\mathbf{v}_c'$ to core nodes (potentials on border nodes are $\mathbf{v}_b$ all the time) and again $\mathbf{v}_c' = \mathbf{v}_c + \delta\mathbf{v}_c$, exactly like before. Using Lemma 3.4.2 it is enough now to prove that $\delta\mathbf{v}_c\widetilde{\mathsf{K}}_c\delta\mathbf{v}_c$ is always positive, unless $\delta\mathbf{v}_c = \mathbf{0}$.

As we have stated $\widetilde{\mathsf{K}}_c$ is not a proper Laplacian for the core network

$$\widetilde{\mathsf{K}}_c = \mathsf{K}_c + \delta\mathsf{K}_c, \qquad (3.4.27)$$

where $\delta\mathsf{K}_c$ is diagonal matrix with non-negative entries

$$(\delta\mathsf{K}_c)_{kl} = \delta_{kl}\left(\gamma_l - \sum_{m\in\mathcal{C}} g_{ml}\right). \qquad (3.4.28)$$

We have

$$\delta\mathbf{v}_c\widetilde{\mathsf{K}}_c\delta\mathbf{v}_c = \delta\mathbf{v}_c\mathsf{K}_c\delta\mathbf{v}_c + \delta\mathbf{v}_c\delta\mathsf{K}_c\delta\mathbf{v}_c, \qquad (3.4.29)$$

K_c being (proper) Laplacian for core network. The first term on the RHS is always positive unless

$$\delta\mathbf{v}_c = v\Theta, \quad v \in \mathbb{R}, \qquad (3.4.30)$$

when it is zero (Theorem 3.4.1). Considering the spectrum of $\delta\mathsf{K}_c$, given by (3.4.28) we see that the second term of RHS is always positive except the case when it is zero for $\delta\mathbf{v}_c$ such that

$$(\delta\mathbf{v}_c)_k = 0, \qquad (3.4.31)$$

k corresponding to core nodes linked to at least one border node and therefore for all core nodes, according to (3.4.30). So always $P - P_0 \geq 0$ and $P = P_0$ iff $\delta\mathbf{v}_c = \mathbf{0}$. □

Corollary. *All eigenvalues of $\widetilde{\mathsf{K}}_c$ belong to $\mathbb{R}_+$ and therefore $\widetilde{\mathsf{K}}_c^{-1}$ exists.*

Proof. Taking Lemma 3.4.2 and Theorem 3.4.3 into consideration we see that expressions like $\delta\mathbf{v}_c\tilde{\mathsf{K}}_c\delta\mathbf{v}_c$ are always positive, except when $\delta\mathbf{v}_c$ is zero. Using the same type of argumentation as in Theorem 3.4.1 we see that all the eigenvalues of $\tilde{\mathsf{K}}_c$ are positive, so the inverse exists. Symmetric matrix with this property is often called positive definite quadratic form. □

Theorem 3.4.4 (Existence/Uniqueness theorem). *If potentials* $\mathbf{v}_b$ *in border nodes are fixed there is one and only one distribution of core potentials obeying current conservation law* (3.4.19).

Proof. We explicitly give the solution

$$\mathbf{v}_c = -\tilde{\mathsf{K}}_c^{-1}\mathsf{R}^T\mathbf{v}_b. \tag{3.4.32}$$

It exists because $\tilde{\mathsf{K}}_c^{-1}$ exists. □

3.4.4 Iterative method for finding $\mathbf{v}_c$

In the previous paragraph we learned how to find solution to our boundary value problem. Here I am going to present another method, more suitable for computer simulations.

Let us consider the linear transformation T, that substitutes all potentials in the core nodes by the averages defined by (3.4.16). Border potentials are left unchanged.

$$\mathsf{T} = \begin{pmatrix} \mathsf{I}_\beta & \mathsf{0}_\beta \\ \tilde{\mathsf{D}}_c^{-1}\mathsf{R}^T & \tilde{\mathsf{D}}_c^{-1}\mathsf{A}_c \end{pmatrix}, \tag{3.4.33}$$

where A_c is an adjacency matrix for core network, $\tilde{\mathsf{D}}_c$ is diagonal matrix of diagonal elements of $\tilde{\mathsf{K}}_c$

$$\tilde{\mathsf{D}}_c = \tilde{\mathsf{K}}_c + \mathsf{A}_c. \tag{3.4.34}$$

I_β and $\mathsf{0}_\beta$ are $\beta \times \beta$ unit and zero matrices respectively. $\tilde{\mathsf{D}}_c^{-1}$ exists, because the network is connected.

Let $\mathbf{v}_c$ be solution of (3.4.19) with boundary conditions $\mathbf{v}_b$ and define

$$\mathbf{u}_c = \mathbf{v}_c + \delta\mathbf{v}_c, \tag{3.4.35}$$

$$\mathbf{u}_c' = \mathbf{v}_c + \delta\mathbf{v}_c' \tag{3.4.36}$$

and

$$\mathbf{u}_c' = \mathsf{T}\mathbf{u}_c. \tag{3.4.37}$$

We have

$$
\begin{aligned}
\mathbf{u}_c' &= \widetilde{\mathsf{D}}_c^{-1}\mathsf{R}^\mathsf{T}\mathbf{v}_b + \widetilde{\mathsf{D}}_c^{-1}\mathsf{A}_c\,(\mathbf{v}_c + \delta\mathbf{v}_c) \\
&= \widetilde{\mathsf{D}}_c^{-1} + \widetilde{\mathsf{D}}_c^{-1}\left(\widetilde{\mathsf{D}}_c - \widetilde{\mathsf{K}}_c\right)(\mathbf{v}_c + \delta\mathbf{v}_c) \\
&= \mathbf{v}_c + \widetilde{\mathsf{D}}_c^{-1}\mathsf{A}_c\delta\mathbf{v}_c,
\end{aligned}
\tag{3.4.38}
$$

so

$$
\delta\mathbf{v}_c' = \mathsf{W}\delta\mathbf{v}_c,
\tag{3.4.39}
$$

where

$$
\mathsf{W} = \widetilde{\mathsf{D}}_c^{-1}\mathsf{A}_c.
\tag{3.4.40}
$$

We can easily conclude that the exact solution $(\mathbf{v}_b, \mathbf{v}_c)$ is invariant under the transformation T.

Let us consider iterative process

$$
\mathbf{u} \rightarrow \mathsf{T}\mathbf{u}.
\tag{3.4.41}
$$

We will now prove, that in the limit of infinite operations we reach exact solution in core nodes $\mathbf{v}_c$, having started from an arbitrary initial guess.

We investigate properties of W

$$
\mathsf{W}_{ii} = 0
\tag{3.4.42a}
$$

$$
0 \leq \mathsf{W}_{ij} \leq 1, \quad i \neq j
\tag{3.4.42b}
$$

$$
\sum_{j=1}^{\kappa} \mathsf{W}_{ij} \leq 1,
\tag{3.4.42c}
$$

and for the core nodes which are linked to at least one border node the last inequality is strong.

There is very useful theorem which allows for the estimation of eigenvalues of a square matrix due to Semyon Aronovich Gerschgorin [36].

Theorem 3.4.5 (Gerschgorin disc theorem). *Let* A *be square complex matrix. Every eigenvalue of* A *lies in one of the following discs*

$$
d_i = \left\{ z : |z - \mathsf{A}_{ii}| \leq \sum_{j \neq i} |\mathsf{A}_{ij}| \right\},
\tag{3.4.43}
$$

called Gerschgorin discs.

Proof. Proof comes from [1]. Let λ be an eigenvalue of A and $\mathbf{v}$ its corresponding eigenvector. Let i be chosen such that $|v_i| = \max_j |v_j|$. $\mathbf{v}$ can't be $\mathbf{0}$ so $|v_i| > 0$. Now, since

$$\mathsf{A}\mathbf{v} = \lambda\mathbf{v}$$

$$(\lambda - \mathsf{A}_{ii})\,v_i = \sum_{j \neq i} \mathsf{A}_{ij} v_j. \tag{3.4.44}$$

Taking norm of both sides we arrive at

$$|\lambda - \mathsf{A}_{ii}| = \left| \sum_{j \neq i} \mathsf{A}_{ij} \frac{v_j}{v_i} \right| \leq \sum_{j \neq i} |\mathsf{A}_{ij}|. \tag{3.4.45}$$

□

We need somewhat different and weaker version.

Theorem 3.4.6 (Markov-Gerschgorin theorem). *Let* W *be matrix with properties* (3.4.42). *All its eigenvalues* λ_i *obey*

$$|\lambda_i| < 1. \tag{3.4.46}$$

Proof. The proof proceeds as in Theorem 3.4.5. We may note that the equality in (3.4.45) may hold only for row i corresponding to core node with no link to border node and to eigenvector of the type $c\Theta$. But for such an eigenvector we may chose any of the rows, so as well the one corresponding to core node with border connection(s) and make the inequality strong. □

It is well known [89] that any square matrix can be decomposed as follows:

$$\mathsf{W} = \mathsf{S}^{-1}\mathsf{J}\mathsf{S}, \tag{3.4.47}$$

where S is a non-singular matrix and J is *Jordan canonical form* of W

$$\mathsf{J} = \begin{pmatrix} \mathsf{J}_1 & & & \\ & \mathsf{J}_2 & 0 & \\ & 0 & \ddots & \\ & & & \mathsf{J}_m \end{pmatrix} \tag{3.4.48}$$

and

$$\mathsf{J}_l = \begin{pmatrix} \lambda_l & 1 & 0 & \dots & 0 \\ 0 & \lambda_l & 1 & 0 & \vdots \\ \vdots & \ddots & \ddots & \ddots & 0 \\ 0 & \dots & 0 & \lambda_l & 1 \\ 0 & \dots & \dots & 0 & \lambda_l \end{pmatrix} \tag{3.4.49}$$

is called Jordan block. It has corresponding eigenvalue repeated on the diagonal and 1's on the superdiagonal. Each Jordan block corresponds to different eigenvalue λ_l;

the number of Jordan blocks m is determined by the number of linearly independent eigenvectors of W and their dimensionality by the multiplicities s_l of the eigenvalues λ_l. The powers of Jordan matrix and Jordan block read respectively

$$\mathsf{J}^k = \begin{pmatrix} \mathsf{J}_1^k & & & \\ & \mathsf{J}_2^k & 0 & \\ & 0 & \ddots & \\ & & & \mathsf{J}_m^k \end{pmatrix}, \qquad (3.4.50)$$

$$\mathsf{J}_l^k = \begin{pmatrix} \lambda_l^k & k\lambda_l^{k-1} & k^2\lambda_l^{k-2} & \dots & k^{s-1}\lambda_l^{k-s-1} \\ 0 & \lambda_l^k & k\lambda_l^{k-1} & k^2\lambda_l^{k-2} & \ddots \\ \vdots & \ddots & \ddots & \ddots & \ddots \\ \vdots & \dots & 0 & \lambda_l^k & k\lambda_l^{k-1} \\ 0 & \dots & \dots & 0 & \lambda_l^k \end{pmatrix}, \qquad (3.4.51)$$

where $s = s_l$ and providing $k \geq s - 1$. Since for $|\lambda| < 1$

$$\lim_{k \to \infty} k^s \lambda^k = 0, \qquad (3.4.52)$$

we see the suggested iterative procedure is convergent

$$\mathsf{W}^n = \mathsf{S}^{-1} \mathsf{J}^n \mathsf{S} \xrightarrow[n \to \infty]{} 0. \qquad (3.4.53)$$

Let us now introduce a notion of *total conductivity* of the network. It makes sense only providing that we divide our set of border nodes in two groups: inflowing and outflowing nodes. All the nodes of the first group have the same potential $U \neq 0$, the nodes in the latter one are kept grounded. The net (total) conductivity of the system is from the definition

$$g_{tot} = \frac{I}{U}, \qquad (3.4.54)$$

where I is the current flowing through the system. Easy calculations show that

$$g_{tot} = \frac{P_{tot}}{U^2}, \qquad (3.4.55)$$

where P_{tot} is the power dissipated in the system.

3.5 Summary

In this chapter I presented the major features of the hydraulic network model for the description of flows in constrained geometries. Its usefulness was proved by direct comparison with experiment. I also showed how to use this formalism to compute permeability of the medium and interphase momentum transfer coefficient β.

The mathematical theory of linear resistor networks, presented in the last part of the chapter, gives some of their fundamental properties. It appears that the resistor networks with Dirichlet boundary conditions can be regarded as well defined variational problem – the solution for nodes potentials which satisfies the current conservation law minimizes also the total power dissipated in the system. It was shown that there was only one such solution. Additional output of the analysis was an iterative procedure for finding potentials in the nodes; its convergence was formally proved. The advantage of the latter method over the direct attempt to solve the set of linear equations, (3.4.19), will be seen in the Chapter 6, where the numerical studies will be presented.

This chapter ends the introductory part of the thesis. From now on we will try to adapt and extend the network model for the purpose of calculating β.

Part II

Studies

The analytic calculation of the interphase drag force exploiting the electrical network analogy became the major goal of my work. I decided to investigate flow in 2D systems past the (possibly disordered) arrays of cylinders, with the main axii perpendicular to the fluid velocity. There were two major reasons for the migration to Flatland. First, it made the problem of flow in disordered systems at least tractable in the sense of analytic solution. Second, such studies have not been undertaken yet; there exists a rich literature (both theoretical and experimental) devoted to flow past systems of spheres, but I am not aware of the similar work concerning flow in the assemblages of cylinders. The resultant porous medium is quite specific, its fragment was presented in the Figure 4.0. Except from this, the rest of the procedure follows ideas presented in the Chapter 3.
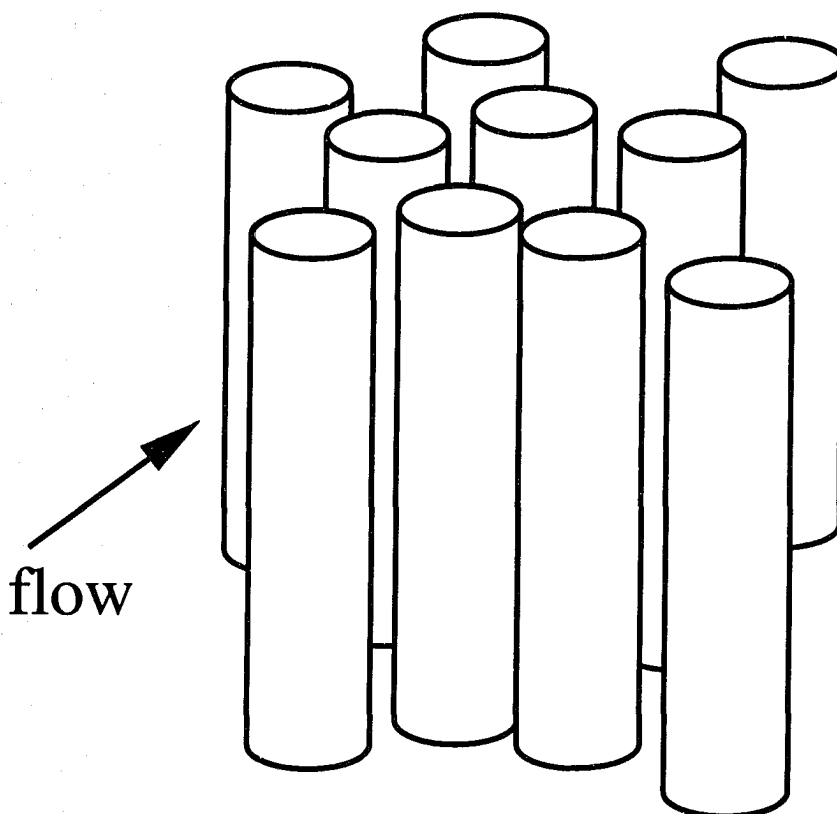
flow

Figure 4.0: Fragment of two dimensional porous medium.

Chapter 4

Flow in periodic media

Study of periodic media has several important advantages. First of all we may construct exact description of flow in the media by solving directly Navier-Stokes equation and utilizing electric analogy matching these two solutions can on the one hand validate the hydraulic network approach and on the other will allow us to gauge one of the models of throat (Sections 4.2 & 4.3). Creating reliable throat functions is another important task accomplished in this chapter (Section 4.1). Finally the chapter reports the first analytic attack on the flows in disordered systems (Section 4.4). The latter issue is especially interesting, since (even exact) calculation of drag for regular systems are feasible. If there were a way to deduce the properties of realistic (disordered) networks from the regular ones our main goal would be fulfilled. The key points of this part of work are summarized in Section 4.5.

The chapter makes use of Voronoi methods for finding nearest neighbors, but in the case of regular sets of generators such identification is easy. The maturer discussion of this issue is therefore postponed to Chapter 5, where in the presence of disorder the problem fails to be trivial.

4.1   Models of throat

Model of the slit between two parallel cylinders makes a cornerstone of the project. During the course of my work I considered many possibilities and here I discuss the three most important of them. The most obvious choice is to assume that the flow between cylinders takes place between two parallel walls of length $L = D$ at a distance $M = s - D$ from each other, where s is a distance between the cylinders centers and D denotes the diameter of the cylinders. The conductance may be then calculated from (3.1.16). This surely overestimates the friction. Below I provide two other models. The first one takes into consideration varying size of the throat ("integrated throat"), the second one is based on the theoretical prediction of the drag experienced by a single row of throats connected in parallel ("Miyagi throat").

4.1.1   Integrated model

Reference [5] points out that the duct with varying geometry may be cut into slices. To each slice a resistance is assigned and the net resistance may be obtained by the integrating of particular slices.
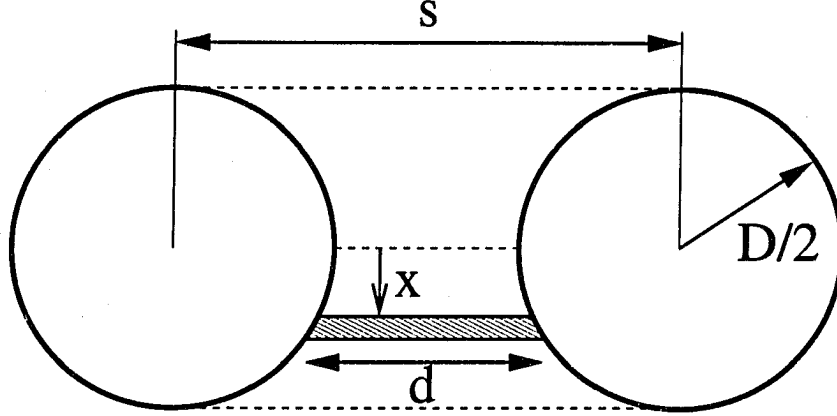
Figure 4.1: The idea of the throat with varying geometry. The conductance of each "slice" is computed using formula (3.1.16).

Resistance of the slice is obtained from equation (3.1.16)

$$dR = \frac{12\mu}{H} \frac{1}{d^3} dx, \qquad (4.1.1)$$

where

$$d = s - 2\sqrt{\frac{D^2}{4} - x^2}, \quad x \in [-D/2, D/2]. \qquad (4.1.2)$$

Please refer to Figure 4.1 for details. The net resistance

$$R = \frac{12\mu}{H} \int_{-D/2}^{D/2} \frac{1}{\left(s - 2\sqrt{\frac{D^2}{4} - x^2}\right)^3} dx = \frac{12\mu}{HD^2} \int_0^1 \frac{1}{\left(\alpha - \sqrt{1 - \xi^2}\right)^3} d\xi, \qquad (4.1.3)$$

with $\alpha = s/D > 1$. After the integration the conductance yields

$$g_I(\alpha) = \frac{HD^2}{\mu} f_I(\alpha), \qquad (4.1.4)$$

where

$$f_I(\alpha) = \frac{\alpha\left(\alpha^2 - 1\right)^{5/2}}{3\left(3\pi\alpha^2 + 2\sqrt{\alpha^2 - 1}\left(1 + 2\alpha^2\right) + 6\alpha^2\mathrm{acot}\left(\sqrt{\alpha^2 - 1}\right)\right)}. \qquad (4.1.5)$$

We have, for $s \approx D$ (narrow throat limit)

$$f_I(\alpha) = c\left(\alpha - 1\right)^{5/2} + \mathcal{O}\left(\left(\alpha - 1\right)^{7/2}\right), \qquad (4.1.6)$$

and

$$c = \frac{2\sqrt{2}}{9\pi} \approx 0.10. \qquad (4.1.7)$$

The importance of the above limit will become clear in Section 6.

4.1.2 Miyagi model
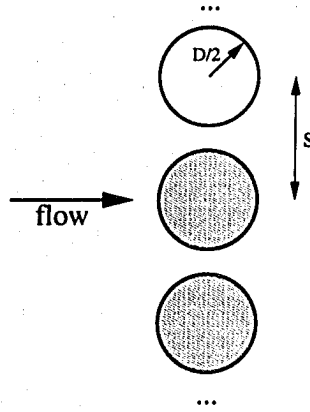
Figure 4.2: The array of Miyagi cylinders.

In [66] Miyagi investigated flow past 1D array of cylinders (Figure 4.2). Using Fourier transform, he gave an expression for a drag in the form of power series in D/s and subsequently extrapolated the result to the regime of narrow throats and got that the force F acting on the cylinder is

$$\frac{F}{\mu U} = \frac{\mathrm{const}}{\left(s/D - 1\right)^2}, \qquad (4.1.8)$$

where U denotes the velocity of the fluid far from the array. We can note characteristic quadratic blow-up, which suggest that the conductance of the single throat in the parallel

network may be written in the following form

$$g_{\mathrm{M}}(\alpha) = \frac{HD^2}{\mu}\gamma_{\mathrm{M}}\,(\alpha-1)^2\,, \tag{4.1.9}$$

where γ_{M} is an dimensionless constant. We will evaluate the optimal value of γ_{M} soon.

In general such extrapolation procedures are risky, but in this case author gave plausible justification to it.

4.2 Regular array of small cylinders

The exact solution of Navier-Stokes equation for the case of flow in periodic environments is due to Hasimoto, [45], and I utilize his work throughout the section. Hasimoto gave the result in a form of expansion up to terms $\mathcal{O}(\log{(1-\epsilon)})$ and only for square lattice. I extended his work to include corrections $\mathcal{O}(1-\epsilon)$ both for square and hexagonal lattices. Another works, which deal with solutions for special periodic setups, are already mentioned [66] and [59].

4.2.1 Green function

We investigate slow steady motion of an incompressible, viscus fluid past a 2D periodic array of small obstacles, placed in the periodic lattice sites

$$\mathcal{L} \ni \mathbf{r}_n = n_1\mathbf{a}_1 + n_2\mathbf{a}_2, \quad n_{1,2} \in \mathbb{Z} \tag{4.2.1}$$

$\mathbf{a}_1$ and $\mathbf{a}_2$ forming the basis of the lattice and $\mathcal{L}$ forming a set of the lattice sites. Our problem may be formulated as follows

$$\mu\nabla^2\mathbf{v} = \nabla p + \mathbf{F}\sum_{\mathbf{r}_n \in \mathcal{L}}\delta(\mathbf{r}-\mathbf{r}_n), \tag{4.2.2a}$$

$$\nabla \cdot \mathbf{v} = 0, \tag{4.2.2b}$$

where μ denotes the viscosity, $\mathbf{v}$ the velocity field and p stands for the pressure. $\mathbf{F}$ is the force exerted on the fluid by each of the obstacles; we assume that the lattice is "simple", i.e. every obstacle is surrounded by the same configuration of other identical obstacles and indeed exerts the same force. In 2D $\mathbf{F}$ is understood as a force acting on the unit length of the system.

Since the problem is periodic we are going to work in the Fourier basis, expanding velocity and pressure gradient respectively ($\mathfrak{i}$ stands for imaginary unit)

$$\mathbf{v} = \sum_{\mathbf{k} \in \mathfrak{R}}\mathbf{v}_{\mathbf{k}}\exp(-2\pi\mathfrak{i}\mathbf{k}\cdot\mathbf{r}), \tag{4.2.3a}$$

$$-\nabla p = \sum_{\mathbf{k} \in \mathfrak{R}}\mathbf{P}_{\mathbf{k}}\exp(-2\pi\mathfrak{i}\mathbf{k}\cdot\mathbf{r}). \tag{4.2.3b}$$

$\mathcal{R}$ stands for the lattice reciprocal to $\mathcal{L}$, i.e. lattice spanned on the basis vectors $\mathbf{A}_1$ and $\mathbf{A}_2$, such that $(i, j = 1, 2)$

$$\mathbf{A}_i \cdot \mathbf{a}_j = \delta_{ij}. \tag{4.2.4}$$

Substituting (4.2.3) into (4.2.2a) and recalling the linear independence of basis functions $\exp(-2\pi i \mathbf{k} \cdot \mathbf{r})$ we obtain the relations between the amplitudes of expansions

$$-4\pi^2 \mu k^2 \mathbf{v_k} = -\mathbf{P_k} + \frac{\mathbf{F}}{\Omega}, \tag{4.2.5a}$$

$$\mathbf{k} \cdot \mathbf{v_k} = 0, \tag{4.2.5b}$$

where we used that fact that Fourier transform of Dirac's delta is simply a constant, inverse of unit cell volume

$$\Omega = \|\mathbf{a}_1 \times \mathbf{a}_2\| = \|\mathbf{A}_1 \times \mathbf{A}_2\|^{-1}. \tag{4.2.6}$$

Additionally, since $\mathbf{P}$ is a gradient of a function

$$\mathbf{k} \times \mathbf{P_k} = 0. \tag{4.2.7}$$

$\mathbf{F}$ can be computed from the mean pressure gradient (eq. (4.2.5a), for $\mathbf{k} = 0$)

$$\mathbf{F} = \mathbf{P}_0 \Omega. \tag{4.2.8}$$

For $\mathbf{k} \neq \mathbf{0}$, taking the scalar product of both sides of (4.2.5a) with $\mathbf{k}$ and recalling relation (4.2.5b) yields

$$\mathbf{k} \cdot \mathbf{P_k} = \frac{1}{\Omega} \mathbf{k} \cdot \mathbf{F} = \mathbf{k} \cdot \mathbf{P}_0 \tag{4.2.9}$$

or, after use of (4.2.7),

$$\mathbf{P_k} = \frac{(\mathbf{k} \cdot \mathbf{F}) \mathbf{k}}{\Omega k^2}. \tag{4.2.10}$$

Relying on (4.2.5a), the amplitudes of velocity are

$$\mathbf{v_k} = \frac{1}{4\pi^2 \mu \Omega} \left(\frac{(\mathbf{k} \cdot \mathbf{F}) \mathbf{k}}{k^4} - \frac{\mathbf{F}}{k^2} \right), \quad \mathbf{k} \neq \mathbf{0}. \tag{4.2.11}$$

Performing inverse Fourier transform and writing the results in the Cartesian coordinates we get

$$\mathbf{v} = \mathbf{v}_0 + \frac{1}{\mu} \mathbf{GF} \tag{4.2.12a}$$

$$-\nabla p = \frac{\mathbf{F}}{\Omega} + \mathbf{G'F}, \tag{4.2.12b}$$

where the operators G and G' are given by

$$G_{ij} = \frac{1}{4\pi}\left(S_1\delta_{ij} - \frac{\partial^2 S_2}{\partial x_i \partial x_j}\right) \tag{4.2.13a}$$

$$G'_{ij} = -\frac{1}{4\pi}\frac{\partial^2 S_1}{\partial x_i \partial x_j}. \tag{4.2.13b}$$

The lattice sums S_1 and S_2 are

$$S_1(\mathbf{r}) = \frac{1}{\pi\Omega}\sum_{\mathbf{k}\in\mathcal{R}'}\frac{\exp(-2\pi i\mathbf{k}\cdot\mathbf{r})}{k^2} \tag{4.2.14a}$$

$$S_2(\mathbf{r}) = -\frac{1}{4\pi^3\Omega}\sum_{\mathbf{k}\in\mathcal{R}'}\frac{\exp(-2\pi i\mathbf{k}\cdot\mathbf{r})}{k^4} \tag{4.2.14b}$$

and the summation goes over all non-zero $\mathbf{k}$'s

$$\mathcal{R}' = \mathcal{R} \setminus \{\mathbf{0}\}. \tag{4.2.15}$$

By explicit calculations we can get that

$$\nabla^2 S_2 = S_1, \tag{4.2.16a}$$

$$\nabla^2 S_1 = -4\pi\left(\sum_{\mathbf{r}_n\in\mathcal{L}}\delta(\mathbf{r}-\mathbf{r}_n) - \frac{1}{\Omega}\right). \tag{4.2.16b}$$

We see that the problem reduces essentially to determination of electrostatic potential coming from a set of point-like positive charges placed on the lattice and neutralized by a surrounding cloud of negative charge density, filling uniformly the unit cell (this is simply description of potential of ionic lattice). It is known that the separate calculations of both contributions lead to divergences. Presence of uniform charge density (being equivalent to the presence of uniform gradient $\mathbf{P_0}$) makes the problem convergent.

The linear operators G and G' may be regarded as Green's functions; they represent the perturbation introduced into the system due to spatially periodic point-like driving $\mathbf{F}$. In the spirit of Green's technique the solutions may be superposed to satisfy non-slip boundary conditions on the obstacles. The zeroth Fourier mode of $\mathbf{v}$, $\mathbf{v_0}$, is the average fluid velocity in the system and may be regarded as the velocity present in the system before the perturbation $\mathbf{F}$ was introduced.

4.2.2 B tensor

The calculations presented above are strict, but there is no easy way (in fact no way that I would be aware of) to fulfill exactly the boundary conditions on the surface of each cylinder. In general we would need to write down the integral equation for $\mathbf{F}$ with G as a kernel. The integration is performed on the surface of the cylinder $\mathcal{C}$, so that the net flow on the cylinder surface would vanish ($\mathcal{F}$ stands for the force per unit area of the cylinder

and L is its length)

$$\mathbf{v}(\mathbf{r})\Big|_{\mathbf{r}\in\mathcal{C}} = \mathbf{v}_0 + \frac{L}{\mu}\int_{\mathcal{C}} \mathsf{G}(\mathbf{r}-\mathbf{r}')\mathcal{F}(\mathbf{r}')dr' = 0 \qquad (4.2.17)$$

Solution of the above equation would give us $\mathcal{F}$ and subsequently $\mathbf{F}$

$$\mathbf{F} = \int_{\mathcal{C}} \mathcal{F}(\mathbf{r}')\hat{\mathbf{n}}(\mathbf{r}')dr', \qquad (4.2.18)$$

where $\hat{\mathbf{n}}(\mathbf{r}')$ stands for the vector normal to the cylinder surface.

The above exact procedure is too complicated. Instead, we follow Hasimoto and use Burgers approximation [14]. We require that the *average* velocity on the surface of the cylinder must vanish ($a = D/2$ stands for the radius of cylinder)

$$\langle\mathbf{v}\rangle = \frac{1}{2\pi a}\int_{r=a} \mathbf{v}dS = 0. \qquad (4.2.19)$$

This condition yields according to (4.2.12a)

$$\mathbf{v}_0 = -\frac{1}{\mu}\langle\mathsf{G}\rangle\mathbf{F} \qquad (4.2.20)$$

or

$$\mathbf{F} = -\mu\langle\mathsf{G}\rangle^{-1}\mathbf{v}_0. \qquad (4.2.21)$$

In other words, instead of a cylinder and a distribution of force, we have point like force applied to the fluid in the center of the cylinder together with the condition that the velocity vanishes in the distance $D/2$. Burgers average (4.2.19) depends on the cylinder diameter and this is exactly the moment where the latter quantity enters our calculations.

The force acting on the cylinder array per unit volume after subtracting the uniform pressure gradient (buoyancy) influence is

$$-\left(\frac{\mathbf{F}}{\Omega} - \frac{\mathbf{F}}{\Omega}\frac{\pi a^2 H}{\Omega H}\right) = -\frac{\mathbf{F}}{\Omega}\epsilon, \qquad (4.2.22)$$

where H is the length of the cylinders. Therefore the drag force $\mathbf{F}_D$ per unit volume for the periodic system reads

$$\mathbf{F}_D = \widetilde{\mathsf{B}}\mathbf{v}_0, \qquad (4.2.23)$$

where

$$\widetilde{\mathsf{B}} = \frac{\epsilon\mu}{\Omega}\langle\mathsf{G}\rangle^{-1}. \qquad (4.2.24)$$

$\widetilde{\mathsf{B}}$ may be regarded as tensor version of β coefficient. If D stands for cylinders' diameter

we get

$$\frac{1}{\Omega} = \frac{4(1-\epsilon)}{\pi D^2}.$$ (4.2.25)

and hence

$$\widetilde{\mathsf{B}} = \frac{4\epsilon(1-\epsilon)}{\pi} \frac{\mu}{D^2} \langle \mathsf{G} \rangle^{-1} = \frac{\mu}{D^2} \mathsf{B}.$$ (4.2.26)

B is dimensionless and depends purely on geometry of the system; we call it *geometrical modifier*. In case of homogeneous and isotropic media it is simply a scalar.

4.2.3 Discussion of the symmetries of tensor G

Definition (4.2.13a) of tensor G_{ij} indicates that the drag tensor defined for periodic media is certainly symmetric

$$\mathsf{G}_{ij} = \mathsf{G}_{ji}.$$ (4.2.27)

The above property may be proved for general permeability tensor, see ref. [77]. The latter source states additionally that G is positive definite matrix.

In the case when the tensor is defined on a certain regular lattice we know that it must feature the same symmetry group as the underlying lattice. If we define Λ as the rotation operator (rotation of angle ϕ)

$$\Lambda(\phi) = \begin{pmatrix} \cos\phi & -\sin\phi \\ \sin\phi & \cos\phi \end{pmatrix}$$ (4.2.28)

we can write the following consistency equation

$$\mathsf{G} = \Lambda^{-1}(\phi)\mathsf{G}\Lambda(\phi)$$ (4.2.29)

if the lattice is invariant with respect to rotations of angle ϕ (e.g. $\phi = 120°$ for triangular lattice and $\phi = 90°$ for square).

Easy calculations show that symmetric tensor on square and triangular lattice must be isotropic, i.e. of the form

$$\mathsf{G}_{ij} = \text{scalar} \times \delta_{ij}.$$ (4.2.30)

4.2.4 Calculation of S_1 & S_2

Solid state physics worked out extremely powerful method for calculating expressions like S_1 or S_2, given by (4.2.14a) and (4.2.14b), called *Ewald theta transformation*. The basic exposition of this technique can be found in [9]. It was born in connection with calculation of Madelung energy of ionic crystals.

We start with the following integral identity

$$\frac{1}{k^{2m}} = \frac{\pi^m}{\Gamma(m)} \int_0^\infty e^{-\pi k^2 \xi} \xi^{m-1} d\xi, \qquad (4.2.31)$$

where $\Gamma(m)$ is the *Euler's gamma function* and define

$$\sigma_m = \sum_{k \in \mathcal{R}'} \frac{e^{-2\pi i k \cdot r}}{k^{2m}} \qquad (4.2.32a)$$

$$= \frac{\pi^m}{\Gamma(m)} \sum_{k \in \mathcal{R}'} \int_0^\infty e^{-\pi k^2 \xi - 2\pi i k \cdot r} \xi^{m-1} d\xi$$

$$= \frac{\pi^m}{\Gamma(m)} \int_0^\infty \xi^{m-1} \left(\sum_{k \in \mathcal{R}} e^{-\pi k^2 \xi - 2\pi i k \cdot r} - 1 \right) d\xi. \qquad (4.2.32b)$$

In the already mentioned Ewald's methods we split the integrals as the one above into two parts, one from zero to α, and the second from α to ∞, where α is an arbitrary constant. Let us note that the parameter ξ bears the unit of m^2 and so does α. The following identity is called *theta transformation*

$$\sum_{k \in \mathcal{R}} e^{-\pi k^2 \xi - 2\pi i k \cdot r} = \frac{\Omega}{\xi} \sum_{r_n \in \mathcal{L}} e^{-\pi (r - r_n)^2 / \xi}. \qquad (4.2.33)$$

This transformation was introduced by Ewald (see e.g. [28]) and proved formally by Born and Huang in [8]. It allows us to write

$$\sigma_m = \frac{\pi^m \alpha^m}{\Gamma(m)} \left(\frac{\Omega}{\alpha} \sum_{r_n \in \mathcal{L}} \phi_{-m} \left(\frac{\pi (r - r_n)^2}{\alpha} \right) - \frac{1}{m} + \sum_{k \in \mathcal{R}'} e^{-2\pi i k \cdot r} \phi_{m-1} \left(\pi \alpha k^2 \right) . \right) \qquad (4.2.34)$$

In the first integral we put $\xi \rightarrow \alpha/\xi$ and in the second $\xi \rightarrow \alpha \xi$. $\phi_m(x)$ is defined using *incomplete Γ-function*

$$\phi_m(x) = \frac{1}{x^{m+1}} \Gamma_{m+1}(x),$$
$$\Gamma_n(x) = \int_x^\infty \xi^{n-1} e^{-\xi} d\xi. \qquad (4.2.35)$$

We obtain

$$S_1 = \frac{\sigma_1}{\pi\Omega} = \sum_{\mathbf{r}_n \in \mathcal{L}} \phi_{-1}\left(\frac{\pi(\mathbf{r} - \mathbf{r}_n)^2}{\alpha}\right) - \frac{\alpha}{\Omega}$$

$$+ \frac{\alpha}{\Omega} \sum_{\mathbf{k} \in \mathcal{R}'} e^{-2\pi i \mathbf{k} \cdot \mathbf{r}} \phi_0\left(\pi\alpha\mathbf{k}^2\right) \qquad (4.2.36\text{a})$$

$$S_2 = -\frac{\sigma_2}{4\pi^3\Omega} = -\frac{\alpha}{4\pi} \sum_{\mathbf{r}_n \in \mathcal{L}} \phi_{-2}\left(\frac{\pi(\mathbf{r} - \mathbf{r}_n)^2}{\alpha}\right) + \frac{\alpha^2}{8\pi\Omega}$$

$$- \frac{\alpha^2}{4\pi\Omega} \sum_{\mathbf{k} \in \mathcal{R}'} e^{-2\pi i \mathbf{k} \cdot \mathbf{r}} \phi_1\left(\pi\alpha\mathbf{k}^2\right) \qquad (4.2.36\text{b})$$

4.2.5 Singular expansion in powers of $1 - \epsilon$

We assume $1 - \epsilon$ to be a small parameter, which corresponds to small ratio D/h, h being distance between centers of neighboring cylinders. To calculate the Burgers average (4.2.19) of G we must be able to express $S_1(\mathbf{r})$ and $S_2(\mathbf{r})$ for $\mathbf{r}$ close to one of $\mathbf{r}_n$'s, let us denote the choice by $\tilde{\mathbf{r}}$. Considering that $S_1(\mathbf{r})$ and $S_2(\mathbf{r})$ are periodic with the periodicity of the lattice, we take $\tilde{\mathbf{r}} = 0$ without any loss of generality. We must now proceed with some care, since the expansion is singular for the terms which correspond to $\mathbf{r}_n = \tilde{\mathbf{r}}$ in our sums.

Here we go. v_i denotes ith Cartesian component of vector $\mathbf{v}$. Expansion of $\phi_{-1}(x)$, far from $x = 0$, $\Upsilon \equiv \pi \mathbf{r}_n^2/\alpha$

$$\phi_{-1}\left(\frac{\pi(\mathbf{r} - \mathbf{r}_n)^2}{\alpha}\right) = \Gamma_0(\Upsilon) + 2e^{-\Upsilon}\frac{(r_{n1}\cos(\varphi) + r_{n2}\sin(\varphi))}{\mathbf{r}_n^2}r$$

$$+ \frac{1}{\mathbf{r}_n^4\Omega}e^{-\Upsilon}\left(\pi\mathbf{r}_n^4 + \left(\pi\mathbf{r}_n^2 + \alpha\right)\left(\left(r_{n1}^2 - r_{n2}^2\right)\cos(2\varphi) + 2r_{n1}r_{n2}\sin(2\varphi)\right)\right)r^2 + \mathcal{O}\left(r^3\right).$$

$$(4.2.37)$$

The expansion around 0 ($\gamma \approx 0.577216$ stands for Euler's gamma)

$$\phi_{-1}\left(\frac{\pi\mathbf{r}^2}{\alpha}\right) = -\gamma - 2\log\left(\frac{\pi r}{\alpha}\right) + \frac{\pi r^2}{\alpha} + \mathcal{O}\left(r^4\right). \qquad (4.2.38)$$

The above results were quoted to give a taste of the problem. In similar manner we expand the rest of the functions: derivatives of $\partial_{r_i}\partial_{r_j}S_2$ and $\exp(-2\pi i \mathbf{k} \cdot \mathbf{r})$.

Next we calculate the averages (4.2.19) for $r = a$. Again only first few results are

quoted

$$\left\langle \phi_{-1}\left(\frac{\pi(\mathbf{r}-\mathbf{r}_n)^2}{\alpha}\right)\right\rangle = \Gamma_0\left(\Upsilon\right) + e^{-\Upsilon}\frac{\pi a^2}{\alpha} + \mathcal{O}\left(a^4\right), \quad \mathbf{r}_n \neq \mathbf{0}. \qquad (4.2.39a)$$

$$\left\langle \phi_{-1}\left(\frac{\pi \mathbf{r}^2}{\alpha}\right)\right\rangle = -\gamma - 2\log\left(\frac{\pi a}{\alpha}\right) + \frac{\pi a^2}{\alpha} + \mathcal{O}\left(a^4\right). \qquad (4.2.39b)$$

In the expansions, most of the terms which vanish during the averaging process. Furthermore even if the term survives, the symmetry of the lattice (especially the inverse point, which all of the lattices under considerations posses) may cause the resultant sum to be zero. Property (4.2.30) and equation (4.2.16a) allow us to calculate all relevant quantities only with the knowledge of $\langle S_1 \rangle$

$$\langle S_1 \rangle = -\gamma - \frac{\alpha}{\Omega} + A + C - \log\left(\frac{\pi a^2}{\alpha}\right) + \frac{a^2}{\Omega}\left(\frac{\pi\Omega}{\alpha} + B + D\right), \qquad (4.2.40)$$

since

$$\left\langle \frac{\partial^2 S_2}{\partial r_1 \partial r_2}\right\rangle = \left\langle \frac{\partial^2 S_2}{\partial r_2 \partial r_1}\right\rangle \equiv 0, \qquad (4.2.41a)$$

$$\left\langle \frac{\partial^2 S_2}{\partial r_1^2}\right\rangle = \left\langle \frac{\partial^2 S_2}{\partial r_2^2}\right\rangle = \frac{1}{2}\langle S_1 \rangle. \qquad (4.2.41b)$$

The constants A, B, C and D are lattice sums and read ($\mathcal{L}' = \mathcal{L} \setminus \{0\}$)

$$A = \sum_{\mathbf{r}_n \in \mathcal{L}'} \Gamma_0\left(\frac{\pi \mathbf{r}_n}{\alpha}\right) \qquad (4.2.42a)$$

$$B = \frac{\pi\Omega}{\alpha} \sum_{\mathbf{r}_n \in \mathcal{L}'} e^{-\pi \mathbf{r}_n^2/\alpha}, \qquad (4.2.42b)$$

$$C = \frac{\alpha}{\Omega} \sum_{\mathbf{k} \in \mathcal{R}'} \phi_0\left(\pi\alpha\mathbf{k}^2\right), \qquad (4.2.42c)$$

$$D = -\pi^2\Omega \sum_{\mathbf{k} \in \mathcal{R}'} \mathbf{k}^2\phi_0\left(\pi\alpha\mathbf{k}^2\right). \qquad (4.2.42d)$$

We still have a freedom in taking a value α and the most convenient choice is

$$\alpha = \Omega. \qquad (4.2.43)$$

The above sums are rapidly convergent and may be easily calculated numerically; some details and the results of calculation are presented in the next section.

4.2.6 Lattice sums

First we discuss briefly the properties of 2D lattice: square and hexagonal (triangular).
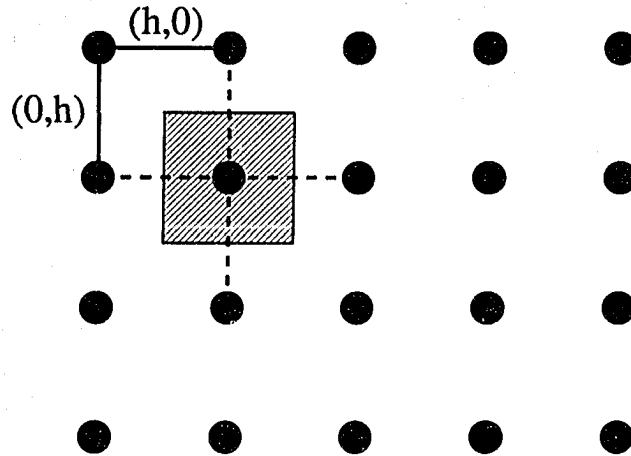
Figure 4.3: Physical square lattice. The shaded region is Voronoi (Wigner-Seitz) cell; it repeats periodically in both directions and its edges are called Voronoi edges. Dashed lines are Delone edges, connecting nearest neighbors.
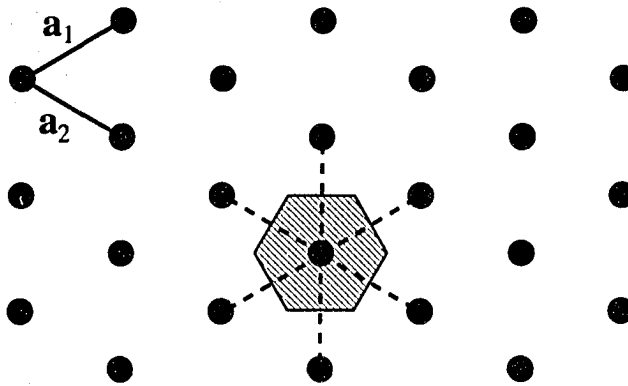
Figure 4.4: Hexagonal lattice. The Voronoi region is an hexagon.
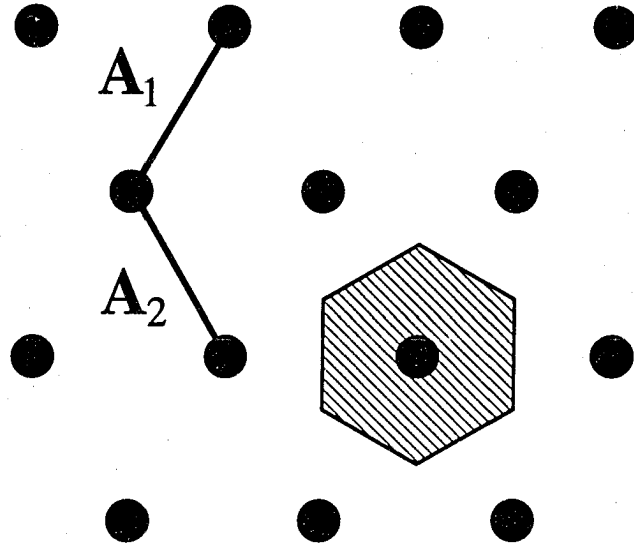
Figure 4.5: The lattice reciprocal to that presented in the Figure 4.4. The Voronoi region for reciprocal lattice is called first Brillouin zone.

Square lattice is spanned on the following two basis vectors (h stands for nearest neighbors distace)

$$h(1,0), \ h(0,1) \tag{4.2.44}$$

and its reciprocal lattice is also a square lattice with the basis:

$$\frac{1}{h}(1,0), \ \frac{1}{h}(0,1). \tag{4.2.45}$$

The volume of the physical unit cell is

$$\Omega_{sq} = h^2. \tag{4.2.46}$$

The lattice is presented in Figure 4.3.

The hexagonal (triangular lattice) was depicted in the Figure 4.4. The basis vectors

$$\mathbf{a}_1 = \frac{h}{2}\left(\sqrt{3}, 1\right) \tag{4.2.47a}$$

$$\mathbf{a}_2 = \frac{h}{2}\left(\sqrt{3}, -1\right). \tag{4.2.47b}$$

The reciprocal lattice basis vectors are (Figure 4.5)

$$\mathbf{A}_1 = \frac{1}{h}\left(\frac{1}{\sqrt{3}}, 1\right) \tag{4.2.48a}$$

$$\mathbf{A}_2 = \frac{1}{h}\left(\frac{1}{\sqrt{3}}, -1\right). \tag{4.2.48b}$$

The volume of the unit cell in the physical space

$$\Omega_{tr} = \frac{\sqrt{3}}{2}h^2. \tag{4.2.49}$$

For all simple lattices we have

$$\frac{a^2}{\Omega} = \frac{1-\epsilon}{\pi}. \tag{4.2.50}$$

The numerical calculations of the constants mentioned were carried out using *Mathematica*. The summation was performed over natural shells surrounding arbitrarily chosen origin. Larger shells have more lattice points, but due to monotonic and exponential decay of the functions under sum symbol, their contributions become less important. The number of shells to be included was determined by the adopted accuracy (10^{-4}). The results are presented in the Table 4.2.6.

	Lattice type	
Sum	square	hexagonal
A	0.044668	0.035737
B	0.566557	0.501383
C	0.056212	0.043973
D	−0.566509	−0.501020

Table 4.1: Lattice sums.

Hasimoto gave the form of second order corrections using elliptic functions. According to this result we have for the square lattice

$$D = -B, \tag{4.2.51}$$

which agrees with our calculations within numerical error.

4.2.7 Results

With the knowledge of matrix elements (4.2.41) we are able to compute $\langle G \rangle$ and subsequently B. The results of the calculations are

$$B_{11}(\epsilon) = B_{22}(\epsilon) = \frac{32\epsilon(1-\epsilon)}{-\gamma - 1 + A + C - \log(1-\epsilon) + (1-\epsilon)(B + D + \pi)/\pi}, \quad (4.2.52a)$$

$$B_{12}(\epsilon) = B_{21}(\epsilon) = 0 \quad (4.2.52b)$$

and they were depicted in the Figure 4.6. The force (both friction and buoyancy) experienced by a single cylinder in the square lattice is

$$\mathbf{F}_{sq} = \frac{4\pi\mu}{c - \log(a/h) + (\pi/2)(a^2/h^2)}\mathbf{v}_0, \quad c \approx -1.3105329. \quad (4.2.53)$$
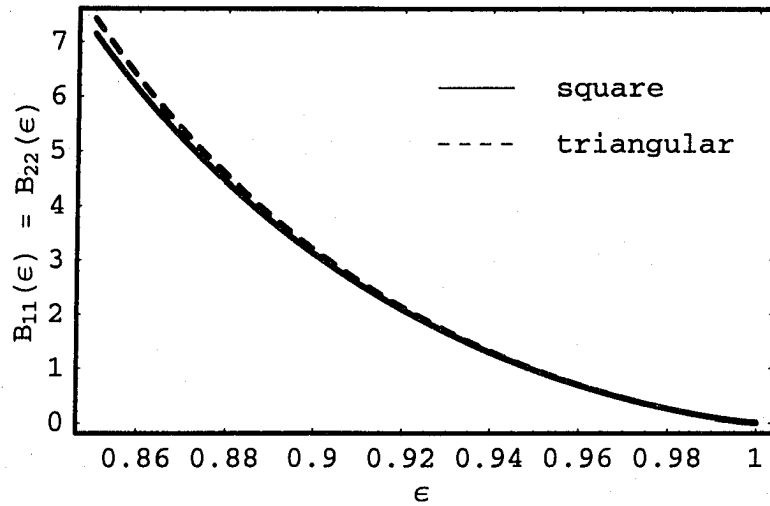
Figure 4.6: Comparison of component B_{11} for square and triangular lattice. For small concentration both lattices have very similar properties. The tensors are isotropic; the off diagonal terms ($B_{12}(\epsilon)$ & $B_{21}(\epsilon)$) vanish.

4.3 Regular lattices of resistors

We will now try to calculate the drag experienced by regular lattices by means of electric formalism. We consider three configurations: square lattice of cylinders, and triangular lattice in two configurations, each configuration rotated by $\pi/2$ with respect to each other. They were presented in the Figure 4.7. Let us assume that the flow takes place in the samples of length L and width M and that L and M are large enough so the boundary effects are negligible.

Let us start with triangular lattice. All the throats have equal conductance and we denote it by g_0. In the orientation as in the Figure 4.7a, from the symmetry of the system we see that the current in the horizontal throats is twice the current flowing in the inclined nodes. With every generator (cylinder) the are associated two inclined throats and one horizontal. The power dissipated in the system is therefore

$$P_{tot} = ML\lambda\frac{1}{g_0}\left(I_0^2 + 2\frac{I_0^2}{4}\right) = ML\lambda\frac{3}{2}\frac{I_0^2}{g_0}, \tag{4.3.1}$$

where I_0 is a current flowing in the horizontal node and λ is a number of cylinders per unit area (Ω^{-1})

$$\lambda = \frac{2\sqrt{3}}{3}\frac{1}{h^2} \tag{4.3.2}$$

The total current flowing through the system is $I_{tot} = (M/h)I_0$ and h is the length of the Delone edge and the total conductance of the network

$$g_{tot} = I_{tot}^2/P_{tot} = g_0\frac{M}{L}\frac{1}{\sqrt{3}}. \tag{4.3.3}$$

Similar calculations for the case presented in the Figure 4.7b, give exactly the same result. Hexagonal lattice of resistors is isotropic; we have already discussed the symmetry properties in Section 4.2.3. For the case of square lattice (Figure 4.7c) simple calculation yields immediately

$$g_{tot} = g_0\frac{M}{L}. \tag{4.3.4}$$

In general we can write

$$g_{tot} = \eta g_0\frac{M}{L}, \tag{4.3.5}$$

where η is a function of the topology of the network.

There is one more interesting fact about the lattices we have discussed. They are not only isotropic but also highly homogeneous. If x denotes the position of the node
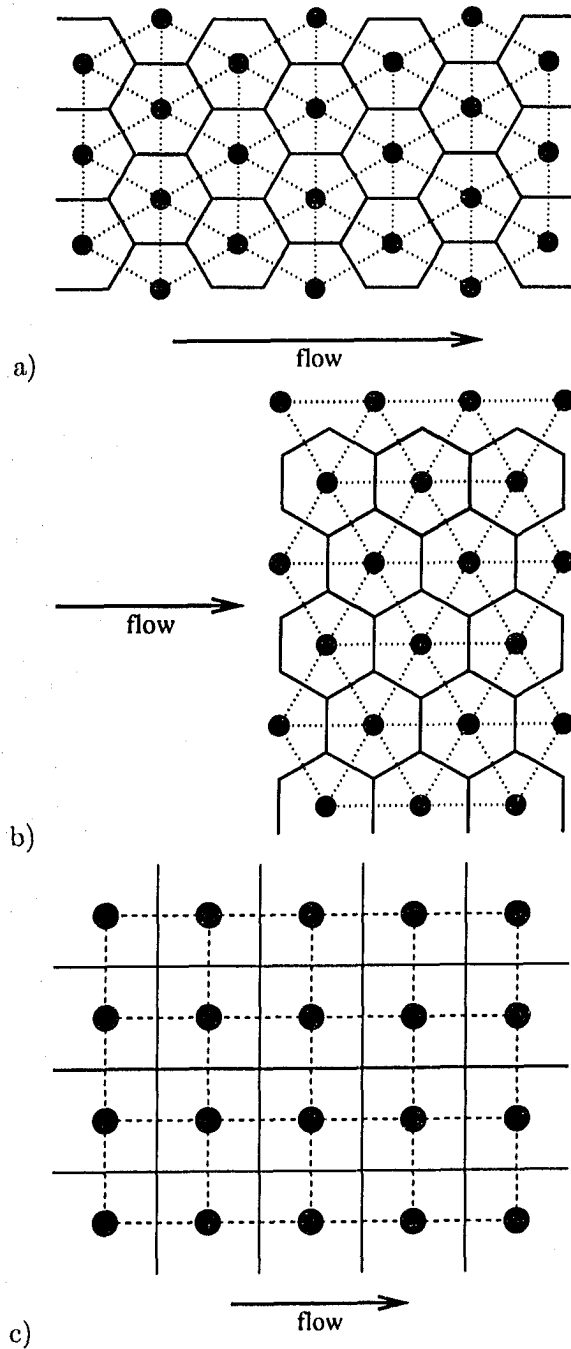
Figure 4.7: Three examined geometries of flow in regular lattices. See the discussion in text. Solid lines represent conductances (flow paths), dashed lines are Delone edges – their length determines the value of conductances.

(Voronoi vertex) projected onto direction of the flow, the pressure in this point reads

$$p_0 - Gx, \tag{4.3.6}$$

where G is a pressure gradient, p_0/L, where p_0 is the pressure of inflow nodes, providing the outflow nodes pressure is zero and the inflow nodes are in position zero. This exactly means that the resistors are decoupled or, in other words, they do not feel the topology of connections: the potentials in the nodes are entirely determined by their positions in simple homogeneous manner described by (4.3.6).

Since, as we soon see, disordered arrays have many common features with hexagonal lattice, we could expect that the above property is to some extent universal. I called this hypothesis **uniform gradient assumption**. Such law, which couples spatial and electrical properties of throats, is essential for every attempts to solve the problem analytically in the disordered case, since all the information we really have about *any* kind of lattice are strictly local. If the resistors "talk to each other" on the large scales we are helpless.

As suggested in the Section 4.1 we write conductance g_0 of a single throat in the form ($\alpha = s/D$, s – inter cylinder distance)

$$g_0(\alpha) = \frac{HD^2}{\mu}\gamma(\alpha). \tag{4.3.7}$$

If the geometry of the system is well defined function $\alpha(\epsilon)$ is single value and we have

$$\alpha(\epsilon) = \left(\frac{\pi}{4}\right)^{1/2}\frac{1}{\sqrt{1-\epsilon}} \qquad \text{(square lattice)} \tag{4.3.8a}$$

$$\alpha(\epsilon) = \left(\frac{\pi\sqrt{3}}{6}\right)^{1/2}\frac{1}{\sqrt{1-\epsilon}} \qquad \text{(hexagonal lattice)}. \tag{4.3.8b}$$

Making use of (3.1.22) we obtain

$$\beta(\epsilon) = f_D(\epsilon)\frac{\mu}{D^2}, \tag{4.3.9}$$

where the geometrical modifier reads

$$f_D(\epsilon) = \frac{\epsilon^2}{\eta\gamma(\alpha(\epsilon))}. \tag{4.3.10}$$

We will try to match now the solutions obtained from Hasimoto treatment and the electrical method. This will allow us to gauge constant γ_M in (4.1.9). We compare $f_D(\epsilon)$ and $B_{11} = B_{22}$ for hexagonal lattice. Since we can control the quality of approximation I chose as a matching point such value ϵ_0, where the second order correction is relatively small. The choice of $\epsilon_0 = 0.9$ yields the relative value of second correction 10%; still it is

arbitrary. The value of γ_M that makes the two solutions match is

$$\gamma_M = \frac{1}{16} = 0.0625. \tag{4.3.11}$$

The results were presented in the Figure 4.8. It is instructive to compare now the integrated (eq. (4.1.4)) and Miyagi (eq. (4.1.9)) model (Figure 4.9). In the region which we are really interested in (cylinders close to each other) they match pretty well, due to the asymptotic behavior of integrated throat given by (4.1.6).

a)   b)
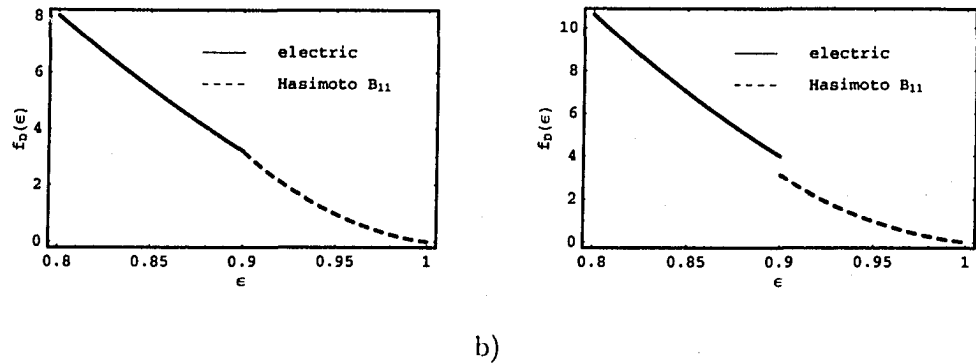
Figure 4.8: Matching of solution obtained from electric formulation and exact predictions based on Fourier series: a) triangular lattice, b) sqaure lattice. The optimal value of γ_M was found to be $1/16 = 0.0625$.

Figure 4.10 presents geometrical modifier of the hexagonal lattice for different models of throat.

4.4 Phonons

What we are really interested in is *disorder*. Having considered regular lattices the next natural step is to investigate what happens if we introduce phonon-like disorder. We must be aware from the very beginning that such oscillatory movements of particles can by no means mimic real interactions with flowing fluid. Rather we assume a presence of interatomic (binding) forces that are much stronger than interactions of the cylinders with the flow field. We work utilizing the uniform gradient assumption, introduced in the previous section.

The phonon model of disorder has no physical significance (the hydrodynamic forces acting between particles are not binding) nevertheless I decided to elaborate it primarily to develop some intuition how the geometrical properties of the medium translate into properties of β.
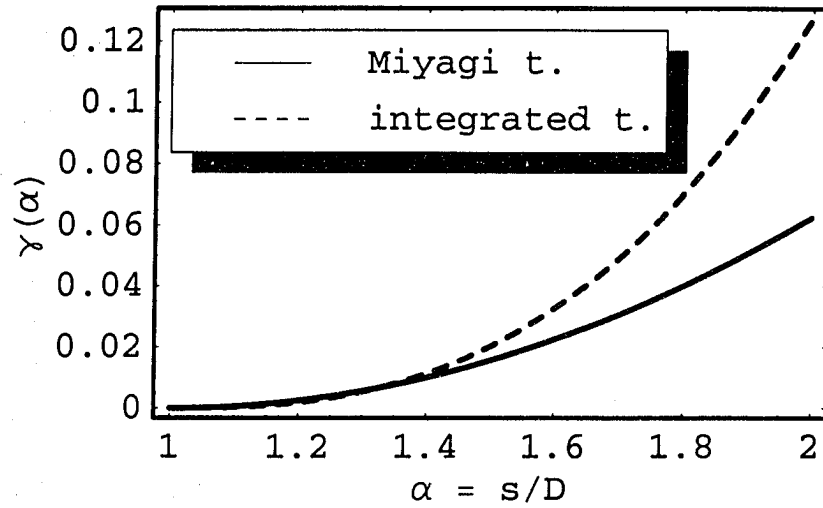
Figure 4.9: Comparison of Miyagi and integrated model of throat.
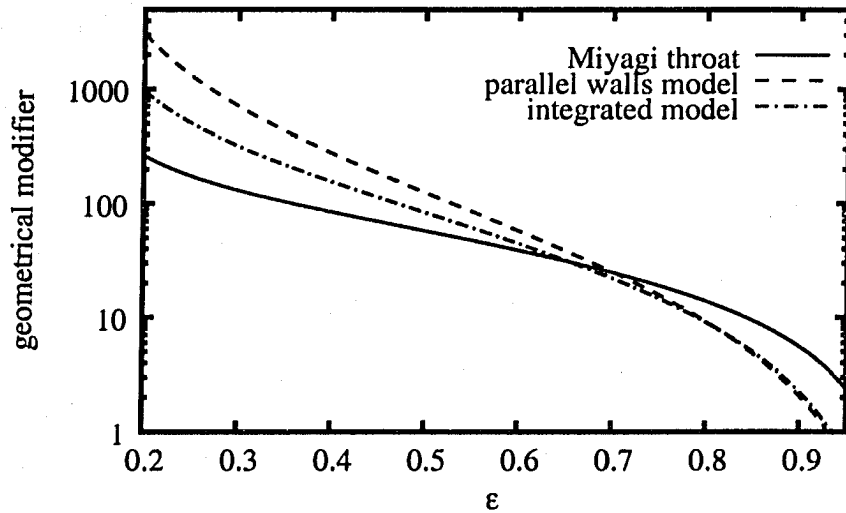
Figure 4.10: Geometrical modifier of hexagonal lattice for different models of throat.

4.4.1 Statement of the problem

We investigate disordered version of the lattice presented in Figure 4.7a. The basis of the physical and reciprocal space were investigated in the Section 4.2.6. The three Delone edges (please refer to the discussion in Section 4.3) adherent to each generator, have the following orientations $\hat{\mathbf{r}}_i$

$$\hat{\mathbf{r}}_1 = \left(\frac{\sqrt{3}}{2}, \frac{1}{2} \right), \tag{4.4.1a}$$

$$\hat{\mathbf{r}}_2 = (0, 1), \tag{4.4.1b}$$

$$\hat{\mathbf{r}}_3 = \left(\frac{\sqrt{3}}{2}, -\frac{1}{2} \right). \tag{4.4.1c}$$

Each one of them have equilibrium length h, where h is interatomic spacing. Undisturbed Voronoi edge has length l_0; please refer to Figure 4.11.
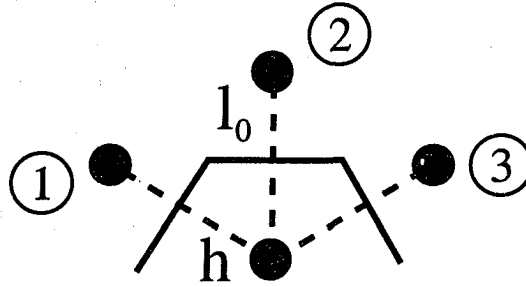
Figure 4.11: Three adjacent gerators that form three throats associated with each cylinder. The equilibrium interatomic distance (Delone edge) and Voronoi edge length are h and l_0 respectively.

According to (3.1.22) and (4.3.9) we have

$$f_D(\epsilon) = \epsilon^2 \frac{HM}{L} \frac{D^2}{\mu} \frac{1}{g_{tot}}. \tag{4.4.2}$$

For several technical reasons it is easier to calculate the inverse of the above quantity:

$$f_D(\epsilon)^{-1} = \frac{1}{\epsilon^2} \frac{\mu}{D^2} \frac{L}{MH} g_{tot} = \frac{\mu}{D^2} \frac{L}{MH} \frac{P_{tot}}{(GL)^2} = \frac{\mu}{D^2} \frac{1}{G^2} \frac{P_{tot}}{MHL}. \tag{4.4.3}$$

G stands for uniform gradient present in the system. $P_{tot}/(MHL)$ is the power dissipated in the system per unit volume. In the spirit of constant gradient assumption we write

$$P_{tot} = G^2 \sum_{i \in \mathcal{G}} g(\alpha_i) l_i^2, \tag{4.4.4}$$

where $g(\alpha_i)$ and l_i are conductance and length projected onto direction of the flow respectively of the ith throat. We adopt Miyagi model (4.1.9) and obtain

$$f_D(\epsilon)^{-1} = \frac{1}{\epsilon^2}\frac{1}{LM}\sum_{i\in\mathcal{G}}\gamma_{\mathrm{M}}\left(\frac{s_i}{D}-1\right)^2 l_i^2. \tag{4.4.5}$$

We assume that vibrational motion does not change the topology of connections and that length of the throat (l_i) may be in the first approximation taken to be equal to that one of the undistorted lattice. The above sum may be written over set of cylinders (lattice sites) $\mathcal{L}$ (note the presence of $\frac{1}{4}$, which comes from the uniform gradient scheme – the length of the inclined throats projected on the direction of the flow is $\frac{1}{2}$ of the throat physical length)

$$f_D(\epsilon)^{-1} = \frac{1}{\epsilon^2}\frac{1}{LM}\gamma_{\mathrm{M}}\sum_{l\in\mathcal{L}}\left(\frac{l_0^2}{4}\left(\frac{s_{1l}}{D}-1\right)^2 + l_0^2\left(\frac{s_{2l}}{D}-1\right)^2 + \frac{l_0^2}{4}\left(\frac{s_{3l}}{D}-1\right)^2\right) \tag{4.4.6}$$

and

$$s_{il} = h + \Delta\mathbf{u}_{il}\cdot\hat{\mathbf{r}}_i, \tag{4.4.7}$$

where $\Delta\mathbf{u}_{il}$ is the relative displacement of two neighboring atoms from their equilibrium positions. We assumed that s_{il} is determined by the projection of the new relative distance onto the original direction of the edge; approximation is surely justified when small distortions are considered.

We have

$$\frac{l_0^2}{LM} = \frac{2}{3\sqrt{3}}\frac{1}{N} \tag{4.4.8}$$

and further manipulations lead to

$$f_D(\epsilon)^{-1} = f_{D0}(\epsilon)^{-1} + \kappa, \tag{4.4.9}$$

with the following notation

$$\kappa = \frac{1}{\epsilon^2}\frac{2}{3\sqrt{3}}\frac{1}{N}\gamma_{\mathrm{M}}\sum_{l\in\mathcal{C}}\sum_{i=1}^{3}\tau_i\left(2\zeta_{il}\left(\frac{2h}{D}-1\right)+\zeta_{il}^2\right), \tag{4.4.10}$$

where $\tau_1 = \tau_3 = \frac{1}{4}$, $\tau_2 = 1$, $\zeta_{il} = \Delta\mathbf{u}_{il}\cdot\hat{\mathbf{r}}_i/D$ and $f_{D0}(\epsilon)$ stands for geometrical modifier for undisturbed lattice. Obviously

$$f_D(\epsilon) = \frac{f_{D0}(\epsilon)}{1 + f_{D0}(\epsilon)\kappa}. \tag{4.4.11}$$

Cylinders are considered as vibrating 2D atoms and the above expressions depends on time – we would like to calculate its time average. In the next section the model of

phonon-like vibrations will be introduced.

4.4.2 Phonon formalism

Theoretical introduction comes from [63], which follows [8]. Our model of vibrating lattice consists simply of a set of atoms connected by means of springs. For simplicity we discuss only mono-atomic lattices, mass of each atom being m. Lattice sites are

$$\mathbf{R}_l = l_1\mathbf{a}_1 + l_2\mathbf{a}_2, \quad l \in \mathcal{L}. \tag{4.4.12}$$

Vibrations cause atoms to leave these equilibrium positions and the displacement of the lth atom is $\mathbf{u}_l$. They are functions of time.

Total kinetic energy of the lattice is

$$K = \frac{1}{2}m \sum_{l \in \mathcal{L}} \dot{\mathbf{u}}_l^2. \tag{4.4.13}$$

The potential Φ energy is assumed to depend only on the instantaneous positions of atoms. We expand it around the equilibrium positions of atoms

$$\Phi = \Phi_0 + \sum_{l \in \mathcal{L}} \sum_{\alpha} \partial_{\alpha;l}\Phi u_{l\alpha} + \sum_{l,l' \in \mathcal{L}} \sum_{\alpha,\beta} \partial_{\alpha;l}\partial_{\beta;l'}\Phi u_{l\alpha}u_{l'\beta} + \text{h.t.} \tag{4.4.14}$$

where $u_{l\alpha}$ stands for α Cartesian component of $\mathbf{u}_l$ and the following shorthand notation was used

$$\partial_{\alpha;l}f = \frac{\partial f}{\partial u_{l\alpha}}. \tag{4.4.15}$$

Omission of higher terms in the expansion is called *harmonic approximation*.

The presence of equilibrium requires that

$$\partial_{\alpha;l}\Phi = 0 \tag{4.4.16}$$

and since lattice is periodic

$$\partial_{\alpha;l}\partial_{\beta;l'}\Phi = \partial_{\alpha;0}\partial_{\beta;l'-l}\Phi \tag{4.4.17}$$

where the notation $\partial_{\beta;l'-l}$ should be understood as differentiation with respect to $u_{\lambda\alpha}$, where λ corresponds to lattice site $\mathbf{R}_\lambda = \mathbf{R}_{l'} - \mathbf{R}_l$. Only the *relative* cell index matters.

Hamiltonian of the system reads

$$H = \Phi + K \tag{4.4.18}$$

and aided by Hamilton's equations

$$\dot{u}_{l\alpha} = \frac{\partial H}{\partial p_{l\alpha}}, \tag{4.4.19a}$$

$$\dot{p}_{l\alpha} = -\frac{\partial H}{\partial u_{l\alpha}}, \tag{4.4.19b}$$

where $p_{l\alpha} = m\dot{u}_{l\alpha}$, we immediately get equation of the motion for the lattice

$$m\ddot{u}_{l\alpha} = -\frac{\partial \Phi}{\partial u_{l\alpha}} = -\sum_{l'\in\mathcal{L}}\sum_{\beta} \partial_{\alpha;l}\partial_{\beta;l'}\Phi u_{l'\beta}. \tag{4.4.20}$$

The problem is linear and we will try to build our solution by means of plane waves

$$u_{l\alpha}(t) = \Lambda_\alpha(\mathbf{k},\omega)\mathfrak{e}^{-i\omega t + 2\pi i\mathbf{k}\cdot\mathbf{R}_l}. \tag{4.4.21}$$

Here we assume that $\Lambda_\alpha(\mathbf{k},\omega)$ does not depend on the site index l. Substitution of the above expression into (4.4.20) yields

$$m\omega^2\Lambda_\alpha = \sum_\beta \mathsf{D}_{\alpha\beta}\Lambda_\beta, \tag{4.4.22}$$

where the *dynamical matrix* reads

$$\mathsf{D}_{\alpha\beta}(\mathbf{k}) = \sum_{l'\in\mathcal{L}} \partial_{\alpha;l}\partial_{\beta;l'}\Phi \mathfrak{e}^{2\pi i\mathbf{k}\cdot(\mathbf{R}_{l'}-\mathbf{R}_l)} = \sum_{l\in\mathcal{L}} \partial_{\alpha;0}\partial_{\beta;l}\Phi \mathfrak{e}^{2\pi i\mathbf{k}\cdot\mathbf{R}_l}. \tag{4.4.23}$$

We can see that D is Hermitian

$$\mathsf{D}_{\alpha\beta}^*(\mathbf{k}) = \mathsf{D}_{\beta\alpha}(\mathbf{k}) \tag{4.4.24}$$

and therefore is has 2 real eigenvalues $m\omega_i^2(\mathbf{k})$. D has the following symmetry

$$\mathsf{D}_{\alpha\beta}(-\mathbf{k}) = \mathsf{D}_{\alpha\beta}^*(\mathbf{k}) \tag{4.4.25}$$

and since it is Hermitian we see that

$$\omega_i^2(-\mathbf{k}) = \omega_i^2(\mathbf{k}). \tag{4.4.26}$$

Eigenvectors of D, $\hat{\mathbf{e}}_i(\mathbf{k})$ form orthonormal basis and may be constructed in such a way that

$$\hat{\mathbf{e}}_i(-\mathbf{k}) = \hat{\mathbf{e}}_i^*(\mathbf{k}). \tag{4.4.27}$$

It is well known, that upon imposing periodic boundary conditions allowed values of $\mathbf{k}$ will occupy first Brillouin zone (Ξ) of reciprocal lattice; we have already discussed the construction of reciprocal space $\mathcal{R}$ in Section 4.2.6 (for triangular lattice example see

Figure 4.5). We will often calculate sums over all possible vectors $\mathbf{k} \in \Xi$. When the size of the system reaches the limit of infinity these vectors start to fill Ξ semi-continuously and uniformly, hence

$$\frac{1}{N}\sum_{\mathbf{k}\in\Xi} \xrightarrow[N\to\infty]{} \Omega\int_{\Xi} d^2\mathbf{k}, \tag{4.4.28}$$

where, let it be recalled, Ω denotes the volume of a Wigner-Seitz cell in physical lattice.

There exists the important relation between physical and reciprocal lattice. In the thermodynamical limit $N \to \infty$ (N stands for number of atoms)

$$\sum_{\mathbf{R}_l\in\mathcal{L}} \mathbb{e}^{2\pi i\mathbf{k}\cdot\mathbf{R}_l} = \frac{1}{\Omega}\sum_{\mathbf{K}\in\mathcal{R}} \delta(\mathbf{k}-\mathbf{K}). \tag{4.4.29}$$

We sum up solutions (4.4.21) and obtain

$$\mathbf{u}_l(t) = \frac{1}{\sqrt{N}}\sum_{\mathbf{k}\in\Xi}(Q_1(\mathbf{k},t)\hat{\mathbf{e}}_1(\mathbf{k}) + Q_2(\mathbf{k},t)\hat{\mathbf{e}}_2(\mathbf{k}))\mathbb{e}^{2\pi i\mathbf{k}\cdot\mathbf{R}_l}$$

$$= \sqrt{N}\Omega\int_{\Xi} d^2\mathbf{k}(Q_1(\mathbf{k},t)\hat{\mathbf{e}}_1(\mathbf{k}) + Q_2(\mathbf{k},t)\hat{\mathbf{e}}_2(\mathbf{k}))\mathbb{e}^{2\pi i\mathbf{k}\cdot\mathbf{R}_l}. \tag{4.4.30}$$

Since $\mathbf{u}_l(t)$ is real the amplitudes $Q_i(\mathbf{k},t)$ must satisfy the condition

$$Q_i(-\mathbf{k}) = Q_i^*(\mathbf{k}). \tag{4.4.31}$$

As a warm up let us calculate the kinetic energy (4.4.13) in terms of Q_i

$$K = \frac{m}{2}\sum_{l\in\mathcal{L}}\dot{\mathbf{u}}_l\cdot\dot{\mathbf{u}}_l = \frac{m}{2}\sum_{l\in\mathcal{L}}N\Omega^2\iint_{\Xi\times\Xi} d^2\mathbf{k}d^2\mathbf{q}\Big(\dot{Q}_1(\mathbf{k})\hat{\mathbf{e}}_1(\mathbf{k}) + \dot{Q}_2(\mathbf{k})\hat{\mathbf{e}}_2(\mathbf{k})\Big)$$

$$\cdot \Big(\dot{Q}_1(\mathbf{q})\hat{\mathbf{e}}_1(\mathbf{q}) + \dot{Q}_2(\mathbf{q})\hat{\mathbf{e}}_2(\mathbf{q})\Big)\mathbb{e}^{2\pi i(\mathbf{k}+\mathbf{q})\cdot\mathbf{R}_l}. \tag{4.4.32}$$

Now, we interchange the order of summation and integration and using relation (4.4.29) arrive at

$$K = \frac{mN\Omega}{2}\iint_{\Xi\times\Xi} d^2\mathbf{k}d^2\mathbf{q}\Big(\dot{Q}_1(\mathbf{k})\hat{\mathbf{e}}_1(\mathbf{k}) + \dot{Q}_2(\mathbf{k})\hat{\mathbf{e}}_2(\mathbf{k})\Big)$$

$$\cdot \Big(\dot{Q}_1(\mathbf{q})\hat{\mathbf{e}}_1(\mathbf{q}) + \dot{Q}_2(\mathbf{q})\hat{\mathbf{e}}_2(\mathbf{q})\Big)\mathbb{e}^{2\pi i(\mathbf{k}+\mathbf{q})\cdot\mathbf{R}_l}\sum_{\mathbf{K}\in\mathcal{R}}\delta((\mathbf{k}+\mathbf{q})-\mathbf{K}). \tag{4.4.33}$$

Since $\mathbf{k}$ and $\mathbf{q}$ lie in the first Brillouin zone the only vector of reciprocal space that they can add up to is $\mathbf{0}$ and the last sum reduces to $\delta(\mathbf{k}+\mathbf{q})$. One integration may be

performed immediately. Using symmetry (4.4.31) and orthogonality of $\hat{e}$'s we get finally

$$K = \frac{mN\Omega}{2} \int_\Xi d^2\mathbf{k} \left(\left| \dot{Q}_1(\mathbf{k}) \right|^2 + \left| \dot{Q}_2(\mathbf{k}) \right|^2 \right). \tag{4.4.34}$$

In the similar manner we are able to calculate potential energy

$$\Phi = \frac{mN\Omega}{2} \int_\Xi d^2\mathbf{k} \left(\omega_1^2(\mathbf{k}) |Q_1(\mathbf{k})|^2 + \omega_2^2(\mathbf{k}) |Q_2(\mathbf{k})|^2 \right). \tag{4.4.35}$$

Using Lagrange formulation we can build the Lagrangian for the lattice

$$L = \Phi - K \tag{4.4.36}$$

and using Euler-Lagrange equations

$$\frac{\partial L}{\partial u_{l\alpha}} - \frac{d}{dt}\left(\frac{\partial L}{\partial \dot{u}_{l\alpha}} \right) \tag{4.4.37}$$

find the equation of motion for Q's

$$\ddot{Q}_i(\mathbf{k}) + \omega_i^2(\mathbf{k})Q_i(\mathbf{k}) = 0. \tag{4.4.38}$$

We can see that our lattice can be regarded as a sum of independent harmonic oscillators. The solution to above equation is

$$Q_i(\mathbf{k},t) = A_i(\mathbf{k})\left(e^{-i\omega_i(\mathbf{k})t + i\delta_i^-(\mathbf{k})} + e^{i\omega_i(\mathbf{k})t + i\delta_i^+(\mathbf{k})} \right). \tag{4.4.39}$$

We assume that amplitudes $A_i(\mathbf{k})$ are real. Due to requirement (4.4.31) the otherwise arbitrary phases must yield

$$\delta_i^-(-\mathbf{k}) = -\delta_i^+(\mathbf{k}) \tag{4.4.40a}$$
$$\delta_i^+(-\mathbf{k}) = -\delta_i^-(\mathbf{k}). \tag{4.4.40b}$$

We switch to another coding of phases

$$\alpha_i(\mathbf{k}) = \frac{\delta_i^+(\mathbf{k}) - \delta_i^-(\mathbf{k})}{2} \tag{4.4.41a}$$

$$\beta_i(\mathbf{k}) = \frac{\delta_i^+(\mathbf{k}) + \delta_i^-(\mathbf{k})}{2}. \tag{4.4.41b}$$

$\alpha_i(\mathbf{k})$ is an even function of $\mathbf{k}$ while $\beta(\mathbf{k})$ is odd. The transformation allows us to write

$$Q_i(\mathbf{k},t) = A_i(\mathbf{k})e^{i\beta_i(\mathbf{k})} \cos\left(\omega_i(\mathbf{k})t + \alpha_i(\mathbf{k})\right). \tag{4.4.42}$$

We adopt now simply Boltzman statistic to estimate A's. According to *equipartition*

theorem we get that each quadratic degree of freedom in Hamiltonian accumulates energy

$$\frac{1}{2}k_{\mathrm{B}}T. \tag{4.4.43}$$

Free harmonic oscillator has two such degrees of freedom while having energy

$$\frac{m\omega^2 A^2}{2}, \tag{4.4.44}$$

so we see that the amplitude of the mode is

$$A_i(\mathbf{k}) = \left(\frac{2k_{\mathrm{B}}T}{m}\right)^{1/2}\frac{1}{\omega_i(\mathbf{k})}. \tag{4.4.45}$$

Let us substitute now the solution (4.4.42) into our expression for kinetic energy (4.4.34)

$$K = \frac{mN\Omega}{2}\int_{\Xi} d^2\mathbf{k}\left(\omega_1^2 A_1^2 \cos^2(\omega_1 t + \alpha_1) + \omega_2^2 A_2^2 \cos^2(\omega_2 t + \alpha_2)\right). \tag{4.4.46}$$

K is a function of time. The time average is defined as

$$\langle f \rangle_t = \lim_{T\to\infty}\frac{1}{T}\int_0^T f(t)dt. \tag{4.4.47}$$

Recalling that $\langle \cos^2(\omega t + \varphi) \rangle_t = \frac{1}{2}$ and utilizing eq. (4.4.45) we get

$$\langle H \rangle_t = \frac{mN\Omega}{2}\int_{\Xi} d^2\mathbf{k}\frac{1}{2}\left(\omega_1^2 A_1^2 + \omega_2^2 A_2^2\right) = Nk_{\mathrm{B}}T, \tag{4.4.48}$$

what is exactly what we would expect from equipartition theorem.

Furthermore, we would expect, that some kind of ergodic theorem should hold indeed, under some assumptions made upon phases $\alpha_i(\mathbf{k})$. Since $\mathbf{k}$ is in fact discrete variable we can enumerate α's, let say that their number is S. Now we can arrange these phases into vector and let us denote the set of these vectors as $\aleph$

$$\boldsymbol{\alpha} \in [0, 2\pi]^S = \aleph \tag{4.4.49}$$

and the probability of the given realization of phases as $\varpi(\boldsymbol{\alpha})$. Ensemble average may be constructed as follows

$$\langle f \rangle_e = \int_{\aleph} d^S\boldsymbol{\alpha} f(\boldsymbol{\alpha})\varpi(\boldsymbol{\alpha}). \tag{4.4.50}$$

When we calculate ensemble average of kinetic energy $\langle K \rangle_e$ it appears that we can recover

result (4.4.48) only when the phases are independent, i.e. uniformly distributed over $\aleph$

$$\varpi(\boldsymbol{\alpha}) = \frac{1}{(2\pi)^S}.$$ (4.4.51)

The same conclusion can be drawn for any other observable. We can regard this result as analogue to molecular chaos assumption introduced in Chapter 1.

4.4.3 Triangular lattice case

As a specific example we consider now triangular lattice with nearest neighbors harmonic interactions, specified simply by a spring with the constant κ, Figure 4.12.
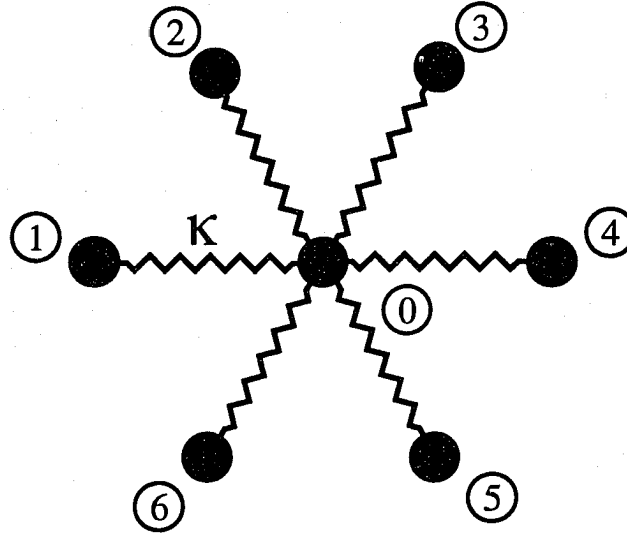
Figure 4.12: For hexagonal lattice with nearest neighbors interactions there are only six terms which contribute to the dynamical matrix, i.e. there are only six terms in the expression for total potential energy that depend explicitly on the position of zeroth atom. They were marked symbolically with springs ∿∿∿.

Let us try to calculate dynamical matrix (4.4.23) for such a case. The part of potential energy that depends on the position of the arbitrarily chosen zeroth atom is

$$\tilde{\Phi} = \tilde{\Phi}_0 + \frac{\kappa}{2} \sum_{s=1}^{6} (\hat{\boldsymbol{\rho}}_i \cdot (\mathbf{u}_s - \mathbf{u}_0))^2,$$ (4.4.52)

where the summation goes over nearest neighbors of zeroth atom and directions of nearest

neighbours $\hat{r}_i$ are given by

$$\hat{\boldsymbol{\rho}}_1 = (0, -1), \tag{4.4.53a}$$

$$\hat{\boldsymbol{\rho}}_2 = \left(-\sqrt{3}, 1\right)/2, \tag{4.4.53b}$$

$$\hat{\boldsymbol{\rho}}_3 = \left(\sqrt{3}, 1\right)/2, \tag{4.4.53c}$$

$$\hat{\boldsymbol{\rho}}_4 = (0, 1), \tag{4.4.53d}$$

$$\hat{\boldsymbol{\rho}}_5 = \left(\sqrt{3}, -1\right)/2, \tag{4.4.53e}$$

$$\hat{\boldsymbol{\rho}}_6 = \left(-\sqrt{3}, -1\right)/2. \tag{4.4.53f}$$

The components of dynamical matrix (4.4.23) read ($\mathbf{k} = (k_1, k_2)$)

$$D_{11} = -3\kappa\left(-1 + \left(\sqrt{3}\sqrt{3}\pi k_1\right)\cos\left(\pi k_2\right)\right), \tag{4.4.54a}$$

$$D_{12} = D_{21} = \sqrt{3}\kappa\left(\sqrt{3}\pi\sqrt{3}\pi k_1\right)\sin\left(\pi k_2\right), \tag{4.4.54b}$$

$$D_{22} = -\kappa\left(-3 + \cos\left(\sqrt{3}\pi k_1\right) + 2\cos\left(2\pi k_2\right)\right). \tag{4.4.54c}$$

What will happen now is sometimes referred to as *Debye* or *long wave approximation*. We will assume that only relatively long wave lengths are important for the problem: our aim is to calculate the distortion of the lattice. $\omega(\mathbf{k})$ is in general increasing function of k and hence, according to (4.4.45), amplitudes of waves with large k are suppressed. I do not quote results of calculations of the eigensystem of D in full, instead I give first order approximation, suitable for small k_1 and k_2. Eigenvalues are

$$\omega_1^2(\mathbf{k}) = \frac{3\pi^2}{2}\frac{\kappa}{m}\mathbf{k}^2 = s_1^2\mathbf{k}^2, \tag{4.4.55a}$$

$$\omega_2^2(\mathbf{k}) = \frac{9\pi^2}{2}\frac{\kappa}{m}\mathbf{k}^2 = s_2^2\mathbf{k}^2 \tag{4.4.55b}$$

and corresponding eigenvectors

$$\hat{e}_1(\mathbf{k}) = i\hat{\mathbf{k}} \qquad \text{(longitudinal waves)}, \tag{4.4.56a}$$

$$\hat{e}_2(\mathbf{k}) = i\hat{\mathbf{q}} \qquad \text{(transverse waves)} \tag{4.4.56b}$$

where $\hat{\mathbf{q}}$ is a unit vector perpendicular to the direction $\hat{\mathbf{k}}$ of the wave vector. The imaginary unit was added to fulfill the symmetry requirement (4.4.27).

It can be noted that the lattice is anisotropic – the velocity of sound s_i depends on the polarization of elastic wave. Since we are going to obtain only qualitative results we discard this property and assume that it is legitimate to use some kind of average, or global, velocity of sound s

$$\omega_1(\mathbf{k}) = \omega_2(\mathbf{k}) = sk. \tag{4.4.57}$$

Our first Brillouin zone is hexagon, but we will approximate it simply with circle of the same area and radius given by

$$k_0 = (\pi\Omega)^{-1/2}.$$ (4.4.58)

Let it be noted that for small values of $\mathbf{k}$, i.e. for long wavelengths, directions of polarizations are parallel or perpendicular to direction of propagation. Similarly, the dispersion relation is linear. This is not the case when we do not make any approximations. The presented equations describe properly long waves. Our formalism resembles classical electromagnetic field in vacuum, except for the fact that that our $\mathbf{k}$'s are constrained to Ξ (we could call it EM theory with cutoff k_0).

4.4.4 Calculations of κ

We must first calculate the average of the following two sums

$$\sigma_i' = \frac{1}{N} \sum_{l \in \mathcal{L}} \Delta\mathbf{u}_{il} \cdot \hat{\mathbf{r}}_i$$ (4.4.59a)

$$\sigma_i'' = \frac{1}{N} \sum_{l \in \mathcal{L}} (\Delta\mathbf{u}_{il} \cdot \hat{\mathbf{r}}_i)^2,$$ (4.4.59b)

where, according to (4.4.30),

$$\Delta\mathbf{u}_{il} = \sqrt{N}\Omega \int_{\Xi} d^2\mathbf{k}(Q_1(\mathbf{k},t)\hat{\mathbf{e}}_1(\mathbf{k}) + Q_2(\mathbf{k},t)\hat{\mathbf{e}}_2(\mathbf{k})) \times$$
$$\times e^{2\pi i \mathbf{k} \cdot \mathbf{R}_l}\left(e^{2\pi i \mathbf{k} \cdot \hat{\mathbf{r}}_i} - 1\right).$$ (4.4.60)

Using eq. (4.4.29) we get immediately

$$\sigma_i' = 0.$$ (4.4.61)

The latter sum is a bit more complicated

$$\sigma_i'' = \frac{1}{N} \sum_{l \in \mathcal{L}} N\Omega^2 \iint_{\Xi \times \Xi} d^2\mathbf{k} d^2\mathbf{q}(Q_1(\mathbf{k},t)\hat{\mathbf{e}}_1(\mathbf{k}) + Q_2(\mathbf{k},t)\hat{\mathbf{e}}_2(\mathbf{k})) \cdot \hat{\mathbf{r}}_i \times$$
$$\times (Q_1(\mathbf{q},t)\hat{\mathbf{e}}_1(\mathbf{q}) + Q_2(\mathbf{q},t)\hat{\mathbf{e}}_2(\mathbf{q})) \cdot \hat{\mathbf{r}}_i \times$$
$$\times e^{2\pi i (\mathbf{k}+\mathbf{q}) \cdot \mathbf{R}_l} \times$$
$$\times \left(e^{2\pi i \mathbf{k} \cdot \hat{\mathbf{r}}_i} - 1\right)\left(e^{2\pi i \mathbf{q} \cdot \hat{\mathbf{r}}_i} - 1\right),$$ (4.4.62)

but it reduces (again (4.4.29)) to

$$\Omega \int_{\Xi} d^2\mathbf{k} |(Q_1(\mathbf{q},t)\hat{\mathbf{e}}_1(\mathbf{q}) \cdot \hat{\mathbf{r}}_i + Q_2(\mathbf{q},t)\hat{\mathbf{e}}_2(\mathbf{q}) \cdot \hat{\mathbf{r}}_i)|^2 \times$$
$$\times 2(1 - \cos(2\pi\mathbf{k} \cdot \hat{\mathbf{r}}_i h)). \tag{4.4.63}$$

Now we utilize (4.4.42), (4.4.45) and our simplification of first Brillouin zone (φ stands for the angle netween $\mathbf{k}$ and $\hat{\mathbf{r}}_i$)

$$\sigma_i'' = \frac{2k_B T \Omega}{ms^2} \int_0^{2\pi} d\varphi \int_0^{k_0} k dk \frac{2\Upsilon}{k^2} (1 - \cos(2\pi ka \cos\varphi)), \tag{4.4.64}$$

where Υ is

$$\Upsilon \equiv \cos^2(skt + \alpha_1(\mathbf{k})) \cos^2\varphi$$
$$+ \cos^2(skt + \alpha_2(\mathbf{k})) \sin^2\varphi$$
$$+ 2\cos(skt + \alpha_1(\mathbf{k})) \cos(skt + \alpha_2(\mathbf{k})) \cos\varphi \sin\varphi \cos(\Delta\beta) \tag{4.4.65}$$

and

$$\Delta\beta = \beta_1(\mathbf{k}) - \beta_2(\mathbf{k}). \tag{4.4.66}$$

$$\langle\sigma_i''\rangle_e = \langle\sigma_i''\rangle_t = \frac{2k_B T \Omega}{ms^2} \int_0^{2\pi} d\varphi \int_0^{k_0} dk \frac{1}{k} (1 - \cos(2\pi kh \cos\varphi))$$
$$= \frac{2k_B T \Omega}{ms^2} \pi^3 k_0^2 h^2 \tilde{\kappa}, \tag{4.4.67}$$

where

$$\tilde{\kappa} = f^*(-\pi^2 k_0^2 h^2) \approx 7.406467 \tag{4.4.68}$$

and $f^*(x)$ is one of the generalized hypergeometric functions

$$f^*(x) = F_3^{-2}((1,1),(2,2,2),x). \tag{4.4.69}$$

Please note the lack of the dependence on i, i.e. on the direction of the throat. The change in the inverse of geometrical modifier κ, given by (4.4.10), reads

$$\kappa = \frac{2\pi^2}{3\sqrt{3}} \frac{\tilde{\kappa}\gamma_M}{\epsilon^2(1-\epsilon)} \frac{k_B T}{ms^2}. \tag{4.4.70}$$

Now we can calculate geometrical modifier for the disordered lattice (4.4.11). Within assumptions made, the thermal disorder always leads to the decrease of the drag.

The above expression is particularly simple in the case of Miyagi model, since it has characteristic quadratic dependence on the separation of the two cylinders constituting

the throat. In any other case the calculations would be much more difficult.

We can notice in the equation (4.4.70) the competition of two energy like-expressions: ms^2, the elastic energy associated with deformation of crystal and $k_{\mathrm{B}}T$, the energy of thermal fluctuations. Neither temperature here, not the elastic constant, determining s, have any direct physical meaning, they just allow us to control the presented model of disorder. Non-zero temperature means that the atoms are vibrating, and as it has already been mentioned it always leads to decrease of the drag. Large stiffness of material (yielding large s) causes the displacements due to thermal motions to be small.

4.5 Summary

Investigation of flows in constrained geometries brought us several advantages. First of all, by introduction of geometrical modifier function, (4.3.9), we could finally justify the claim, that for small Reynolds numbers the drag can be regarded as a function of the topology of the system and the single dimensionless parameter ϵ. We could see where the topology enters the game and how to deal with it.

Another outcome of studying regular media was more reliable model of throat. To gauge a constant in Miyagi model (4.1.9) we matched electric and exact solutions. The outcome of these studies was an observation that flows in regular lattices appeared to have series of non-trivial symmetries. 2D periodic media are not only isotropic (providing the underlying lattice has sufficient symmetry), but also highly homogeneous. The latter observation was called uniform gradient hypothesis (equation (4.3.6)); we will try to use it also for irregular networks.

As pointed in [37], Voronoi diagram for a set of discs interacting via hard-core potentials may be regarded as "disordered" honeycomb lattice – it seemed to be instructive to investigate the influence of disorder on the drag force. As the first toy model of disorder we shook the triangular lattice by means of artificially introduced phonons. This exercise was primarily meant to understand how the impact of disorder should be (in general) incorporated into the geoemtrical modifier.

In the next two chapters we will try to learn how to incorporate the more realistic model of disorder into the formalism of hydraulic networks.

Chapter 5

Stochastic geometry

Previous chapter brought us some insight into the flow in regular porous media; our main concern is nevertheless simultaneous flow of particles and fluid. This requires in general the solution of Navier-Stokes equation with dynamic boundary conditions on the surface of the bodies. The formalism was presented in the Section 1.3; there is no method (neither analytical nor numerical) that would be able to exactly solve the presented problem. For example Batchelor's solution, discussed in Section 2.4.1, utilizes model of spatial correlations between flowing spheres, which is completely unaffected by the flow field – simply it is assumed that the spheres cannot overlap. In the first approximation it seems to be justified to retain this assumption and calculate the drag averaged over some artificially constructed ensemble of spheres' (discs') configurations. It might be regarded as infinite granular density assumption – motion of grains does not depend on the motion of fluid and it is driven solely by the collisions between grains. We can recall that the the same assumption of spatial homogeneity was made by Batchelor in reference [6]. We reuse it here in the context of hydraulic networks. In Chapter 7 a possible way of putting the fluid dynamics back into the system will be presented.

5.1 Uniform gradient hypothesis

The major problem with the application of hydraulic network method lies in the fact that we are not able to deduce the net conductance of the network solely from the knowledge of the values of resistors. The way in which they are connected, i.e. the topology of the network, is crucial when determining the total conductance. We were able to overcome this issue in case of regular lattice taking advantage of the periodicity and high symmetry of the regular lattices. The uniform gradient assumption is a plausible, but still heuristic, way of doing the same in the disordered case. At the present moment, without such a simplification, we are helpless.

The idea of uniform gradient was introduced in the previous chapter, where we noted that for (at least some) regular lattices so called uniform gradient property held. Resistors in such a lattice are independent. It means that if we disconnect them and set the potentials in their endings according to mean field rule, (4.3.6), neither the power

produced nor the total resistance will change with comparison to original lattice and the current will be automatically conserved.

Let us first apply the idea for a single resistor. What we need is a joint probability, $p(g, v)$, that the resistor has a conductance g and the pressure drop across it is v. Let us denote the number of throats per unit area as λ. The total power dissipated in the system is

$$P_{tot} = LM\lambda \int\!\!\int_0^\infty gv^2 p(g, v) dg dv, \qquad (5.1.1)$$

where L is the length of the system and M is its width. The net conductance of the system can be calculated as

$$g_{tot} = \frac{P_{tot}}{(GL)^2}, \qquad (5.1.2)$$

where G is the macroscopic pressure gradient in the system. With aid of equation (3.1.22) we can calculate β as

$$\beta = \epsilon^2 \frac{HM}{L} \frac{(GL)^2}{LM\lambda \int\!\!\int_0^\infty gv^2 p(g, v) dg dv} = \epsilon^2 \frac{G^2}{\lambda} \frac{1}{\int\!\!\int_0^\infty g'v^2 p(g', v) dg' dv}, \qquad (5.1.3)$$

where g' stands for conductance per unit height of the throat. All the quantities on the right hand side are intensive. The above expression is exact, but useless, unless we can give $p(g', v)$ explicitly. Now comes the simplification and we write

$$p(g', v) = \tilde{p}(g', l) Gl \cos \varphi, \qquad (5.1.4)$$

where l is the length of the resistor (the length of the corresponding Voronoi edge) and φ the angle that the resistor makes with the macroscopic direction of flow. The simplification encompasses two steps. First, we related the topological property (pressure drop v) to spatial properties of the throat and second, we postulated simple form for this dependence (in the spirit of uniform gradient). Plugging this expression into equation (5.1.3) yields

$$\beta = \frac{\epsilon^2}{\lambda} \frac{2}{\langle g'l^2 \rangle}. \qquad (5.1.5)$$

Once again we have convinced ourselves that β is purely geometrical quantity; the statement is true even without any approximations.

In general we could include the impact of the correlations trying to investigate not a single resistors, but larger structures immersed in the pressure field of constant gradient, Figure 5.1. The pressure in the peripheral nodes is set using uniform gradient assumption, the pressure in the internal nodes results from the flow of current. I could be expected that having taken the average over sufficiently large cluster, the permeability of the network could be reproduced with an arbitrary accuracy. In the case of any shape and size of the
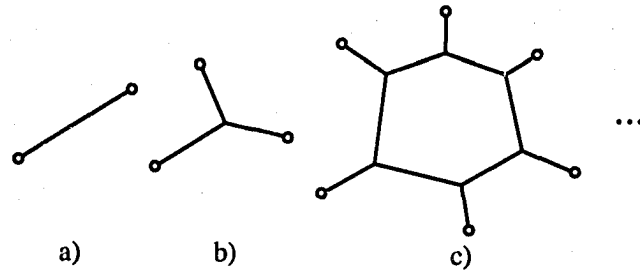
Figure 5.1: Structures that might be considered in the uniform gradient approach. The lines represent resistors; the empty circles o are the nodes in which the pressure is set according to mean field. The pressure in the rest of the nodes is such that the flow in them is conserved.

cluster the calculations proceed in the similar way.

The current chapter has the following structure. First, I discuss possible models of random points arrangements (with substantial focus on the models preserving hard core distance between points) and subsequently several methods of their statistical description. Next, a more formal introduction of Voronoi/Delaunay tessellations is provided and supplemented with the methods of their stochastic analysis. The methods presented should, in principle, allow us calculation of the probability $\tilde{p}(g', l)$.

5.2 Random point fields

The definitions come form [83, 84]. The notion of point field or point process may be introduced very formally in the language of measure theory; this is not necessary on this stage of the work. We consider only 2D patterns. Random point field is a subset $\varphi = \{\mathbf{x}_n\} \subset \mathbb{R}^2$, with the following two properties

i. φ is *locally finite*, i.e. each bounded subset of $\mathbb{R}^2$ contains only a finite number of the elements of φ,

ii. φ is *simple* what mean that $\mathbf{x}_i \neq \mathbf{x}_j$ if $i \neq j$.

The family of all φ's with the above properties is denoted by $\mathcal{N}$.

One remark. The fascinating use of random point fields is that they may be regarded as patterns (point sets) or as measures. We denote $\varphi(B)$, where B is a Borel set, as the number of points of φ in B and define integral as follows

$$\int_B f(x)\varphi(dx) = \sum_{\mathbf{x}_n \in \varphi} \mathbb{1}_B(\mathbf{x}_n)f(\mathbf{x}_n), \qquad (5.2.1)$$

where the indicator function is

$$\mathbb{1}_B(\mathbf{x}) = \begin{cases} 1 & (\mathbf{x} \in B) \\ 0 & (\mathbf{x} \notin B). \end{cases} \tag{5.2.2}$$

Probability that B contains n points of φ is denoted by $P(\varphi(B) = n)$. $\langle \varphi(B) \rangle$ stands for mean number of points of φ in B and it is called *intensity measure*, $\Lambda(B)$. We treat φ as a random variable.

A point field φ is called homogeneous (or stationary) if φ and the *translated process* $\varphi_\Delta = \{\mathbf{x}_n + \Delta\}$ yields the same probabilities, i.e. $P(\varphi(B) = n) = P(\varphi_\Delta(B) = n)$. Similarly the process is *isotropic* if the rotation of the rotations of the field keep the probability invariant. Random point field we consider will always have these two properties.

If $K \subset \mathbb{R}^2$ is a compact set (closed and bounded) then the *emptiness probability* is defined as

$$\text{void}(K) = P(\varphi(K) = 0). \tag{5.2.3}$$

Second order moment measure $\mu^{(2)}$ denotes the following average

$$\mu^{(2)}(B_1 \times B_2) = \langle \varphi(B_1)\varphi(B_2) \rangle = \left\langle \sum_{\mathbf{x} \in \varphi} \sum_{\mathbf{y} \in \varphi} \mathbb{1}_{B_1}(\mathbf{x}) \mathbb{1}_{B_2}(\mathbf{y}) \right\rangle, \tag{5.2.4}$$

while the *factorial moment measure* $\alpha^{(2)}$ stands for

$$\alpha^{(2)}(B_1 \times B_2) = \langle \varphi(B_1)(\varphi(B_2) - 1) \rangle = \left\langle \sum_{\mathbf{x} \in \varphi} \sum_{\substack{\mathbf{y} \in \varphi \\ \mathbf{x} \neq \mathbf{y}}} \mathbb{1}_{B_1}(\mathbf{x}) \mathbb{1}_{B_2}(\mathbf{y}) \right\rangle. \tag{5.2.5}$$

Often $\alpha^{(2)}$ has density function (*second order product density*):

$$\alpha^{(2)}(B_1 \times B_2) = \int_{B_1} \int_{B_2} d^2\mathbf{x}_1 d^2\mathbf{x}_2 \rho^{(2)}(\mathbf{x}_1, \mathbf{x}_2). \tag{5.2.6}$$

The last quantity has an infinitesimal interpretation: of B_1, B_2 are two infinitesimally small disjoint Borel sets of volumes dV_1, dV_2 and if $\mathbf{x}_1 \in B_1$ and $\mathbf{x}_2 \in B_2$ then

$$\rho^{(2)}(\mathbf{x}_1, \mathbf{x}_2) dV_1 dV_2 = \lambda^2 dV_1 dV_2 \tag{5.2.7}$$

stands for the number of processes that place points both in B_1 and B_2. Or, when infinite and ergodic processes are considered, number of pairs of points in φ from which one lies in B_1 and the second in B_2.

Quantity $g_2(\mathbf{x}_1, \mathbf{x}_2) = \rho^{(2)}(\mathbf{x}_1, \mathbf{x}_2)/\lambda^2$ is called *pair correlation function*. The higher order correlation functions g_n are defined in such a way that

$$\lambda^n g_n(\mathbf{x}_1, \mathbf{x}_2, \dots \mathbf{x}_n) d^2\mathbf{x}_1 d^2\mathbf{x}_2 \dots d^2\mathbf{x}_n \tag{5.2.8}$$

stands for the number of processes that put points in elements $d^2\mathbf{x}_m$ centered at $\mathbf{x}_m$ ($m = 1, 2, \ldots n$).

5.2.1 Poisson point field

The prototype of all point processes is *Poisson point field* defined by its two fundamental properties:

    i. if $B_1 \ldots B_n$ are disjoint Borel sets, $\varphi(B_1) \ldots \varphi(B_n)$ are stochastically independent,

    ii. for any bounded Borel set $\varphi(B)$ has Poisson distribution

$$P(\varphi(B) = k) = \frac{\lambda(L(B))^k}{k!} \exp(-\lambda L(B)), \qquad (5.2.9)$$

    where λ is called *point density*, i.e. number of points per unit volume, and L is the Lebesgue measure of B.

In the case of Poisson point process points are scattered completely randomly, they do not interact with each other. We have

$$\Lambda(B) = \langle \varphi(B) \rangle = \lambda L(B). \qquad (5.2.10)$$

We immediately see that

$$\text{void}(B) = \exp\left(-\lambda L(B)\right). \qquad (5.2.11)$$

All correlation functions, g_n, like in the case of an ideal gas, are identically equal to 1.

5.2.2 Hard-core point processes

The interactions of grains in the fluidized system may be very well described by means of hard-core pairwise potential with range D equal to the diameter of the disc/sphere. Therefore we should primarily investigate properties of the point processes preserving this minimal distance. Let us note that the problem immediately starts to complicate. D introduces the second ($1/\sqrt{\lambda}$ being the first one) length scale; these too scales are usually not separated, especially for dense systems.

Matérn processes & SSI

There are three types of hard-core point fields, which are constructed by specially constructed inhibition rule: Matérn process type I & II ([64]) and simple sequential inhibition (SSI). In all of these processes points are scattered randomly (Poisson field) without preserving HC distance. At the time of scattering each point receives a birthmark t, representing time of birth. The differences in spheres' inhibition algorithms are presented in the Figure 5.2.

    Let us suppose that only the four points were scattered. Point D will be retained (in all types of processes) regardless of its birthmark, since it does not overlap with anything.
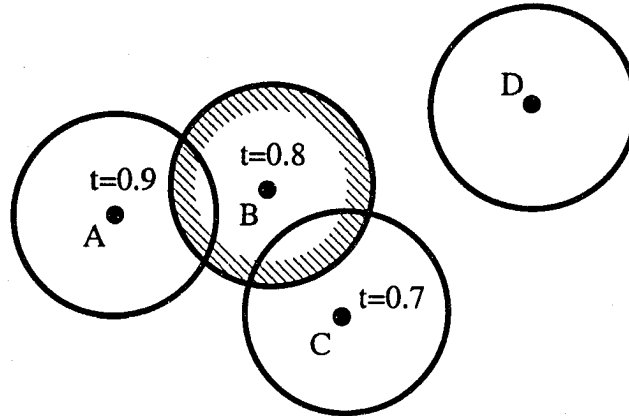
Figure 5.2: Idea of inhibition algorithms in Matérn and SSI processes. Small black dots represent centers of the discs, the circles are excluded regions. Shaded circle is a "ghost area" in type II process. Please refer to the description in the text.

In the Matérn type I process all intersecting discs are removed (A, B and C). In the type II process if two discs overlap only the one with the lower birthmark is retained, hence we need to remove both A (because of B) and B (because of C): only C and D survive. We see that the latter schema introduces "ghost areas" (B). Recognizing it leads to SSI: if we removed point B right after its birth (because of the presence of C) it would not interfere with A and A would be retained. This is the most natural method of creating hard-core point fields. Immediately after the new point is added we check if it overlaps with the points already present and if this is the case we remove it instantly. In the other case we let it be.

The densest possible packing of discs in 2D is the traingular lattice mentioned in Chapter 4. Combining (4.2.49) and (4.2.50) we see that that minimal void volume is as low as

$$\epsilon_{cp}^{2D} = 1 - \frac{\pi}{2\sqrt{3}} \approx 0.0931. \tag{5.2.12}$$

Random packings are usually ill defined in 2D, since they can bear similarities to triangular lattice; we will come back to this problem in the next section, but they may yield ϵ lower than 0.3. The three mentioned processes bring much larger void volumes. According to [83], the intensity for the Matérn type II is

$$\frac{1 - \mathbb{e}^{-\lambda \pi D^2}}{\pi D^2}, \tag{5.2.13}$$

where λ is the intensity of the underlying Poisson point process. If we let λ approach infinity we see that the minimal void volume for tis process is $\frac{3}{4}$. The type I process leads to even lower concentrations. The lowest void volume for SSI was found numerically

to be 0.587, [92]. Although we are in general interested in much denser discs systems I believed that the models presented here were important since there is a possibility of their analytical study. There exists analytical form for the pair correlation function for Matérn type II process. In the limiting case of $\lambda \to \infty$

$$g(r) = \begin{cases} 0 & (r \le D) \\ \frac{2\pi D^2}{\Gamma(r)} & (r > D), \end{cases} \tag{5.2.14}$$

where

$$\Gamma(r) = 2\pi D^2 - 2D^2 \arccos\left(\frac{r}{2D}\right) - \frac{r}{2}\sqrt{4D^2 - r^2}. \tag{5.2.15}$$

The pair correlation functions for some interesting cases are presented in the Figure 5.3.
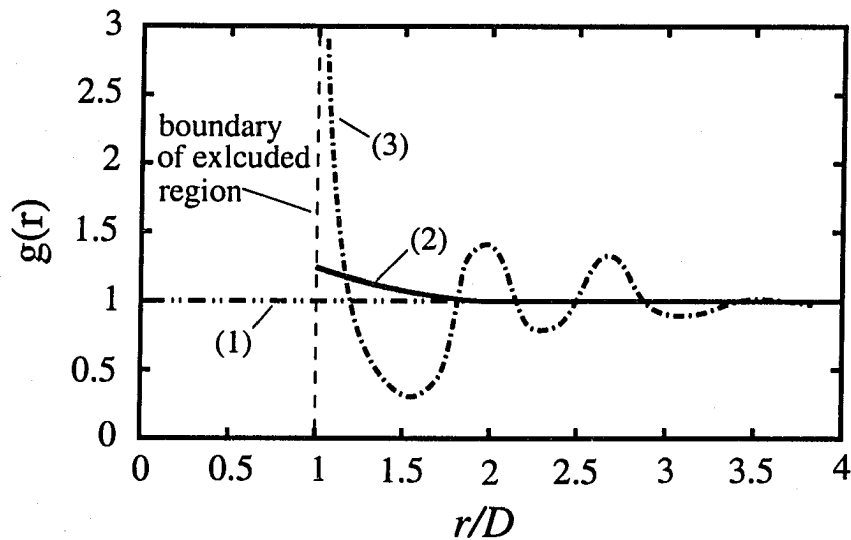
Figure 5.3: Pair correlation functions $g(r)$ for several points patterns discussed. (1) Poisson process (ideal gas); (2) Matérn type II given by (5.2.14); (3) dense random packing. The last shape is very characteristic for processes with repulsive hardcore interactions. Figure was adapted from [83].

Gibbs hard-core process

Gibbs processes are simply configurations of gas atoms interacting with the given pair potential. Liquids of hard discs were studied thoroughly, both numerically and analytically. Despite the apparent simplicity of interactions they express rich behavior; see [62] for references. The systems is believed to undergo phase transition. Around $\epsilon = 0.29$ fluid (gaseous) phase changes into "hexatic-phase" possessing quasi-long-range bond orientation but no long-range translational order. For even lower void volumes system has

to exists in the solid phase, with distinct peaks in the Fourier spectrum.

The pair correlation function for dense systems of spheres features not only "excluded region" for $r < D$, but also high peak at the edge of it (Figure 5.3); presence of such peaks is always a sign of the emergence of order in the system; we could notice it even for the very dilute Matérn process. After a minimum the second peak occurs at the distance $2D$, the next is a bit closer than $3D$. Gradually the function reaches its asymptotic value 1, indicating the lack of long-range correlations. The characteristic nearest neighbor peak was substituted by Batchelor with a delta function.

There are several analytic results, which try to approximate $g(r)$ for the HC case, like BGY approximation or Percus-Yevick theory, please refer to [42].

Since the HC model can yield much higher densities I decided to use this model in the numerical simulations.

5.2.3 Kirkwood approximation

Unfortunately there is no easy way to calculate higher order correlation-functions. It was suggested [58] that they might be obtained by means of pair correlation functions; this is so called *Kirkwood approximation*:

$$g_{123} \cong g_{12}g_{13}g_{23}, \tag{5.2.16}$$

with the notation $g_{lk} \equiv g(\mathbf{x}_l, \mathbf{x}_k)$. The above relation is exact for the case where there would be no 3-body correlation; this is not true even if the potential is pairwise. Higher functions may be, in general, approximated in the same manner.

5.3 Introduction to Voronoi diagrams

The comprehensive review of properties and applications of Delaunay and Voronoi diagrams can be found in [69] and the following definitions and theorems originate there. Let $\mathcal{G} = \{\mathbf{g}_1, \mathbf{g}_1, \ldots, \mathbf{g}_n\} \subset \mathbb{R}^2$, $3 \le n < \infty$, be a finite simple point field, i.e. $\mathbf{g}_i \ne \mathbf{g}_j$ for $i \ne j$, $i, j \le n$. $\mathbf{g}_i$'s are called *generators*. The *Voronoi polygon (region)* associated with generator $\mathbf{g}_i \in \mathcal{G}$ is denoted by $V(\mathbf{g}_i)$ and equals

$$V(\mathbf{g}_i) = \{\mathbf{x} : \|\mathbf{x} - \mathbf{g}_i\| \le \|\mathbf{x} - \mathbf{g}_j\|, j \ne i, j \le n\}. \tag{5.3.1}$$

The set of Voronoi polygons

$$\mathcal{V}(\mathcal{G}) = \{V(\mathbf{g}_i) : \mathbf{g}_i \in \mathcal{G}\} \tag{5.3.2}$$

is called *Voronoi diagram* induced by the set of generators $\mathcal{G}$.

The boundary $\partial V(\mathbf{g}_i)$ may consist of line segments, half lines or lines. If $e(\mathbf{g}_i, \mathbf{g}_j) = V(\mathbf{g}_i) \cap V(\mathbf{g}_j) \ne \emptyset$ and it is not an empty set, then $e(\mathbf{g}_i, \mathbf{g}_j)$ is called *Voronoi edge*. If $e(\mathbf{g}_i, \mathbf{g}_j)$ is a Voronoi edge, generators $\mathbf{g}_i$ and $\mathbf{g}_j$ are *adjacent*. $\mathcal{E}$ stands for the set of edges. The end point of Voronoi edge is called *Voronoi vertex*; their set is denoted by $\mathcal{Q}$.

Let us denote by $\mathcal{G}'_i$ set of generators, whose polygons share the Voronoi vertex $q_i \in \Omega$. *Delaunay region* is defined as

$$T_i = \left\{ x : x = \sum_{g_j \in \mathcal{G}'_i} l_j g_j, \text{ where } \sum_j l_j = 1, \; l_j \geq 0 \right\} \tag{5.3.3}$$

and

$$\mathcal{D} = \{T_i\} \tag{5.3.4}$$

is called *Delaunay pretriangulation*. In the same manner as before we define *Delaunay edges* and *vertices*. Delaunay edges connect adjacent generators.

The example of Voronoi/Delaunay diagram for ten points was presented in the Figure 5.4. The physical significance of the Voronoi diagram had been already explained in Section 3.3.
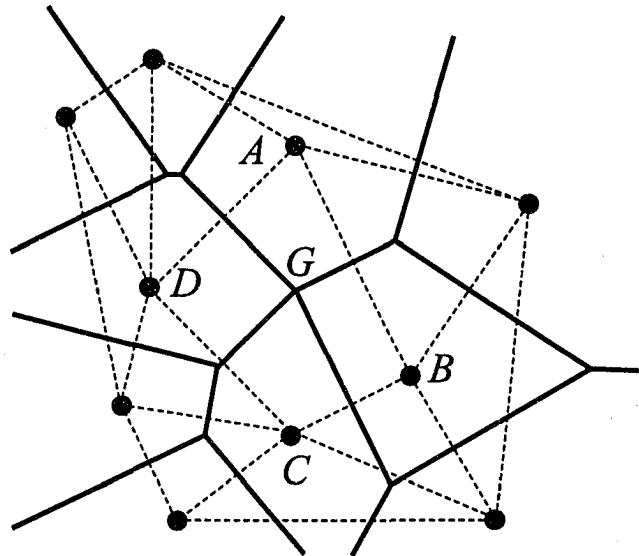
Figure 5.4: Example of Voronoi and Delaunay diagram for 10 points. Vertex G is called degenerated since it has rank larger than 3.

If the number of edges originating in every Voronoi vertex is exactly 3, the diagram is called non-degenerated. In this case every Delaunay region is a triangle and the pretriangulation is simply a *triangulation*. In the other case some Delaunay regions are polygons with more than three edges and they may be divided into triangles to produce triangulation, but this operation is not unique. Such situation happened in the presented example: vertex G is degenerated and the quadrangle $ABCD$ may be divided into trian-

gles by adding Delaunay edge AC or BD. The extracted Voronoi and Delaunay diagrams were presented in the Figures 5.5ab respectively.

Every Voronoi and associated Delaunay diagram posses the following properties:

(P1) A Voronoi edge is part of perpendicular bisector of the two adjacent generators constituting this edge.

(P2) A Voronoi vertex is the center of the circle circumscribing the generators, whose regions are adjacent to that vertex.

(P3) The circle from property (P2) contains no generators in its interior. From this it follows that all Delaunay regions can be circumscribed by a circle and this circle is empty. This property is called *empty circle law*.

(P4) Voronoi region always contains the corresponding generator in its interior. If the the region is finite it is a convex polygon.

(P5) Voronoi diagram partitions the plane into as many region as the generators.

(P6) Two Voronoi regions do not share two or more edges as a common part of their boundaries.

Furthermore if we assume that the diagram is non-degenerated, $n \geq 3$ and that not all generators lie on a single straight line we have

(P'7) All Voronoi vertexes have rank exactly 3.

(P'8) All Delaunay regions are triangles.

5.4   Local configurations for Poisson fields

The presented methods were developed by Collins [18] to investigate properties of fluids.

5.4.1   Distribution of Delaunay edges

Let us consider triangle as presented in the Figure 5.6. It is known that the probability that the Delaunay region is not a triangle is 0 for Poisson field. The number of triangles in the 2D field with N points occupying volume V is from the definition (5.2.8)

$$\lambda^3 g_3(\mathbf{x}_1, \mathbf{x}_2, \mathbf{x}_3) d^2\mathbf{x}_1 d^2\mathbf{x}_2 d^2\mathbf{x}_3. \tag{5.4.1}$$

According to the empty circle law, (P3), page 110, such triangle $(\mathbf{x}_1, \mathbf{x}_2, \mathbf{x}_3)$ is Delaunay triangle if the circle γ is devoid of further points. Let us denote this probability by $E(\mathbf{x}_1, \mathbf{x}_2, \mathbf{x}_3)$. Since the fluid is homogeneous and isotropic we can expect that both g_3 and E should be solely functions of (θ, r, s), see Figure 5.6. Let us denote by $\psi(r)$ the density of probability that randomly chosen Delaunay edge has length r. If the average

a)

b)
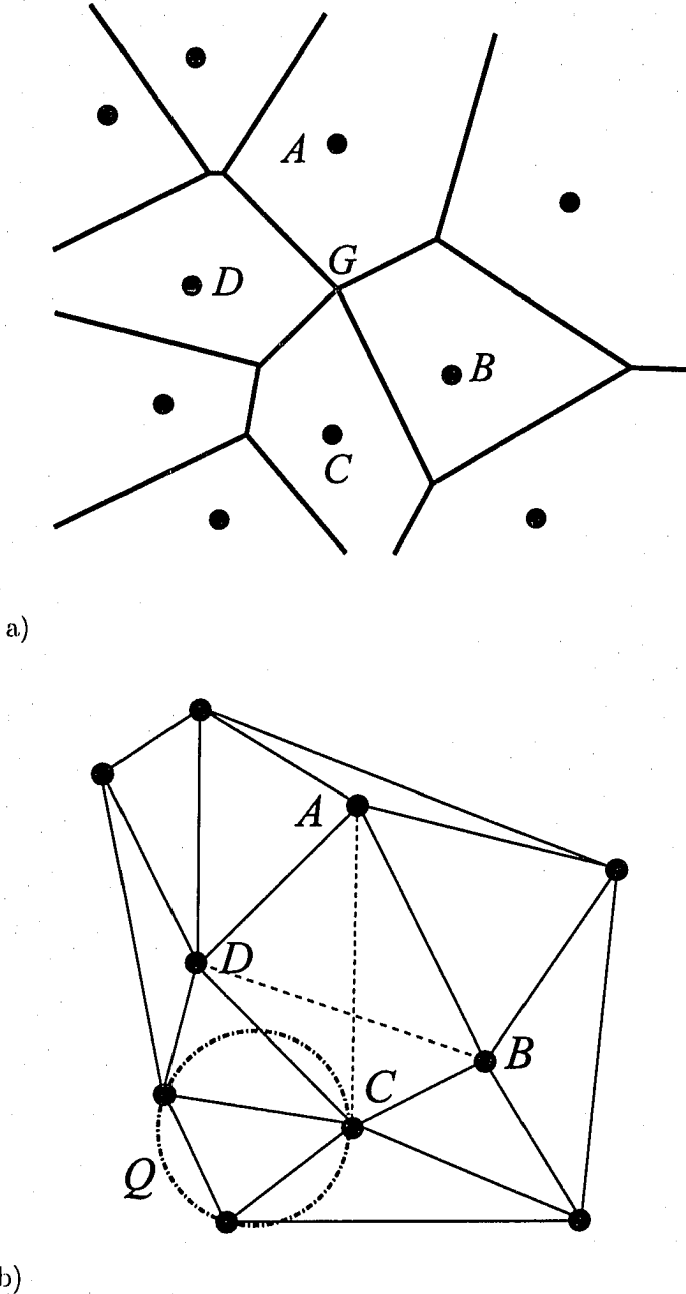
Figure 5.5: Extracted Voronoi and Delaunay diagrams from the presented example. Circle Q circumscribed on every three generators forming Delaunay region contains no generators in its interior.
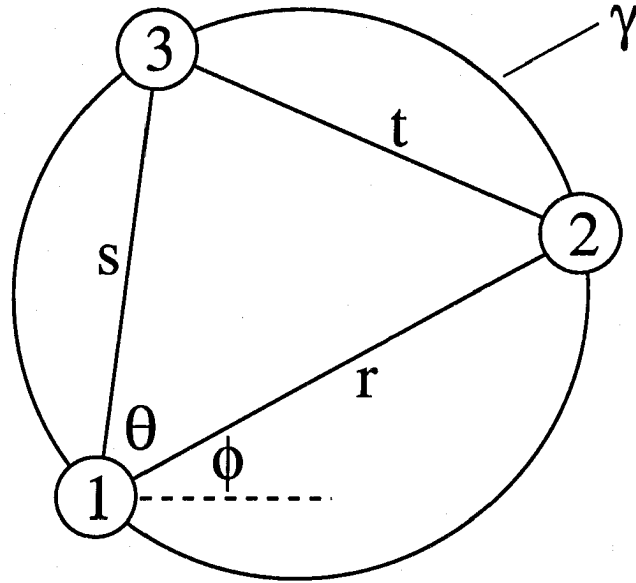
Figure 5.6: Delaunay triangle. The Figure is reproduced from [18].

number of nearest neighbors is q, the number of Delaunay edges with the length in the range $(r, r + dr)$ is

$$qN\psi(r) = \lambda^3 \int d^2\mathbf{x}_1 d^2\mathbf{x}_2 d^2\mathbf{x}_3 g_3(\mathbf{x}_1, \mathbf{x}_2, \mathbf{x}_3) E(\mathbf{x}_1, \mathbf{x}_2, \mathbf{x}_3) \qquad (5.4.2)$$

and the integration is performed over the subset of configuration space for which $\|\mathbf{x}_1 - \mathbf{x}_2\| = r$. If we switch the parameterizations

$$(\mathbf{x}_1, \mathbf{x}_2, \mathbf{x}_3) \longrightarrow (\mathbf{x}_1, \phi, r, \theta, s) \qquad (5.4.3)$$

we obtain the following

$$qN\psi(r) = r\lambda^3 \int_V d^2\mathbf{x}_1 \int_0^{2\pi} d\phi \int_0^\pi d\theta \int_0^\infty s\, ds\, g_3(\theta, r, s) E(\theta, r, s). \qquad (5.4.4)$$

As we have seen for the Poisson field the emptiness probability is (cf. (5.2.11))

$$E(\theta, r, s) = \exp(-\lambda\pi R^2), \qquad (5.4.5)$$

where

$$R = R(\theta, r, s) = \frac{r^2 + s^2 - 2rs\cos\theta}{2\sin\theta} \qquad (5.4.6)$$

is the radius of the circle γ. As shown in [65] q for Poisson field is equal exactly 6. Integration over $\mathbf{x}_1$ and ϕ can be performed immediately and we obtain

$$\frac{3\psi(r)}{\pi\lambda^2 r} = \int_0^\pi d\theta \int_0^\infty s\,ds\,\exp\left(-\rho\pi R^2\right). \qquad (5.4.7)$$

The evaluation of the latter integral will become feasible if we switch the parameterization one more time

$$(\theta, r, s) \longrightarrow (\theta, r, t). \qquad (5.4.8)$$

We must proceed with care, since for acute angles θ the mapping is not 1-1, as shown in the Figure 5.7 and we have ($\theta \le \frac{\pi}{2}$):

$$s_\pm = r\cos\theta \pm \sqrt{t^2 - r^2\sin^2\theta}. \qquad (5.4.9)$$

$r \in (r, r\sin\theta)$ corresponds to s_- while $r \in (r\sin\theta, \infty)$ to s_+. The range $(r\sin\theta, \infty)$ is swept two times for acute θ. In the case of $\theta > \frac{\pi}{2}$ only s_+ is possible and $t \in (r, \infty)$
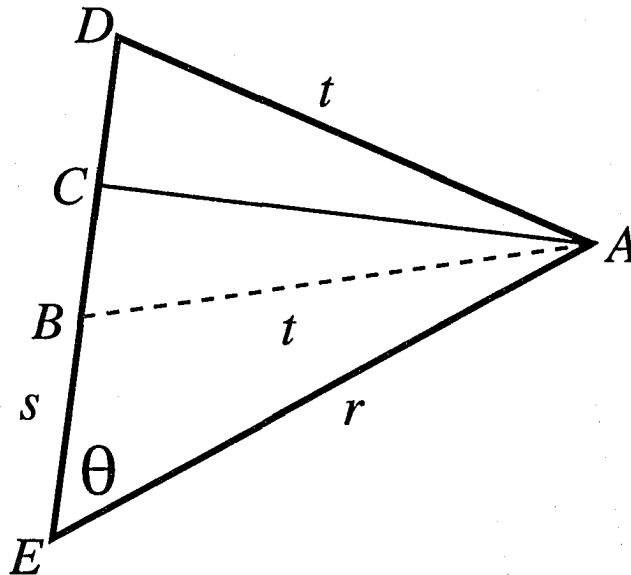
Figure 5.7: Transformation (5.4.8) is not 1-1; for acute angles θ single value of $t = |AB| = |AD|$ corresponds to two values of s: $s_- = |EB|$ and $s_+ = |ED|$.

Jacobian of the transformation is

$$J = \frac{t}{\sqrt{t^2 - r^2\sin^2\theta}}. \qquad (5.4.10)$$

Thus we have

$$\frac{3\psi(r)}{\pi\lambda^2 r} = \int_0^{\pi/2} d\theta \left(\int_{r\sin\theta}^r dt\, s_- J \mathrm{e}^{-\lambda\pi R^2} + \int_{r\sin\theta}^\infty dt\, s_+ J \mathrm{e}^{-\lambda\pi R^2} \right)$$

$$+ \int_{\pi/2}^\pi d\theta \int_r^\infty dt\, s_+ J \mathrm{e}^{-\lambda\pi R^2}$$

$$= \int_0^{\pi/2} d\theta (I_1 + I_2 + I_3) + \int_{\pi/2}^\pi d\theta (I_2 + I_3), \qquad (5.4.11)$$

where

$$I_1 = 2r \int_{r\sin\theta}^r dt\, \cos\theta \frac{t\mathrm{e}^{-at^2/(r^2\sin^2\theta)}}{\sqrt{t^2 - r^2\sin^2\theta}} = r^2 \cos\theta\sin\theta\mathrm{e}^{-a}\sqrt{\frac{\pi}{a}}\, \mathrm{erf}(\sqrt{a}|\cot\theta|), \quad (5.4.12\mathrm{a})$$

$$I_2 = \int_r^\infty dt\, \cos\theta \frac{t\mathrm{e}^{-at^2/(r^2\sin^2\theta)}}{\sqrt{t^2 - r^2\sin^2\theta}} = r^2\cos\theta\sin\theta\frac{\mathrm{e}^{-a}}{2}\sqrt{\frac{\pi}{a}}\, \mathrm{erfc}(\sqrt{a}|\cot\theta|), \qquad (5.4.12\mathrm{b})$$

$$I_3 = \int_r^\infty dt\, t\mathrm{e}^{-at^2/(r^2\sin^2\theta)} = \frac{r^2\sin^2\theta}{2a}\mathrm{e}^{-a/\sin^2\theta}. \qquad (5.4.12\mathrm{c})$$

$$a = \frac{\lambda\pi r^2}{4} \qquad (5.4.13)$$

and the *error* and *complementary error functions* read respectively

$$\mathrm{erf}(x) \equiv \frac{2}{\pi} \int_0^x \mathrm{e}^{-t^2} dt, \qquad (5.4.14\mathrm{a})$$

$$\mathrm{erfc}(x) \equiv 1 - \mathrm{erf}(x). \qquad (5.4.14\mathrm{b})$$

Now we obtain

$$\frac{3\psi(r)}{\pi\lambda^2 r} = I_4 + I_5 \qquad (5.4.15)$$

where

$$I_4 = \mathrm{e}^{-a}\sqrt{\frac{\pi}{a}} \int_0^{\pi/2} d\theta\, \cos\theta\sin\theta\, \mathrm{erf}(\sqrt{a}\cot\theta) = \frac{\pi}{2}\, \mathrm{erfc}(\sqrt{a}), \qquad (5.4.16\mathrm{a})$$

$$I_5 = \frac{1}{a} \int_0^{\pi/2} d\theta\, \sin^2\theta\mathrm{e}^{-a/\sin^2\theta} = \frac{1}{a}\left(\frac{\sqrt{a\pi}}{2}\mathrm{e}^{-a} - \frac{\pi}{4}(2a-1)\mathrm{erfc}(\sqrt{a}) \right). \qquad (5.4.16\mathrm{b})$$

Finally we arrive at

$$\psi(r) = \frac{\pi\lambda^2 r}{3}\left(\frac{r}{\sqrt{\lambda}}\mathrm{e}^{-\lambda\pi r^2/4} + \frac{1}{\lambda}\, \mathrm{erfc}\left(r\frac{\sqrt{\lambda\pi}}{2} \right) \right). \qquad (5.4.17)$$

Collins quotes this result without explicit calculations.

Since Poison field has only one parameter it is possible to introduce normalized length scale

$$l = \frac{1}{2} r \sqrt{\lambda \pi}.$$

(5.4.18)

After changing variables as above we obtain the universal distribution of the normalized lengths of Delaunay edges:

$$\widetilde{\psi}(l) = \frac{4}{3} l \left(\frac{2l}{\sqrt{\pi}} e^{-l^2} + \mathrm{erfc}\, l \right).$$

(5.4.19)

Quantity of interest might be integrated probability

$$\widetilde{\Psi}(l) = \int_0^l d\xi\, \widetilde{\psi}(\xi) = \frac{2}{3} l \left(l - \frac{3 e^{-l^2}}{\sqrt{\pi}} \right) + \left(1 - \frac{2}{3} l^2 \right) \mathrm{erf}\,(l).$$

(5.4.20)

The distributions are plotted in the Figure 5.8.
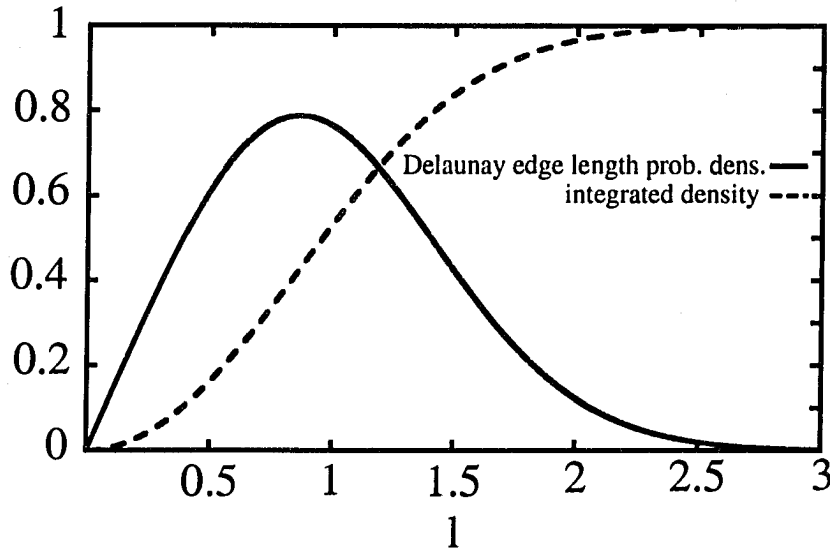
Figure 5.8: $\widetilde{\psi}(l)$ and $\widetilde{\Psi}(l)$ for Poisson field. Lengths are in the universal units.

5.4.2   Joint probability

Even if we want to utilize uniform gradient approach for a single resistor we must at least know the joint probability $\varkappa(r, l)$ for lengths of corresponding Delaunay (r) and Voronoi (l) edges. This requires the investigation of properties of two neighboring Delaunay triangles, spanned on four points, see Figure 5.9. Two neighboring triangles form two

valid Delaunay triangles if both of the two circles spanned on them are empty.

As before we can write

$$qN\varkappa(r,l) = \lambda^4 \int d^2\mathbf{x}_1 \ldots d^2\mathbf{x}_4 \, g_4(\mathbf{x}_1, \mathbf{x}_2, \mathbf{x}_3, \mathbf{x}_4) E(\mathbf{x}_1, \mathbf{x}_2, \mathbf{x}_3, \mathbf{x}_4) \qquad (5.4.21)$$

and the integration is taken over such configurations for which the two triangles are indeed two neighboring Delaunay triangles and for which $r = |AB| = $ const and $l = |O_1O_2| = $ const. The emptiness probability for the two overlapping circles is

$$E(\mathbf{x}_1, \mathbf{x}_2, \mathbf{x}_3, \mathbf{x}_4) = E(r, l, x) = \exp(-\lambda v), \qquad (5.4.22)$$

where the area of the overlaping circles is

$$v \equiv \frac{1}{2}lr + \frac{\pi}{2}(l^2 + r^2 + 4x^2) - \frac{1}{4}\left(r^2 + (l - 2x)^2\right) \arccos\left(\frac{l - 2x}{\sqrt{r^2 + (l - 2x)^2}}\right)$$
$$- \frac{1}{4}\left(r^2 + (l + 2x)^2\right) \arccos\left(\frac{l + 2x}{\sqrt{r^2 + (l + 2x)^2}}\right) \quad (5.4.23)$$

The circles always overlap and one circle cannot encompass the other one in full (this would violate the empty circle rule).

We switch to the parameterization presented in in the Figure 5.9:

$$(\mathbf{x}_1, \mathbf{x}_2, \mathbf{x}_3, \mathbf{x}_4) \longrightarrow (\mathbf{x}_1, \phi, r, l, x, \theta_1, \theta_2). \qquad (5.4.24)$$

The mapping is 1-1. $r, l \in (0, \infty)$, $x \in (-\infty, \infty)$ and $\theta_i \in (-\theta_{gi}, \theta_{gi})$, where

$$\theta_{g1} = \pi - \arccos\left(\frac{l + 2x}{\sqrt{r^2 + (l + 2x)^2}}\right), \qquad (5.4.25a)$$

$$\theta_{g2} = \pi - \arccos\left(\frac{l - 2x}{\sqrt{r^2 + (l - 2x)^2}}\right). \qquad (5.4.25b)$$

Jacobian of the transformation reads

$$\frac{r}{4}\left(l + 2x + \sqrt{r^2 + (l + 2x)^2}\cos\theta_1\right)\left(l - 2x + \sqrt{r^2 + (l - 2x)^2}\cos\theta_2\right); \qquad (5.4.26)$$

the above expression is always positive. We can immediately perform integration over $\mathbf{x}_1$ and ϕ; due to symmetry of the integrands (primarily due to factorization of the dependences on $\theta_{1,2}$ and the fact that v does not depend on $\theta_{1,2}$) integration over $\theta_{1,2}$ is relatively easy (although messy). In the end we are left with integration over x alone.
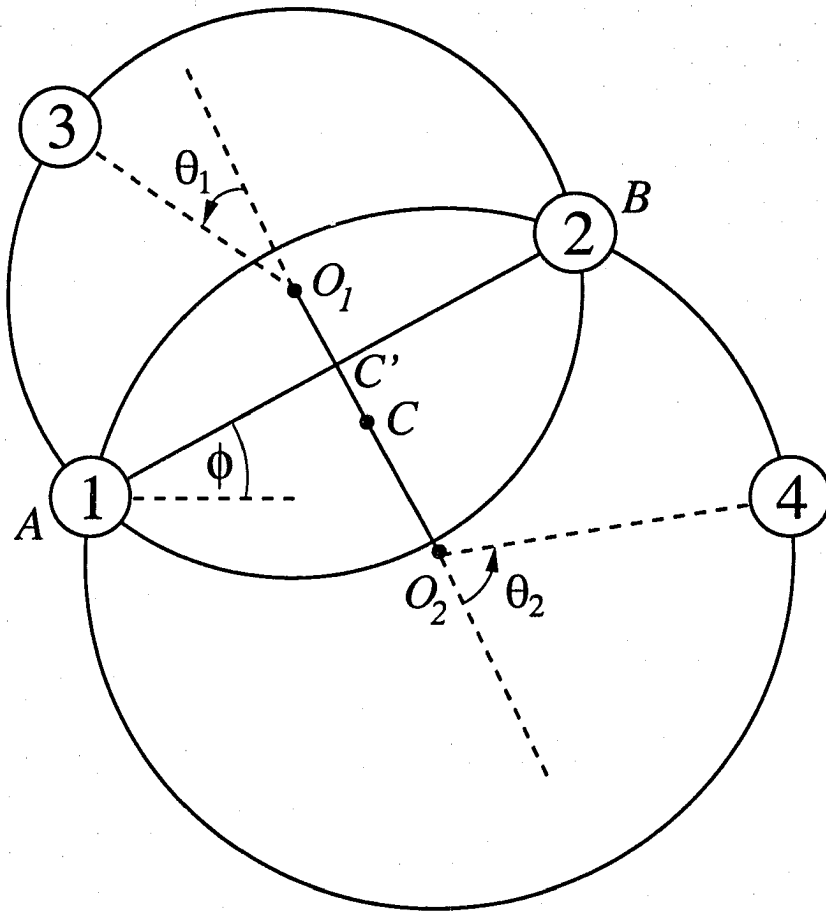
Figure 5.9: Geometry considered during calculations of joint probability $\varkappa(r, l)$. Delaunay edge is $r = |AB|$ and the Voronoi edge $l = |O_1O_2|$, where O_1 and O_2 are centers of the circles circumscribed on the triangles 123 and 124 respectively. C is the center of the segment O_1O_2 and C' stands for the point of the intersection of the directions of Voronoi and Delaunay edges. θ_1 and θ_2 measure the directions of points x_1 and x_2 respectively from as seen from O_1 and O_2 with respect to the direction of Voronoi edge. $|CC'| = |x|$ and the sign of x is positive if C lies on the same side of the AB as O_1. Radius of the circles centered on O_1 and O_2 are R_1 and R_2 respectively.

After switching to normalized units (5.4.18) we obtain (r, l are normalized):

$$\widetilde{\varkappa}(r,l) = \frac{64rl}{3\pi} \int_0^\infty d\omega\, j_+ j_- \mathbb{e}^{-v'} \tag{5.4.27}$$

where

$$j_\pm(\omega,r,l) = r + l(1 \pm \omega)\left(\pi - \arccos \frac{l(1 \pm \omega)}{\sqrt{r^2 + l^2(1 \pm \omega)^2}}\right) \tag{5.4.28}$$

and

$$v'(\omega,r,l) = \frac{2}{\pi}rl + 2\big(r^2 + l^2(1 + \omega^2)\big) - \frac{1}{\pi}(\xi_- + \xi_+) \tag{5.4.29}$$

with

$$\xi_\pm = \big(r^2 + l^2(1 \pm \omega)^2\big) \arccos \frac{l(1 \pm \omega)}{\sqrt{r^2 + l^2(1 \pm \omega)^2}}. \tag{5.4.30}$$

I found no way to calculate the last integral. It seems however that it may not be necessary. Any quantity of interest (any moment of l and r) will probably have to be calculated numerically anyway; all we need to do is to add one more integral. I checked the obtained formula using Monte Carlo integrator. It is normalized and and after integration over l and ω I arrived at the known expression for $\tilde{\psi}(r)$. Note that in general it allows calculation of the distribution of l. I am not aware of any such result in the literature.

The above calculation have unfortunately only pedagogical meaning. In order to calculate any relevant quantities for set of discs we must abandon $g \equiv 1$ assumption. We know in general how to build correlation functions for hard-core fields and the next section I present the Collins summation formula, which allows a calculation of the void probability, $E(\gamma)$.

5.5   General expression for void probability

The calculations presented come from [18], however argumentation is slightly altered and generalized.

We state the problem as follows. Let us suppose we have a field of N points interacting via potential Φ, which depends on their instantaneous positions $\mathbf{x}_\alpha$, $\alpha = 1, \ldots N$. We fix positions $\mathbf{f}_i$ of n points ($i = 1, \ldots n$), "spanning" a subset of $\mathbb{R}^2$, γ; we assume that γ is an open set, i.e. a point lying on its boundary does not belong to it. In our previous examples it was an interior of the circle circumscribed on the three points or the interior of the two overlapping discs spanned by four points. We want to know the probability

$E_n(\gamma)$ that γ contains no points. The condition for that reads

$$\prod_{\alpha=n+1}^{N} (1 - \mathbb{1}_\gamma(\mathbf{x}_\alpha)) = 1, \tag{5.5.1}$$

where $\mathbb{1}_\gamma$ is the indicator function defined by (5.2.2). By means of canonical ensemble average with integrated kinetic energy part we can write the general expression for emptiness probability

$$E_n(\gamma) \equiv E = \frac{1}{Q_n} \int_{V^N} d(N)\delta(n) e^{-\Phi/T} \prod_{\alpha=n+1}^{N} (1 - \mathbb{1}_\gamma(\mathbf{x}_\alpha)). \tag{5.5.2}$$

We use the following notation

$$\delta(n) = \prod_{i=1}^{n} \delta^{(2)}(\mathbf{x}_i - \mathbf{f}_i), \tag{5.5.3a}$$

$$d(N) = \prod_{\alpha=1}^{N} d^2 \mathbf{x}_\alpha. \tag{5.5.3b}$$

The reduced configurational integral reads

$$Q_n(\mathbf{f}_1, \ldots \mathbf{f}_n) = \int_{V^N} d(N)\delta(n) e^{-\Phi/T}. \tag{5.5.4}$$

(5.5.1) may be expanded to obtain

$$1 - \sum_{n<\alpha} \mathbb{1}_\alpha + \sum_{n<\alpha<\beta} \mathbb{1}_\alpha \mathbb{1}_\beta - \ldots, \tag{5.5.5}$$

where $\mathbb{1}_\alpha$ is a shorthand notation of $\mathbb{1}_\gamma(\mathbf{x}_\alpha)$. E reads

$$E = 1 + \sum_{m=1}^{\infty} E^{(m)}, \tag{5.5.6}$$

where

$$E^{(m)} = \frac{(-1)^m}{Q_n} \int_{V^N} d(N)\delta(n) e^{-\Phi/T} \underbrace{\sum_{n<\alpha \,<\, \beta \,<\, \ldots \,<\, \delta}}_{m} \mathbb{1}_\alpha \mathbb{1}_\beta \ldots \mathbb{1}_\delta$$

$$= \frac{(-1)^m}{Q_n} \binom{N-n}{m} \int_{V^N} d(N)\delta(n) \mathbb{1}_{n+1} \mathbb{1}_{n+2} \ldots \mathbb{1}_{n+m} e^{-\Phi/T}, \tag{5.5.7}$$

where we exchanged the order of integration and summation and noticed that for all

arrangements of α, β, etc. the integrals are the same. The last integral can be written as

$$\int_{\gamma^m} d^2\mathbf{y}_{n+1}\ldots d^2\mathbf{y}_{n+m} \int_{V^N} d(N)\delta(n)\delta(\mathbf{x}_{n+1}-\mathbf{y}_{n+1})\ldots\delta(\mathbf{x}_{n+m}-\mathbf{y}_{n+m})\mathrm{e}^{-\Phi/T}. \tag{5.5.8}$$

From the definition of correlation functions we have (here k is arbitrary)

$$\lambda^k g_k(\mathbf{y}_1,\ldots\mathbf{y}_k) = \frac{1}{Q}\binom{N}{k}k!\int_{V^N}d(N)\delta(k)\mathrm{e}^{-\Phi/T} = \frac{Q_k(\mathbf{y}_1,\ldots\mathbf{y}_k)}{Q}\binom{N}{k}k!, \tag{5.5.9}$$

where the configurational integral reads

$$Q = \int_{V^N} d(N)\mathrm{e}^{-\Phi/T}. \tag{5.5.10}$$

The justification of the above is the following. We are asking how many configurations in the fluid places atoms around $(\mathbf{y}_1,\ldots\mathbf{y}_k)$. We pick up k atoms (it can be done in $\binom{N}{k}k!$ ways including their permutations on the fixed positions). The rest of the atoms may be arranged arbitrarily. We obtain

$$Q_k(\mathbf{y}_1,\ldots\mathbf{y}_k) = \frac{(N-k)!}{N!}Q\lambda^k g_k(\mathbf{y}_1,\ldots\mathbf{y}_k) \tag{5.5.11}$$

and we can write

$$E^{(m)} = \frac{(-1)^m}{Q_n}\binom{N-n}{m}\int_{\gamma^m}d^2\mathbf{y}_{n+1}\ldots d^2\mathbf{y}_{n+m}Q_{n+m}(\mathbf{f}_1,\ldots\mathbf{f}_n,\mathbf{y}_{n+1},\ldots\mathbf{y}_{n+m})$$

$$= \frac{(-1)^m\lambda^m}{m!}\int_{\gamma^m}d^2\mathbf{y}_{n+1}\ldots d^2\mathbf{y}_{n+m}\frac{g_{n+m}(\mathbf{f}_1,\ldots\mathbf{f}_n,\mathbf{y}_{n+1},\ldots\mathbf{y}_{n+m})}{g_n(\mathbf{f}_1,\ldots\mathbf{f}_n)}. \tag{5.5.12}$$

We have been able to express $E_n(\gamma)$ in the form of power series in density λ. The expression can be easily evaluated in the case of Poisson field

$$E(\gamma) = \exp(-\lambda L(\gamma)). \tag{5.5.13}$$

I devoted a lot of time and effort to approximate E at least for the simplest possible form of hard-core correlation functions, but without any significant progress.

5.6 Delaunay tessellations of hard discs

Due to tremendous difficulties in handling the large integrals presented in the previous section a little analytic work has been done in that field for hard-core fields. On the other hand the Poisson case has been studied thoroughly, please refer to [69]. [37] deals mainly with topological properties of Voronoi diagrams of hard-core discs. As mentioned earlier the researchers found that probability of generated Voronoi vertex is indeed zero and that the average number of the generator adjacent to typical generator is around
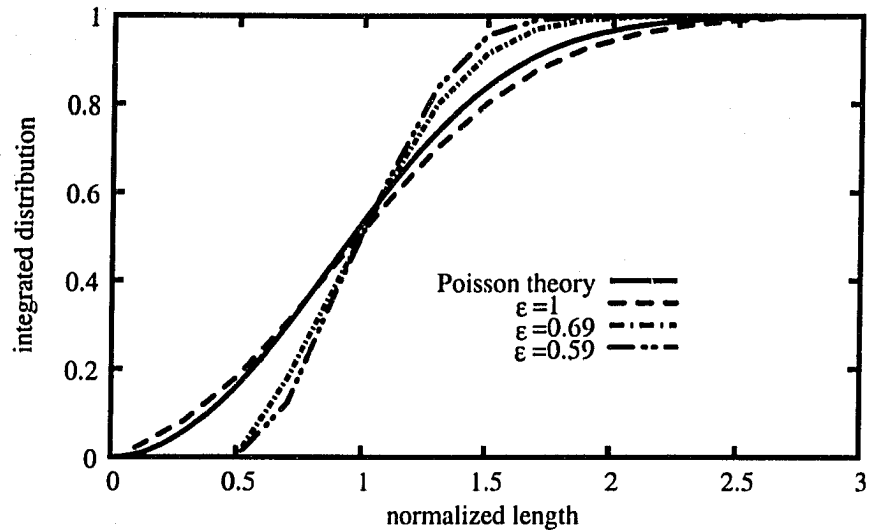
Figure 5.10: Integrated distributions from [92] compared to Poisson case. I can be seen that form smaller void volumes variance of the distribution becomes smaller; the system becomes more ordered.

6 (the results is exact for Poisson case). It is therefore reasonable to think about the tessellations of hard discs as of disordered triangular lattices.

The only attempt to calculate the Delaunay edge distribution known to me is [68], but it seems to disagree with the numerical experiments presented in [92], which are reported in the Figure 5.10. The last work clearly indicates that the systems becomes more regular with the decreasing void volume – for the case of very high concentrations the (unintegrated) distribution should approach delta function, like for the case of the triangular lattice.

5.7 Summary

The studies on local properties of point fields were developed in parallel to the computer studies. After I had obtained the first numerical results, presented in Chapter 6, it became clear, that mean gradient hypothesis needs to be refuted. The size of the cluster that would reproduce the permeability of the network appeared to be much too large to be handled analytically. Small clusters/single resistors will not do.

Nevertheless I believe that the work presented in this chapter is important for any analytic attack on the random hydraulic networks. Any description I can imagine will have to, at some point, calculate some average properties of single throats. Let me therefore recall what has been done here. I showed how to investigate the statistical properties of of Voronoi/Delaunay diagrams: the knowledge of many body correlation functions is needed (which under some assumptions may be expressed using pair correlation function $g(r)$) and void probability for our point field. I investigated the latter quantity using Collins

approach in Section 5.5. Different hard-core point precesses were suggested; among them the one that was used in the computer simulations, so called gas of hard discs. Pair correlation functions for these processes were also studied.

Chapter 6

Numerical studies

6.1 Introduction

The main object of numerical study is the calculation of geometrical modifier for the flow through disordered quasi two dimensional systems of cylinders, as discussed in Chapter 4. The gas of hard discs constitutes the source of configurations. Effective resistivity of the network is computed using relaxation methods. In the following section details of implementation are presented. The numerical project is called `Drag`; its structure is presented in Figure 6.1.
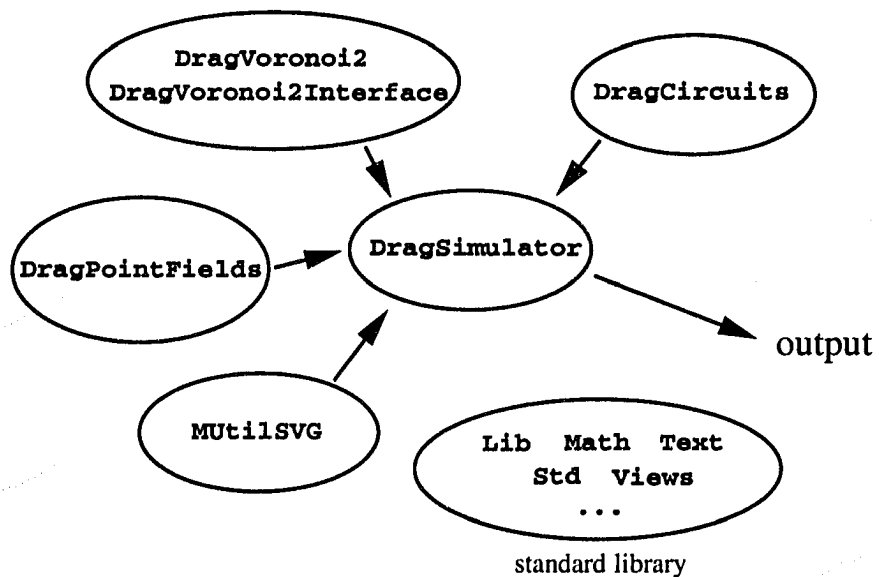

Figure 6.1: `Drag` module system.

6.2 Implementation

The programing language chosen was **Component Pascal (CP)** under programming environment BlackBox Component Builder 1.4. The language seems to be very convenient for middle size projects: it is object oriented, has garbage collector and comes with user friendly development environment. The language design is such that the code is easy to develop and to debug. The operating system used was Windows XP (Version 2002) installed on Dell INSPIRON 9100 portable computer. System resources are: CPU 2.80GHz Intel®, Pentium® IV, RAM 1.00 GB. All the development, testing and calculations were performed on this machine.

 `Drag` consists of four main modules:

- `DragVoronoi2` (with the interface `DragVoronoi2Interface`) with the library `Voronoi2.dll` compiled from FORTRAN77 sources. The module constructs Voronoi diagrams for the set of generators

- `DragCircuits`: constructs the circuit equivalent to obtained Voronoi diagram. It calculates net conductances of general resistors networks.

- `DragPointFields`: Monte Carlo configuration generator. Also set of tools to create and manipulate 2D point fields.

- `DragSimulator`: main module, where the actual simulations are performed.

Additionally graphical output was realized using `MUtilSVG` module. Several other modules from standard CP library was used, mainly to facilitate output. The whole code developed has about 7000 lines.

 In the subsequent section some details of implementation are given.

6.2.1 Configurations generator

As already suggested, we will use the configuration of points that appear in the gas with hard-core potential. In the beginning simulation starts with triangular lattice, Figure 6.2. We sample the configuration after every m steps of Monte Carlo procedure. The number of points is n and we assume the periodic boundary conditions.

Lattice generation

Generation of lattice require some caution, because the discrete translational symmetry may lead to frustration. The size of the computational domain ($\Delta x \times \Delta y$) cannot be arbitrary – after adding copies of the system around (periodic boundary conditions) we must obtain infinite lattice without any defects. The task is performed by procedure `TriangularLattice` in module `DragPointFields`. User supplies the requested void volume of the system ϵ and diameter of the cylinders D. These two parameters are unchanged in the procedure. Additionally user specifies the approximate ratio $\eta = \Delta y / \Delta x$

and number of generators n. Procedure calculates approximate length Δx from the expression

$$\Delta x = D\left(\frac{\pi n}{4\eta(1-\epsilon)}\right)^{1/2} \tag{6.2.1}$$

and subsequently the interparticle distance as

$$a = \left(\frac{2\sqrt{3}}{3}\right)^{1/2}\left(\frac{\pi}{4(1-\epsilon)}\right)^{1/2}D = \sqrt{\frac{2\sqrt{3}}{3}}\frac{1}{\sqrt{\lambda}}. \tag{6.2.2}$$

Δx has to be the multiplicity of a:

$$n_x = \mathtt{ENTIER}(\Delta x/a), \tag{6.2.3a}$$

$$\Delta x = n_x a. \tag{6.2.3b}$$

If the result is zero, than it is set to a. $\mathtt{ENTIER}$ denotes the standard CP function, which returns integer part of the number (floor).
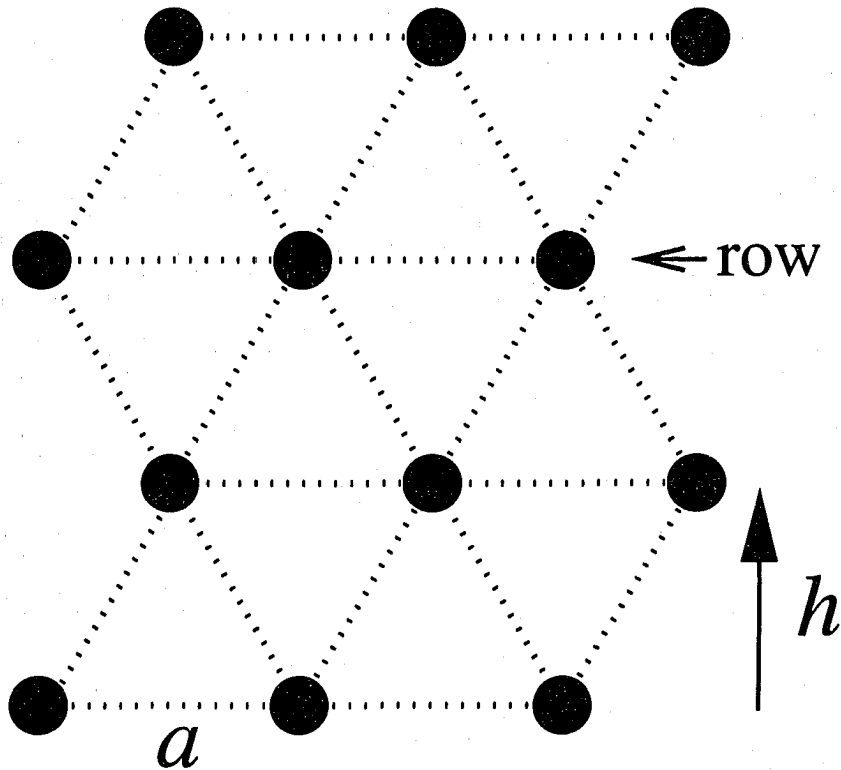
Figure 6.2: Triangular lattice generation. $n_x = 3$, $n_y = 4$.

The actual number of generators in the computational domain is calculated as the closest even multiplicity of n_x

$$n \longrightarrow \text{ENTIER}(n/2n_x)2n_x. \tag{6.2.4}$$

n_x stands for the number of particles in the row, while

$$n_y = n/n_x \tag{6.2.5}$$

is the number of rows, which must be even. Δy is now calculated as

$$\Delta y = n_y h, \tag{6.2.6}$$

where

$$h = a\frac{\sqrt{3}}{2}. \tag{6.2.7}$$

Finally

$$\eta \longrightarrow \Delta y/\Delta x. \tag{6.2.8}$$

Building of actual point field is now easy, example was presented in the Figure 6.2.

Monte Carlo configuration sampling

Strictly speaking we are simulating melting of 2D crystal of atoms interacting via HC potential under constant volume (density) condition. Such system has only one parameter, ϵ. Temperature is absent in the classical simulations of hard sphere gas.

One Monte Carlo step is the following. We try to displace every atom by vector $\Delta \mathbf{r}$, where

$$\mathbf{r} \in [-\Delta/2, \Delta/2]^2 \tag{6.2.9}$$

and all possible realizations of $\mathbf{r}$ are equally probable. Uniform random number generator from the standard library module LibRandom was used. If the disc in the new position overlap with any of the other discs the step is rejected, otherwise is accepted.

The rule of the thumb in this kind of simulations is to keep the *acceptance ratio* α (the number of accepted displacements to the total number of attempted displacements) close to $\mathfrak{m} = 0.5$. This is achieved by adjusting the value of Δ. After each few MC steps α is calculated and

$$\text{if } \alpha < \mathfrak{m} - \delta/2, \text{ then } \Delta \to \Delta \cdot \kappa, \text{ or}$$
$$\text{if } \alpha > \mathfrak{m} + \delta/2, \text{ then } \Delta \to \Delta/\kappa.$$

In general we may expect that the larger displacement, the smaller probability of accepting the step.

Algorithm requires certain number of steps to remove correlations, I call this process *thermalization*.

6.2.2 Computing the tessellations

The exhaustive discussion of the numerical aspects of construction Voronoi/Delaunay diagrams can be found in [69]. The construction of the accurate Voronoi tessellation of point fields generated by the Monte Carlo section is crucial, since we need both the correct numerical values of distances, determining the resistances of particular throats, and exactly reproduced topological ordering. Especially this second property is prone to numerical instabilities.

First of all we should decide whether to concentrate on creation of Delaunay or Voronoi diagram. There are several reasons to choose the second option: the data structures for this case are easier to construct and manipulate; at the same numerical cost they carry more information. Furthermore, it is generally much easier to obtain Delaunay tessellation having constructed Voronoi diagram than build topologically correct Voronoi tessellation from Delaunay diagram.

Reference [69] discusses several algorithms for computing Voronoi graphs: *plane sweep method*, *divide and conquer algorithm* and finally *incremental method*, which we will concentrate on later. All these algorithms, by utilizing quite sophisticated algorithmic techniques, can approach time complexity $\mathcal{O}(n)$ on average and $\mathcal{O}(n \log n)$ in the worst case, what has been shown to be a theoretical limit for these kind of computations. Nevertheless only the incremental method was refined enough to give a robust algorithm insensitive to unavoidable numerical errors.

The algorithm was developed by Kokichi Sugihara and Masao Iri in the late 80's and was called VORONOI2. The code was written in FORTRAN77 language and makes fairly large library, having almost 2000 lines (with additional 1000 line of code designed to facilitate graphical output) and about 20 COMMON blocks (64 global variables). This code, compiled to *dynamic link library*, constitutes the core of my subprogram for determining the structure of the electric networks. The sources, as well as the user guide, [85], are distributed solely by authors.

I had to modify slightly the original code. Also the internal FORTRAN77 data structures had to be ported to CP language, since the direct access was impossible. The CP interface contains also the algorithms for constructing Voronoi diagrams with periodic (or semi-periodic) boundary conditions and several other subroutines to extract necessary data. Subsequent sections serve as report and short user guide to this part of my CP code. They also reveal some basics concepts that guided authors of VORONOI2.

Incremental method

The idea of incremental method is simple. We start with Voronoi diagram for limited number of generators, e.g. 3. This can be done easily and exactly. Successively we add subsequent generators, each time modifying the diagram. Let us say we add generator $\mathbf{g} = \mathbf{g}_l$ and want to modify Voronoi diagram $\mathcal{V}_{l-1}$ to obtain V_l. Modification encompasses

removing part of edges and vertices of the old diagram and adding new ones, as presented in the Figure 6.3. First we find the perpendicular bisector between **g** and the nearest generator, say **g'** among those already added (line 1-2 in the figure). Bisector crosses edges bounding region of **g'** and enters regions of two others, let us call one of them **g''**. We can now find bisector between g_l and **g''**, which enters the next region in point 3. We can continue this *boundary growing procedure* until we close the region ascribed to **g**.
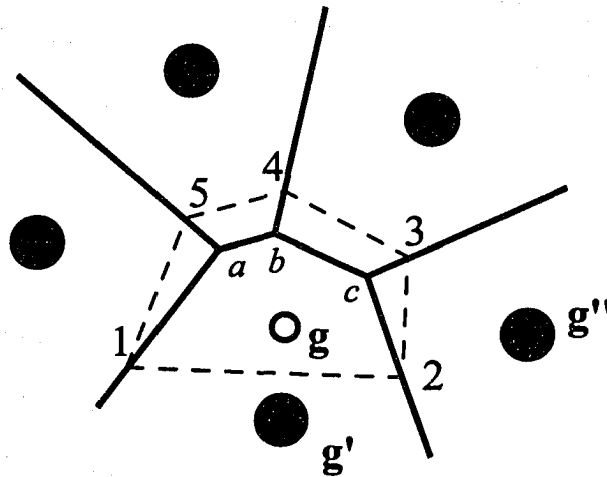
Figure 6.3: An idea of the incremental method. Thick lines represent diagram $\mathcal{V}_{l-1}$. After an addition of generator **g** old Voronoi vertices *a*, *b* and *c* have to be removed; the old Voronoi edges must be split in points 1, 2, 3, 4 and 5 and new edges 1-2, 2-3, 3-4, 4-5, 5-1 are added (dashed lines). Similar figure can be found in [69].

The algorithm works under assumption that the new Voronoi region is finite. This is not always true, but the infinite regions may be eliminated by a simple trick, which is discussed later.

If there would be no errors we could judge which vertices of $\mathcal{V}_{l-1}$ should be removed by the following procedure. Let assume that three generators g_i, g_j and g_k span the circle $\mathcal{C}$ and are ordered in such a way that going on the circle in the counterclockwise direction we visit generators in the order $ijki$. We are interested in the position of fourth

generator **g** with respect to the circle $\mathcal{C}$. Let us define

$$
H(\mathbf{g}_i, \mathbf{g}_j, \mathbf{g}_k, \mathbf{g}) = \begin{vmatrix} 1 & x_i & y_i & x_i^2 + y_i^2 \\ 1 & x_j & y_j & x_j^2 + y_j^2 \\ 1 & x_k & y_k & x_k^2 + y_k^2 \\ 1 & x & y & x^2 + y^2 \end{vmatrix},
\tag{6.2.10}
$$

where notation $x_{(l)} = \mathbf{g}_{(l)} \cdot (1,0)$, etc. It can be proved that that

if $H(\mathbf{g}_i, \mathbf{g}_j, \mathbf{g}_k, \mathbf{g}) < 0$ **g** is inside $\mathcal{C}$,

if $H(\mathbf{g}_i, \mathbf{g}_j, \mathbf{g}_k, \mathbf{g}) = 0$ **g** lies on the boundary of $\mathcal{C}$ and

if $H(\mathbf{g}_i, \mathbf{g}_j, \mathbf{g}_k, \mathbf{g}) > 0$ **g** is outside $\mathcal{C}$.

If we want to judge if the vertex $q(\mathbf{g}_i, \mathbf{g}_j, \mathbf{g}_k)$ adjacent to generators $\mathbf{g}_i, \mathbf{g}_j$ and $\mathbf{g}_k$ is to be removed, we need to check sign of $H(\mathbf{g}_i, \mathbf{g}_j, \mathbf{g}_k, \mathbf{g}_l)$. If it is non-positive the vertex should be removed.

Let it be noted that in the case of $H(\mathbf{g}_i, \mathbf{g}_j, \mathbf{g}_k, \mathbf{g}_l) = 0$ we deal with degeneracy. The degeneracy can be removed using simple *symbolic perturbation* technique: we remove the vertex only if $H < 0$. This procedure should be understood as delicate deformation of old Voronoi diagram. The idea underlying this procedure is such that the degeneracy might be judged correctly only if there would be no numerical errors. Since real data always bear this stigma, we can say that in the real world the degeneracy never occurs.

The time complexity of the program depends greatly on the ability of the algorithm to find fast the nearest generator for $\mathbf{g}_l$. This is achieved by *bucketing technique*, where the generators are distributed over the specially constructed *quaternary three*.

Numerical accuracy depends on the uniformity of generators, i.e. the more uniformly the generators taken in order fill the region the better. This is achieved by renumeration based on the bucket tree.

Data structure

The most popular data structure to store information about Voronoi diagram is so called *winged-edge data structure*. Such data structure had been used before in connection with Voronoi diagrams in [40]. We start with adding one additional generator, $\mathbf{g}_\infty$, which lies in the (complex) infinity. In this way we achieve that all Voronoi regions associated with ordinary generators are finite. In the case when no degeneracy takes place all vertices are rank three, what means that the number of vertices and respectively edges is

$$
n_v = 2n - 2,
\tag{6.2.11a}
$$

$$
n_e = 3n - 3,
\tag{6.2.11b}
$$

where n stands for the number of generators. The graph we obtained is called *augmented geometric graph*. Its all edges are finite, please confront Figure 6.4 (all the figures in this section comes from [69]).
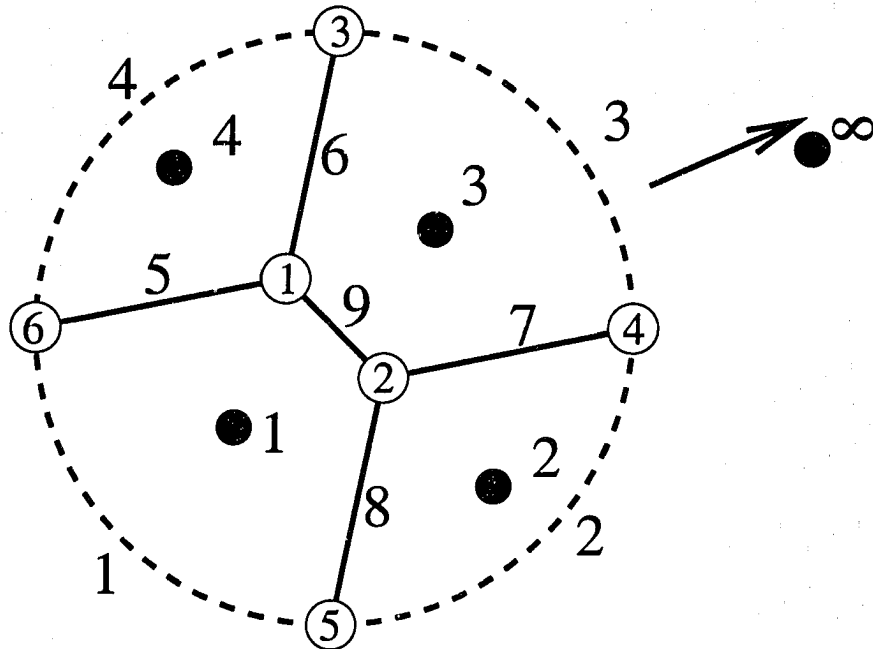
Figure 6.4: Augmented geometric graph. Ordinary diagram is generated by four points denoted with filled circles (1 ... 4); it has five edges (5 ... 9) and two vertices 1 and 2. By adding ∞-generator we obtain augmented graph with additional vertices 3 ... 6 and edges marked with dashed lines.
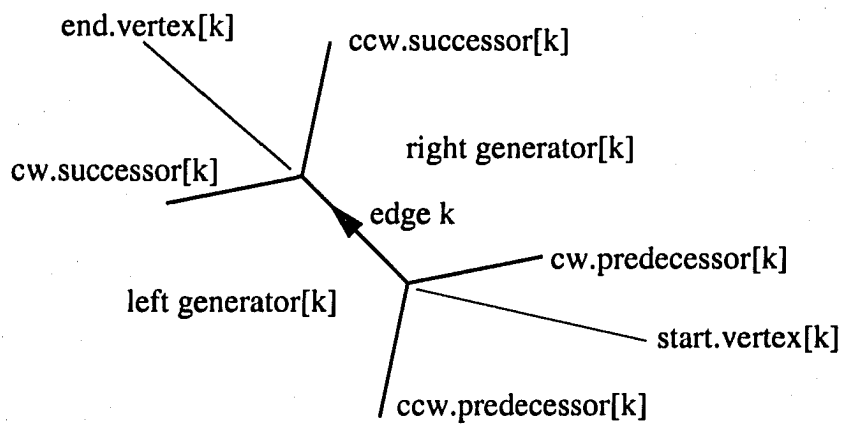
Figure 6.5: Winged edge data strucure for edges. To get the order (cw vs. ccw) we must stand on the vertex and look in the direction of the second vertex (regardless the direction of the edge).

Every edge, vertex and generator is marked with a unique number. The next step is to impose a direction of every edge. Every edge has now starting and ending vertex. Additionally we can define successors and predecessors of every edge, clockwise (cw) or counterclockwise (ccw) in order. To every edge we can ascribe right and left generator. Please refer to Figure 6.5. Additionally we record number of one of the edges on the boundary of each Voronoi region and number of one of the edges on incident to every vertex. Every vertex is given a mark "Euclidean" or "infinity" depending if the vertex belongs to the ordinary diagram (Euclidean, like 1 and 2 in the Figure 6.4) or is in the infinity (like 3...6). Every vertex has two coordinates. In case of Euclidean points they are ordinary Cartesian components of it; when the point lies in the infinity they code the direction of the infinite Voronoi edge. The last convention is sometimes referred as *homogeneous coordinates*.

To avoid building infinite Voronoi region in the incremental method, the following trick is used. In the beginning algorithm adds three extra generators placed on the triangle and construct (augmented) diagram for them. If the triangle is large enough (comparing to the region containing all regular generators), the sequential adding of regular generators will not disturb the outermost structure of the three infinite vertices and edges.

Topological consistency

VORONOI2 does not attempt to build exact Voronoi diagram, rather it constructs (always) the (augmented) graph $\mathcal{V}$ that is *topologically consistent* in the sense that it possesses the following properties:

(T1) The degree of any vertex in $\mathcal{V}$ is exactly three.

(T2) $\mathcal{V}$ posses $n + 1$ primary cycles (i.e. closed paths built of adjacent edges, which contain no other cycles inside)

(T3) Every region, except the one associated with g_∞ is simply connected (does not have any holes).

(T4) Two regions share at most one common edge.

(T5) The region associated with g_∞ has exactly three edges and three vertices (this property is imposed by adding the three additional generators mentioned in the previous paragraph).

Every augmented Voronoi graph posses these properties, but the inversion of this statement is not true.

Initial graph for three ($+\infty$-generator) fake generators is topologically consistent. The process of modification, as described in Section 6.2.2, will always produce topologically consistent graph if the set of vertices and edges T which is removed in every step express the following features

(T'6) T is non-empty (what follows from the fact that each generator must have its own region).

(T'7) T does not contain vertex in infinity.

(T'8) T is a tree, i.e. connected acyclic graph.

(T'9) Deletion of T cannot lead to the situation when two (or more) Voronoi regions have more than one edge in common.

Figure 6.6 presents some examples, please refer to the caption for short comment. The point that fulfills H-criterion is included into T if resulting T fulfills T'6÷T'9. This makes the algorithm robust against numerical errors. Furthermore, as pointed by authors when the errors become negligible, the diagram converges to exact Voronoi diagram.
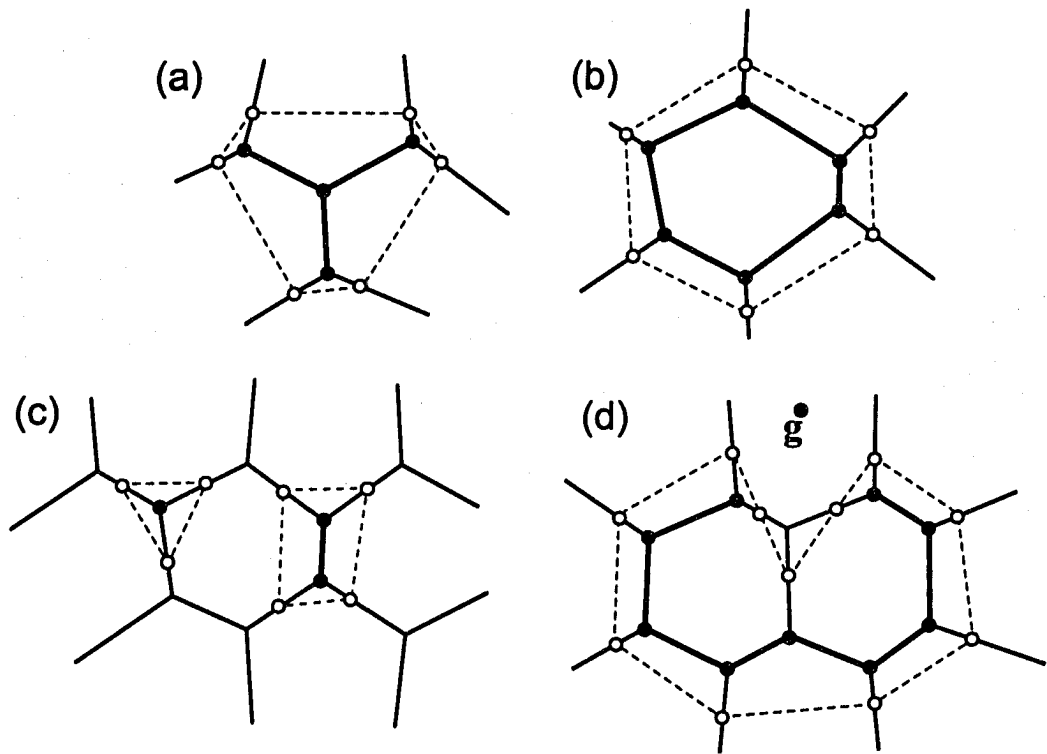

Figure 6.6: Example of allowed and forbidden shapes of set T. (a) presents legal deletion of a tree; (b) violates T'8, one generator would loose its region; (c) forbidden, since T must be connected; (d) example of violation of T'9.

VORONOI2 under CP

VORONOI2 takes as an input number and positions of generators and builds (stored inside the COMMON blocks) winged-edge data structure. CP first initializes the right blocks of memory, calls the functions responsible for diagram computation and in the end reads the blocks containing the desired output.

Several modification of the original code had to be done on the level of FORTRAN code. For some reason (that are still unclear) CP can call efficiently only those functions from the dll libraries compiled from FORTRAN code, which have single argument (possibly pointer to an array). Therefore, instead of single initialization procedure, a chain of them must be called. The same applies to reading out the results. This forced me to create a set of "setters" and "getters" (the library resembles now static Java class).

I added to each subprogram in FORTRAN code explicit declaration of common blocks and variables, getting rid of the extensive use of IMPLICIT statement. I also parametrized the code, so now almost no "magic numbers" appear. These decorations were not crucial, nevertheless facilitate future development of the code. Also, without them I would never be able to understand it on the implementation level. Finally, the subroutines and global variables used to plotting the output were commented out.

To compile the library g77 compiler under MinGW32 system was used. MinGW32 is a minimalistic emulator of Unix system under Windows. Below the version of g77 is given and the listing of Makefile used.

```
$ g77 --version
GNU Fortran (GCC 3.2.3 (mingw special 20030504-1)) 3.2.3 20030425 (release)
Copyright (C) 2002 Free Software Foundation, Inc.

$ cat Makefile
../../Voronoi2.dll: Voronoi2.o
  dllwrap \
    --export-all \
    --output-def Voronoi2.def \
    --implib Voronoi2.a \
    --driver-name g77 \
    -o Voronoi2.dll Voronoi2.o

Voronoi2.o: Voronoi2.f Parametrization.f
  g77 -c -g -fno-underscoring \
    -fexpensive-optimizations -ffast-math \
    -malign-double -fforce-addr \
    -fstrength-reduce -fcaller-saves \
    -funroll-loops \
    -o Voronoi2.o Voronoi2.f
```

Prior to use, we have to define interface for dll library in CP. It is also a good idea to "wrap" every subroutine called from the library into CP procedure. Frequent direct calls

of procedures from the library within single CP procedure may cause (and caused) stack overflow.

The CP builds its own version of winged-edge data structure, since the direct access of FORTRAN COMMON blocks is impossible.

Original VORONOI2 builds, as mentioned, the diagram with fixed boundary conditions. It is however desirable to build diagram with periodic boundary conditions: it saves the problem of nodes on the boundary and weaken the finite size effects. The idea is simple: 8 copies of the system (Figure 6.7) are added around the original one and for such expanded system the Voronoi diagram is computed. Next, the edges, which cross the borders between images, are "wrapped around". However trivial it might sound the actual task appeared to be pretty involving combinatorial challenge. The periodic boundary condition may be imposed in two directions or only in one. We can of course still work with fixed boundaries.
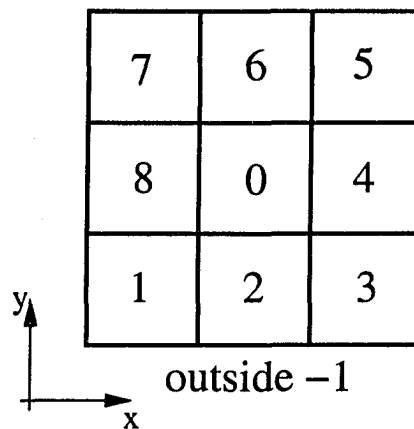
Figure 6.7: 8 copies of the original system (0) used to construct boundary conditions. Schema of quadrants enumeration is presented. Edges originating in 0 and ending outside are "wrapped".

DragVoronoi2 module — short user manual

DragVoronoi2Interface is the interface module between the dll library and the CP code. No procedures from this module should be ever directly called by user, nevertheless there are several important constants defined in it. Types of vertices:

- VT_inf_point — vertex in infinity,

- VT_Euclidean — Euclidean vertex.

If the type of vertex, t is negative, then $-t$ denotes the number of quadrant in which the vertex lie. Minimum and maximum number of generators

- max_gen_no = 50000 — maximum number of generators,

- `min_gen_no` = 2 – minimum number of generators.

NOTE: when periodic boundary conditions are imposed (even in one direction), the maximum number of generators defined by user must be `max_gen_no DIV 9`.

DragVoronoi2 is the fundamental module for computing and manipulating Voronoi diagrams. Four basic data structures and types:

```
CONST
  all_periodic* =  0; (*periodic boundary conditions in 2D*)
  x_periodic*   = -1; (*periodic boundary conditions in x-dir*)
  y_periodic*   =  1; (*periodic boundary conditions in y-dir*)
  no_periodic*  =  2; (*fixed boundary conditions*)


TYPE
  Generator* = POINTER TO RECORD
    no-: INTEGER;
    x-, y-: REAL;
    be-: VEdge; (*bounding edge*)
  END;
  Vertex* = POINTER TO RECORD (SVG.Shape) (*Voronoi vertex*)
    no-: INTEGER; (*number of the vertex*)
    x-, y-: REAL;
    type-: INTEGER; (*type of vertex*)
    ie-: VEdge; (*incident edge*)
    marker: BOOLEAN; (*internal flag*)
  END;
  VEdge* = POINTER TO RECORD (*Voronoi edge*)
    no-: INTEGER;
    start-, end-: Vertex;
    rg-: Generator; (*right hand side generator*)
    lg-: Generator; (*left hand side generator*)
    sce-:  VEdge; (*start clockwise         edge*)
    scce-: VEdge; (*start counter-clockwise edge*)
    ece-:  VEdge; (*end   clockwise         edge*)
    ecce-: VEdge; (*end   counter-clockwise edge*)
  END;
  VDiagram* = POINTER TO RECORD (*Voronoi diagram*)
    periodicity-: INTEGER; (*type of boundary conditions*)
    genDone-: BOOLEAN; (*Generators has been initialized*)
    VoronoiDone-: BOOLEAN; (*Voronoi Diagram has been calculated*)
    genNo-: INTEGER; (*no of generators*)
    VEdgeNo-: INTEGER; (*number of Voronoi edges*)
    VVertexNo-: INTEGER; (*number of Voronoi vertices*)
    generators-: POINTER TO ARRAY OF Generator; (*generators*)
    VVertices-: POINTER TO ARRAY OF Vertex; (*vertices*)
```

```
        VEdges-: POINTER TO ARRAY OF VEdge; (*Voronoi edges*)
      END;
```

The basic procedures available:

```
PROCEDURE BuildVoronoiDiagramFBC* (
  gx, gy: ARRAY OF REAL;
  gno: INTEGER
): VDiagram;
```

returns Voronoi Diagram for gx generators with positions specified in gx (x-components), gy (y-components) with fixed boundary conditions.

```
PROCEDURE BuildVoronoiDiagramPBC* (
  direction: INTEGER;    (*periodicity direction*)
  eta: REAL;             (*ratio of y_len to x_len*)
  gx, gy: ARRAY OF REAL; (*generators coordinates*)
  gno: INTEGER           (*number of generators*)
): VDiagram;
```

direction can have one of the values: all_periodic, x_periodic, y_periodic or no_periodic. eta stands for the ratio $\Delta y/\Delta x$, where the latter are the length of the edges (respectively in y and x direction) of the rectangle bounding all generators. The larger among Δx and Δy must be equal to 1. The subroutine does not check carefully the accuracy of the diagram when the number of points is small. It will surely fail for the number of generators less than 3. The generators are assumed to fill the rectangle uniformly. This drawback requires future development, but it does not affect the numerical studies of this chapter, since the systems we deal with are much larger (it has been carefully tested).

6.2.3 Conductivity calculations

Example of the hydraulic network obtained for small thermalized system of generators is presented in the Figure 6.8. The Voronoi diagram is periodic in one direction, the dashed edges are "wrapped around".

Conductances associates with every edge is calculated, each node is given flag "boundary" or "core". Inflowing nodes $(1 \ldots 5)$ have their pressures set to p, outflowing nodes $6 \ldots 10$ to zero. Module designed to deal with electrical (hydraulic) properties is DragCircuits. As we have seen, it is possible to calculate the pressure in each node and subsequently power and geometrical modifier.

As discussed in Section 3.4, there are two ways to calculate the potentials in the core nodes. We can try the direct attack and construct matrices K_c and R^T and solve the system of equations (3.4.19). The standard method is to LU-decompose matrix K_c and obtain solution v_c via back substitution (e.g. [72]). There are standard libraries (LibMatrices and LibVectors) written in CP to achieve that. The method is exact.

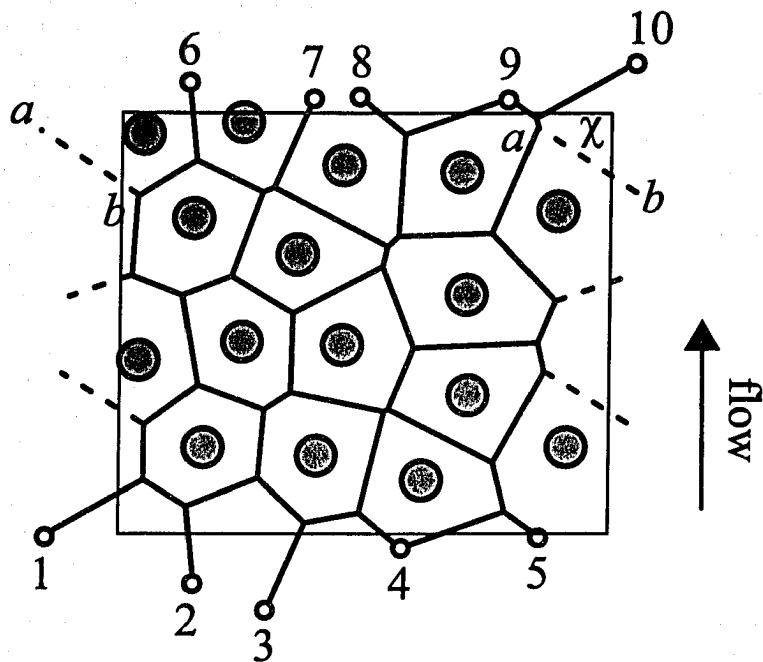Figure 6.8: Calculations of conductivity. Filled circles denotes generators (with reduced radius) and the open ones contacts, to which the pressure is applied. Nodes 6 . . . 10 have pressure 0, while nodes 1 . . . 5 have pressure p. Voronoi edges marked with dashed lines are "wrapped". For example edge χ connects points a and b. The solid rectangle marks the borders of basic computational domain.

The only problem with the above method is that its time complexity is $\mathcal{O}(N^3)$, where N stands for the number of Voronoi vertices. It appears that for 1000 generators (about 2000 vertices) this method needs about 7h to find potential for one configuration of points. Since we must perform hundreds of such operations (and for even larger systems) this approach cannot be used.

Fortunately we have the second method, based on relaxation scheme. It appeared to be much faster (order of seconds for the mentioned example) and brought no loss in accuracy. The important step is the initial guess of pressure in the vertices ans it was simply computed as if the pressure gradient in the system was uniform. The relaxation scheme is simple. The potential in each node l is substituted by the potential averaged (with weights) over the nodes connected to l, as given by the formula (3.4.16). The iteration procedure is terminated when the absolute value of change in every node is smaller the given value.

Geometrical modifier, f_ϵ, is computed from the eq. (4.4.2):

$$f_D(\epsilon) = \epsilon^2 \frac{HM}{L} \frac{D^2}{\mu} \frac{1}{g_{tot}} \qquad (6.2.12)$$

with g_{tot} coming from (3.4.55). H cancels in our calculation, as well as D^2 and μ, so the code always operated on the non-dimensional quantities. Because of periodic boundary conditions M is known exactly. L is calculated as the difference between the average positions of inflow and outflow nodes respectively.

6.2.4   Graphical output

I decided to adopt the *scalable vector graphics* SVG format as the graphical output from my code. SVG is modularized language for describing two-dimensional vector and mixed vector/raster graphics in XML. SVG specification can be found in [2].

6.3   Statistical analysis

Any Monte Carlo simulation requires building suitable statistics. Lets assume we performed n measurements of quantity x, $\{x_1, x_2, \ldots x_n\}$. The estimator for the population mean, ("sample mean") reads

$$\langle x \rangle = \frac{1}{n} \sum_{k=1}^{n} x_k. \qquad (6.3.1)$$

The central moment (measure of noise in the system) of the sample is

$$S\left[x\right] = \sqrt{\frac{1}{n} \sum_{k=1}^{n} \left(x_k - \langle x \rangle\right)^2} = \sqrt{\langle x^2 \rangle - \langle x \rangle^2}. \qquad (6.3.2)$$

Note, that this estimator is biased. *Mean standard deviation* (quality of $\langle x \rangle$ estimation) is

$$\sigma[x] = \frac{S}{\sqrt{n-1}} \tag{6.3.3}$$

and it is not biased.

6.4 Validation tests and code tuning

Several checks were made to confirm that the Voronoi diagrams produced by the code are accurate (for example by comparison with output produced by *Mathematica*). Example for $n = 300$ generators for $\epsilon = 0.6$ can be found in Figure 6.9.

As described in the Section 6.2.1, Monte Carlo generator has internal tuning mechanism. Its performance was presented in Figure 6.10. Please refer to the caption for details.

We discuss now the tests performed to confirm the numerical adequacy of the code. The first obvious check is the comparison of theoretical prediction of geometrical modifier for the regular triangular lattice, eq. (4.3.10), with the program output. It was done in Figure 6.4, full agreement exists.

Since we have to relay on the iterative procedure, which was written from scratch, we must make sure it is correct. The first test was presented in the Figure 6.12 and verifies relation (6.2.12):

$$g_{tot} \frac{\mu}{HD^2} = \epsilon^2 \frac{M}{L} \frac{1}{f_D(\epsilon)}. \tag{6.4.1}$$

Void volume $\epsilon = 0.3$, number of cylinders 500. In the case when the lattice underwent thermalization initial number of MC steps was 50. After that 10 samples were collected, each separated by 2 Monte Carlo steps (2 attempts to displace every discs). The immediate conclusion is that the above equation works. Also the example serves as additional proof that both iterative and exact method lead to the same solution (also in the case of disordered systems).

It is also quite important to see how the systems reaches the thermodynamical equilibrium. Figure present the "time" evolution of the system slowly melting from the initial triangular ordering for three different system sizes. It seems that smaller systems produces much more noise. The time of reaching equilibrium state may be safely taken to be 50 MC steps and weakly depends on the size of the system. ϵ was kept 0.3 and the system was approximately square.

Next we may investigate finite size effects in our simulations. Mean standard deviation (6.3.3) obeys power law

$$\sigma \sim n^\alpha, \tag{6.4.2}$$
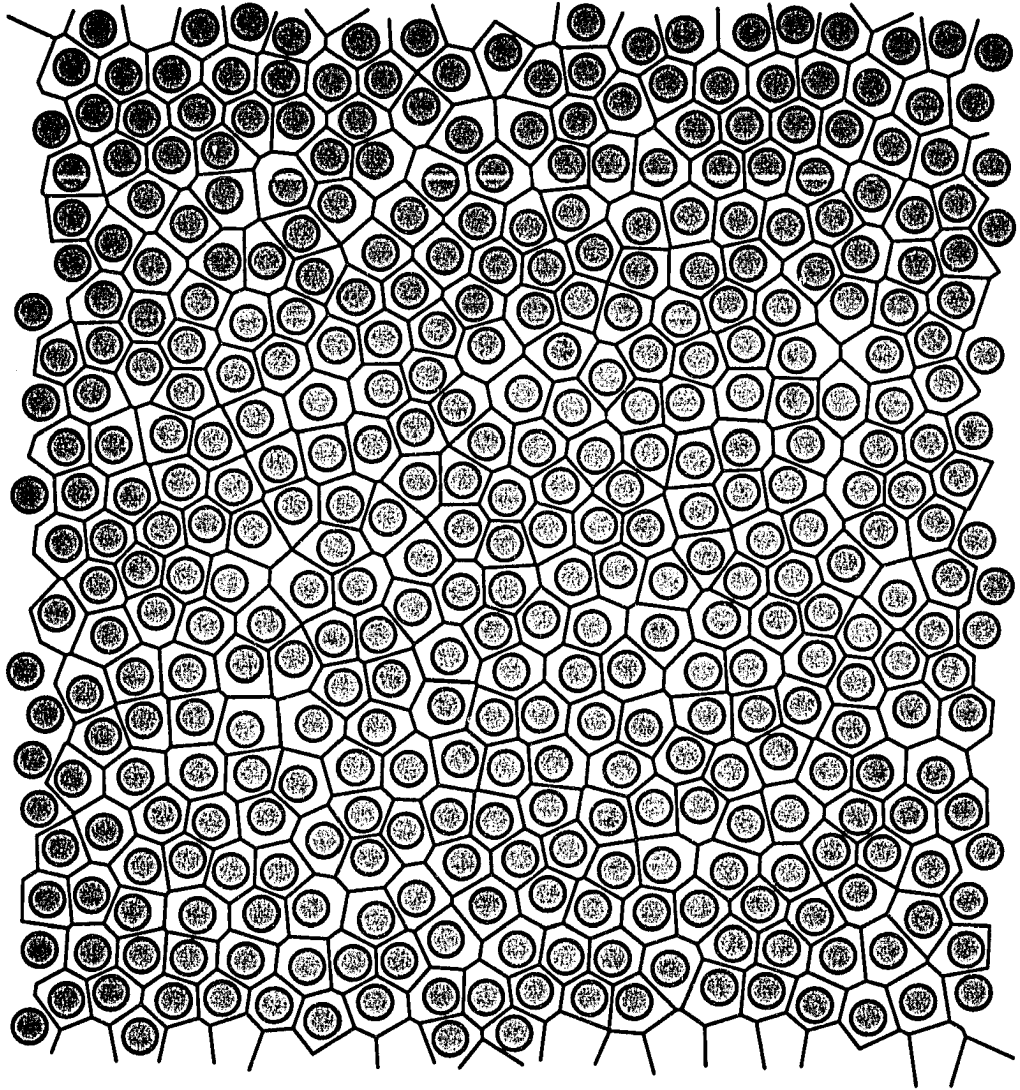
Figure 6.9: Example of Voronoi diagram for 400 generators, $\epsilon = 0.4$. Wrapped edges were removed and computational domain is approximately a square. Flow points upward. Figures 6.19 to 6.23 pertain to the same configuration of cylinders.

a)

b)
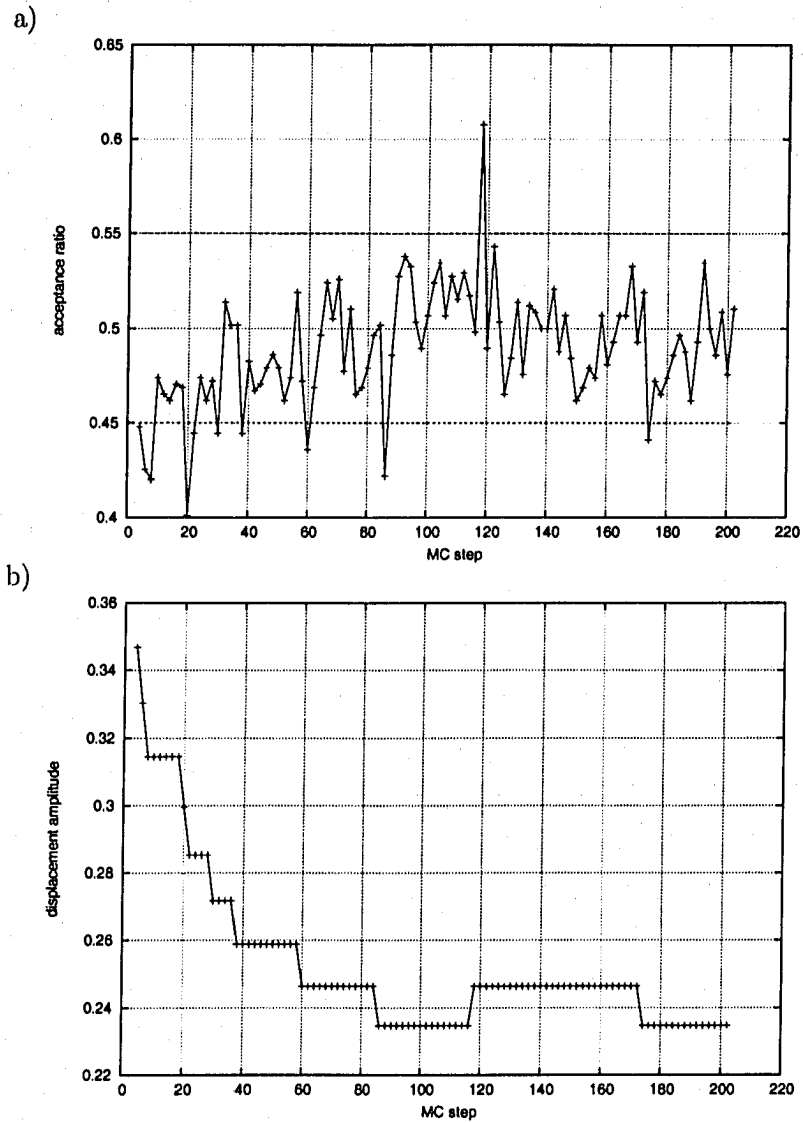
Figure 6.10: Example of the performance of internal tuning mechanism in the Monte Carlo generator. System features: $n = 300$, $\epsilon = 0.5$ and $\eta \approx 1.0$. Panel a) presents evolution of acceptance ratio, b) displacement amplitude d. If the acceptance ratio leaves the interval $[\mathfrak{m} - \delta/2, \mathfrak{m} + \delta/2]$, the code increases or decreases the amplitude as described in Section 6.2.1. With MC steps the value seems to approach asymptotic value. $\mathfrak{m} = 0.5$ and $\delta = 0.1$ were used throughout the simulations.

Figure 6.11: Comparison of geometrical modifier computed by the code with the theoretical prediction (4.3.10) for triangular lattice. Full agreement exists. The system consists of about 200 cylinders and $\Delta x \approx \Delta y$.

Figure 6.12: System conductivity (in units $\frac{HD^2}{\mu}$) as a function of sample shape.

Figure 6.13: Thermalization of three systems with different sizes.

where α was found to be equal to

$$\alpha = -0.456 \pm 0.050. \tag{6.4.3}$$
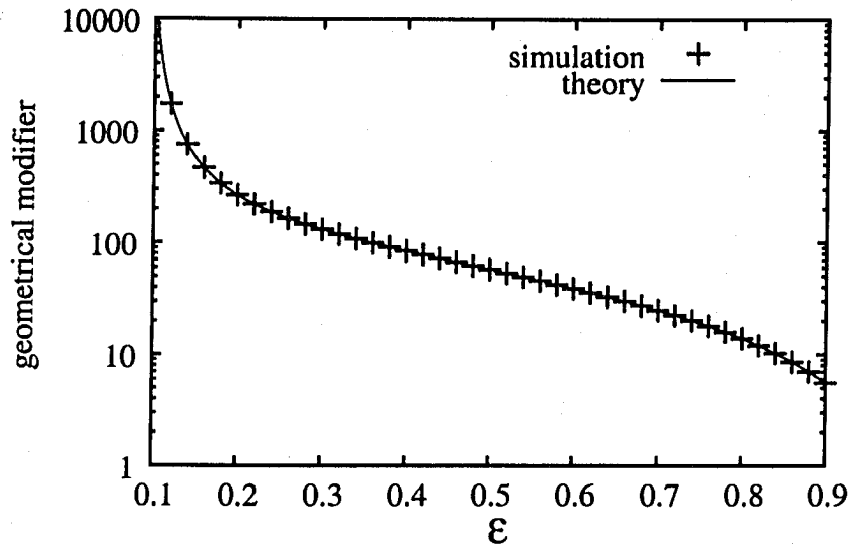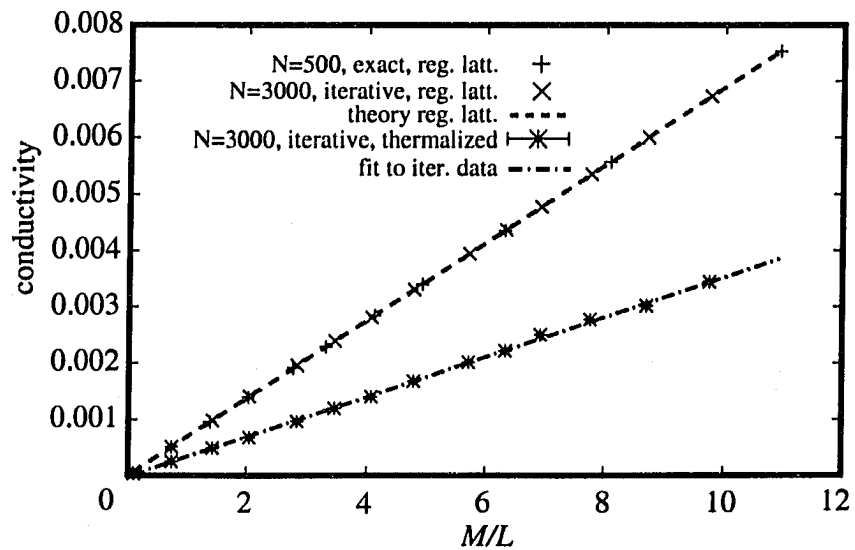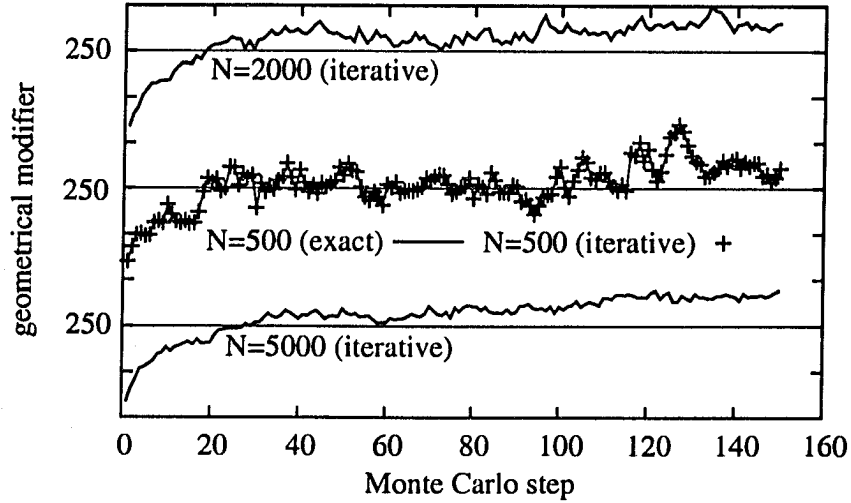
The above result suggests that geometrical modifier is well defined thermodynamical observable.

There is a finite size effect present in the system, see Figure 6.14; it seems that for smaller systems the geometrical modifier is slightly smaller and approaches certain asymptotic value for large number of particles. The source of the effect is probably connected with the way how the actual size of the system is computed (Section 6.2.3). It was found that the system of size $n = 3000$ is large enough to safely work with.

6.5 Results

6.5.1 Calculations of the drag

Figures presents the results of numerical calculations of the geometrical modifier for disordered assemblage of cylinders. Number of cylinders used in the simulation was 3000. Thermalization of the system took 50 MC steps. The averages for each ϵ were calculated using 25 samples, taken after each 2 MC steps.

The geometrical modifier was calculated for all three models of throat: Miyagi model, flow between parallel walls and the integrated throat. In all cases the disorder lead to increase of the drag force. Results were presented in the Figure 6.15abc. It appears that for $\epsilon \lesssim 0.5$ the drag is simply

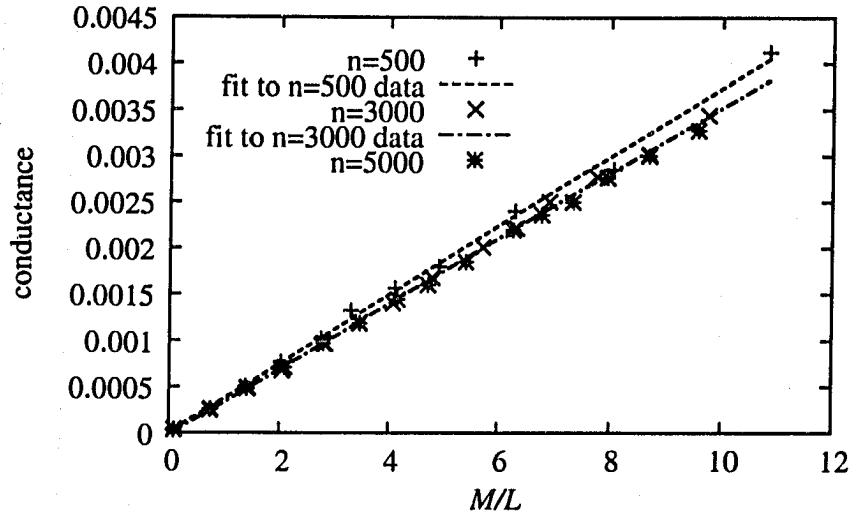$$f_D(\epsilon) = cf_{Dhex}(\epsilon), \tag{6.5.1}$$

Figure 6.14: There is a finite size effect present in the simulation: geometrical modifier seems to depend on the size of the system (slightly increasing with n). For the presented example $\epsilon = 0.3$. Fits to data for $n = 3000$ and $n = 5000$ do not differ within the numerical error, but are different from the fit to data for $n = 500$. The effect is an artifact caused by the algorithm for system size estimation.

where $f_{Dhex}(\epsilon)$ denotes the geometrical modifier for triangular lattice. Below $\epsilon \approx 0.5$ the shape of the function changes. Constant c depends on the model of the throat and more precisely on the leading order in the powers of $\frac{s}{D} - 1$ expansion of conductance function, where s denotes separation of cylinders and D their diameter. The following artificial conductance function was used

$$g(\alpha) = (\alpha - 1)^q, \tag{6.5.2}$$

where $q \geq 0$ and $\alpha = \frac{s}{D}$. Next function $c(q)$ was computed. It is presented in the Figure 6.16. $c(q)$ appeared to be ruled by simple empirical exponential law:

$$c(q) = \exp(aq). \tag{6.5.3}$$

Optimal fit was found for

$$a = 0.3488 \pm 0.0014. \tag{6.5.4}$$

Figure 6.17 presents the calculations of geometrical modifier for the network, where each throat has equal conductance, set to 1 in units HD^2/μ. For small void volumes the geometrical modifier for both regular and irregular networks are equal, what supports the observation that at high densities the topology is primarily that of triangular lattice. For larger void volumes, i.e. for increasing topological disorder, drag for regular lattices
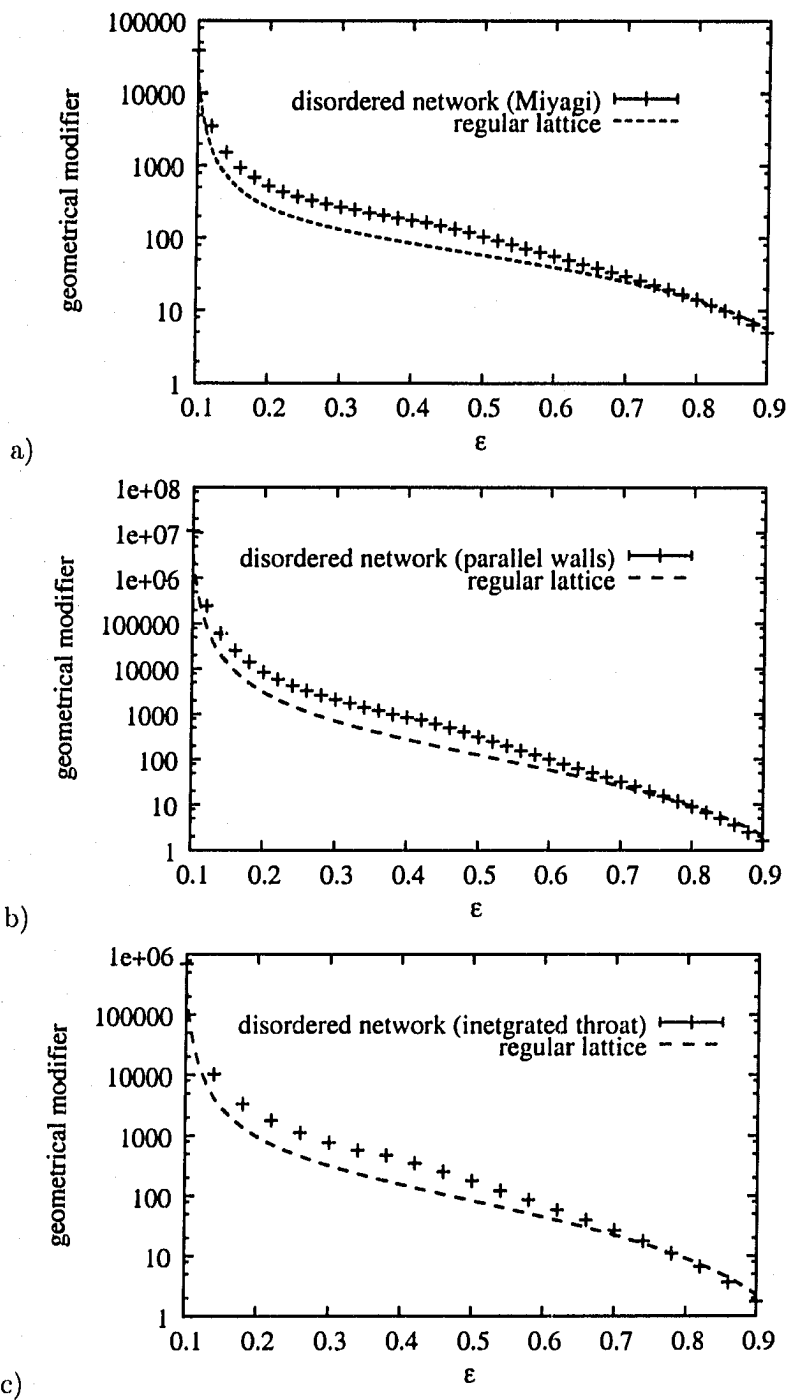
a)

b)

c)

Figure 6.15: Effect of disorder for the systems with different model of throat: a) Miyagi model, b) parallel walls throat, c) integrated model.
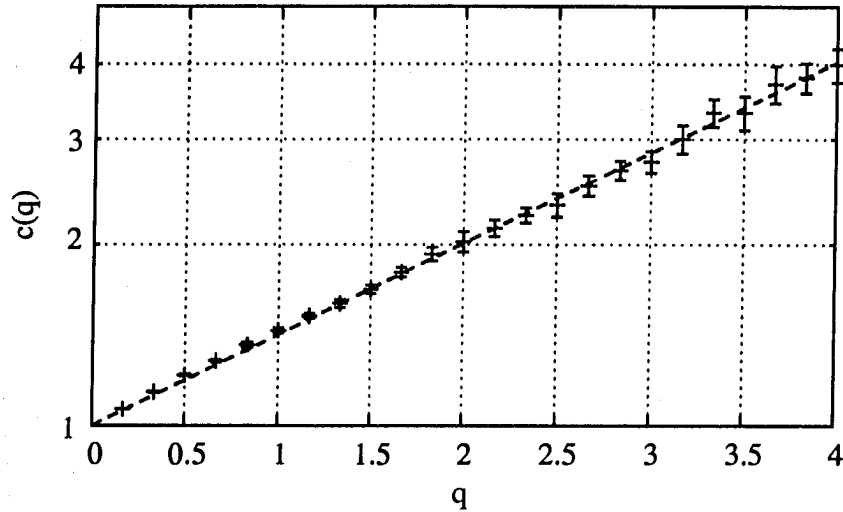
Figure 6.16: Function $c(q)$ seems to follows exponential law given by (6.5.3).

is slightly smaller. The change however is not significant comparing to impact of changes in the values of conductances.

We have a chance to verify uniform gradient hypothesis. We focus on the Miyagi model. For the system from the previous section geometrical modifier was calculated as if the endings of resistors (Voronoi vertices) were placed in the field with constant pressure gradient. The same was done for "3-stars", please refer to Figure 5.1 and comments in the beginning of Chapter 5. Additionally the total resistance of network was computed as if the network of resistors had hexagonal topology with values of all resistors equal to average resistance of the throats in the system. The results are plotted in the Figure 6.18.

None of the quantities serve as good approximation to total conductance of the lattice, also in the case of other models of throat. The uniform gradient hypothesis needs to be refuted, at least when we insist on using small clusters. Surprisingly both of the uniform gradient approximations lead to similar results and recover the geometrical modifier for undisturbed triangular lattice. It seems to be one more piece of evidence that locally the lattice is hexagonal and that non-locality plays important role in the problem.

6.5.2 Correlations

To understand, at least qualitatively, the results presented in the previous subsection, we must investigate the correlations emerging in our models with the introduction of disorder.

We could be tempted to explain the change in the drag using some kind of form factor, saying that conductance of disordered lattice is basically that of the hexagonal (shape of the function does not change after all), but the internal topology somehow changes. This
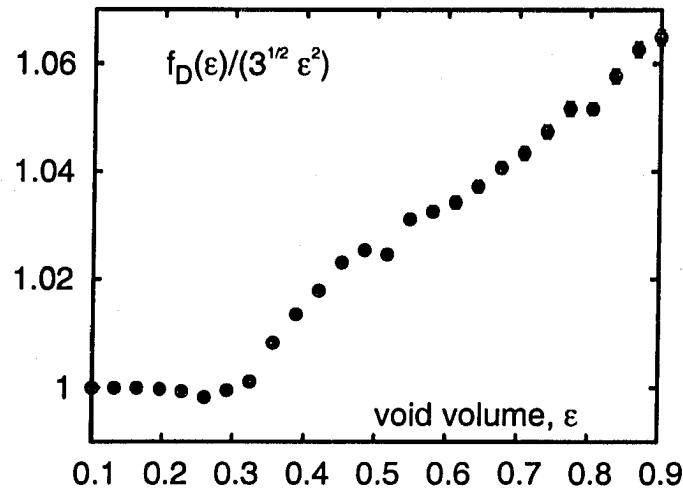
Figure 6.17: Geometrical modifier for the networks where each existing link has constant conductivity.

statement cannot grasp the actual phenomena in the system. Let us have a look on the flow fields presented in the Figures 6.19, 6.20 & 6.21. Lines thickness in the Figures is proportional to volumetric flow through the throats. Void volumes for all examples was $\epsilon = 0.4$, the computational domain was approximately square and "wrapped" edges were removed. Macroscopic flows point upward and all pictures pertain to the same cylinders' configuration, presented in the Figure 6.9. If the conductances of all links are equal, the flow in the network is naturally uniform and resembles strongly the flow in regular lattice (as shown in the previous section): flow field is homogeneous and very often links perpendicular to macroscopic flow are dead (Figure 6.19). But once the throats are given natural weights (i.e. smaller openings have smaller conductances) the picture changes dramatically. We can clearly see the emergence of well defined mesoscopic patterns of flow. Most of the system does not conduct and I call this regions clusters. When the conductance function becomes steeper, the patterns become more distinct, but generally do not change (6.21). The phenomenon may be easily understood qualitatively. The system is uniform, but for the stronger dependence of conductances on openings local inhomogeneities can more effectively block the whole clusters of network, which then become unaccessible for flow and hence lead to jump in the conductivity.

It seems that the blockades are localized not on the boundaries of the clusters, but rather in their centers and corresponds to throats with much larger than average pressure drop, Figure 6.22. These drops in turn are clearly correlated with tight throats. The
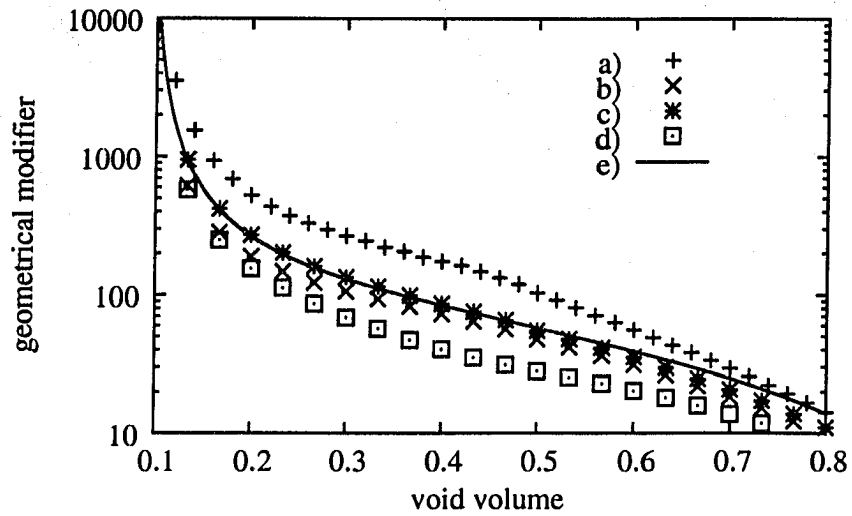
Figure 6.18: Possible observables in case of Miyagi model of throat. a) pertains to exact calculations, b) and c) utilize mean gradient hypothesis (for single resistor and for 3-stars), d) was calculated as if the lattice were triangular (all throats identical) with the value of conductance g_0 equal to average throat conductance in the system. e) is theoretical prediction for regular triangular lattice. Error bars are smaller then the size of the data points.
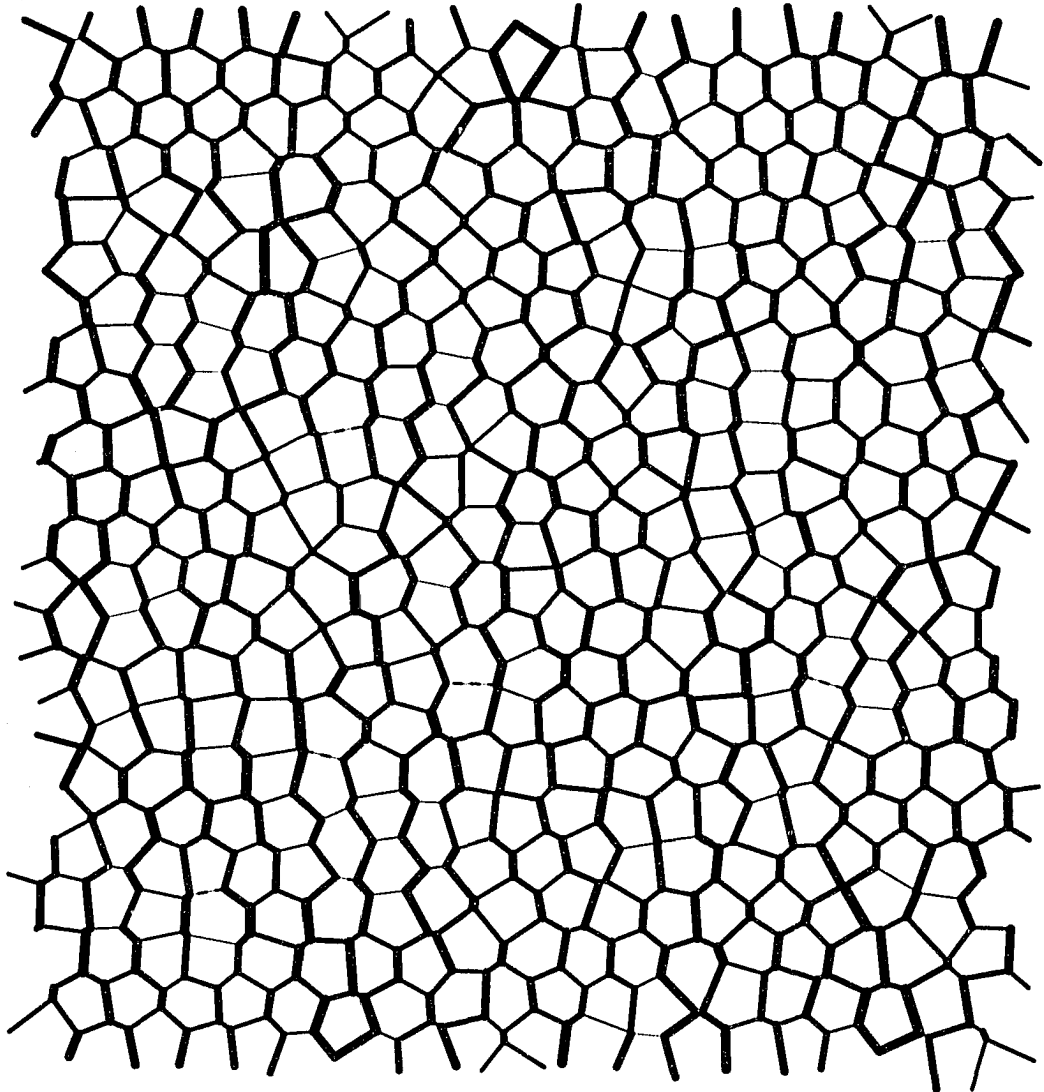
Figure 6.19: Flow in the disordered topology: all throats have the same conductance.
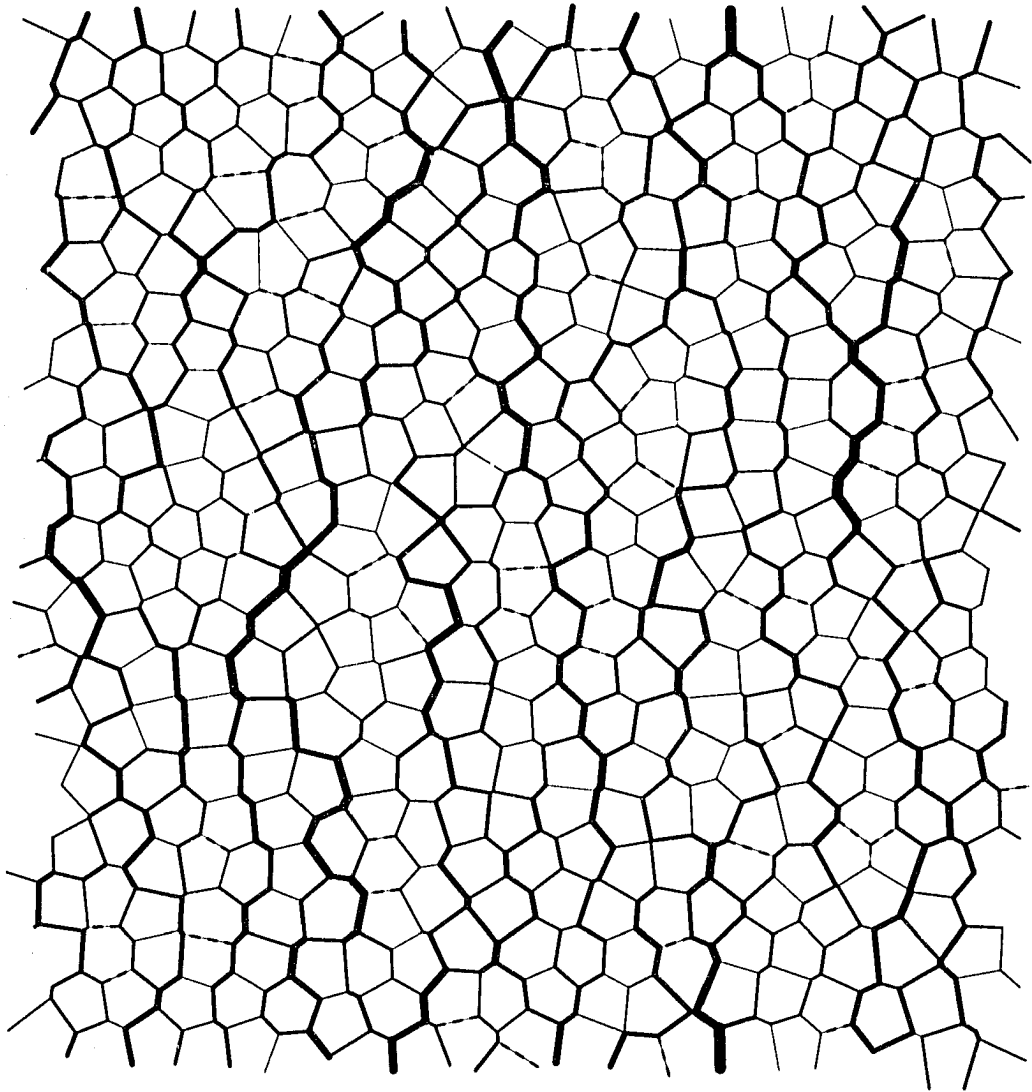
Figure 6.20: Flow in the disordered topology for the throat model $g \sim \left(\frac{s}{D} - 1\right)$. The dashed lines denote links that carry current smaller than 1% of maximal current found in the system.
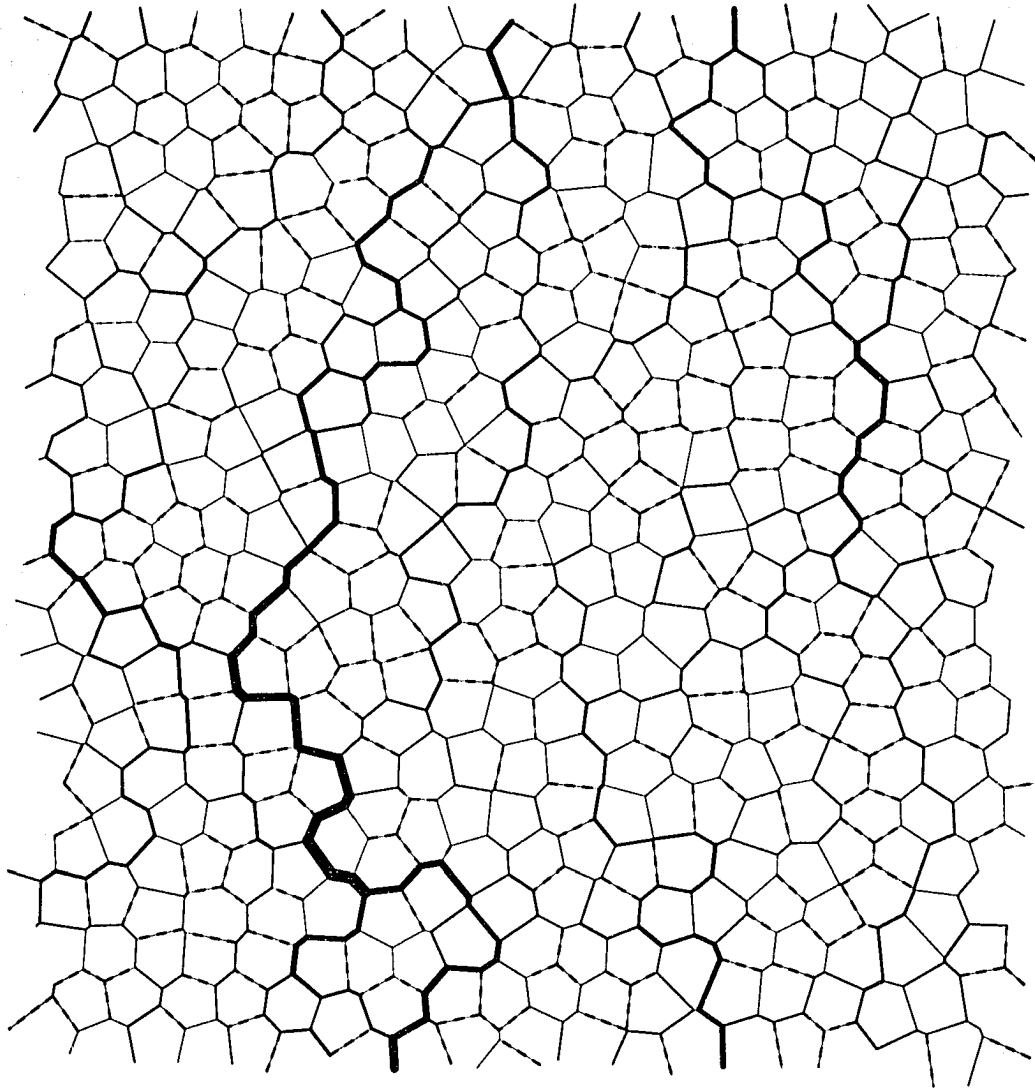
Figure 6.21: Flow in the disordered topology for the throat model $g \sim \left(\frac{s}{D} - 1\right)^3$. The dashed lines denote links that carry current smaller than 1% of maximal current found in the system.
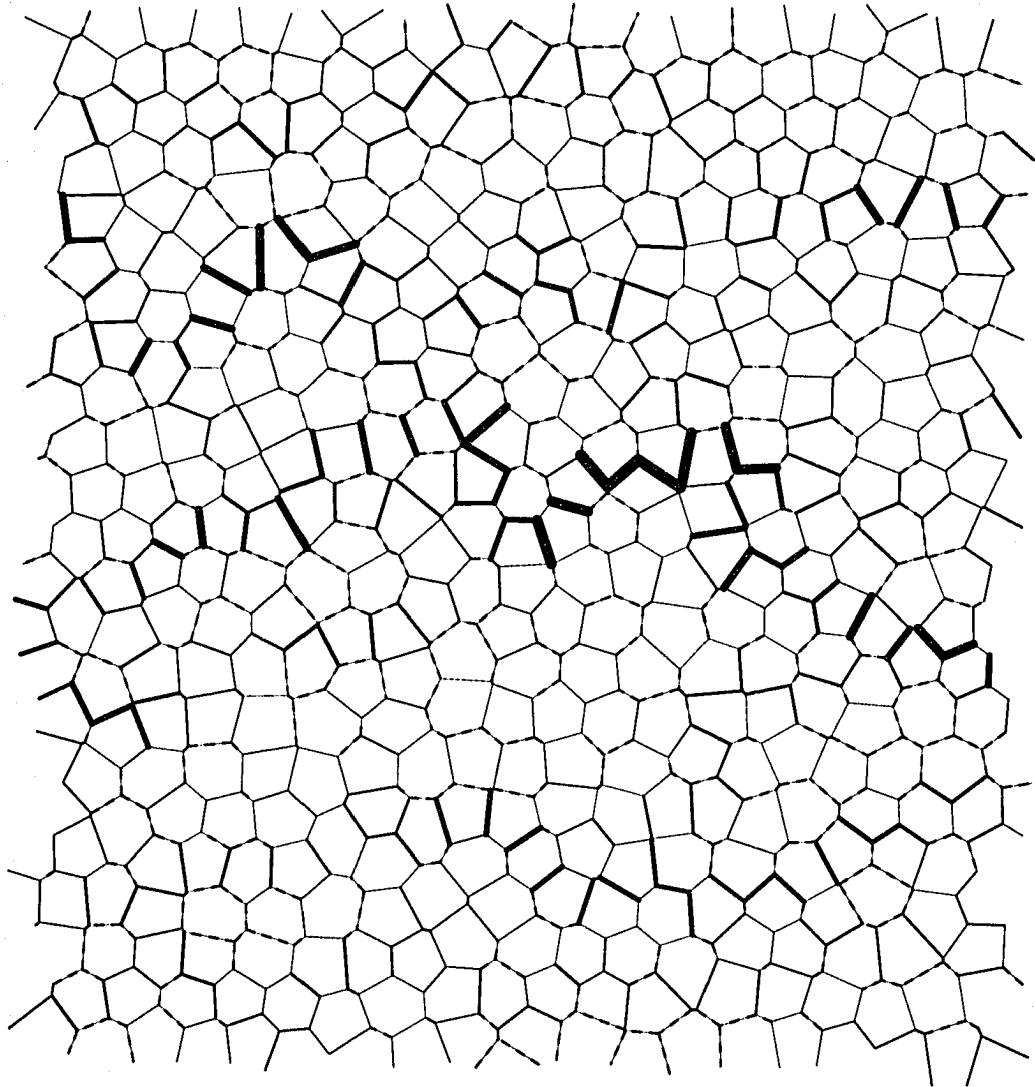
Figure 6.22: Pressure drop on the throats. The setup is identical to that presented in the Figure 6.21.

complexity of the picture is amplified by the fact that the clusters have in fact internal, hierarchical structure. The flow field may posses fractal-like structure, flow resembles a bit river deltas.

We can now understand the failure of mean field (uniform gradient) hypothesis: the system is strongly correlated. The key to analytical description is not only understanding properties of local configuration but tracing the mentioned mesoscopic structures. We see that the solution should concentrate on *percolations* in the system.

To estimate the size of inhomogeneities we investigate the distribution of powers dissipated in the diagram, Figure 6.23. The "hot throats" (those producing the most of the power) do not form agglomerates but are rather dispersed and it seems that their separation should be good estimate of the sizes of clusters. As the throat function become steeper, positions of hot throats do not change, but as in the case of currents their pattern become clearer (the hottest throats become even hotter and the cold and warm cool down) and their mutual distances should increase. By the "distance" we understand the distance from the given hot throat to the nearest hot neighbor. The throat is regarded as "hot" if the power dissipated on it is larger than

$$P_{min} + \tau(P_{max} - P_{min}),$$

$$P_{min} + \tau(P_{max} - P_{min}), \tag{6.5.5}$$

where P_{min} and P_{max} are respectively the smallest and the largest powers dissipated on any of the resistors and $\tau \in [0,1]$ is a certain threshold. Indeed, when the conductance function become steep we can see that average distance between the nearest neighbors approach an asymptotic value, which could serve as an estimate of correlation length in the system. The calculations were presented in the Figure 6.24. These kind of computations demands a lot of computational time if we want to keep the errors reasonable: the number of hot throats is rather small fraction of total links and we need to sample much more configurations than in the case of f_D.

6.5.3 Emergence of large deviations

In this section we study the distributions of flow parameters assigned to single throats, namely powers dissipated and flows. To allow comparison of distributions for different models we consider normalized quantities.

Normalized power is defined as

$$\tilde{P}_k = \frac{\mu}{D^2 H} \frac{\lambda'}{G^2} P_k, \tag{6.5.6}$$

where H is the height of the cylinders, D their diameter, μ viscosity of fluid, G macroscopic pressure gradient in the system, P_i the power dissipated in the given throat and λ' stands for the number of throats per unit area of the system:

$$\lambda' = 3\lambda. \tag{6.5.7}$$
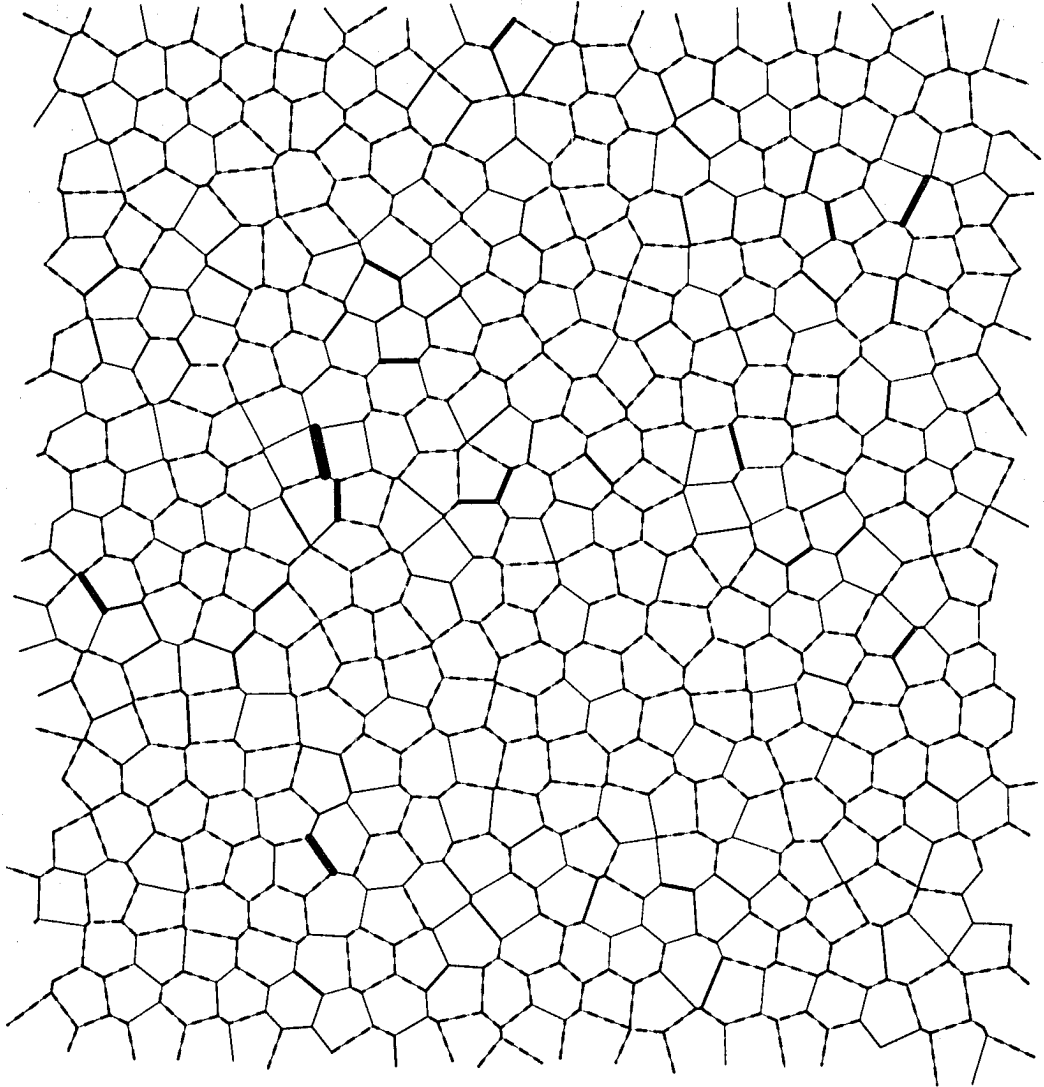
Figure 6.23: Distribution of powers produced in the throats. The setup is identical to that presented in the Figure 6.21.
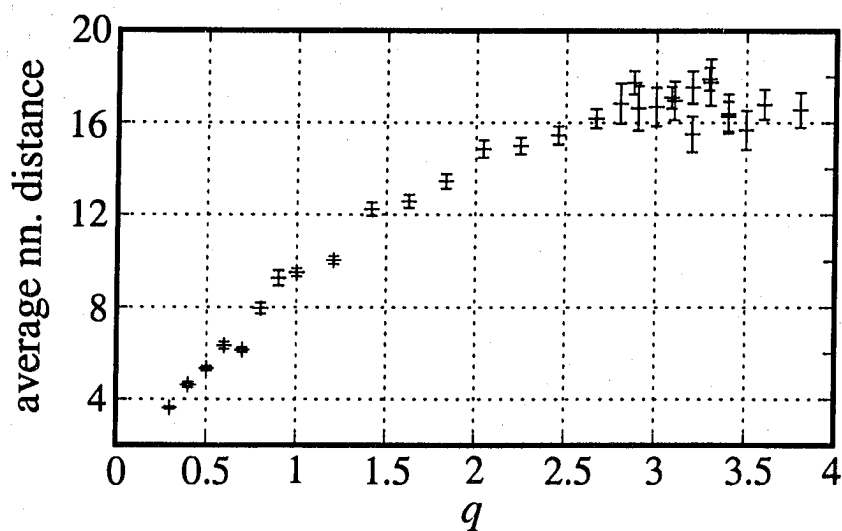
Figure 6.24: Average distance between nearest hot neighbors as a function of exponent q, as defined for function (6.5.2). Length scales in the system are: $D = 1$ and $1/\sqrt{\lambda} \approx$ 1.05924, where λ is number of cylinders per unit area. $\epsilon = 0.3$. Number of cylinders was around 3000 and the computational domain was approximately square. Threshold τ was set to 0.75. The saturation of the distance can be clearly visible. The asymptotic value appears to be around 16.

Easy calculation show that

$$f_D(\epsilon) = \epsilon^2 \left\langle \widetilde{P}_k \right\rangle^{-1}. \tag{6.5.8}$$

Normalized current reads similarly

$$\widetilde{I}_k = \frac{\mu}{D^2}\frac{\theta}{HG}I_k, \tag{6.5.9}$$

where

$$\frac{\theta}{H} = \frac{\sqrt{\lambda}}{H} \tag{6.5.10}$$

is the average number of links per unit area crossing given cross section plane perpendicular to macroscopic flow. I_k denotes volumetric flow in the throat k. We have

$$f_D(\epsilon) = \epsilon^2 \left\langle \widetilde{I}_k \right\rangle^{-1}. \tag{6.5.11}$$

Let us first take a look on the probability density of currents presented in the Figure 6.25ab. For the unweighted networks (a) two clear peaks can be pointed. For the regular lattice the correspond to the throat perpendicular to the direction of the flow (peak around zero) and to throats with current. We see that if we disorder topology leaving the conductances of the throats unchanged, positions of peaks do not change, but they are somewhat broaden. When the throats become weighted the pictures changes completely. The densities become strongly peaked around zero and feature long fat tails. We can note that for the steeper the conductance function becomes the more its tail approaches the exponential distribution.

We could expect that the "rivers" clearly present in the system should form peak for large values of current. This is however not the case. Large currents in the system are rare events and most of the system is dead. Similar emergence of current rivers for exponentially weighted square lattice of resistors was recently reported in [97]. According to authors of this paper large currents are associated with so called "optimal paths", ie. sequences of links that minimize the total resistivity between source and sink.

Densities of normalized powers can be described in similar terms, however the tails of the distributions are not as fat as in the case of currents. They were presented in the Figure 6.26. Underlying networks are random and weighted.

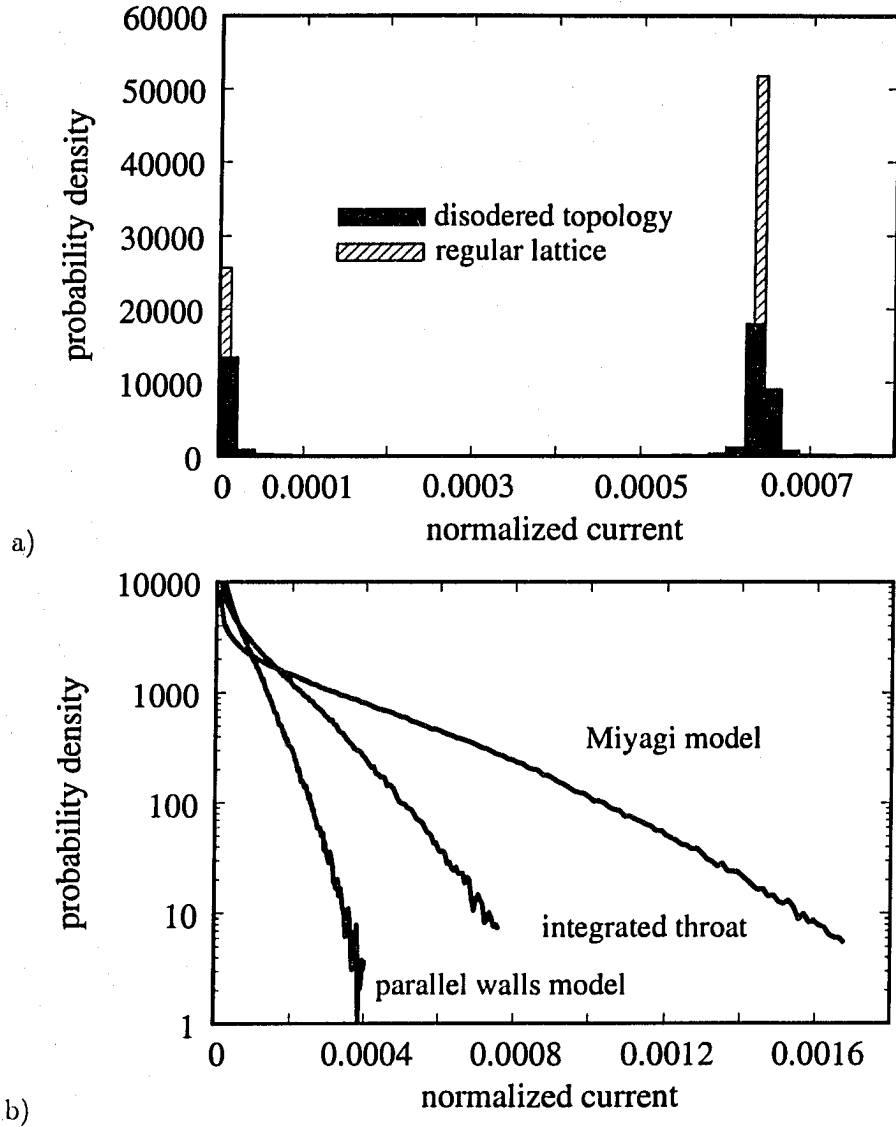Figure 6.25: Distribution of normalized currents. Panel a) pertains to unweighted networks constructed with Miyagi model. Panel b) presents the distributions for the weighted networks. $\epsilon = 0.3$, compuational domain was approximately a square. The number of cylinders used was 3000. Please refer to the discussion in the text.
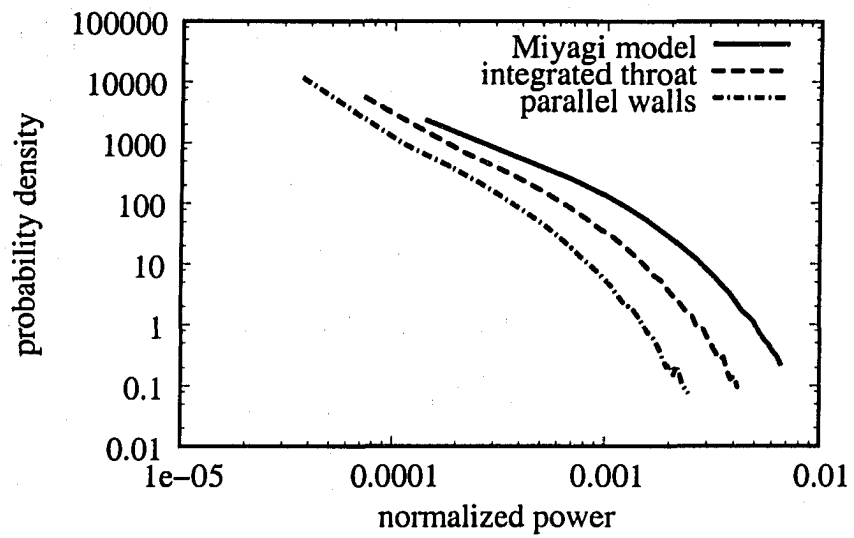
Figure 6.26: Distribution of normalized powers for the examples discussed.

Chapter 7

Summary

7.1   Retrospection

The oil refineries processing heavy bituminous hydrocarbons utilize fluidized beds, i.e. columns filled with fluidized coke suspended in the stream of steam. The coke particles serve both as a source of heat and as a surface for the process of thermocracking. Numerical simulations of multiphase flows in such systems are an essential tool for designing modern chemical reactors. The standard method used is to treat both phases as continuous interpenetrating media and to solve the pair of Navier-Stokes equations for them. An indispensable closure relation for this problem is the term which couples the two equations, interphase drag.

The drag is defined as a force acting between the phases per unit volume of the system. The natural way to calculate this quantity analytically is to abandon the continuous approximation and investigate the flow of fluid between particles. Since we do not need to track the history of each grain, usually the momentum transfer is constructed as a statistical quantity; in this work we utilized the method of spatial averages. This requires the introduction of an additional length scale, defining the size of the region over which the forces are averaged. The most general and straightforward method for dealing with our problem is to solve simultaneously the equations of motion for each particle (they possess both translational and rotational degrees of freedom) and for the fluid surrounding them (Navier-Stokes equation), fulfilling the proper boundary conditions on the surface of particles. The force and momentum acting on the grains are calculated by integration of fluid stress tensor over their area. We do not have tools to solve this problem exactly at the present time.

The only existing exact analytic solutions are constrained to void volumes (void volume ϵ is a fraction of the system not occupied by the solids) close to 1, where only pairwise hydrodynamical interaction can be taken into account. Furthermore, it is often assumed that the system is quasi steady, i.e. that for each configurations of grains we need to solve steady state Navier-Stokes equation with non-slip boundary conditions on the particles' surface. Another standard assumption adopted is that the relative Reynolds number for particle and fluid phase is small and therefore the inertial terms may be discarded.

Finally we have to assume that the microdynamics of grains is not affected by the flow field, i.e. the probability that the given configuration of particles occurs is solely a function of the mutual interaction between solids. This may be regarded as infinite solids density assumption. The drag may be then computed as an average over an ensemble of particles' configurations.

Let us briefly discuss these assumptions. We must surely abandon the first one: the drag strongly increases when the void volume decrease and becomes important exactly where particles are close to each other and many-body interaction cannot be discarded. The other assumptions are surprisingly good. Reactor is in general a turbulent system, but the turbulence occurs on the scales which are very large compared to interparticle distance; relative motion of the phases in the most interesting regime of large concentration is rather smooth. Nonetheless the last assumption that the granular dynamics is flow-independent is at least questionable. It may serve as a good starting point, but ultimately we must also investigate the impact of the flow on the phase space of grains. Surprisingly, there exists an evidence [70], that the rotational movement of particles may be more important in this case than translational; rotation is usually a good way to release the hydrodynamical stresses in the fluid-particle system.

There exists a method of dealing with creeping flows in the constrained geometries, used for the first time in the studies of flow through porous media [13]. It is based on the observation that in such systems flow occurs in the well defined paths defined by contractions between particles (in throats). For small Reynolds numbers such throats behave like Ohmic resistors, the pressure drop along them is proportional to the mass flow. From this point of view the interface drag may be computed as the net resistivity of a random resistor network. The model has two important advantages. First of all it appeared to be useful; it allowed to predict the permeability of porous medium spanning 5 orders of magnitude and agreeing perfectly with experimental data. Second, the electric analogy seems to be much more tractable than the direct attack on the Navier-Stokes equation. Finally we can obtain some analytical insight into the low ϵ regime. The drawbacks are obvious. The method is purely heuristic, we cannot control the quality of our approximation and it hardly gives us any chance to release the infinite solids density assumption.

The electric method requires three key elements. First of all we need a solid formalism to deal with a linear electric network, which this work provides. Second we must elaborate the accurate model of the throat, based on the properties of local configurations of particles. Finally, having calculated the conductance of every throat, we must find the net conductance of the whole network.

We build model of the throat by investigation of flows in regular network of resistors. There exists an exact periodic solution of Navier-Stokes equation based on Fourier techniques and constructed as (singular) perturbation series in powers of $1 - \epsilon$. We match it with the electric solution suitable for small ϵ and in this way get the throat conductance function. Regular lattice has a very pleasant property, namely we can deduce the macroscopic properties of the medium just by investigating the local configurations of particles. This observation was called the uniform gradient hypothesis. We suspected that the same law might be applied to disordered systems. Briefly, uniform gradient

hypothesis is a mean filed theory which assumes that the throats are independent and the pressure drop on their ends may be calculated as if they lied in the pressure field with a constant gradient. The refinement of this method might include consideration of larger groups of connected resistors.

Every reasonable analysis of the electric model must be based on the statistical studies of local structures formed by the particles. The identification of nearest neighbors is performed by means of Voronoi diagrams. To obtain the solution, at least under independent resistor assumption, we need joint probability density for Voronoi edge and corresponding interparticle distance (Delaunay edge). Analytic solution of this problem was obtained, but in general calculations are possible only for Poisson point field (i.e. for the case of non-interacting points). Also building the relevant distributions for larger structures (clusters) is hopeless.

We undertook series of numerical simulations of the lattices emerging in our problem, primarily to understand the role of correlations in the system and to verify the uniform gradient assumption. As the source of configurations the gas of hard discs was taken. We were working with the constant density ensemble. The configurations were sampled using self adjusting Monte Carlo generator. Voronoi diagrams were built utilizing slightly modified VORONOI2 library written in FORTRAN77 and ported to Component Pascal, which was chosen as the primary programming language for this project. Finding the net conductance of the network requires basically the solution of a set of linear equations. The exact methods to achieve that appeared to be extremely expensive as far as the computational time is concerned, so an iterative method was developed, together with the proof of its convergence. The engine for the project was carefully tested.

Numerical studies demonstrated that even the severely simplified electric model posses number of interesting properties. It appeared that the drag is well defined thermodynamical observable. Standard deviation of its mean vanishes in the thermodynamical limit of infinite grains number, obeying $1/\sqrt{n}$ power law. It was generally found that the drag for the lattice is generally smaller than for disordered network. Studies showed also that mean gradient hypothesis had to be refuted, the system appeared to be strongly correlated.

The disordered network arising when assemblages of hard discs are concerned resembles topologically hexagonal lattice. When the throats are given equal conductances the topological disorder leaves the interphase drag almost unaltered. The factors responsible for the increase of drag are natural weight attached to the throats (smaller openings have higher resistivity). This leads to formation of clusters (regions devoid of flow) and rivers, carrying most of the current. Disordered networks are strongly non local as opposed to flow in regular lattices, where the flow patterns are repeated with the periodicity of the lattice, necessarily much smaller that averaging region. We pointed the way to estimate the correlations length scale, but at this stage we cannot explain quantitatively its value.

The difference between weighted and unweighted nets can be also visible in the distributions of current flowing through particular throats and powers dissipated. Unweighted networks feature distinct peaks in their distribution of currents (and powers), while the distributions for weighted networks are gathered around zero and have very long fat tails, which in case of current distributions are clearly exponential. It is interesting to

note that the rivers, so apparent when inspecting the flow field, cannot be seen in these distributions. Significant currents are merely large deviations in weighted systems.

The emergence of large currents has significant implications. We started with a picture of two continuous fluids that move smoothly though each other – the already discussed scale separation is the necessary assumption if we want to simulate reactors by means of partial differential equations, which necessarily deal with the quantities that are defined strictly locally. We end up with the correlation scale that is of order of 10 particle diameters. Usual coke particles used in Syncrude cokers are around 0.1mm, which means that our correlation are of order of millimeters, ie. macroscopic. It signifies in turn that our procedures of spatial averaging should be carefully reexamined. It seems that the assumption of scales separation ("granular details wash out") may be not appropriate in the real life problems.

Every source I used is acknowledged, nevertheless it is desirable to state explicitly which part of the work is my original contribution. The literature review from Chapter 2 was prepared by me. Also the translation of interphase drag into language of resistors networks is original (Chapter 3) together with the presented models of throats (Section 4.1). The matrix formulation of linear resistors network given in Section 3.4 is mine. I Chapter 4 I extended the work of Hasimoto, used it to gauge Miyagi model of throat and calculated the flow in the presence of phonon disorder. In Chapter 5 I repeated calculations of Collins (they were not given explicitly) for the probability density for Delone edge of Poisson point field and extended the method to give integral representation for joint probability for Delone and Voronoi edges for the case mentioned. The whole material from Chapter 6 is original (as well as the code in CP with exception of `Voronoi2` library).

7.2 Vision

We can think of the future of this project in two categories. First we could refine the network model and second take completely different approach to analytical calculations of drag.

Network model has to take into account movement of particles driven by the flow. The easiest scheme could be the following. We solve NS equation (by means of electric method) for given configuration of particles and then calculate the forces and momenta acting on them. In the next step the particles are moved and the scheme continues. In this approach we would need to modify our throat model to take into account the movement of the contractions' walls.

Also it seem that emergence of rivers makes the problem closer to percolation theory, which gives us another chance of an analytical study. Percolation theory is a well developed discipline, but existing solution have been found almost only for regular, unweighted graphs, without correlations between bonds [48]. Our graphs hardly follow this assumptions.

We should move toward 3D systems. Although most of ready-to-use algorithms for computing Voronoi diagram are concerned with 2D sets of generators, there are in general

no obstacles to repeat our simulations in 3D.

On the other hand it becomes possible to simulate the flow in porous media by direct numerical solution of Navier-Stokes equation. It seems also that we are approaching slowly the moment when taking into account not only the dynamics of fluid but also that of the grains will be feasible. With the growing power of computers the problem can be solved by brute force.

Nevertheless we should remember that it is analytical solution of the problem that we are really aiming for. It is unclear at the present moment if the theory of stochastic differential equations (taking into account non regularity of boundary conditions), will be any help, but clearly the key to understanding of the drag is hidden in statistical physics.

Bibliography

[1] http://planetmath.org/encyclopedia/GerschgorinDisc.html.

[2] Scalable Vector Graphics (SVG) 1.1 Specification. http://www.w3.org, 2003. NET.

[3] ALBERT, R., AND BARABÁSI, A. L. Statistical mechanics of complex networks. *Rev. Mod. Phys. 74*, 47 (2002). arXiv:cond-mat/0106096.

[4] ANDERSON, T. B., AND JACKSON, R. A fluid mechanical description of fluidized beds. *Ind. Eng. Chem. Fund. 6*, 4 (1967), 527–539. SCI/TECH TP 1 I1.

[5] BATCHELOR, G. K. *An introduction to fluid dynamics.* Cambrigde University Press, New York, 1967. SCI/TECH QA 911 B32 1967.

[6] BATCHELOR, G. K. Sedimentation in a dilute dispersion of spheres. *J. Fluid. Mech. 52* (1972), 245–268. SCI/TECH QA 901 J86.

[7] BELLISSARD, J., COMBE, P., ESSOH, C., AND SIRUGUE-COLLIN, M. Thermodynamic limits for Euclidean random resistors network. In *Stochastic Processes, Physics and Geometry II* (1995), S. Albeverio, Ed., vol. II, World Scientific, pp. 107–116. ILL.

[8] BORN, M., AND HUANG, K. *Dynamical theory of crystal lattices.* The Interantional Series of Monographs on Physics. Claredon Press, Oxford, 1956. SCI/TECH QD 931 B73 1956.

[9] BORN, M., AND MISRA, R. D. *Proc. Camb. Phil. Soc. 36* (1940), 466. UABARD P 11 C17.

[10] BRYANT, S., AND BLUNT, M. Prediction of relative permeability in simple porous media. *Phys. Rev. A 46* (August 1992), 2004–2011. UAINTERNET.

[11] BRYANT, S., AND CADE, C. Permeability prediction from geological models. In *Proceedings of the 3rd European Conference on the Mathematics of Oil Recovery* (Delft, 1992), M. A. C. et al., Ed., Delft University Press, pp. 209–224. ARC TN 871 E88 3rd 1992.

[12] BRYANT, S. L. Private communication, September 2004.

[13] BRYANT, S. L., KING, P. R., AND MELLOR, D. W. Network model evaluation of permeability and spatial correlation in a real random sphere packing. *Transport in Porous Media 11* (1993), 53–70. SCI/TECH TA 357 T77.

[14] BURGERS, J. M. *2nd Report on Viscosity and Plasticity*. Koninklÿke Nederlandse Akademie van Wetenschappen, Amsterdam, 1938.

[15] BURGERS, J. M. On the influence of concentration of a suspension upon the sedimentation velocity. *Proc. Kon. Ned. Akad. Wetensch. 44 & 45* (1942), 1045–, 1177– (in vol. 44), 9–, 126– (in vol. 45). ILL.

[16] CAFLISCH, R. E., AND LUKE, H. C. Variance in the sedimentation speed of a suspension. *Phys. Fluids 28*, 3 (March 1985), 759–760. PHYSCI QC 145 P57.

[17] CHANDRA, A. K., RAGHAVAN, P., RUZZO, W. L., SMOLENSKY, R., AND TIWARI, P. The electrical resistance of a graph captures its commute and cover times. In *Proceedings of 21st Annual Symposium on Theory of Computation* (Seattle, 1989), pp. 574–586. NET/PRIV.

[18] COLLINS, R. A geometrical sum rule for two-dimensional fluid correlation functions. *J. Phys. C 1* (1968), 1461–1471. UABARD QC 1 P57 C.

[19] CROWE, C. T., SOMMERFELD, M., AND TSUJI, Y. *Multiphase flows with droplets and particles*. CRC Press, Boca Raton, 1998. PRIV.

[20] DALLA VALLE, J. M. *Micromeritics, the technology of fine particles*. Pitman, London, 1948. SCI/TECH TA 407 D14 1948.

[21] DARCY, H. *Fontaines publiques de la ville de Dijon*. Victor Dalmont, Paris, 1856.

[22] DI FELICE, R. The voidage function for fluid-particle systems. *Int. J. Mult. Flow 20*, 1 (1993), 153–159. SCI/TECH QA 922 I62.

[23] DONEV, A., CISSE, I., SACHS, D., VARIANO, E. A., CONNELLY, F. H. S. R., TORQUATO, S., AND CHAIKIN, P. M. Improving the density of jammed disordered packings using ellipsoids. *Science 303* (2004), 990–993. UAINTERNET.

[24] DOROGOVTSEV, S. N., AND MENDES, J. F. F. The shortest path to complex networks. arXiv:cond-mat/0404593, to be published, 2004.

[25] DOYLE, P. G., AND SNELL, J. L. *Random Walks and Electric Networks*, vol. 22 of *The Carus Mathematical Monographs*. The Mathematical Association of America, 1984. MATH QA 274.73 D75 1984.

[26] EINSTEIN, A. Eine neue Bestimmung der Moleküldimensionen. *Ann. Phys. 19* (1906), 289–. UABARD QC 1 A61 4.F.

[27] ERGUN, S. Fluid flow through packed columns. *Chem. Eng. Prog. 48* (1952), 89. SCI/TECH TP 1 C515.

[28] EWALD, P. P. *Ann. Phys. 54* (1917), 519-. UABARD QC 1 A61.

[29] FATT, I. The network model of porous media (in three parts). *Pet. Trans. AIME 207* (1956), 144–181. ILL.

[30] FEYNMAN, R. P., LEIGHTON, R. B., AND SANDS, M. *Feynmana wykłady z fizyki*, second ed., vol. II. Państwowe Wydawnictwo Naukowe, Warszawa, 1974. PRIV.

[31] FINNEY, J. *Random packings and the structure of the liquid state.* PhD thesis, University of London, 1968. ILL.

[32] FINNEY, J. Random packings and the structure of simple liquids. I. the geometry of random close packing. *Proc. Roy. Soc. 319A* (1970), 479–494. NET JSTOR.

[33] FIXMAN, C. W., AND FIXMAN, M. Frictional coefficient of polymer molecules in solution. *J. Chem. Phys. 41*, 4 (August 1964), 937–944. UABARD QD 1 J86 v.41: no.1-4 1964.

[34] FRISCH, U., HASSLACHER, B., AND POMEAU, Y. Lattice-gas automata for the Navier-Stokes equation. *Phys. Rev. Lett. 56* (1986), 1505 – 1508. PHYSCI QC 1 P43.

[35] GARSIDE, J., AND AL DIBOUNI, M. R. The voidage function for fluid-particle systems. *Int. J. Mult. Flow 20*, 1 (1977), 153–159. SCI/TECH QA 922 I62.

[36] GERSCHGORIN, S. Über die Abgrenzung der Eigenwerte einer Matrix. *Izv. Akad. Nauk. USSR Otd. Fiz.-Mat. Nauk 7* (1931), 749–754. ILL.

[37] GERVOIS, A., TROADEC, J. P., AND LEMAÎTRE, J. Universal properties of Voronoi tesselations of hard discs. *J. Phys. Math. Gen. 25* (1992), 6169–6177. PHYSCI QC 1 J861.

[38] GIDASPOW, D. *Multiphase Flow and fluidization.* Academic Press, San Diego, 1994. ILL.

[39] GUERRA, F., AND TALEVI, M. On the thermodynamic limit in random resistors networks. *J. Phys. A-Math. Gen. 29* (1996), 7287–7299. UAINTERNET.

[40] GUIBAS, L., AND STOLFI, J. Primitives for the manipulation of general subdivisions and the computation of Voronoi diagrams. *ACM Transactions on Graphics 4*, 2 (April 1985), 74–123. PRIV.

[41] HALES, T. C. The sphere packing problem. *J. Comput. Appl. Math 44* (1992), 41–76. MATH QA 1 J856.

[42] HANSEN, J. P., AND MACDONALD, I. R. *Theory of simple liquids.* Academic Press, San Francisco, 1976. SCI/TECH QC 175.3 H24 1976.

[43] HAPPEL, J. Viscous flow in multiparticle systems: slow motion of fluids relative to beds of spherical particles. *AIChE Journal 4*, 2 (1958), 197–201. SCI/TECH TP 1 A11.

[44] HAPPEL, J., AND BRENNER, H. *Low Reynolds number hydrodynamics with special applications to particulate media.* Noordhoff International Publishing, Leyden, 1973. SCI/TECH QC 151 H25 1973.

[45] HASIMOTO, H. On the periodic fundamental solutions and their application to viscous flow past a cubic array of spheres. *J. Fluid Mech. 5* (1959), 317. SCI/TECH QA 901 J86.

[46] HJELMFELT, A. T., AND MOCKROS, L. F. Motion of discrete particles in a turbulent fluid. *Appl. Sci. Res. 16* (1966), 149–. BARD QC 1 A66.

[47] HUANG, K. *Statistical Mechanics.* John Wiley & Sons, Inc., New York, 1963. PHYSCI QC 175 H87 1963.

[48] HUGHES, B. D. *Random Walks and Random Environments*, vol. 1: Random Walks, 2: Random Environments. Clarendon Press, Oxford, 1995. MATH QA 274.73 H84 1995 v.1.

[49] ISHII, M. *Thermo-fluid dynamic theory of two phase flow.* Direction des Etudes et Recherches de Electricité de France, Eyrolles, Paris, 1975.

[50] JACKSON, R. *Fluidization*, second ed. Academic Press, Toronto, 1985, ch. Hydrodynamic stability of fluid-particle systems, pp. 47–72. SCI/TECH TP 156 F65 D25 1985.

[51] JACKSON, R. Locally averaged equations of motion for a mixture of indentical spherical particles and a Newtonian fluid. *Chem. Eng. Sci. 52* (1997), 2457–. PHYSCI TP 1 C516.

[52] JACKSON, R. Erratum. *Chem. Eng. Sci. 53* (1998), 1955–. PHYSCI TP 1 C516.

[53] JÄGER, H. M., AND NAGEL, S. R. Physics of granular states. *Science 255* (1992), 1524–. PHYSCI Q 1 S41.

[54] JONES, R. A. L. *Soft Condensed Matter*, first ed. Oxford University Press, Inc., New York, 2002. PRIV.

[55] KADANOFF, L. P. Private communication, September 2004.

[56] KEMENY, J. G., AND SNELL, J. L. *Finite Markov Chains.* D. van Nostrand Company, Inc., Princeton, New Jersey, 1960. MATH QA 273 K31.

[57] KHAN, A. R., AND RICHARDSON, J. F. The resistance to motion of a solid sphere in a fluid. *Chem. Eng. Commun. 62* (1987), 135–150. SCI/TECH TP 155 C57.

[58] KIRKWOOD, J. G. *J. Chem. Phys. 3* (1935), 300–. UABARD QD 1 J86 v.3 1935.

[59] KUWABARA, S. The forces experienced by a lattice of equal flat plates in the uniform flow at small Reynolds numbers. *J. Phys. Soc. Jpn. 13*, 12 (December 1958), 1516–1523. UABARD QC 1 P578.

[60] LAMB, H. *Hydrodynamics.* Cambridge University Press, Cambridge, 1932. PHYSCI QA 911 L22 1932.

[61] LANDAU, L. D., AND LIFSHITZ, E. M. *Fluid mechanics.* Pergamon Press, London, 1959. SCI/TECH QA 901 L25 1959.

[62] MAK, C. H. Large-scale simulations of the two-dimensional melting of hard disks. 2005.

[63] MARADUDIN, A. A., MONTROL, E. W., AND WEISS, G. H. *Theory of lattice dynamics in the harmonic approximation,* vol. 3 of *Solid State Physics, Advances in Research and Applications.* Academic Press, New York and London, 1963. PHYSCI QC 176 S68 suppl. no. 3 1953.

[64] MATÉRN, B. Spatial variation. *Meddelanden från Statens Skogsforskningsintitut 49,* 5 (1960), 1–144. ILL.

[65] MEIJERING, J. L. Interface area, edge length and number of vertices in crystal aggregates with random nucleation. *Philips Res. Rep. 8* (1953), 270–290. SCI/TECH Q 1 P55 v.8 1953.

[66] MIYAGI, T. Viscous flow at low Reynolds numbers past an infinite row of equal circular cylinders. *J. Phys. Soc. Jpn. 13,* 5 (May 1958), 493–496. UABARD QC 1 P578.

[67] NADIM, A., AND STONE, H. A. The motion of small particles and droplets in quadratic flows. *Stud. Appl. Mech. 85* (1991), 53–73. ILL.

[68] OGAWA, T., AND TANEMURA, M. Geometrical consideratations on hard core problems. *Progress of Theoretical Physics 51,* 2 (February 1974), 399–417. PHYSCI QC 1 P96.

[69] OKABE, A., BOOTS, B., AND SUGIHARA, K. *Spatial Tesselations, Concepts and Applications of Voronoi Diagrams.* Wiley Series in Probability and Mathematical Statistics. John Wiley & Sons, Toronto, 1992. SCI/TECH QA 278.2 O412 1992.

[70] PANCHENKO, A. Private communication, March 2005.

[71] POESCHEL, T., AND BRILLIANTOV, N., Eds. *Granular Gas Dynamics,* vol. 624 of *Lecture notes in physics.* Springer Verlag, Berlin, 2003. SCI/TECH QC 168 G68 2003.

[72] PRESS, W. H. *Numerical recipes in Pascal: the art of scientific computing.* Cambridge University Press, New York, 1989. SCI/TECH QA 76.73 P2 N972 1989.

[73] PROUDMAN, I., AND PEARSON, J. R. A. Expansion at small Reynolds numbers for the flow past a sphere and a circular cylinder. *J. Fluid. Mech. 2* (1957), 237–262. SCI/TECH QA 901 J86.

[74] RICHARDSON, J. F., AND ZAKI, W. N. Sedimentation and fluidisation: Part I. *Trans. Inst. Chem. Eng. 32* (1954), 35–53. SCI/TECH TP 1 C493.

[75] ROWE, P. N. Drag forces in a hydraulic model of a fluidised bed – Part II. *Trans. Inst. Chem. Eng. 39* (1961), 175–180. SCI/TECH TP 1 C493.

[76] ROWE, P. N. A convenient empirical equation for estimation of the Richardson-Zaki exponent. *Chem Engng Sci. 42* (1987), 2795–2796. SCI/TECH TP 1 C516.

[77] SANCHEZ-PALENCIA, E. *Non-Homogeneous Media and Vibration Theory*, vol. 127 of *Lecture Notes in Physics*. Springer-Verlag, Berlin, Heidelberg, New York, 1980. UABARD QC 20.7 P47 S19 1980.

[78] SCHEIDEGGER, A. E. *The physics of flow through porous media*, 3rd ed. University of Toronto Press, Toronto, 1974. SCI/TECH QC 151 S31 1974.

[79] SCHILLER, L., AND NAUMANN, A. *Z. Ver Deut. Ing. 77* (1933), 318–.

[80] SLICHTER, C. S. Theoretical investigation of the motion of ground waters. *U.S. Geological Survey, 19th Ann. Rep.* (1899), 301–384. SCI/TECH QE 75 B93.

[81] SMOLUCHOWSKI, M. On the practical applicability of Stokes' law. *Proc. 5th Intern. Cong. Math. 2* (1912), 192–. ILL.

[82] STOKES, G. G. *Mathematical and physical papers*. University Press, Cambridge, 1901.

[83] STOYAN, D., KENDALL, W. S., AND MECKE, J. *Stochastic geometry and its applications*. Wiley Series in Probability and Mathematical Statistics. John Wiley & Sons, Toronto, 1987. MATH QA 273.5 S893 E5 1987.

[84] STOYAN, D., AND STOYAN, H. *Fractals, random shapes and point fields*. Wiley Series in Probability and Mathematical Statistics. John Wiley & Sons, Toronto, 1995. MATH QA 614.86 S7613 1995 c.1.

[85] SUGIHARA, K., AND IRI, M. VORONOI2 *reference manual*, second ed., December 1993. Manual is sent by authors upon request, sugihara@mist.i.u-tokyo.ac.jp.

[86] SYAMLAL, M., AND O'BRIEN, T. J. Simulation of granular layer inversion in liquid fluidized beds. *Int. J. Mult. Flow 14*, 4 (1988), 473–481. SCI/TECH QA 922 I62.

[87] SYAMLAL, M., ROGDERS, W., AND O'BRIEN, T. J. MFIX documentation theory guide. Technical Note, U.S. Department of Energy, Office of Fossil Energy, 1993. NET http://www.netl.doe.gov/osta/gaseous/simulate/mfix/theory.pdf.

[88] TORQUATO, S., TRUSKETT, T. M., AND DEBENEDETTI, P. G. Is random close packing of spheres well defined? *Phys. Lev. Lett. 84* (2000), 2064–2067. UAINTERNET.

[89] TURNBULL, H. W., AND AITKEN, A. C. *An introduction to the theory of canonical matrices*. Blackie & Son Ltd., London, 1932. MATH QA 263 T94.

[90] VAN DYKE, M. *Perturbation methods in Fluid Mechanics*, vol. 8 of *Applied Mathematics and Mechanics*. Academic Press, New York and London, 1964. SCI/TECH TA 350 V24 1964.

[91] VAN WACHEM, B. G. M., SCHOUTEN, J. C., VAN DEN BLEEK, C. M., KRISHNA, R., AND SINCLAIR, J. L. Comparative analysis of CFD models of dense gas-solid systems. *AIChE Journal 47*, 5 (May 2001), 1035–1051. SCI/TECH TP 1 A5118.

[92] VINCENT, P. J., AND HAWORTH, J. A theoretical note on spatial pattern of discs and properties of simplicial graph. *Forest Sci. 28*, 1 (1982), 181–186. SCI/TECH SD 1 F655 v.28 1982.

[93] WALLIS, G. B. *One dimesional two-phase flow*. McGraw-Hill, New York, 1969.

[94] WEISSTEIN, E. W. Sphere packing. From MathWorld – A Wolfram Web Resource. http://mathworld.wolfram.com/SpherePacking.html.

[95] WEN, C. Y., AND YU, Y. H. Mechanics of fluidization. *Chem. Eng. Prog. Symp. Ser. 62* (1966), 100. ILL.

[96] WOLFRAM, S. Computation theory of cellular automata. *Commun. Math. Phys. 96* (1984), 15–57. PHYSCI QC 20 C73.

[97] WU, Z., LOPEZ, E., BULDYREV, S. V., BRAUNSTEIN, L. A., HAVLIN, S., AND STANLEY, H. E. Current flow in random resistors networks: The role of percolation in weak and strong disorder, 2005.

"See how he lies at random, carelessly diffused."
John Milton, *Samson Agonistes*